Organisation for Economic Co-operation and Development

**ENV/CBC/MONO(2026)7**

**Unclassified** **English - Or. English**

**8 July 2026**

**ENVIRONMENT DIRECTORATE**
**CHEMICALS AND BIOTECHNOLOGY COMMITTEE**

# Validation report of methods to determine the dustiness of materials containing nano-objects and their aggregates and agglomerates

## OECD Series on Testing and Assessment

E-mail: ehscont@oecd.org

**JT03590512**

This work was approved and declassified by the Chemicals and Biotechnology Committee on 22/06/2026.

**Please cite this publication as:**

OECD (2026), *Validation report of methods to determine the dustiness of materials containing nano-objects and their aggregates and agglomerates*, OECD Series on Testing and Assessment, No. 429, OECD Environment, Health and Safety, Paris, https://one.oecd.org/document/ENV/CBC/MONO(2026)7/en/pdf.

**Contact us**

**OECD Environment Directorate,**
**Environment, Health and Safety Division**
**2 rue André-Pascal**
**75775 Paris Cedex 16**
**France**

**E-mail: ehscont@oecd.org**

# About the OECD

The Organisation for Economic Co-operation and Development (OECD) is an intergovernmental organisation in which representatives of 38 countries in North and South America, Europe and the Asia and Pacific region, as well as the European Union, meet to co-ordinate and harmonise policies, discuss issues of mutual concern, and work together to respond to international problems. Most of the OECD's work is carried out by more than 200 specialised committees and working groups composed of member country delegates. Observers from several Partner countries and from interested international organisations attend many of the OECD's workshops and other meetings. Committees and working groups are served by the OECD Secretariat, located in Paris, France, which is organised into directorates and divisions.

The Environment, Health and Safety Division publishes free-of-charge documents in twelve different series: **Testing and Assessment**; **Good Laboratory Practice and Compliance Monitoring**; **Pesticides**; **Biocides**; **Risk Management**; **Harmonisation of Regulatory Oversight in Biotechnology**; **Safety of Novel Foods and Feeds; Chemical Accidents; Pollutant Release and Transfer Registers; Emission Scenario Documents; Safety of Manufactured Nanomaterials;** and **Adverse Outcome Pathways.** More information about the Environment, Health and Safety Programme and EHS publications is available on the OECD's World Wide Web site (https://www.oecd.org/en/topics/chemical-safety-and-biosafety.html).

This publication was developed in the IOMC context. The contents do not necessarily reflect the views or stated policies of individual IOMC Participating Organizations.

The Inter-Organisation Programme for the Sound Management of Chemicals (IOMC) was established in 1995 following recommendations made by the 1992 UN Conference on Environment and Development to strengthen co-operation and increase international co-ordination in the field of chemical safety. The Participating Organisations are FAO, ILO, UNDP, UNEP, UNIDO, UNITAR, WHO, World Bank, Basel, Rotterdam and Stockholm Conventions and OECD. The purpose of the IOMC is to promote co-ordination of the policies and activities pursued by the Participating Organisations, jointly or separately, to achieve the sound management of chemicals in relation to human health and the environment.

# Foreword

This document contains the report of a validation study of methods to determine the dustiness of materials containing nano-objects and their aggregates and agglomerates. The study was conducted across several laboratories (inter-laboratory comparison) testing the same methods and the same materials. The project to establish harmonise Test Guidelines for the determination of dustiness of materials containing nano-objects and their aggregates and agglomerates was added to the OECD work plan in 2019 and was jointly led to completion by Germany and Denmark.

The validation report and the associated Test Guideline 127 were endorsed and approved, respectively, in April 2026 by the Working Party of the National Coordinators of the Test Guidelines Programme.

# Table of Contents

# List of figures

# List of tables

# Acknowledgements

The authors would like to thank Joint research center (JRC) for providing the samples used in the ILCs. Furthermore, the laboratories having participated in this inter-laboratory comparison are kindly acknowledged (list below).

National Laboratories:

- NFA-NRCWE (Denmark)
- BAuA (Germany)
- INERIS (France)
- ITC University Jaume I (Spain)
- INRS (France)
- CEA (France)
- Delft Solids Solutions (The Netherlands)
- LNE (France)
- TNO (The Netherlands)
- The Cyprus Institute (Cyprus)
- CDC-NIOSH (US)
- ITGA (France)
- Chemours (US)
- BASF (Germany)
- TÜV NORD (Germany)
- IBEVE (Belgium)
- INL (Portugal)

We also thank the experts for providing their feedback and shared knowledge towards the development of this TG, including its validation report.

# List of abbreviations

| Abbreviation | Definition |
|---|---|
| APS® [1] | Aerodynamic Particle Sizer / Aerodynamic Particle Size Spectrometer |
| CPC | Condensation Particle Counter |
| ELPI® [2] | Electrical Low Pressure Impactor |
| EM | Electron Microscopy |
| HARFO | High Aspect Ratio Fibrous Object |
| HARFA | High Aspect Ratio Fibrous Agglomerate |
| HEPA | High-Efficiency Particulate Arresting |
| LARFA | Low Aspect Ratio Fibrous Agglomerate |
| LARPO | Low Aspect Ratio Particulate Object |
| NOAA | Nano-Objects, and their Aggregates and Agglomerates |
| PSD | Particle Size Distribution |
| RH | Relative Humidity |
| SEM | Scanning Electron Microscopy |
| SMPS | Scanning Mobility Particle Sizer |
| TG | OECD Test Guideline |
| WPMN | OECD Working Party on Manufactured Nanomaterials |
| WNT | OECD Working Party of National Coordinators of the Test Guidelines Programme |

[1]APS® is the trademark of a product supplied by TSI. [2]ELPI® is the trademark of a product supplied by Dekati. This information is given for the convenience of users of this TG and does not constitute an endorsement by OECD of the product named. Equivalent products may be used if they can be shown to lead to the same results.

# 1. Introduction

2. The dustiness of a powdered material is a key parameter which describes the ability to generate airborne dust during agitation. Dustiness has been recognised not only as a relevant parameter for workplace health and safety [1–3] but also for assessing exposure risk [4–6], designing safe-by-design solutions [7], and quantifying exposure using control banding tools or mass balance models [8–10].

3. Several dustiness testing methods, both standardised and non-standardised, are currently available. Two major standards, EN 15051 and EN 17199-series, outline methodologies for determining material dustiness. EN 15051-series includes two methods - the Rotating Drum (RD) and the Continuous Drop (CD). EN 17199-series builds on this by adding two more methods, the Small Rotating Drum (SRD) and the Vortex Shaker (VS), specifically tailored for nano-objects and their agglomerates and aggregates (NOAA). Other methods, such as the Venturi, is described as dynamic method in ISO/TS 12025:2021 while the Fluidizer is described by Broßell et al. (2019) [11]. Each dustiness method is based on different agitation mechanisms (e.g., conveying, dropping, mixing, vibration, worst-case scenarios), leading to variations in dust generation, energy levels applied, test durations, and the amount of powder required. These differences result in variability in dustiness levels [1,4,12,13]. Therefore, for dustiness data to be reliable and comparable, it is essential to harmonize, validate, and standardize these various testing methods.

4. The Test Guideline (TG 127) [57] for the determination of dustiness of manufactured nanomaterials was developed in response to the need for standardised dustiness tests that address the unique requirements of nanomaterials and support regulatory needs now and in the future. Denmark (NFA-NRCWE), with support from Germany (BAuA), led the development and validation of this TG.

5. The TG development was informed by experimental data generated through intra- and inter-laboratory exercises conducted under the EU Horizon 2020 projects NanoHarmony (Grant agreement No 885931) and Gov4Nano (Grant agreement No 814401). This document reports on the international inter- and intra-laboratory comparisons (ILCs) carried out to validate the methods included in the TG on dustiness determination of manufactured nanomaterials. The ILCs aimed to assess the applicability and reproducibility of the proposed methods, identify factors contributing to variability, and analyse the statistical variability of results. Two ILCs were conducted-one focused on powders containing granular NOAA and the other on powders containing fibrous NOAA. The study design, execution, and results are described separately for each ILC. The methods, procedures, and outcomes were reviewed by both scientific and regulatory experts from the OECD's Joint Working Party of National Coordinators of the Test Guidelines Programme (WNT) and Working Party on Manufactures Nanomaterials (WPMN) Expert Group on Physical-Chemical Properties of Manufactured Nanomaterials. Subsequently it was reviewed by the WNT.

# 2. Scope and aim

6. The purpose of this validation report is to present the results of the ILCs conducted to support the development of the TG 127 [57] on dustiness determination of manufactured nanomaterials. These comparisons evaluated various dustiness test methods, including both standardised (EN 17199- series [14–18], ISO/TS 12025:2021 [19]) and non-standardised approaches, with the goal of generating reliable dustiness data. Additionally, the ILC aimed to help providing recommendations for selecting suitable measurement devices

7. The assessment of the reported results was conducted in accordance with requirements set out in international standards and guidelines, including ISO 5725-2:2025, ISO 13528:2022, EN 16897:2017,

ISO 27891:2015, CEN/TC 137 C 13/2023, OECD TG 125:2023, ISO 14966:2019, ISO 15900:2020, and VDI 3492:2013-06 [20–28].

# 3. ILC for powders containing granular NOAA

## 3.1. Time frame and instructions to participants

8. The schedule of the ILC is outlined in Table 1. A call for contributions to the dustiness testing program, involving both intra- and inter-laboratory comparisons, was circulated in October 2019 via the OECD National Coordinators group, reaching national scientific networks. Laboratories interested in participating were required to register by October 15, 2019. Participants provided details that included contact information, dustiness testing methods, and the minimum amounts of powders required per method. Notifications of acceptance or rejection were sent by October 25, 2019.

9. Initially, 18 collaborators expressed interest, covering seven different dustiness methods. Five of these methods had contributions from three or more laboratories. The final comparison study involved 12 laboratories, covering six well-established dustiness methods (see section 4.3). These methods included four standardised approaches as described in EN 17199-series: the large Rotating Drum (EN 17199-2:2019 [15]), the Continuous Drop (EN 17199-3:2019 [16]), the Small Rotating Drum (EN 17199-4:2019 [17]), and the Vortex Shaker (EN 17199-5:2025 [18]). Additionally, two methods were included: the Venturi method described as dynamic method in ISO/TS 12025:2021 [19], originally designed for pharmaceuticals, [29,30], and the Fluidizer method [11], developed for fibrous materials.

10. The samples were dispatched to participants, and the dustiness testing program was officially launched in June 2020. Nearly monthly meetings were organised to discuss experimental setups, procedures, and data analysis with all participating laboratories. Subgroup meetings were also held to address method-specific issues and ensure harmonisation of the procedures to maintain data comparability. Section 5.3 provides more details on the study design. Discussions covered topics such as test materials conditioning, weighing procedures, aerosol instrumentation, filters for mass collection, limits of quantification, and testing conditions.

**Table 1. Timeline of main activities in the ILC for powders containing granular NOAA.**

| Activities | Date |
| --- | --- |
| Call for contributions to the ILC | October 2019 |
| Start of the ILC experiments | June 2020 |
| Finalisation of the ILC experiments | September 2022 |
| Data treatment, and discussion of the ILC results | October 2022-March 2024 |
| Joint expert group meeting | April 2024 |
| Joint expert group meeting | November 2024 |
| Finalisation of the TG and validation report | February 2025 |

## 3.2. Participating institutions

The dustiness testing programme presented in this report had participation from 12 laboratories, located in 7 different countries (Cyprus, Denmark, France, Germany, Netherlands, Spain and the USA). Each laboratory conducted dustiness tests using at least one of the selected dustiness methods, as outlined in Table 2 below.

**Table 2. List of selected test methods and name, abbreviation and country of participating institutions in the dustiness determination.**

| Method | Number of participating laboratories | Laboratory | Number of tests¥ per material |
|---|---|---|---|
| Rotating Drum [15] | 5 | Lab 1 | TiO2 PC 105: 3 tests<br>TiO2 NM 103: 1 test<br>TiO2 NM 105: 1 test<br>SiO2 NM 203: 1 test<br>SiO2 NM 204: 1 test<br>SiO2 244 FP: 3 tests |
| | | Lab 2 | TiO2 PC 105: 2 tests<br>TiO2 NM 103: 1 test<br>TiO2 NM 105: 1 test<br>SiO2 NM 203: 1 test<br>SiO2 NM 204: 1 test<br>SiO2 244 FP: 1 test |
| | | Lab 3 | TiO2 PC 105: 3 tests<br>TiO2 NM 103: 2 tests<br>TiO2 NM 105: 2 tests<br>SiO2 NM 203: 3 tests<br>SiO2 NM 204: 2 tests<br>SiO2 244 FP: 3 tests |
| | | Lab 4 | TiO2 PC 105: 3 tests<br>TiO2 NM 103: 1 test<br>TiO2 NM 105: 1 test<br>SiO2 NM 203: 1 test<br>SiO2 NM 204: 1 test<br>SiO2 244 FP: 3 tests |
| | | Lab 5 | TiO2 PC 105: 2 tests<br>TiO2 NM 103: 1 test<br>TiO2 NM 105: 2 tests<br>SiO2 NM 203: 2 tests<br>SiO2 NM 204: 2 tests<br>SiO2 244 FP: 2 tests |
| Small Rotating Drum [17] | 2 | Lab 6 | TiO2 PC 105: 3 tests<br>TiO2 NM 103: 3 tests<br>TiO2 NM 105: 3 tests<br>SiO2 NM 203: 3 tests<br>SiO2 NM 204: 3 tests<br>SiO2 244 FP: 3 tests |

| | | | |
|---|---|---|---|
| | | Lab 7 | TiO2 PC 105: 1 test<br>TiO2 NM 103: 1 test<br>TiO2 NM 105: 1 test<br>SiO2 NM 203: 1 test<br>SiO2 NM 204: 1 test<br>SiO2 244 FP: 1 test |
| Vortex Shaker [18] | 4 | Lab 8 | TiO2 PC 105: 1 test<br>TiO2 NM 103: 1 test<br>TiO2 NM 105: 1 test<br>SiO2 NM 203: 1 test<br>SiO2 NM 204: 1 test<br>SiO2 244 FP: 1 test |
| | | Lab 9 | TiO2 PC 105: 1 test*<br>TiO2 NM 103: 1 test*<br>TiO2 NM 105: 1 test*<br>SiO2 NM 203: 1 test*<br>SiO2 NM 204: 1 test*<br>SiO2 244 FP: 1 test* |
| | | Lab 10 | TiO2 PC 105: 1 test<br>TiO2 NM 103: 1 test<br>TiO2 NM 105: 1 test<br>SiO2 NM 203: 1 test<br>SiO2 NM 204: 1 test<br>SiO2 244 FP: 1 test |
| | | Lab 5 | TiO2 PC 105: 1 test<br>TiO2 NM 103: 1 test<br>TiO2 NM 105: 1 test<br>SiO2 NM 203: 1 test<br>SiO2 NM 204: 1 test<br>SiO2 244 FP: 1 test |
| Continuous Drop [16] | 2 | Lab 1 | TiO2 PC 105: 1 test<br>SiO2 244 FP: 1 test<br>Micro Alumina: 3 tests |
| | | Lab 2 | TiO2 PC 105: 1 test<br>SiO2 244 FP: 1 test<br>Micro Alumina: 3 tests |
| Fluidizer [1<br>1] | 2 | Lab 11 | TiO2 PC 105: 3 tests<br>TiO2 NM 103: 2 tests<br>TiO2 NM 105: 3 tests<br>SiO2 NM 203: 3 tests<br>SiO2 NM 204: 3 tests<br>SiO2 244 FP: 2 tests |
| | | Lab 12 | TiO2 PC 105: 3 tests<br>TiO2 NM 103: 2 tests<br>TiO2 NM 105: 3 tests<br>SiO2 NM 203: 3 tests<br>SiO2 NM 204: 3 tests<br>SiO2 244 FP: 1 test |
| Venturi [29,30] | 1 | Lab 3 | TiO2 PC 105: 3 tests |

| | | | |
|---|---|---|---|
| | | | TiO2 NM 103: 3 tests<br>TiO2 NM 105: 3 tests<br>SiO2 NM 203: 3 tests<br>SiO2 NM 204: 3 tests<br>SiO2 244 FP: 3 tests |

¥ each test consist of three replicates.
* One test of five replicates performed.

## 3.3. Study design

### 3.3.1. Dustiness methods

11. A total of six dustiness methods applicable to powders containing NOAA were employed (Table 2). Each participating laboratory conducted a harmonisation process for the methods and procedures to be followed during the testing. For the Rotating Drum, Small Rotating Drum, Vortex Shaker, and Continuous Drop methods, the procedures were based on the existing CEN standards (EN 17199-series), with any deviations explicitly documented in the procedures provided in the TG 127 [57]. For the Fluidizer and Venturi methods, the procedures described by Broßell et al. (2019) [11] and Boundy et al. (2006) [29] and Evans et al. (2013) [30] were followed, respectively. Detailed descriptions of each method and their key characteristics are provided in the TG 127 [57].

12. To facilitate an inter-laboratory comparison, each participating laboratory performed one dustiness test per material with three replicates for each method. Additionally, some laboratories conducted an intra-laboratory validation by performing extra tests on different days, each consisting of three replicates, for all or selected materials. The number of tests conducted for both intra-laboratory validation and inter-laboratory comparison for each method is outlined in Table 2.

13. Considering that dustiness is sensitive to environmental conditions such as relative humidity, temperature and electrostatic effects, in order to ensure the repeatability and reproducibility of the results, the test atmosphere was controlled for temperature and relative humidity (RH) (21 ± 3ºC and 50 ± 5% RH, respectively). The environmental conditions were documented along with the dustiness results. The dustiness test apparatus were also electrically grounded to prevent charge accumulation.

### 3.3.2. Metrics and measurands

14. Each dustiness method, as currently established, includes different parameters that are measured depending on the setup and the intended use of the generated data. Some parameters, such as the respirable dustiness index or the number-based dustiness index, are common across several tests. However, dustiness kinetics, which describe the rate of particle release over time, are only considered in certain methods (e.g., Small Rotating Drum).

15. Table 3 summarizes the validated metrics and measurands for each method described in this TG 127 [57] for powders containing granular NOAA. In addition, Table 4 lists optional measurands that may be of interest when assessing the dustiness of powders containing granular NOAA.

16.

**Table 3. Summary of the validated (Yes/No) metrics and measurands for granular NOAA and for each dustiness method.**

| Measurand | Symbol | Unit | Test method | | | | | |
|---|---|---|---|---|---|---|---|---|
| | | | Rotating Drum | Small Rotating Drum | Vortex | Continuous Drop | Fluidizer | Venturi |
| Respirable, dustiness mass fraction | $DI_R$ | mg/kg | Yes | Yes | Yes | Yes | No | Yes |
| Thoracic dustiness mass fraction | $DI_T$ | mg/kg | Yes | No | No | No | No | No |
| Inhalable/Total dustiness mass fraction | $DI_I$ / $DI_{tot}$ | mg/kg | Yes | No | No | Yes | Yes | Yes |
| Number-based dustiness index of respirable particles (10 nm to about 1 µm)* | $DI_N$ | #/mg | Yes | Yes | Yes | Yes | Yes | No |
| Number-based average emission rate of respirable particles (10 nm to about 1 µm)* | $E$ | #/mg·s | Yes | Yes | Yes | Yes | Yes | No |
| Number-based initial dustiness kinetics considering the number of particles released (10 nm to about 1 µm)* | $D_k$ | #/mg·s$^2$ | Yes | Yes | No | No | No | No |
| Time-based dustiness kinetics assessed as the time required to generate 50 % of the total number of particles released (10 nm to about 1 µm) | $n_{50}$ | s | Yes | Yes | No | No | No | No |
| Number of modes of the time-averaged number-based PSD as d$N$/dlog$D_i$ * | $M_N$ | — | Yes | Yes | Yes | Yes | Yes | No |
| Modal aerodynamic equivalent diameters corresponding to the highest mode (M1N) and to the second highest mode (M2N) of the time-averaged number-based PSD as d$N$/dlog$D_i$* | $M_{1N}$ and $M_{2N}$ | µm | Yes | Yes | Yes | Yes | Yes | No |

* The number-basis measurand refers to particles released by the powder during the measurement, with agglomerates and aggregates each counted as a single particle.

**Table 4. Summary of optional measurands for granular NOAA.**

| Measurand | Symbol | Unit |
|---|---|---|
| Number of modes of the time-averaged mass-based PSD as d*M*/dlog$D_i$ | $M_M$ | — |
| Modal aerodynamic equivalent diameters corresponding to the highest mode (M1M) and to the second highest mode (M2M) of the time-averaged mass-based particle size as d*M*/dlog$D_i$ | $M_{1M}$ and $M_{2M}$ | µm |
| Morphological and chemical characterisation of the particles including NOAA | None | — |

17. As detailed in Table 3, the validated measurands for the dustiness methods covered in this TG vary by method. However, some metrics are common across nearly all methods, such as the respirable mass fraction (except for the Fluidizer) and the number-based dustiness measurands. For comparability between methods, the parameters assessed in this ILC were harmonised based on their relevance and applicability:

i) *Respirable mass-based dustiness index ($DI_R$; mg/kg)* - This is the most common measurand traditionally used for dustiness determination for both general powders (EN 15051-series) and nanomaterials (EN 17199-series). The respirable mass-based dustiness index is a mandatory measurand for all methods according to their respective standards, except for the Fluidizer method due to its unique characteristics, such as longer test duration and lower aerosol generation. This parameter is critical due to the existence of occupational exposure limits (OELs) based on the respirable fraction and its significance for human health.

ii) *Number based dustiness index ($DI_N$; #/mg) and number based powder normalised average emission rate (E; #/mg.s)* - Both are mandatory parameters for all methods per the standards for dustiness determination of nanomaterials (EN 17199-series). Measuring nanoparticle emissions in terms of particle number concentration is valuable because of the strong correlation of effects with the number of particles, which also aligns with provisional particle number concentration exposure limits set by Germany and the Netherlands [31]. Consequently, dustiness data in this study were also evaluated using $DI_N$ and *E* for all methods.

iii) *Particle size distribution (PSD) and size modes* - These are mandatory measurands according to existing standards for nanomaterial dustiness determination (EN 17199-series). The PSD of aerosols generated during powder handling provides valuable insights, such as filtration efficacy, inhalation dose, and health risks. When combined with the number-based average emission rate, this information aids in safer material selection, exposure prioritisation during powder handling, and better understanding of release and exposure mechanisms.

iv) *Time-based number dustiness kinetics ($n_{50}$; s)* - This metric defines the time (in seconds) required to generate 50% of the total emitted particles during agitation. It is currently mandatory only for the Small Rotating Drum (EN 17199-4:2019 [17]). Dustiness kinetics provide insight into a powder's resistance to attrition and energy demand. Powders with lower dustiness kinetics (i.e., longer time to generate 50% of the particles) demonstrate higher resistance to attrition and energy consumption. This metric is valuable for exposure modeling, as it explains variations between dustiness and exposure under specific processes [9,10,13,32]. Dustiness kinetics were measured for both the Small Rotating Drum and Rotating Drum, with the goal of: 1) comparing kinetic differences across methods to improve understanding of dynamics, and 2) providing data for future exposure modeling.

v) *Total, inhalable, or thoracic mass-based dustiness indices* - These indices were reported for the

Rotating Drum and/or Venturi methods but are not discussed in further detail in this document.

vi) *Morphological and chemical characterisation of airborne particles* - For powders containing granular NOAA, optional sampling and qualitative analysis of airborne particles' morphology and chemical composition using offline analytical techniques (e.g., electron microscopy (EM), X-ray fluorescence spectroscopy, inductively coupled plasma mass spectrometry (ICP-MS), or inductively coupled plasma atomic emission spectroscopy (ICP-AES)) can provide complementary information. Such analysis reveals the morphology and chemical makeup of the NOAA generated by resuspended powder during agitation, supplementing the data from time-resolving instruments. However, this aspect is not further discussed in the present document.

18. Each dustiness method has slight variations, and the equations described in the corresponding standard methods for determining the aforementioned measurands differ slightly. However, to improve comparability between methods, efforts were made to harmonize the equations where possible. The equations used for each method are provided in the dustiness TG 127 [57].

### 3.3.3. Instruments and samplers

19. The specifics of the online aerosol instrumentation and filters used for the gravimetric determination of particle mass by the participating laboratories, as well as the instruments applied for each method, are summarised in Table 5.

**Table 5. Overview of filters used for mass-based dustiness index determination and online instrumentation for number-based dustiness index and size distribution for each dustiness method and laboratory.** ***N/A: not applicable.***

| Method | Laboratory | Respirable gravimetrical fraction | Particle number concentration | Number-based Size distribution data | Cyclone prior online instruments |
|---|---|---|---|---|---|
| Rotating Drum | Lab 1 | Back-up filter | CPC 3775, TSI [a] | ELPI+™, Dekati [b] | CPC: Respirable cyclone at 4.2 L/min |
| | Lab 2 | Back-up filter | CPC 3775, TSI [a] | ELPI+™, Dekati [b] and NanoScan SMPS 3910, TSI [c] | CPC: Respirable cyclone at 4.2 L/min on CPC and ELPI cyclone |
| | Lab 3 | Back-up filter | Not measured | Not measured | N/A |
| | Lab 4 | Back-up filter (Pall P/N 61663; 76mm filter) | CPC 3776, TSI [d] | ELPI+™, Dekati [b] | CPC: Respirable cyclone at 4.2 L/min |
| | Lab 5 | Back-up filter | Not measured | Not measured | N/A |
| Small Rotating Drum | Lab 6 | Sensidyne GK2.69 (PTFE filter 37 mm) at 4.2 L/min | CPC 3007, TSI [e] | ELPI+™, Dekati [b] | No |
| | Lab 7 | Sensidyne GK2.69 (PTFE filter 37 mm) at 4.2 L/min | N-WCPC 3788, TSI[f] | OPS 3300, TSI [g] | No |
| Vortex Shaker | Lab 8 | Sensidyne GK2.69 (PTFE filter 37 mm) at 4.2 L/min | CPC 3007, TSI [e] | Not measured | CPC: Respirable cyclone at 4.2 L/min |

| | | | | | |
|---|---|---|---|---|---|
| | Lab 9 | Sensidyne GK2.69 (PTFE filter 37 mm) at 4.2 L/min | CPC 3007, TSI [e] | Not measured | CPC: Respirable cyclone at 4.2 L/min |
| | Lab 10 | Sensidyne GK2.69 (PTFE filter 37 mm) at 4.2 L/min | CPC 3007, TSI [e] | ELPI+™, Dekati [a] | CPC: Respirable cyclone at 4.2 L/min |
| | Lab 5 | Sensidyne GK2.69 (PTFE filter 37 mm) at 4.2 L/min | CPC 3007, TSI [e] | Not measured | Not measured |
| Continuous Drop | Lab 1 | Glass microfiber filter (37 mm Ø and 1.6 um pore size) and Sensidyne GK2.69 | CPC 3775, TSI [a] | APS 3321, TSI [h] and SPMS 3034, TSI [i] | CPC: Respirable cyclone at 4.2 L/min |
| | Lab 2 | Glass microfiber filter (37 mm Ø and 1.6 um pore size) and Sensidyne GK2.69 | CPC 3775, TSI [a] | ELPI+™, Dekati [b] | ELPI pre-separator cyclone with 10 µm cut point at 10 L/min. |
| Fluidizer | Lab 11 | Ø 37 mm, 0.8 µm pore size, AAWP, Millipore | CPC 5.403, GRIMM Aerosol Technik [j] | SMPS (CPC 5.403 with DMA 55-900), GRIMM Aerosol Technik [k] and APS 3321, TSI [h] | No |
| | Lab 12 | Ø 37 mm, 0.8 µm pore size, AAWP, Millipore | CPC 3022A, TSI [L] | SMPS (TSI 3080 classifier, L-DMA TSI 3081, 85Kr Neutralizer and TSI 3786 CPC) [m] and APS 3321, TSI [h] | No |
| Venturi | Lab 3 | 37mm PVC filters (#225-5-37-P, SKC Inc., Eighty Four, PA) and Cyclone (GK 2.69) with metallic cassette | Not measured | Not measured | N/A |

[a] Condensation Particle Counter (CPC) 3775, TSI: down to 4 nm at 1 s time resolution
[b] Electrical Low-Pressure Impactor, ELPI+™, Dekati: 14 size channels between 6 nm and 10 µm with 1 s intervals
[c] NanoScan Scanning Mobility Particle Sizer (SMPS) 3910, TSI: 13 size channels between 10 and 420 nm with 1 minute intervals
[d] Condensation Particle Counter (CPC) 3776, TSI: down to 2.5 nm at 1 s time resolution
[e] Condensation Particle Counter (CPC) 3007, TSI: 10 nm to >1 µm at 1 s time resolution
[f] Nano Water-Based Condensation Particle Counter (N-WCPC) 3788, TSI: down to 2.5 nm at 1 s time resolution
[g] Optical particle sizer (OPS) 3300, TSI: 16 channels from 0.3 to 10 µm with 60 s intervals
[h] Aerodynamic Particle Sizer (APS) 3321, TSI: 51 size channels between 0.5 and 20 µm with 1 s time intervals
[i] Scanning Mobility Particle Sizer (SMPS) 3034, TSI: 32 size channels between 10 and 487 nm with 1 s intervals
[j] Condensation Particle Counter (CPC) 5.403 GRIMM Aerosol Technik: 4.5 nm to >3 µm at 1 s time resolution
[k] SMPS (CPC 5.403 with DMA 55-900), GRIMM Aerosol Technik
[L] Condensation Particle Counter (CPC) 3022A, TSI: down to 7 nm at 1 s time resolution
[m] SMPS (TSI 3080 classifier, L-DMA TSI 3081, 85Kr Neutralizer and TSI 3786 CPC)

### 3.3.4. Test materials

20. Six test materials were selected to represent various classes of powders containing NOAA, differing chemical compositions, and varying levels of dustiness (Table 6). According to data from the French R-nano database (https://www.r-nano.fr/), the selected substances, titanium dioxide ($TiO_2$) and silicon dioxide ($SiO_2$), are among the most produced, distributed, and imported nanomaterials, with tonnages exceeding 10 000 and 100 000 tons, respectively. Additionally, microalumina was included in the study to facilitate dustiness tests with the Continuous Drop method, which requires a significant amount of material.

**Table 6. Selection of materials, producers/providers, descriptions, densities, surface specific areas (SSA), sizes, and justifications for choice.** ***N/A: not available. *Based on Small Rotating Drum results tested by Lab 6. *1 Green density (90 MPa); equivalent circular diameter (ECD).***

| Code | Producer/ provider | Description | Dustiness Index* (mg/kg) | Bulk density ($g/cm^3$) | BET SSA ($m^2/g$) | NOAA ECD size (nm) | Remarks and motivation for choice |
|---|---|---|---|---|---|---|---|
| TiO2 PC105 | CRYSTAL | Photocatalytic $TiO_2$ (anatase) | 9.52 (very low) | N/A | 86.0 | N/A | CEN Mandate material. Sufficient material to include methods with a high material requirement. |
| TiO2 NM-103 | -/JRC Nanomaterials Repository | Thermal, hydrophobic $TiO_2$ (rutile) (90.7% purity) | 323 (high) | 0.44 | 51.4 | 13.1 | JRC repository for representative nanomaterials and linked to the OECD WPMN. |
| TiO2 NM-105 | -/JRC Nanomaterials Repository | Thermal, hydrophilic $TiO_2$ (rutile) (99.9% purity) | 28 (low) | 0.1 | 46.2 | 10.9 | JRC repository for representative nanomaterials and linked to the OECD WPMN. |
| SiO2 NM-203 | -/JRC Nanomaterials Repository | Thermal, synthetic amorphous $SiO_2$ (99.6% purity) | 354 (high) | 0.03 | 194.6 | 18.9 | JRC repository for representative nanomaterials and linked to the OECD WPMN. |
| SiO2 NM-204 | -/JRC Nanomaterials Repository | Precipitated, synthetic amorphous $SiO_2$ (92.1% purity) | 1058 (very high) | 0.16 | 136.6 | 5.2 | JRC repository for representative nanomaterials and linked to the OECD WPMN. |
| SiO2 244FP | Silica Grace | | 638.3 (very high) | N/A | 142 | N/A | CEN Mandate material. Sufficient material to include methods with a high material requirement. |
| Micro alumina CT3000 LS SG | Almatis GmbH | Low soda high reactive calcide alumina. High fired density and low impurities ($Al_2O_3$ 99.8%) | N/A | 2.24*1 | 7.8 | 500 | This material was selected to be used for intra-laboratory testing for the CD dustiness method, due to amount of sample requirements. |

#### *Sampling from bulk material*

21. It is crucial to ensure that samples of bulk material taken for dustiness measurement accurately represent the overall bulk material supplied. The settlement of larger particles in the container during transport can result in significant variations in PSD across different sections of the container. To maximize the homogeneity of materials distributed among all participating laboratories, the materials were acquired from the same batch. The distributors of the materials, handled the subsampling, packing,

and shipping of the samples, ensuring that each laboratory received the required amounts from their specially designed and authorised facilities.

22. To ensure proper mixing of the powder, each container containing the bulk material for replicate samples had sufficient free space. The container was inverted several times to promote uniformity. A sample was then extracted from the top of the container and immediately sealed. This procedure was repeated based on the number of replicate samples required by each laboratory.

#### *Conditioning of the test material and test equipment*

23. Conditioning of the test material and test equipment was performed according to the specifications provided in the TG 127 [57]; Sections 4.3 and 4.4). In brief, samples were stored and conditioned at standard conditions (21 ± 3 °C and 50 ± 5% RH) prior to testing to ensure equilibrium with the ambient environment.

24. During dustiness testing, the apparatus was maintained under standard controlled conditions (21 ± 3 °C and 50 ± 5% RH) as specified in the TG. Equipment was electrically grounded to prevent static charge accumulation.

25. 25. For gravimetric quantification of the mass-based dustiness index, filters were pre-conditioned and weighed under the same controlled environmental conditions. In cases where laboratories could not ensure fully controlled temperature and humidity, the actual conditions during pre-conditioning and weighing were documented.

#### *Moisture content and bulk density*

26. Prior to the dustiness tests and following the pre-conditioning of bulk materials, six participating laboratories determined the moisture content of six materials. The oven-drying method was employed as the standard approach, with samples heated at 110-120 °C for a minimum of 12 hours, in accordance with EN 17199-1:2019 [14] and as described in Section 5 of the TG 127 [57]. One laboratory (Lab 7) determined moisture content using a Moisture Analyser HR73.

27. The bulk density of the test materials was measured and documented according to EN 15051-1:2025 [33], as detailed in Section 6 of the TG 127 [57]. Measurements were performed using calibrated volumetric containers and analytical balances.

### 3.3.5. Harmonisation efforts

28. The experimental procedure was harmonised as much as possible, and several key points were the subject of discussion and agreement. The most important topics of discussion are summarised below, along with a brief description of the decisions made.

#### *Aerosol instrumentation*

29. After extensive discussion, it was concluded that complete harmonisation of the instrumentation used was not feasible. However, all partners were requested to provide detailed information about the instrumentation utilised to assess any potential impacts on the measured data. The online instrumentation used by the different partners is outlined in Table 5.

30. In addition to variations in instrumentation, some partners employed a cyclone prior to the CPC inlet, while others did not (Table 5). The effect of the cyclone was investigated for one material, $TiO_2$ NM-105, using a Small Rotating Drum at Lab 6. To study the cyclone's effect, an additional set of three replicates was conducted with $TiO_2$ NM-105, utilizing a respirable cyclone before the CPC inlet, which

was then compared to three tests conducted without the cyclone under identical setup and conditions. All tests were performed by the same laboratory, except for the CPC unit used in the additional cyclone test, as the CPC unit employed in the other three tests required repairs. Notably, the CPC model used (TSI 3007) has a concentration accuracy of ± 20%. Consequently, utilizing a different instrument could introduce a variation complicating the interpretation of the results.

31. For $TiO_2$ NM-105, the difference in measured particle number concentrations (#/cm³) between tests conducted without a cyclone ranged from 2% to 9%. In contrast, the difference between tests conducted with and without the cyclone was between 29% and 38%. Similarly, the differences in particle number emission rate and the number-based dustiness index showed variances of 5% to 12% without the cyclone, while the differences when comparing tests with and without the cyclone ranged from 23% to 34%.

32. Specifically, the difference in test results obtained without using the cyclone was between 5% and 12% for the number-based average emission rate per mg of powder and 5% to 23% for the number-based dustiness index. Conversely, the differences between tests conducted without the cyclone and those with the cyclone ranged from 23% to 35% for both metrics. The differences observed were slightly higher (12% to 23%) when comparing tests with and without the cyclone prior to the CPC. This discrepancy can partially be attributed to the use of a different CPC unit, as previously noted. The CPC 2007 model from TSI has a reported concentration accuracy of ± 20%.

33. In summary, the differences in results when using the cyclone were greater than those observed when no cyclone was employed. However, it remains challenging to determine whether the increased variability is solely due to the cyclone effect or if other influencing factors, such as the use of a different CPC unit for measurements, contributed to this variation. To draw robust conclusions regarding the cyclone's impact on particle number concentrations, further testing is necessary.

### *Filter samples and foams used for gravimetric analysis*

34. Filters conforming to ISO 15767:2009 [34] were employed by all laboratories. The limit of quantification was established as 10 times the standard deviation of the method's uncertainty, calculated from the mean value of the difference in mass gain or loss on blind filters.

35. For the Rotating Drum method, all partners utilised the same foams as specified in EN 15051-2:2025 [35].

### *Good weighing practices*

36. Proper weighing practices are crucial for accurate quantification (ISO 15767:2009 [34]). It was agreed that weighing would occur under controlled temperature and humidity conditions (21 ± 3ºC and 50 ± 5% RH). Filter media should be pre-conditioned for several hours, or at least overnight, prior to both pre-weight and post-weight measurements. If these conditions could not be met, laboratories were required to monitor and record the temperature and humidity during the weighing process. A balance capable of measuring to at least 5 decimal places would be used.

### *Equations used for dustiness characterisation.*

37. Each dustiness method possesses slightly different characteristics, resulting in slight variations in the equations applied to calculate the dustiness parameters. To enhance comparability and consistency across methods, efforts were made to harmonize the calculated dustiness parameters and to understand the underlying rationale and assumptions behind these equations. A detailed description of the applied and, where applicable, modified equations (in comparison to those in the original CEN standards) along with their implications, is provided in the TG 127 [57] within the Sections 6-11.

### 3.3.6. Data gathering

38. A common dustiness data template was developed and utilised by all laboratories to systematically collect and organize information on the characteristics of the dustiness methods employed, as well as to report dustiness results. This approach ensured comparability across the produced results and allowed for the traceability of all reported data.

39. Laboratories were instructed to adhere to their routine procedures for dustiness testing while providing specific details related to gravimetric dustiness determination. This included information on filter weighting, such as blank filter correction and limit of quantification as well as data on the volume and flow rates of the dustiness method, the volume and mass of the test sample, and the dustiness mass fraction in mg/kg. The template also contained detailed information on the online data produced, including average particle number concentration, emission rate time series, average emission rate, emission rate per mg of test powder, number-based dustiness index (#/mg), and PSD and modes. Additionally, specific sheets were included to report on the instruments and samplers used, operating conditions, moisture content of the test powder, and powder characteristics such as density and specific surface area. Dustiness data was reported using the standardised template (Annex A), supported by a macro script for calculating dustiness parameters (Annex B). Each laboratory was also required to maintain a logbook template, which documented testing dates, file names containing raw data, the amount of material used in each test, and any relevant notes or observations. The structure of the logbook is detailed in Annex C.

## 3.4. Dustiness data evaluation

40. The equations used to calculate the measurands described in Table 3, including the mass- and number-based dustiness indexes and emission rates, are provided in the TG 127 [57]; sections 6-12). In this validation report, only the resulting data and their evaluation are presented.

41. To support consistent data processing among participating laboratories, an Excel-based calculation tool (macro script) was developed to automatically derive the relevant dustiness parameters from the concentration data recorded with the particle counter (e.g. CPC). A step-by-step user guide for this tool is provided in Annex B.

## 3.5. Validation of the ILC results

### 3.5.1. Data quality criteria

42. To ensure high data quality, the criteria adopted for this task were based on considerations from relevant OECD documents (OECD GD 34 ENV/JM/MONO(2005)14; [36]), and OECD Nanomaterial documents 90 (ENV/JM/MONO(2019)12 [37]) and 91 (ENV/JM/MONO(2019)13 [38]).

i) The quality criteria encompass four essential types of information:
ii) Information on the material as prepared and delivered to the laboratories.
iii) Information on the powders containing NOAA conditions during storage, handling, and dustiness testing.
iv) Information on test parameters that are specific or particularly relevant for powders containing NOAA.
v) General information on reporting.

43. In this regard, information regarding the selected materials for testing and handling conditions has been provided, along with documentation of testing instrumentation and conditions. All relevant raw results are included as annexes to this report.

### 3.5.2. Data assessment and statistics

44. ISO 5725-1:2023 and ISO 5725-2:2025 [26,39] and ISO 13528:2022 [22] were used to assess the accuracy (trueness and precision) of measurement methods and results, as well as laboratory performance. The steps followed are summarised in Figure 1.

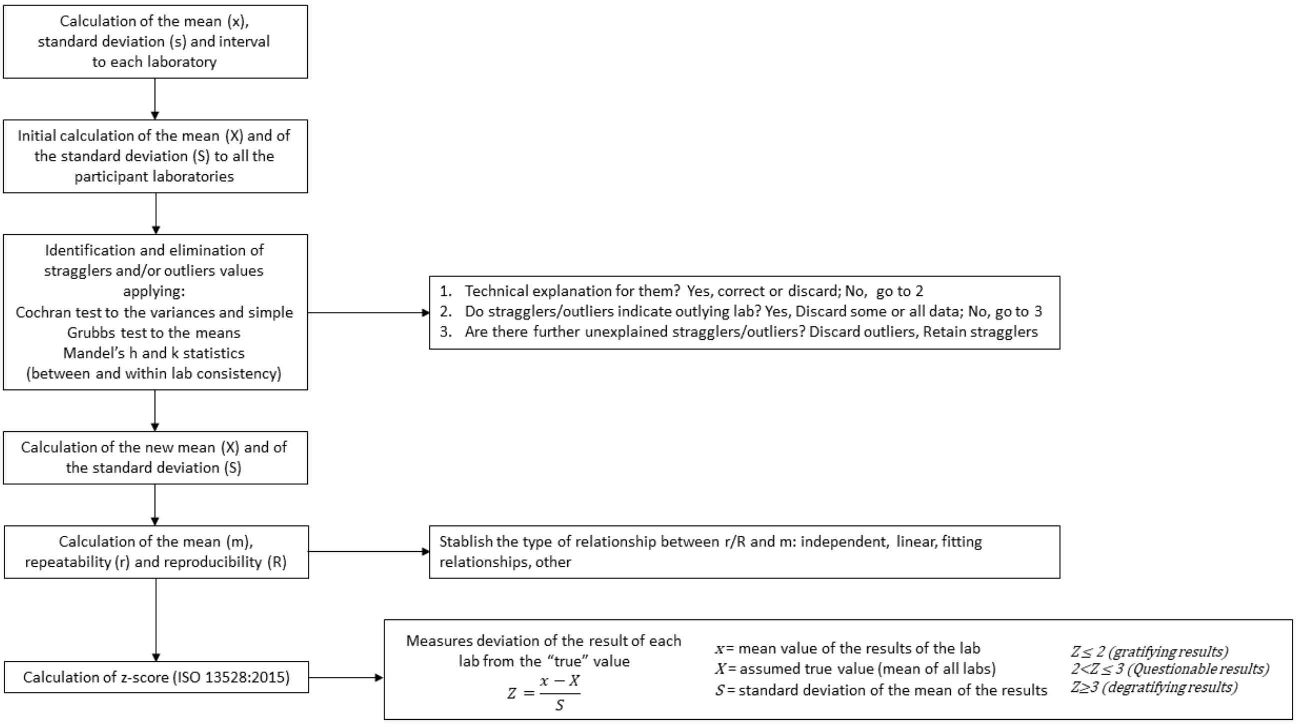


**Figure 1. Schematic figure of the steps followed for ILC data treatment based on ISO 5725-2:2025 and ISO 13528:2022.**

45. For methods with participation from three or more laboratories (i.e., Rotating Drum and Vortex Shaker), ISO 5725-2:2025 [26] was used to assess repeatability and reproducibility of the different measurands for the various methods, as well as for the detection and removal of outliers. Initially, data were organised for each method and parameter, and means and standard deviations were calculated based on all data. To identify and remove outliers, Mandel's h and k statistics, as well as Cochran and Grubbs tests, were computed and plotted. Mandel's test helps describe the variability of the measurement method; the h statistic assesses between-laboratory consistency, while the k statistic measures within-laboratory consistency. Cochran's test evaluates within-laboratory variability, whereas Grubbs' test assesses between-laboratory variance. For the application of Mandel's, Cochran, and Grubbs tests, three randomly selected repetitions were used to harmonize the number of repetitions across laboratories. For laboratories with three tests (nine replicates), one test composed of three replicates was selected.

46. Stragglers are observations with statistics that lie between the 5% and 1% critical values, while outliers exceed the 1% critical value. According to ISO 5725-2:2025 [26], stragglers should be retained

unless they can be attributed to technical errors or outlying laboratories. After the removal of stragglers and outliers, the mean, repeatability variance, and reproducibility variance were computed for each analysed level, and their relationships were analysed.

47. For methods with fewer than three participant laboratories (i.e., Small Rotating Drum, Continuous Drop, Fluidizer, and Venturi), all data were retained for evaluation, except for outliers linked to mistakes or malfunctions during testing. The statistical analysis was conducted using R Statistical Software version 4.1.0 (R Core Team 2021).

48. Additionally, for all methods, regardless of the number of participant laboratories, the following analyses were conducted:

i. Intra-laboratory data was explored, and coefficient of variation % (CV) was calculated as:

   $CV = \cdot 100$ where σ is the standard deviation and μ the mean of the considered data.

ii. Differences and correlations between laboratories and methods were studied.

iii. Following ISO 13528:2022 [22], the z-score ($z$) was determined, which measures the deviation of each laboratory's result from the "true" value. The equation used for calculating the z-score is included in Figure 1. The performance criteria based on the z-score are as follows:

   - if $\leq 2$: performance is satisfactory/acceptable
   - if $2 < \leq 3$: performance is questionable/warning signal
   - if $> 3$: performance is unsatisfactory/unacceptable.

## 3.6. Results

### 3.6.1. Rotating Drum

49. Five laboratories participated in the Rotating Drum method. Respirable dustiness data was provided by all five laboratories, though only three submitted results for particle number measurements (see combined dustiness report in Annex D).

50. The respirable dustiness data from lab 2 for $TiO_2$ NM-105 and $SiO_2$ NM-203, as well as Lab 5 data for $TiO_2$ PC105, $TiO_2$ NM-105, and $SiO_2$ NM-203, were excluded from the analysis because the results were below the detection limit. One straggler and one outlier were identified for respirable dustiness index (Lab 1 $SiO_2$ 244FP and Lab 1 $SiO_2$ NM-204) when assessing the between-lab consistency, and 2 stragglers (Lab 2 $TiO_2$ PC105 and Lab 5 $TiO_2$ NM-103) when assessing the within-lab consistency (Figure 2). Additionally, two stragglers were found in the within-laboratory consistency assessment using Mandel's k: Lab 2 $TiO_2$ PC105 and Lab 5 $TiO_2$ NM-103 (Figure 3). $TiO_2$ PC105 was also flagged as a straggler by the Cochran test (Figure 3).

51. For particle number data ($DI_N$ and $PNE_i$), no outliers or stragglers were identified in the between-laboratory consistency assessment. However, the within-laboratory consistency analysis for Lab 4, using Mandel's k and the Cochran test, identified four outliers/stragglers (Figure 5).

52. For the inhalable dustiness index, a few stragglers were found in the between-laboratory ($TiO_2$ NM-103) and within-laboratory consistency assessments ($TiO_2$ PC105, NM-105, and $SiO_2$ NM-203) for Lab 5, based on Mandel's h and k.

53. For the thoracic dustiness index, $SiO_2$ NM-204 from Lab 1 was identified as a straggler in the between-laboratory consistency assessment (Mandel's h; Figure 6). In the within-laboratory consistency assessment, Lab 3 $SiO_2$ NM-204 and 244FP were flagged as an outlier and a straggler, respectively,

using Mandel's k (Figure 7). The Cochran test supported these findings, identifying $SiO_2$ NM-204 as a straggler. The standard deviations for reproducibility were smaller when excluding $SiO_2$ NM-204 from Lab 1 and Lab 3. However, since the differences in standard deviations were minimal, the data was retained for further analysis. A full statistical assessment is included in Annex E.

54. Overall, the stragglers and outliers identified could not be clearly linked to technical errors or laboratory issues, and no laboratory was consistently flagged as problematic. Furthermore, the CV was generally around or below 20%. Considering the limited number of datasets, all data was retained for further analysis. Additional removal of data points could result in parameter estimates for standard deviations that overlook the normal variability expected in such measurements.

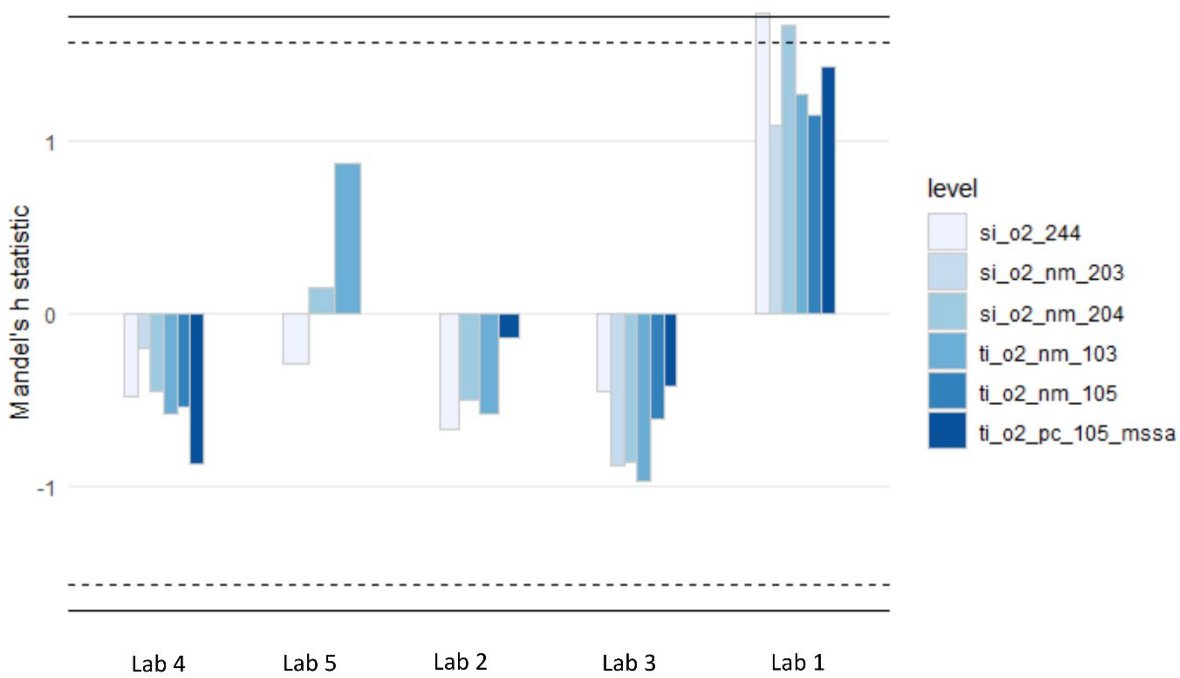

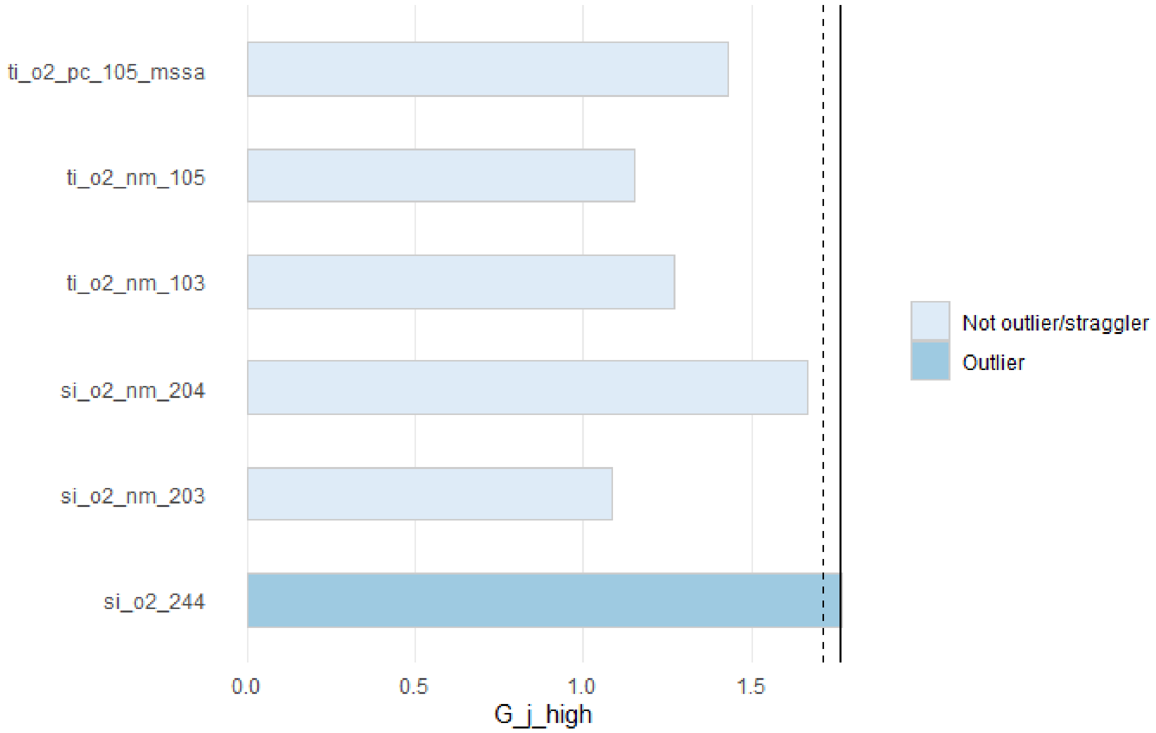


**Figure 2. Mandel's h statistic (top), and Grubb's test (bottom) assessing between laboratory consistency results for respirable mass-based dustiness index determined with the Rotating Drum. Dashed and solid line indicate 1% and 5% critical values, respectively.**

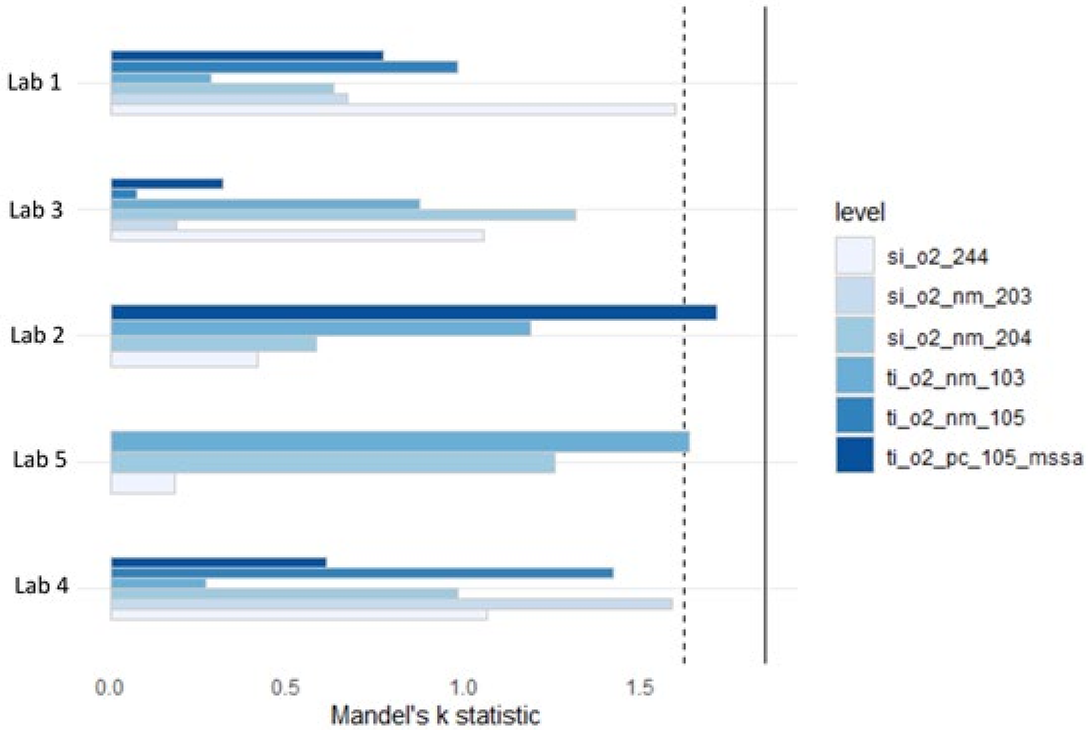

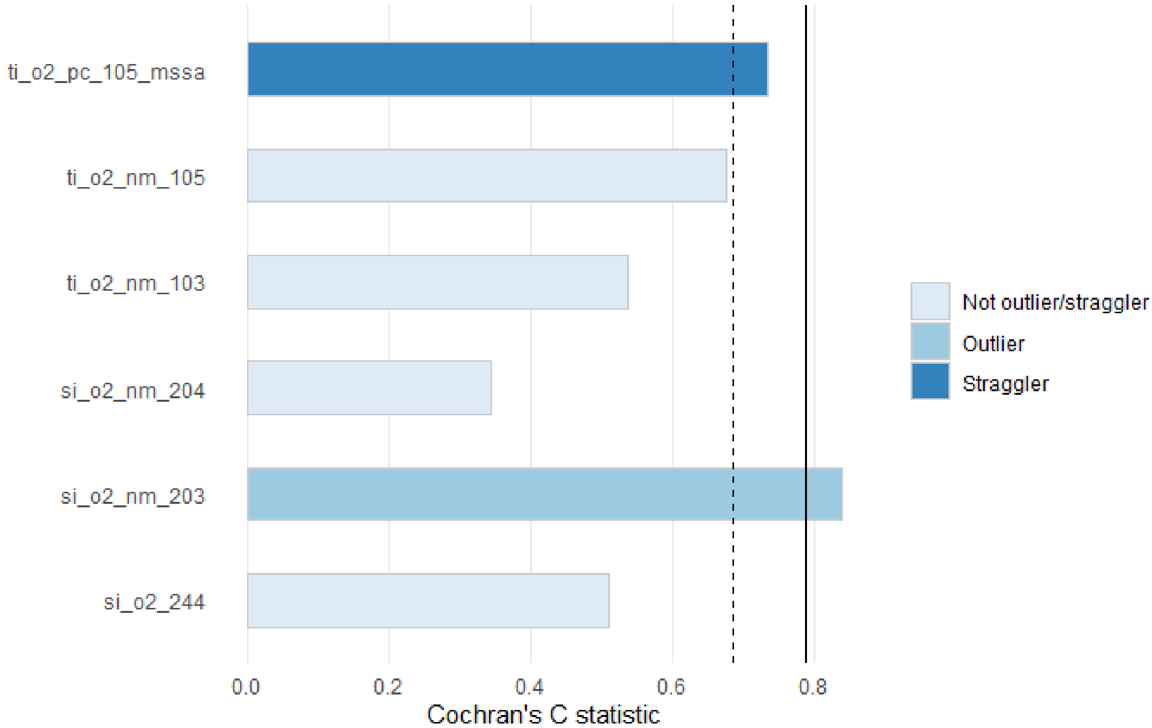


**Figure 3. Mandel's k statistic (top), and Cochran's test (bottom) assessing within laboratory consistency results for respirable mass-based dustiness index determined with the Rotating Drum. Dashed and solid line indicate 1% and 5% critical values, respectively.**

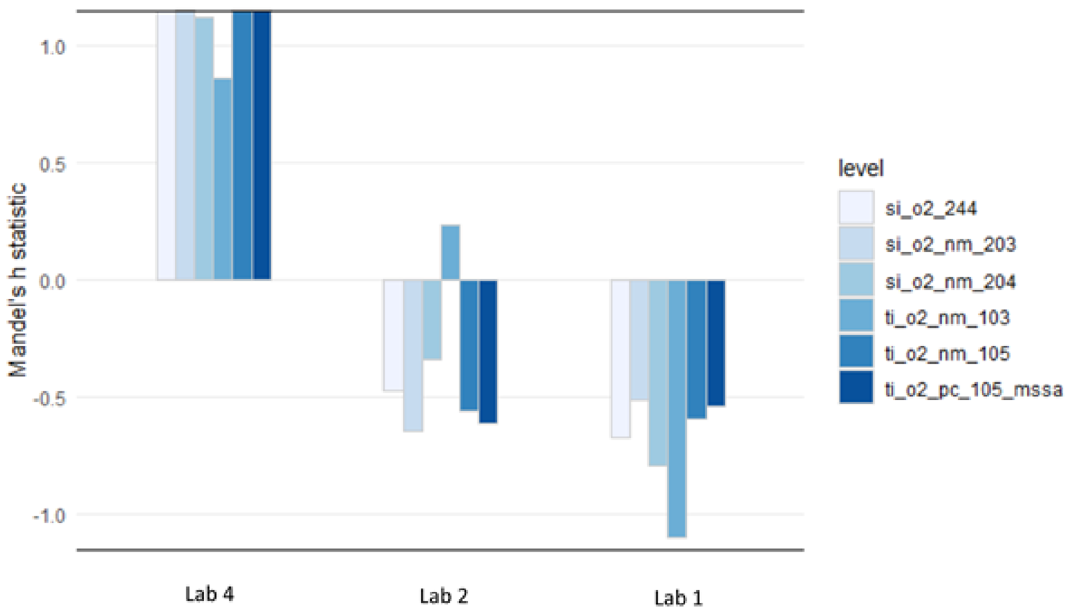

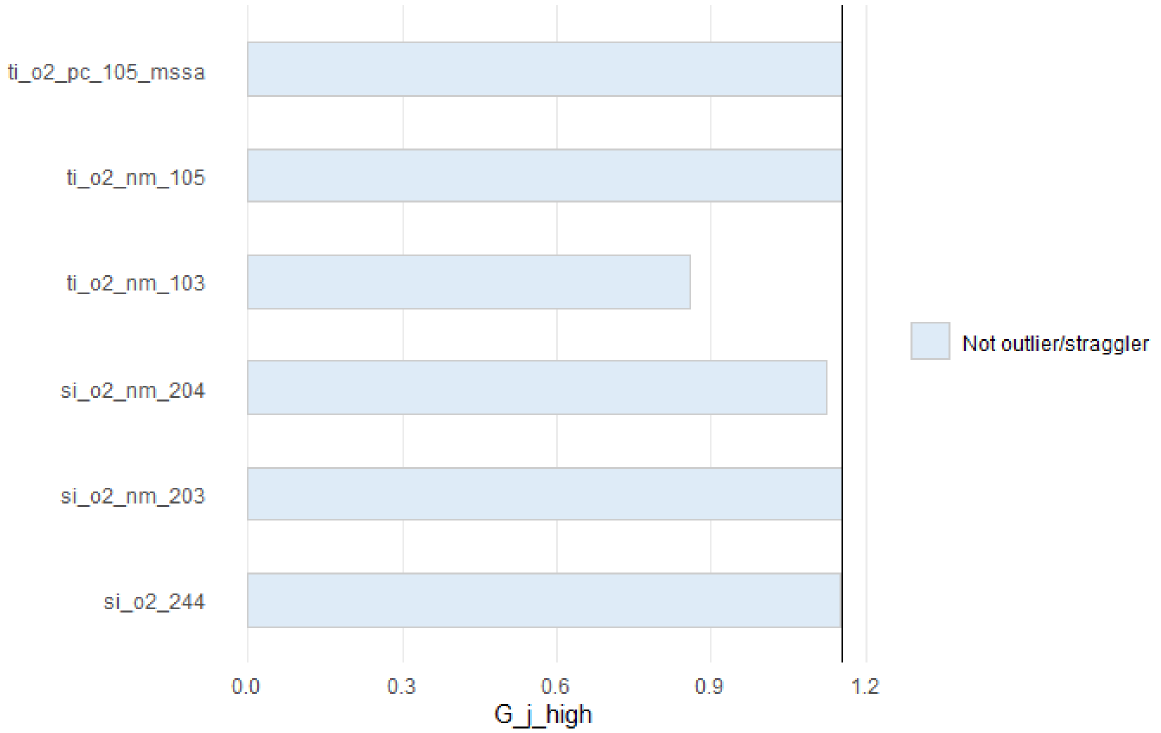


**Figure 4. Mandel's h statistic (top), and Grubb's test (bottom) assessing between laboratory consistency results for particle number-based dustiness index determined with the Rotating Drum. Dashed and solid line indicate 1% and 5% critical values, respectively.**

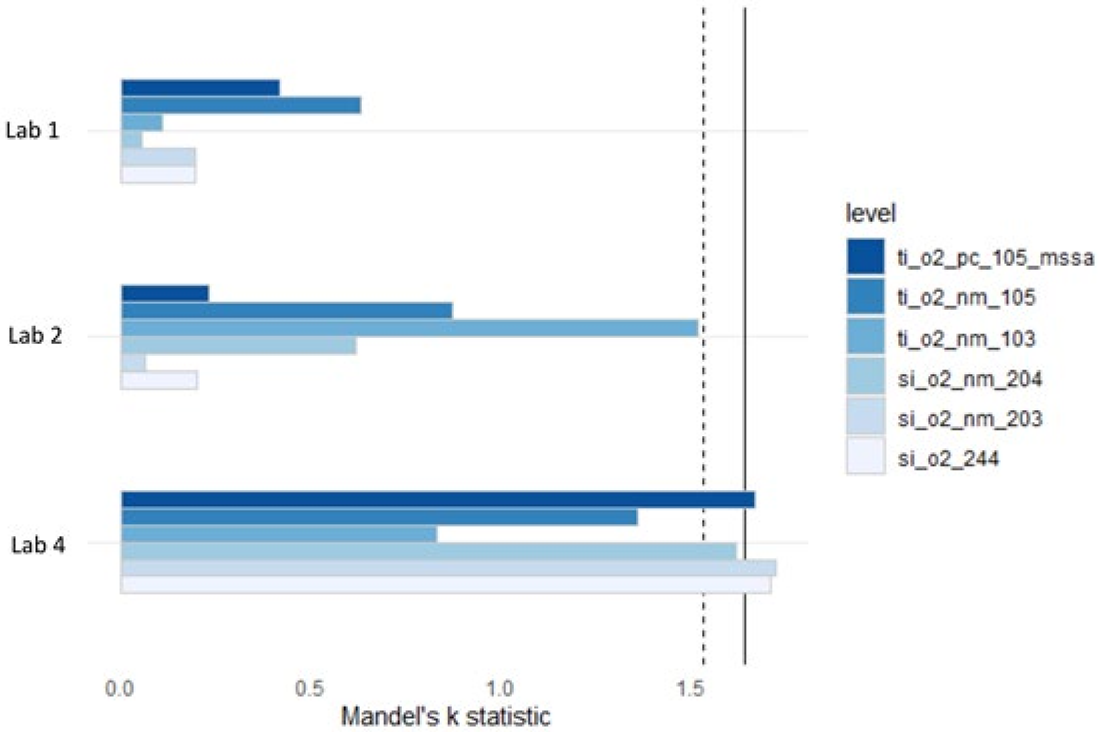

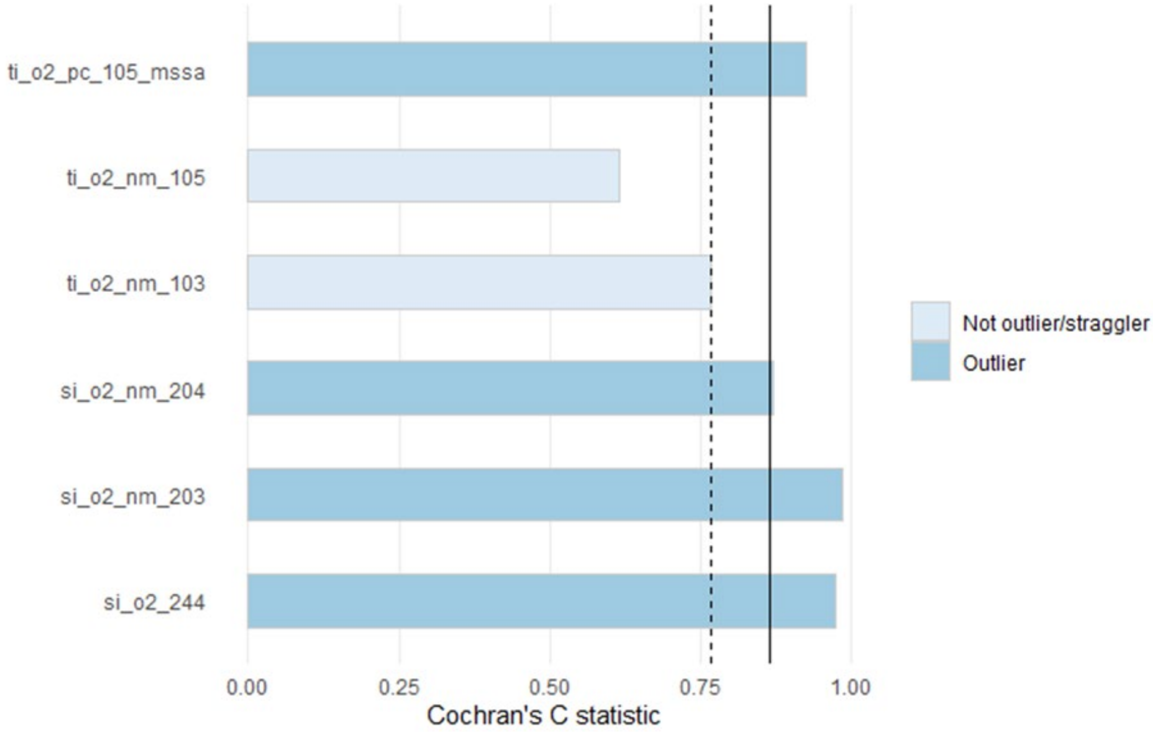


**Figure 5. Mandel's k statistic (top), and Cochran's test (bottom) assessing within laboratory consistency results for particle number-based dustiness index determined with the Rotating Drum. Dashed and solid line indicate 1% and 5% critical values, respectively.**

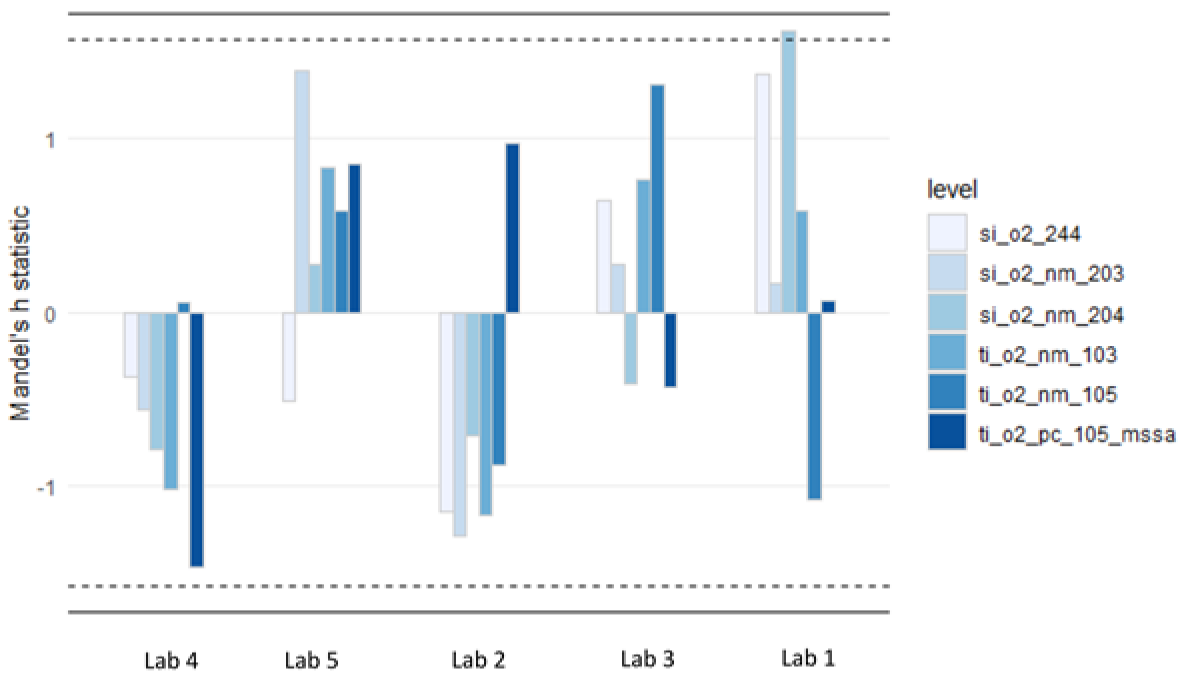

**Figure 6. Mandel's h statistic (between laboratory consistency) results for thoracic mass-based dustiness index determined with the Rotating Drum. Dashed and solid line indicate 1% and 5% critical values, respectively.**

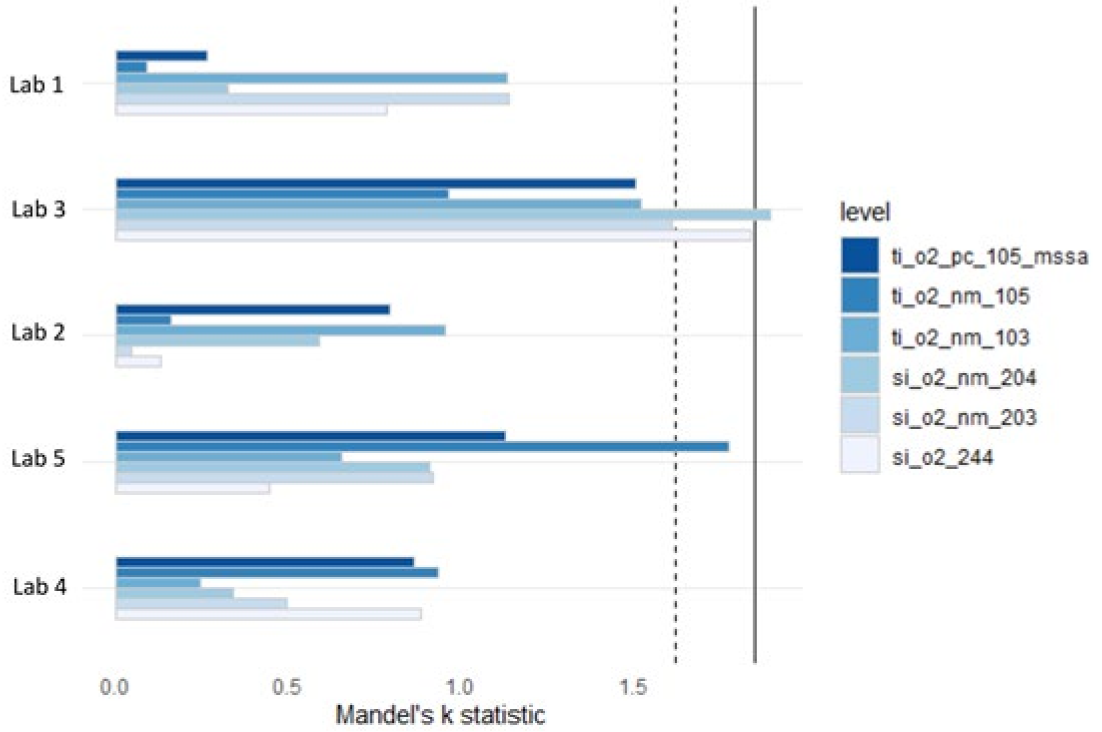


**Figure 7. Mandel's k statistic (within laboratory consistency) results for thoracic mass-based dustiness index determined with the Rotating Drum. Dashed and solid line indicate 1% and 5% critical values, respectively.**

55. Data for the respirable mass dustiness index for each laboratory is presented in Figure 8, while the particle number dustiness index is shown in Figure 9. Thoracic and inhalable mass dustiness index data are provided in Figures A1 and A2 (Appendix). The variability across laboratories was generally below 20%, although higher variability was observed in certain cases (Table 7). Notably, for the respirable mass dustiness index, about one-third of the values exceeded 20%, with some reaching 50% or higher, particularly for Lab 2 $TiO_2$ PC105 and Lab 3 $SiO_2$ NM-203.

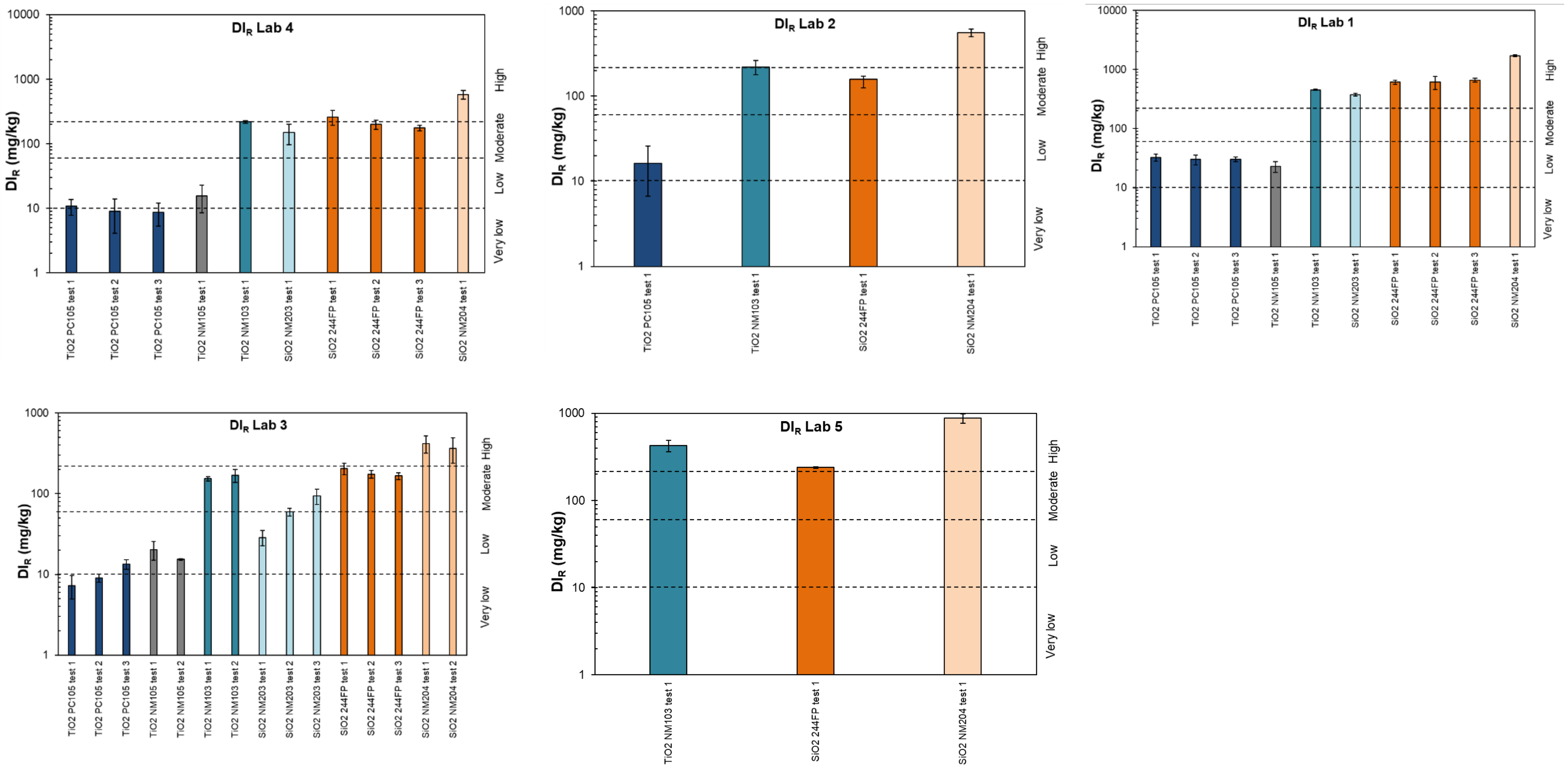
DI$_R$ Lab 4
DI$_R$ (mg/kg)
10000
1000
100
10
1
High
Moderate
Low
Very low
TiO2 PC105 test 1
TiO2 PC105 test 2
TiO2 PC105 test 3
TiO2 NM105 test 1
TiO2 NM103 test 1
SiO2 NM203 test 1
SiO2 244FP test 1
SiO2 244FP test 2
SiO2 244FP test 3
SiO2 NM204 test 1
DI$_R$ Lab 2
DI$_R$ (mg/kg)
1000
100
10
1
High
Moderate
Low
Very low
TiO2 PC105 test 1
TiO2 NM103 test 1
SiO2 244FP test 1
SiO2 NM204 test 1
DI$_R$ Lab 1
DI$_R$ (mg/kg)
10000
1000
100
10
1
High
Moderate
Low
Very low
TiO2 PC105 test 1
TiO2 PC105 test 2
TiO2 PC105 test 3
TiO2 NM105 test 1
TiO2 NM103 test 1
SiO2 NM203 test 1
SiO2 244FP test 1
SiO2 244FP test 2
SiO2 244FP test 3
SiO2 NM204 test 1
DI$_R$ Lab 3
DI$_R$ (mg/kg)
1000
100
10
1
High
Moderate
Low
Very low
TiO2 PC105 test 1
TiO2 PC105 test 2
TiO2 PC105 test 3
TiO2 NM105 test 1
TiO2 NM105 test 2
TiO2 NM103 test 1
TiO2 NM103 test 2
SiO2 NM203 test 1
SiO2 NM203 test 2
SiO2 NM203 test 3
SiO2 244FP test 1
SiO2 244FP test 2
SiO2 244FP test 3
SiO2 NM204 test 1
SiO2 NM204 test 2
DI$_R$ Lab 5
DI$_R$ (mg/kg)
1000
100
10
1
High
Moderate
Low
Very low
TiO2 NM103 test 1
SiO2 244FP test 1
SiO2 NM204 test 1

**Figure 8. Respirable mass dustiness index *($DI_R$)* obtained per test (with replicates standard deviation) and material (represented in different colours) for each participant Rotating Drum laboratory. EN 15051-2:2025 Rotating Drum ranking values (very low, low, moderate and high) plotted. Error bars show standard deviation of the three replicates. Note: log scale used.**

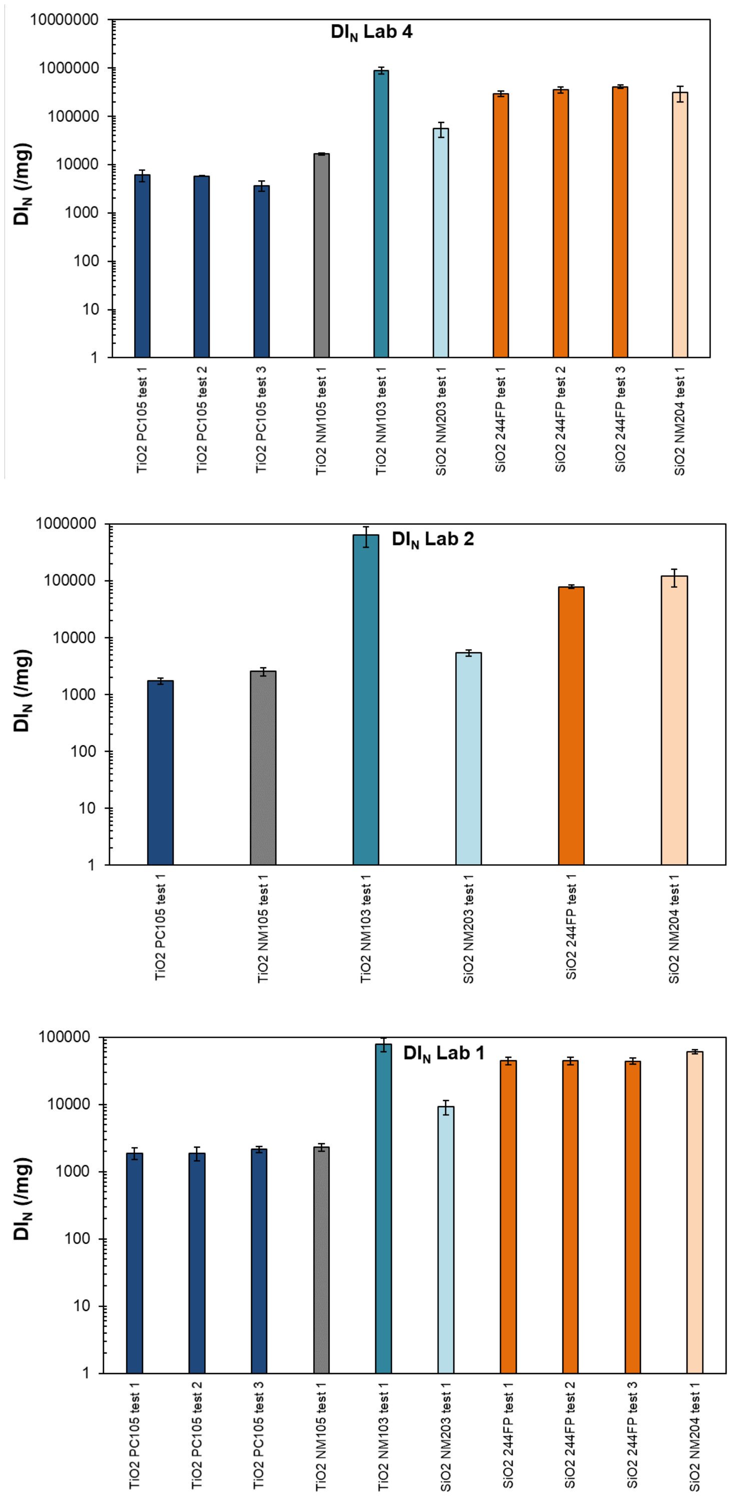


**Figure 9. Particle number dustiness index ($DI_N$) obtained per test (with replicates standard deviation) and material (represented in different colours) for each participant Rotating Drum laboratory. Error bars show standard deviation of the three replicates. Note: log scale used.**

**Table 7. Rotating Drum method variability (%) for each laboratory and material. $DI_R$: respirable dustiness index $DI_I$: inhalable dustiness index; $DI_T$: thoracic dustiness index; $DI_N$: number-based dustiness index; N/A: not available. Variability values >20% are indicated in italics.**

| Laboratory (n) | Material | $DI_R$ | $DI_I$ | $DI_T$ | $DI_N$ |
|---|---|---|---|---|---|
| Lab 4 (9) | $TiO_2$ PC105 | 36.6 | 9.0 | 13.0 | 28.3 |
| Lab 4 (3) | $TiO_2$ NM-105 | 45.2 | 15.1 | 17.9 | 4.0 |
| Lab 4 (3) | $TiO_2$ NM-103 | 4.3 | 3.4 | 5.8 | 15.1 |
| Lab 4 (3) | $SiO_2$ NM-203 | 35.2 | 0.8 | 14.7 | 34.4 |
| Lab 4 (9) | $SiO_2$ 244FP | 25.2 | 22.5 | 20.0 | 17.2 |
| Lab 4 (3) | $SiO_2$ NM-204 | 16.2 | 8.1 | 6.7 | 35.6 |
| Lab 2 (3) | $TiO_2$ PC105 | 58.9 | 11.6 | 16.1 | 12.0 |
| Lab 2 (3) | $TiO_2$ NM-105 | N/A | 30.0 | 10.6 | 16.5 |
| Lab 2 (3) | $TiO_2$ NM-103 | 18.9 | 22.6 | 24.7 | 39.0 |
| Lab 2 (3) | $SiO_2$ NM-203 | N/A | 13.3 | 11.8 | 13.1 |
| Lab 2(3) | $SiO_2$ 244FP | 8.2 | 16.3 | 8.2 | 7.1 |
| Lab 2 (3) | $SiO_2$ NM-204 | 10.1 | 16.5 | 10.8 | 2.9 |
| Lab 1 (9) | $TiO_2$ PC105 | 13.1 | 12.2 | 17.4 | 16.6 |
| Lab 1 (3) | $TiO_2$ NM-105 | 21.3 | 3.7 | 5.9 | 13.2 |
| Lab 1 (3) | $TiO_2$ NM-103 | 2.2 | 14.0 | 14.6 | 22.6 |
| Lab 1 (3) | $SiO_2$ NM-203 | 5.9 | 17.7 | 18.1 | 23.8 |
| Lab 1 (9) | $SiO_2$ 244FP | 14.1 | 9.1 | 13.9 | 10.2 |
| Lab 1 (3) | $SiO_2$ NM204 | 3.6 | 6.5 | 2.0 | 6.3 |
| Lab 3 (9) | $TiO_2$ PC105 | 31.6 | 15.8 | 41.7 | N/A |
| Lab 3 (6) | $TiO_2$ NM-105 | 38.0 | 12.4 | 9.5 | N/A |
| Lab 3 (6) | $TiO_2$ NM-103 | 13.6 | 13.9 | 18.3 | N/A |
| Lab 3 (9) | $SiO_2$ NM-203 | 50.0 | 16.3 | 23.1 | N/A |
| Lab 3 (9) | $SiO_2$ 244FP | 15.0 | 15.6 | 26.9 | N/A |
| Lab 3 (6) | $SiO_2$ NM-204 | 27.4 | 22.8 | 23.4 | N/A |
| Lab 5 (6) | $TiO_2$ PC105 | N/A | 26.5 | 17.8 | N/A |
| Lab 5 (6) | $TiO_2$ NM-105 | N/A | 23.6 | 21.1 | N/A |
| Lab 5 (6) | $TiO_2$ NM-103 | 14.8 | 15.1 | 13.5 | N/A |
| Lab 5 (6) | $SiO_2$ NM-203 | N/A | 19.1 | 23.9 | N/A |
| Lab 5 (6) | $SiO_2$ 244FP | 2.4 | 12.6 | 15.8 | N/A |
| Lab 5 (6) | $SiO_2$ NM-204 | 11.9 | 9.7 | 7.2 | N/A |

56. Data from all participating laboratories is plotted together for each assessed metric (respirable, inhalable, thoracic, and particle number-based dustiness index) and shown in Figure 10. Overall, for all metrics, the ranking of materials by dustiness index values followed a consistent trend across all laboratories, with relatively low dispersion. However, a few exceptions showed higher variability, such as the respirable mass dustiness index for $SiO_2$ NM-203 and $TiO_2$ PC105. In general, the respirable dustiness index classification, following EN 15051-2:2025 [35], placed materials in the same dustiness band or between two consecutive bands, as seen with $TiO_2$ PC150 or $SiO_2$ 244FP (Figure 8). The same pattern was observed for the inhalable mass dustiness index (Figure A2 in the Appendix).

57. Lab 1 tended to report higher respirable dustiness index values, while Lab 4 recorded the highest values for particle number dustiness. The small variations could be attributed to the different CPC models used: Lab 4 employed the TSI 3776 (2.5 nm - 1 µm), whereas Lab 1 and Lab 2 used the TSI 3775, which measures down to 4 nm. For the thoracic mass fraction, Lab 2 generally reported lower

values than the other laboratories (Figure 10). Correlations between the laboratories' results are provided in Figures A3-A8 in the Appendix.

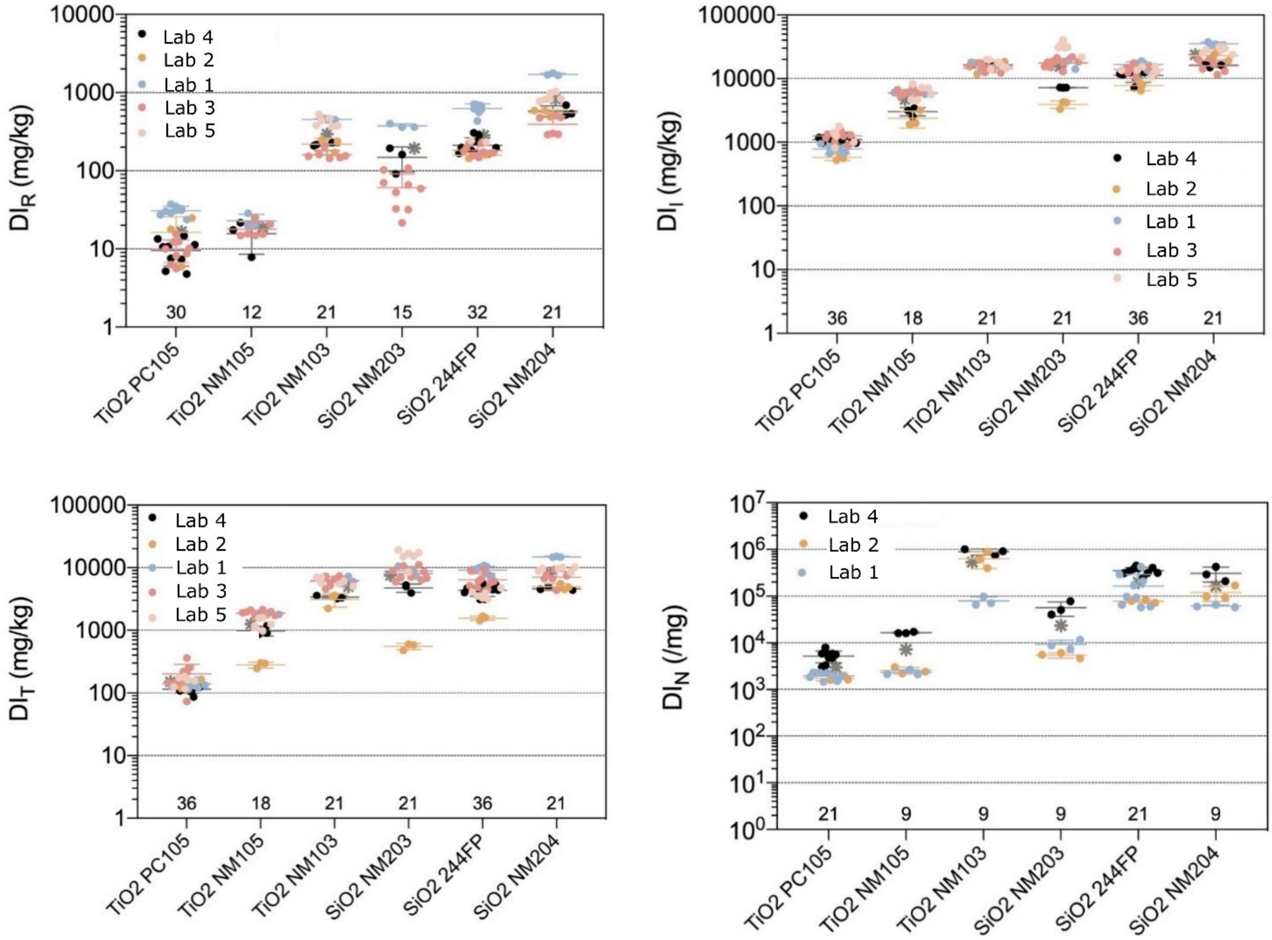


**Figure 10. Individual data points obtained per laboratory and material for each metric assessed for the Rotating Drum method (upper left: respirable mass dustiness index ($DI_R$); upper right: inhalable mass dustiness index ($DI_I$); lower left: thoracic mass dustiness index ($DI_T$); lower right: particle number-based dustiness index). Error bars show standard deviation of all the replicates for each laboratory. Note: log scale used.**

58. The effect of material moisture content on both the respirable mass and particle number dustiness indices was investigated. Overall, moisture content variations among different materials and laboratories ranged between 0.14% and 0.76%. Significant negative correlations were found between moisture content and respirable mass dustiness index for $TiO_2$ PC105 (n7) and $SiO_2$ 244FP (n8), with Pearson correlation coefficients of -0.86 and -0.78, respectively. In contrast, significant positive correlations were observed for the particle number-based dustiness index, with correlation coefficients of 0.92 and 0.97, respectively (n7). Graphs illustrating the correlations for $TiO_2$ PC105 and $SiO_2$ 244FP are provided in Appendix Figure A9. For all other materials, no significant correlations were identified, though it is important to note that the number of replicates was less than 4.

59. The z-scores, calculated based on ISO 13528:2022 [22], which measure the deviation of each laboratory's results from the "true" value, are shown in Table 8 and Table 9 for the respirable and particle number-based dustiness indices. Z-scores for the inhalable and thoracic dustiness indices are provided

in Appendix Tables A1 and A2. All calculated z-scores for the assessed metrics were below 2, except for Lab 1 $SiO_2$ NM-204, which yielded questionable results. This indicates that the ILC results obtained for the Rotating Drum method are generally satisfactory.

Table 8. Rotating Drum respirable dustiness index calculated z-score. In bold values which are higher than 2, but lower or equal than 3.

| Laboratory | $TiO_2$ PC105 | $TiO_2$ NM-105 | $TiO_2$ NM-103 | $SiO_2$ NM-203 | $SiO_2$ 244FP | $SiO_2$ NM-204 |
|---|---|---|---|---|---|---|
| Lab 4 | 0.69 | 0.60 | 0.58 | 0.06 | 0.51 | 0.42 |
| Lab 2 | 0.05 | N/A | 0.58 | N/A | 0.77 | 0.48 |
| Lab 1 | 1.35 | 0.43 | 1.20 | 1.80 | 1.51 | 2.11 |
| Lab 3 | 0.65 | 0.07 | 1.02 | 0.62 | 0.66 | 0.85 |
| Lab 5 | N/A | N/A | 0.99 | N/A | 0.38 | 0.25 |

Table 9. Rotating Drum particle number dustiness index calculated z-score.

| Laboratory | $TiO_2$ PC105 | $TiO_2$ NM-105 | $TiO_2$ NM-103 | $SiO_2$ NM-203 | $SiO_2$ 244FP | $SiO_2$ NM-204 |
|---|---|---|---|---|---|---|
| Lab 4 | 0.98 | 1.33 | 0.92 | 1.24 | 1.09 | 1.15 |
| Lab 2 | 0.82 | 0.65 | 0.26 | 0.69 | 0.65 | 0.34 |
| Lab 1 | 0.70 | 0.68 | 1.18 | 0.55 | 0.87 | 0.81 |

### 3.6.2. Small Rotating Drum

60. Two laboratories participated in the dustiness ILC using the Small Rotating Drum method (Lab 6 and Lab 7; see the combined dustiness report in Annex F). Data for the respirable and particle number dustiness indices for each laboratory is presented in Figure 11 and Figure 12. Kinetics data for the Small Rotating Drum dustiness method is shown in Figure 13, and laboratory variability is detailed in Table 10. Overall, the variability was around or below 20%, but in a few cases, higher variability was observed. This higher variability was always due to one of the three replicates showing a significant deviation from the others, and it was not consistent across metrics and laboratories (e.g., for Lab 6, the $DI_R$ for $SiO_2$ NM-203 had a variability of 25.5%, while the $DI_N$ variability was 6.1%). The specific data points causing the increased variability could not be attributed to any testing issues or equipment malfunctions.

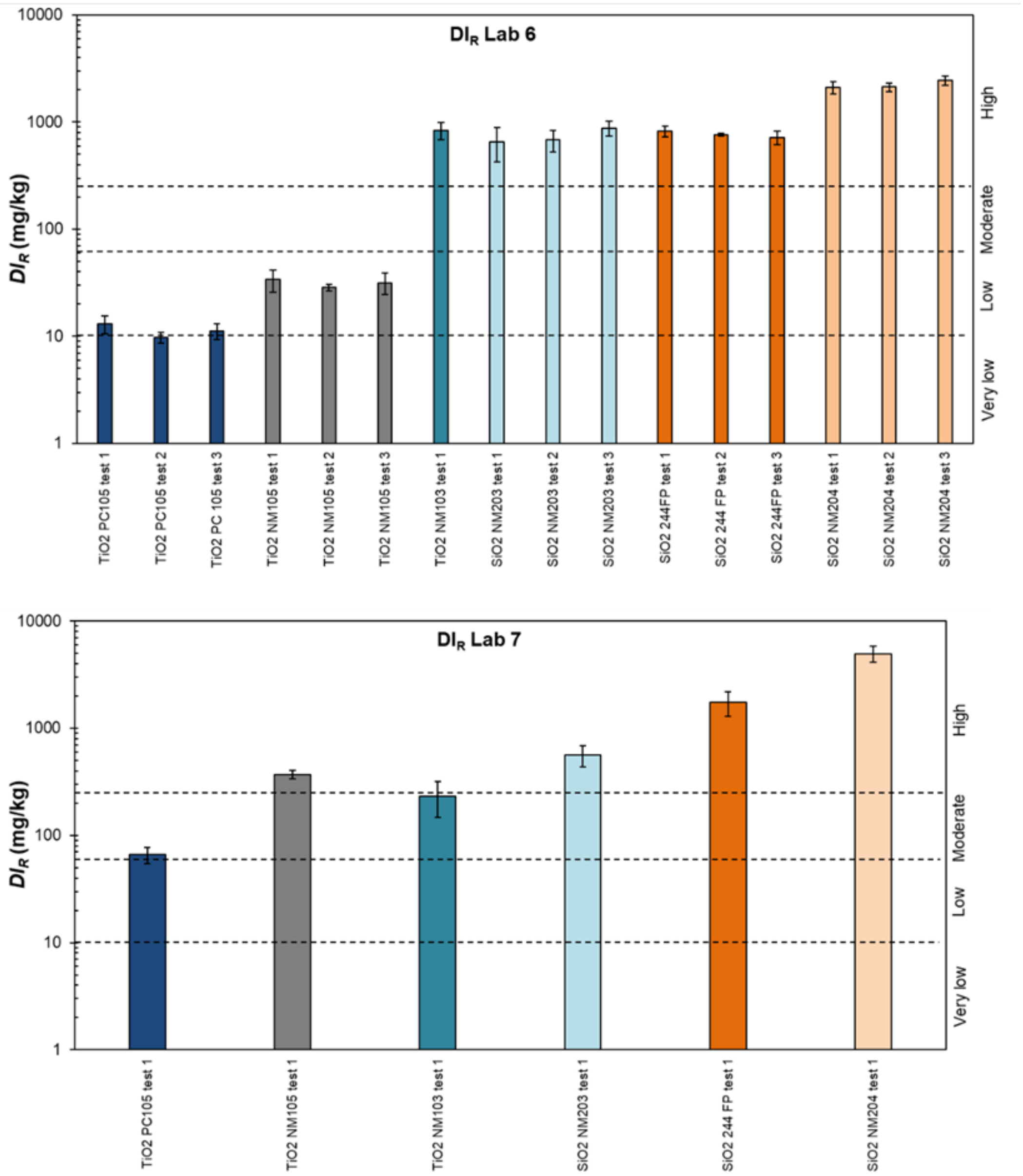


**Figure 11. Respirable mass dustiness index (DI$_R$) obtained per test (with replicates standard deviation) and material (represented in different colours) for each participant Small Rotating Drum laboratory. Rotating drum ranking values (EN 15051-2:2025) plotted for discussion (very low, low, moderate and high). Error bars show standard deviation of the three replicates. Note: log scale used.**

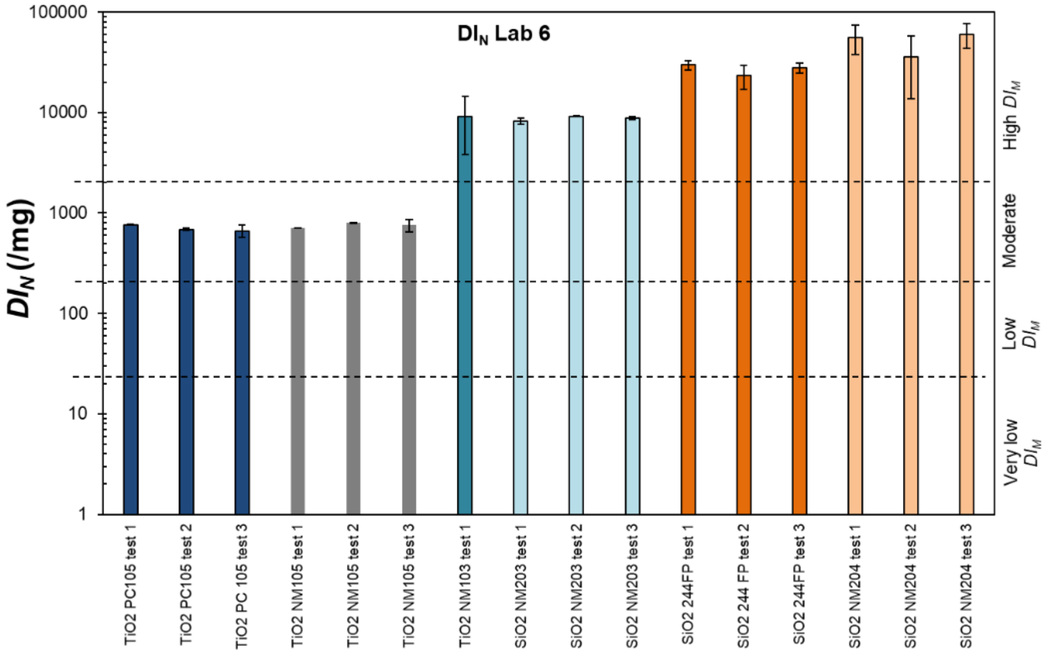

DIN Lab 6
DIN (/mg)
100000
10000
1000
100
10
1
High DIM
Moderate
Low DIM
Very low DIM
TiO2 PC105 test 1
TiO2 PC105 test 2
TiO2 PC 105 test 3
TiO2 NM105 test 1
TiO2 NM105 test 2
TiO2 NM105 test 3
TiO2 NM103 test 1
SiO2 NM203 test 1
SiO2 NM203 test 2
SiO2 NM203 test 3
SiO2 244FP test 1
SiO2 244 FP test 2
SiO2 244FP test 3
SiO2 NM204 test 1
SiO2 NM204 test 2
SiO2 NM204 test 3


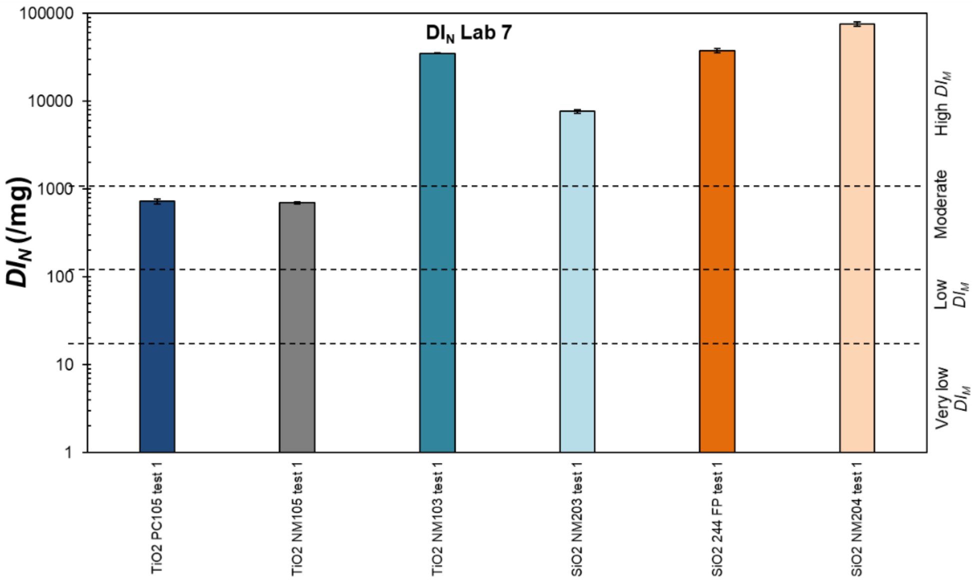

DIN Lab 7
DIN (/mg)
100000
10000
1000
100
10
1
High DIM
Moderate
Low DIM
Very low DIM
TiO2 PC105 test 1
TiO2 NM105 test 1
TiO2 NM103 test 1
SiO2 NM203 test 1
SiO2 244 FP test 1
SiO2 NM204 test 1

**Figure 12. Particle number dustiness index ($DI_N$) obtained per test (with replicates standard deviation) and material (represented in different colours) for each participant Small Rotating Drum laboratory. Error bars show standard deviation of the three replicates. Note: log scale used.**

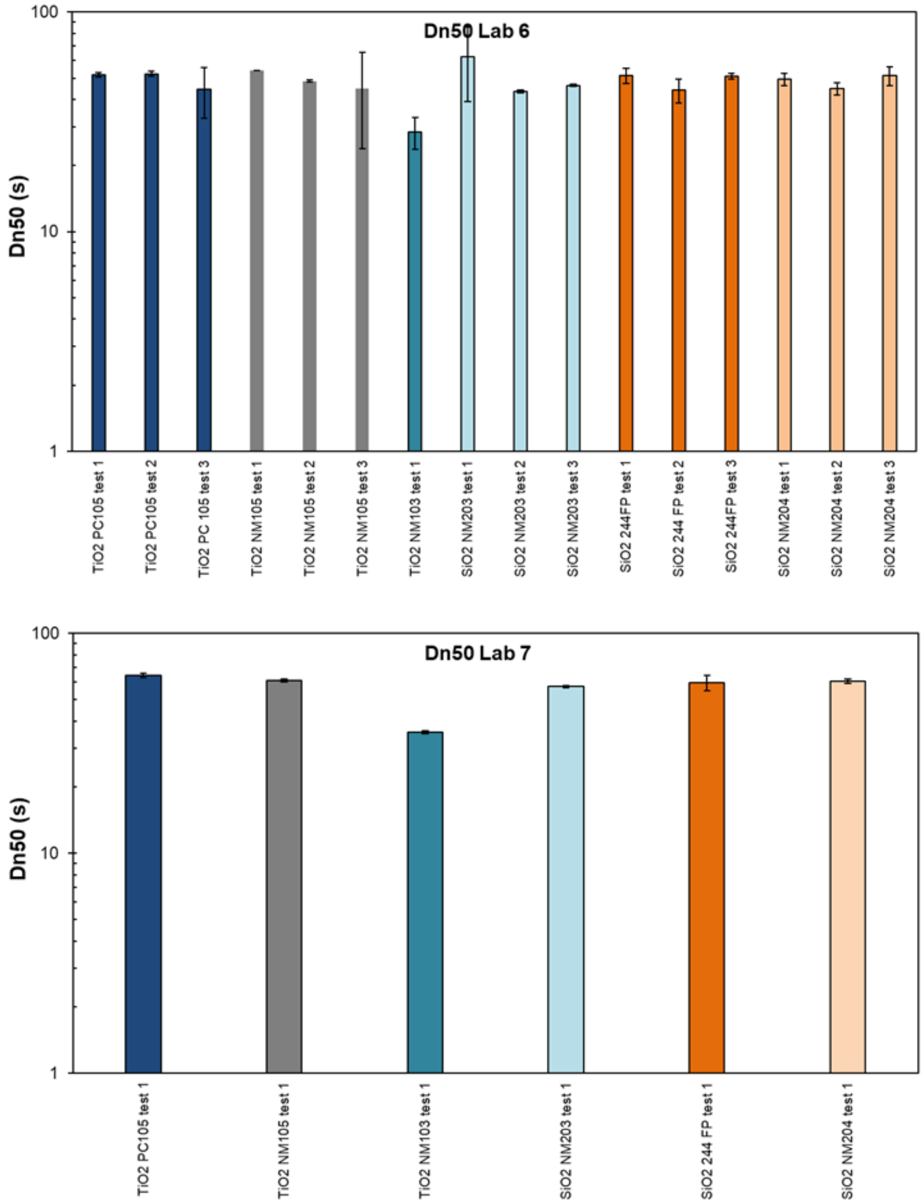


**Figure 13. Number-based dustiness kinetics (*n50*) obtained per test (with replicates standard deviation) and material (represented in different colours) for each participant Small Rotating Drum laboratory. Error bars show standard deviation of the three replicates. Note: log scale used.**

**Table 10. Small Rotating Drum method variability (%) for each laboratory and material. $DI_R$: respirable dustiness index; $DI_N$: number-based dustiness index; *n50*: time-based dustiness kinetics. Variability values >20% are indicated in italics.**

| Laboratory (n) | Material | $DI_R$ | $DI_N$ | $n_{50}$ |
|---|---|---|---|---|

| | | | | |
|---|---|---|---|---|
| Lab 6 (9) | $TiO_2$ PC105 | 19.2 | 9.3 | 14.2 |
| Lab 6 (9) | $TiO_2$ NM-105 | 18.7 | 10.0 | 28.8 |
| Lab 6 (3) | $TiO_2$ NM-103 | 17.9 | 58.6 | 16.4 |
| Lab 6 (9) | $SiO_2$ NM-203 | 25.5 | 6.1 | 29.6 |
| Lab 6 (9) | $SiO_2$ 244FP | 11.0 | 17.8 | 10.3 |
| Lab 6 (9) | $SiO_2$ NM-204 | 12.2 | 39.4 | 9.2 |
| Lab 7 (3) | $TiO_2$ PC105 | 17.5 | 5.9 | 2.4 |
| Lab 7 (3) | $TiO_2$ NM-105 | 9.2 | 2.7 | 1.6 |
| Lab 7 (3) | $TiO_2$ NM-103 | 36.2 | 1.1 | 1.6 |
| Lab 7 (3) | $SiO_2$ NM-203 | 22.5 | 4.5 | 1.0 |
| Lab 7 (3) | $SiO_2$ 244FP | 26.1 | 6.1 | 7.7 |
| Lab 7 (3) | $SiO_2$ NM-204 | 16.8 | 5.4 | 2.5 |

61. In Figure 14, data from both laboratories testing the Small Rotating Drum method is plotted together for each metric ($DI_R$, $DI_N$, *and* $n_{50}$), including a comparison between the two laboratories. The results indicate that both laboratories classify the materials in a similar order based on the respirable and number-based dustiness indices, with the exception of $TiO_2$ NM-103. However, in general, Lab 7 consistently reported higher values across most metrics compared to Lab 6, with a few exceptions, such as $DI_R$ for $TiO_2$ NM-103 and $SiO_2$ NM-203.

62. A significant discrepancy was observed in the respirable mass dustiness index, with Lab 7 values ranging from 2 to 10 times higher than those from Lab 6. This resulted in the three $TiO_2$ materials with lower dustiness levels (PC105, NM-105, and NM-103) being ranked one or two dustiness levels higher according to Lab 7 data, based on the Rotating Drum ranking system (EN 15051-2:2025 [35]), compared to Lab 6 data. Conversely, for the particle number-based dustiness index, the results were generally comparable between the two laboratories, except for $TiO_2$ NM-103.

63. The correlation between the data from the two laboratories shows a slope and $R^2$ value of 0.48 and 0.83 for $DI_R$, 0.25 and 0.89 for $DI_N$, and 0.20 and 0.89 for $n_{50}$, indicating strong correlations for $DI_N$ and $n_{50}$ despite some variability in the $DI_R$ measurements.

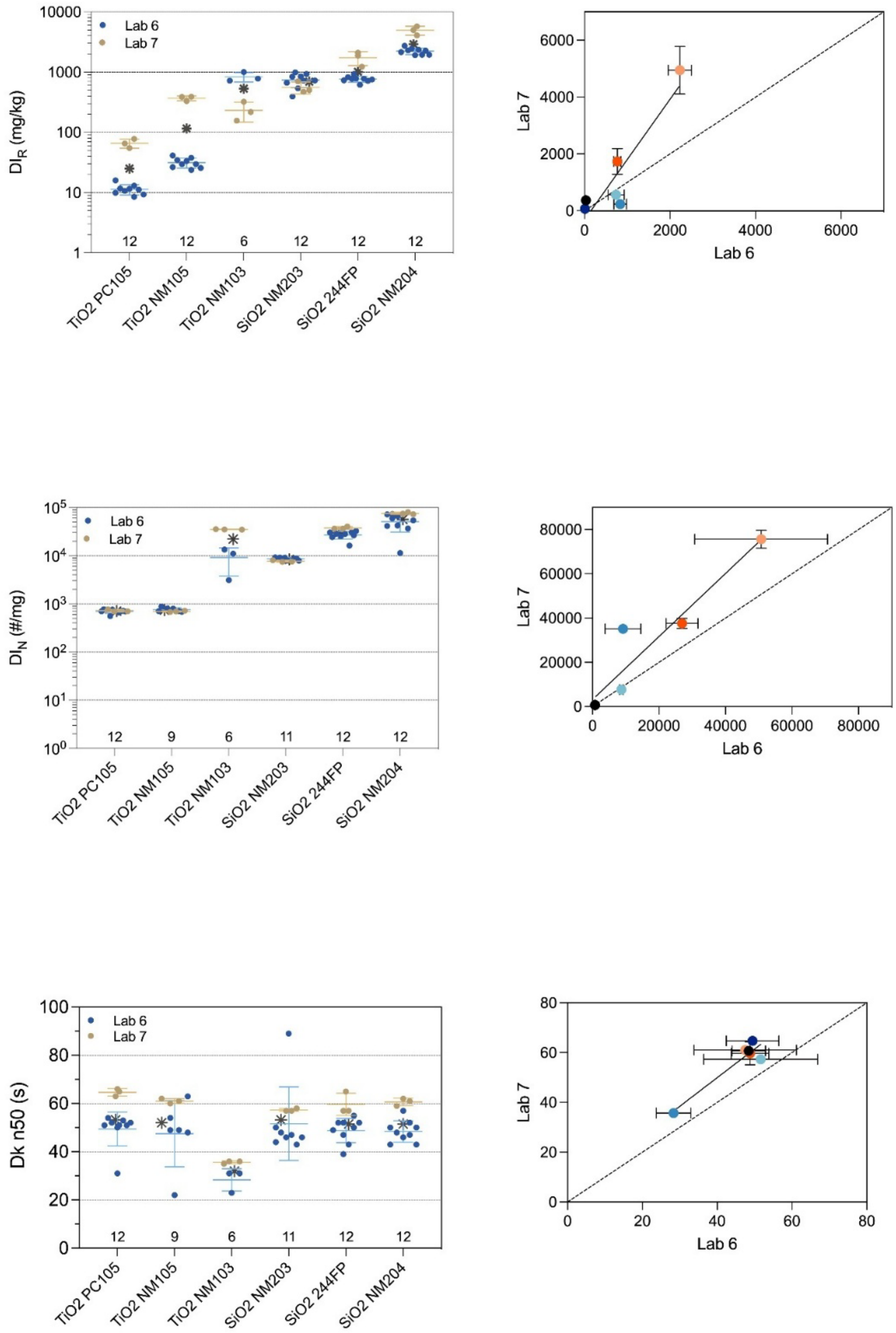


**Figure 14. Individual data points obtained per laboratory and material for each metric assessed for the Small Rotating Drum method and correlation between laboratories (Lab 6 and Lab 7).** ***$DI_R$*****: respirable dustiness index;** ***$DI_N$*****: number-based dustiness index;** ***n50*****: number-based dustiness kinetics. Error bars show standard deviation of all the replicates for each laboratory. Note: log scale used. For correlation plots, materials are identified with colours: dark blue-$TiO_2$**

**PC105; black-$TiO_2$ NM105; dark turquoise-$TiO_2$ NM103; light turquoise-$SiO_2$ NM203; dark orange-$SiO_2$ 244; light orange-$SiO_2$ NM204.**

64. The dustiness kinetics were determined solely for the Small Rotating Drum method. Specifically, the $Dk_{50}$ metric indicates the time required to generate 50% of the total number of particles released during the test. These dustiness kinetics provide additional relevant information that can be valuable for prioritisation, risk assessment, or improving modelling efforts. Dispersion among laboratories was relatively stable across the materials included in the ILC, and both laboratories ranked the materials similarly.

65. The relationship between materials' moisture content and respirable and particle number dustiness levels was also examined. The differences in moisture content among the materials ranged from 0.30% to 1.85%. For the respirable dustiness index, significant positive correlations were found for $TiO_2$ PC105, NM-105, and $SiO_2$ NM-204 (n=4), with Pearson correlation coefficients of 0.999, 0.9999, and 0.993, respectively (see Appendix Figure A10). A negative, non-significant correlation was observed for $SiO_2$ NM-203. In contrast, for the particle number-based dustiness index, non-significant correlations were noted. It is important to emphasize that data from only two laboratories are currently available, which limits the results and their interpretation.

66. The z-scores calculated for the respirable and particle number-based dustiness indices are presented in Table 11. All calculated z-scores (including those for dustiness kinetics, data not shown) were below 2, indicating that the results obtained from the Small Rotating Drum method are satisfactory.

**Table 11. Small Rotating Drum respirable mass and particle number dustiness index calculated z-score.**

| Metric | Lab | $TiO_2$ PC105 | $TiO_2$ NM-105 | $TiO_2$ NM-103 | $SiO_2$ NM-203 | $SiO_2$ 244FP | $SiO_2$ NM-204 |
|---|---|---|---|---|---|---|---|
| $DI_R$ | Lab 6 | 0.54 | 0.55 | 0.87 | 0.24 | 0.50 | 0.52 |
| | Lab 7 | 1.62 | 1.65 | 0.87 | 0.72 | 1.50 | 1.57 |
| $DI_N$ | Lab 6 | 0.08 | 0.31 | 0.89 | 0.41 | 0.42 | 0.30 |
| | Lab 7 | 0.24 | 0.62 | 0.89 | 1.09 | 1.25 | 0.91 |

### 3.6.3. Vortex Shaker

67. Four laboratories participated in the dustiness assessment using the Vortex Shaker method: Lab 8, Lab 9, Lab 10, and lab 5 (see the combined dustiness report in Annex G).

68. To apply the statistical tests recommended by ISO, an equal number of replicates per laboratory is required. Since Lab 9 reported five replicates, three replicates conducted on the same day were randomly selected for analysis.

69. For the respirable dustiness index, between-laboratory consistency was assessed using Mandel's h and Grubbs tests, which identified Lab 10 $SiO_2$ 244FP and $TiO_2$ PC105 as outliers and/or stragglers (Figure 15 and Annex H). In contrast, within-laboratory consistency, evaluated with Mandel's k, identified three outliers: Lab 10 $SiO_2$ NM-203, $SiO_2$ NM-204, and $TiO_2$ PC105 (Figure 16). The same materials were flagged as stragglers and outliers using the Cochran test (data shown in Annex H). No issues were reported for Lab 10 data, and the variability percentage was below 30%, similar to that of the other laboratories. Given these factors and the limited number of participating laboratories, we have decided to retain Lab 10 data for the current analysis.

70. Regarding the particle number dustiness index, two stragglers were identified in the between-laboratory consistency analysis using Mandel's h and Grubbs tests (Lab 10 $TiO_2$ PC105 and Lab 9 $SiO_2$ NM-203) (Figure 17 and Annex H). Within-laboratory consistency assessment revealed only one outlier identified by both Mandel's k and Cochran tests (Lab 9 $SiO_2$ NM-203) (Figure 18 and Annex H). This outlier was attributed to a single data point that showed 100% variability, resulting from an initial mass

loaded in the dustiness setup that was considerably lower than expected. Consequently, it was decided to exclude this material from Lab 9 in the calculations for repeatability and reproducibility.

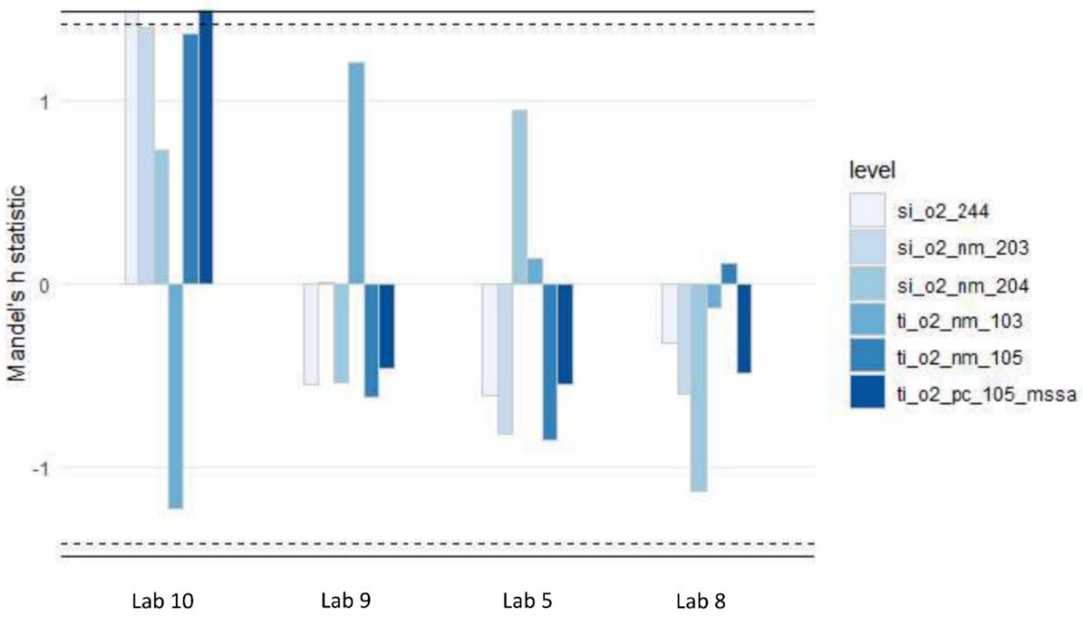


**Figure 15. Mandel's h statistic for respirable dustiness index determined with the Vortex Shaker. Dashed and solid line indicate 1% and 5% critical values, respectively.**

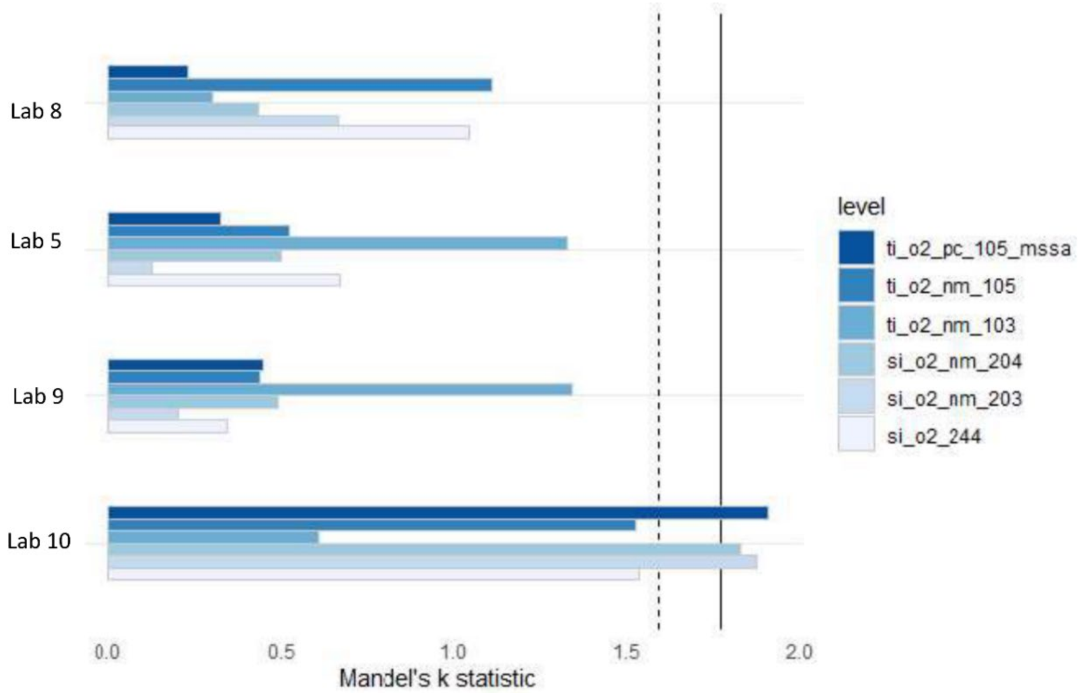

**Figure 16. Mandel's k statistic results for respirable dustiness index determined with the Vortex Shaker. Dashed and solid line indicate 1% and 5% critical values, respectively.**

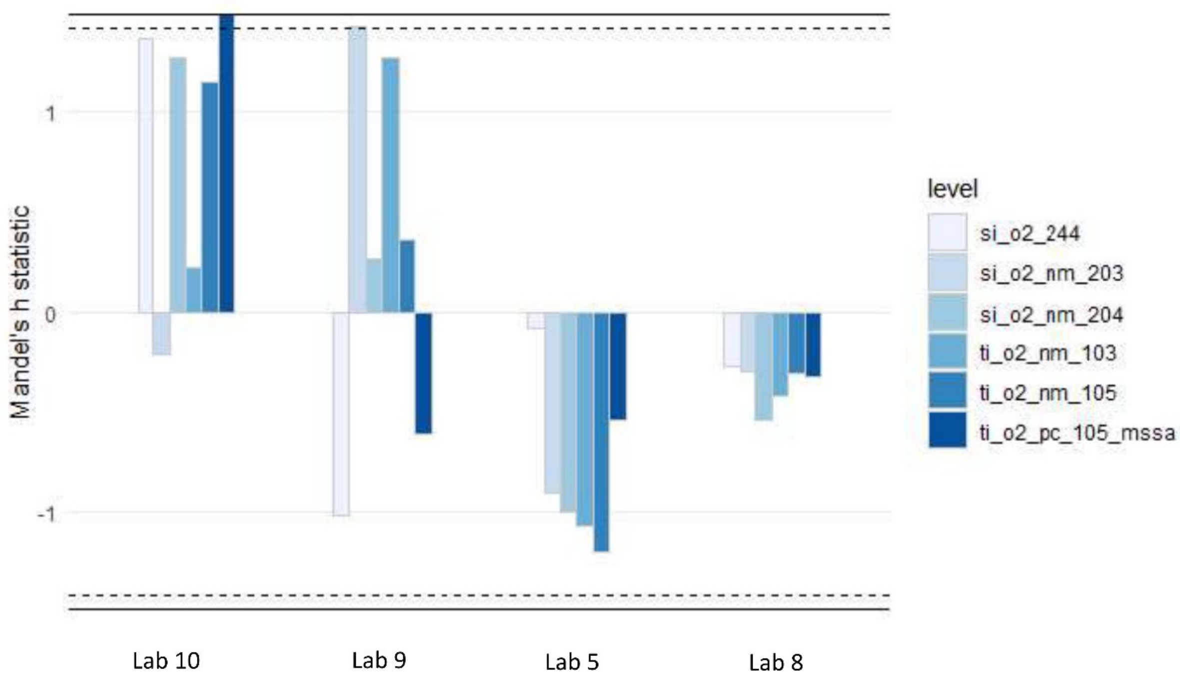

**Figure 17. Mandel's h statistic for particle number dustiness index determined with the Vortex Shaker. Dashed and solid line indicate 1% and 5% critical values, respectively.**

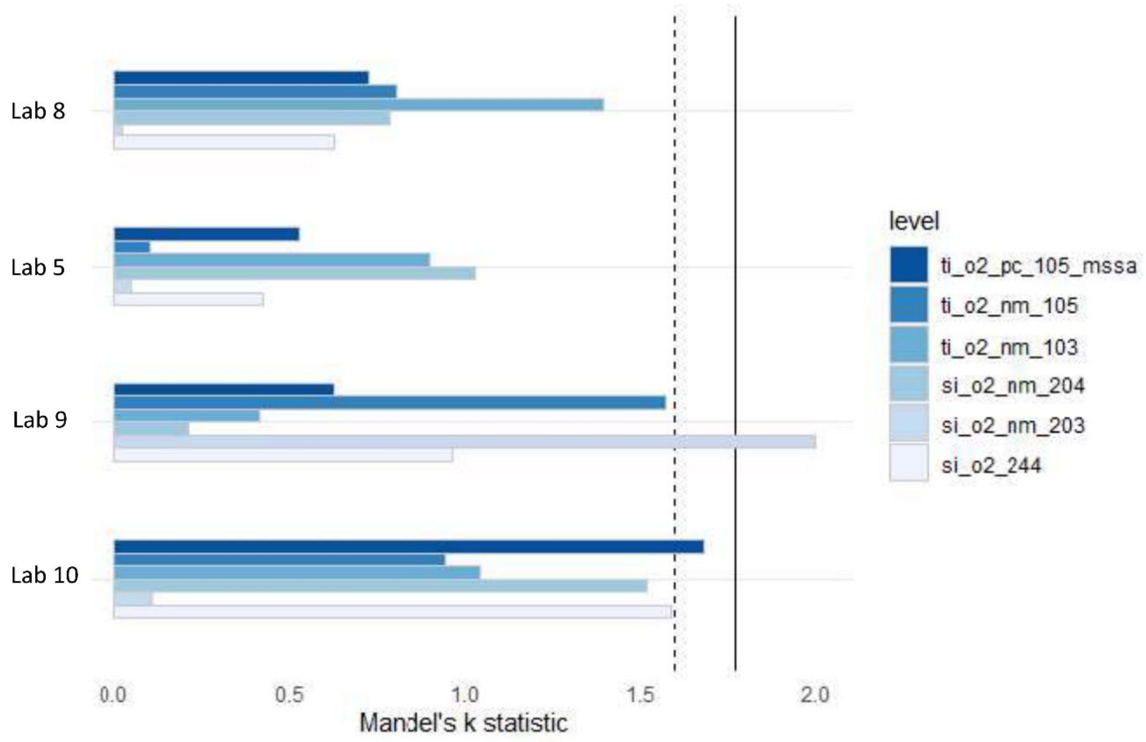


**Figure 18. Mandel's k statistic results for particle number-based dustiness index determined with the Vortex Shaker. Dashed and solid line indicate 1% and 5% critical values, respectively.**

71. Results for the respirable mass and number-based dustiness indices are presented in Figure 19 and Figure 20, respectively. Laboratory variability is summarised in Table 12. Overall, variability was found to be below 20%, with a few exceptions where it reached up to 30%. Notably, after the removal of the outlier for particle number from Lab 9 $SiO_2$ NM-203, the variability decreased significantly from over 100% to 25.5%.

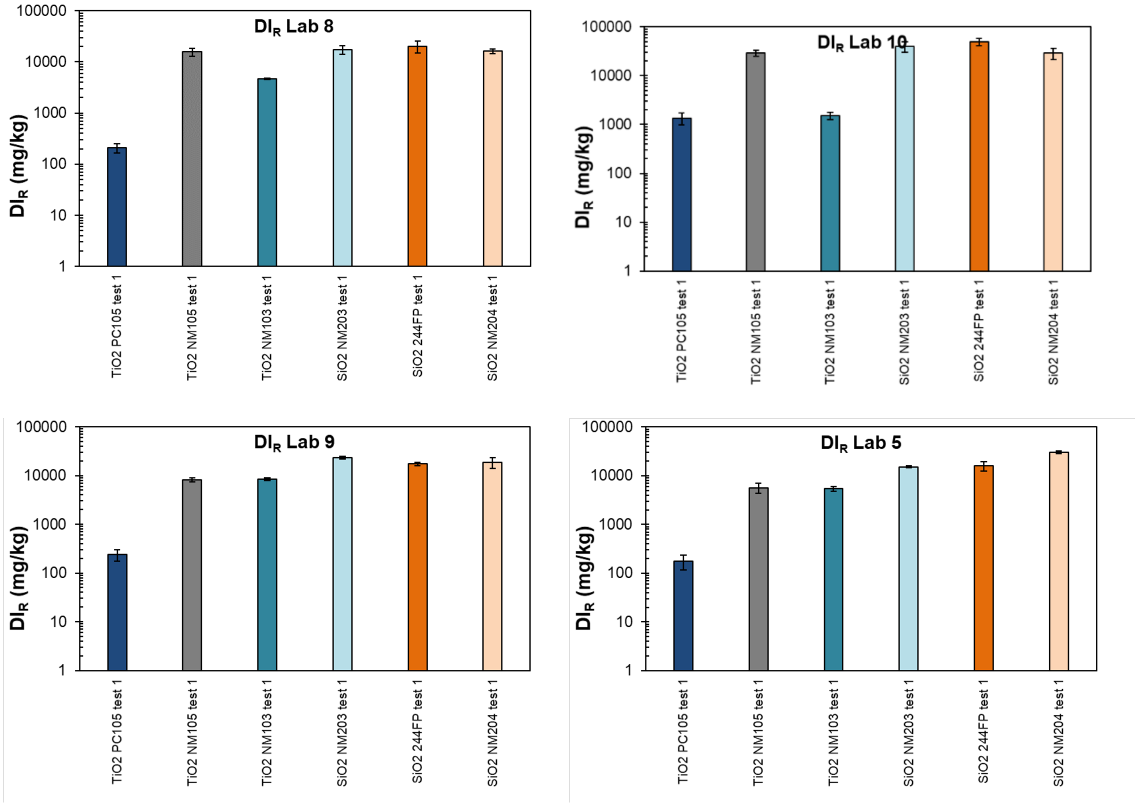


**Figure 19. Respirable mass (*DIR*) dustiness index obtained per test (with replicates standard deviation) and material (represented in different colours) for each Vortex Shaker participant laboratory. Error bars show standard deviation of the three replicates. Note: log scale used.**

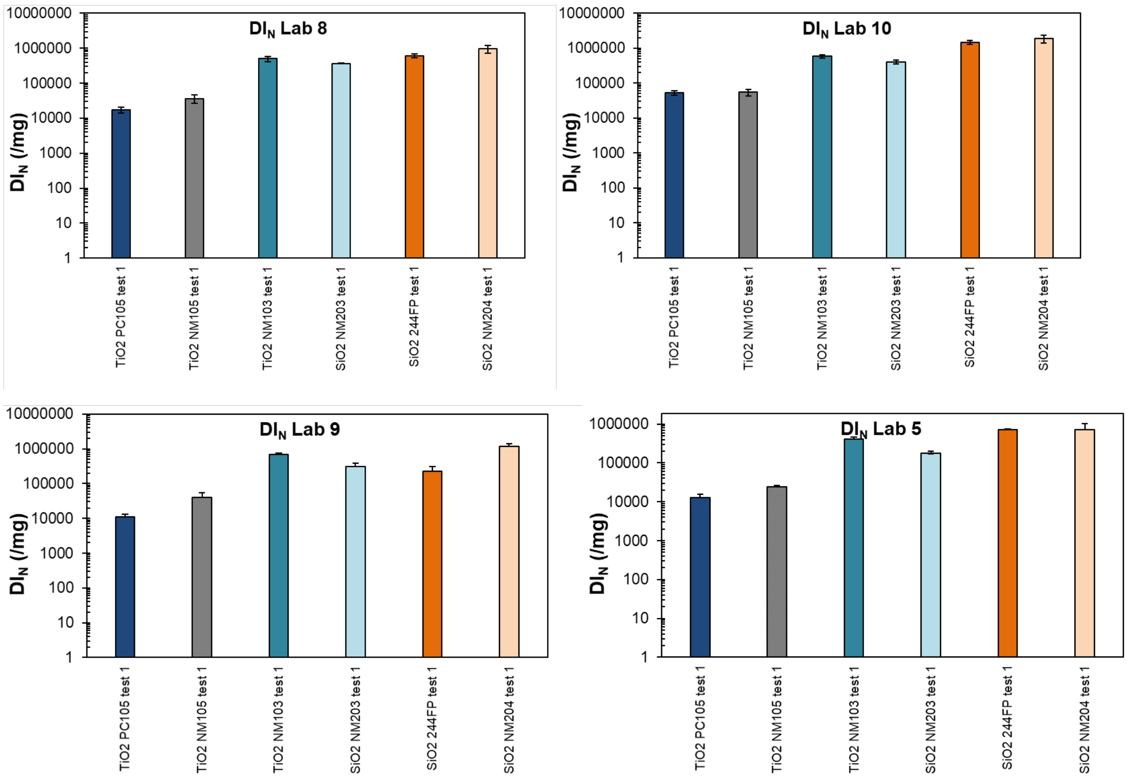


**Figure 20. Particle number ($DI_N$) dustiness index obtained per test (with replicates standard deviation) and material (represented in different colours) for each Vortex Shaker participant laboratory. Error bars show standard deviation of the three replicates. Note: log scale used.**

**Table 12. Vortex Shaker method variability (%) for each laboratory and material. $DI_R$: respirable dustiness index; $DI_N$: number-based dustiness index. * 5 replicates for respirable dustiness index and 4 for number-based dustiness index. Variability values >20% are indicated in italics.**

| Laboratory (n) | Material | $DI_R$ | $DI_N$ |
|---|---|---|---|
| Lab 8 (3) | $TiO_2$ PC105 | 20.4 | 18.8 |
| Lab 8 (3) | $TiO_2$ NM-105 | 17.8 | 27.7 |
| Lab 8 (3) | $TiO_2$ NM-103 | 2.9 | 17.0 |
| Lab 8 (3) | $SiO_2$ NM-203 | 19.7 | 3.0 |
| Lab 8 (3) | $SiO_2$ 244FP | 27.1 | 12.0 |
| Lab 8 (3) | $SiO_2$ NM-204 | 11.4 | 25.4 |
| Lab 10 (3) | $TiO_2$ PC105 | 26.7 | 14.3 |
| Lab 10 (3) | $TiO_2$ NM-105 | 13.4 | 21.5 |
| Lab 10 (3) | $TiO_2$ NM-103 | 17.6 | 10.9 |
| Lab 10 (3) | $SiO_2$ NM-203 | 24.8 | 13.1 |
| Lab 10 (3) | $SiO_2$ 244FP | 16.5 | 12.8 |
| Lab 10 (3) | $SiO_2$ NM-204 | 27.1 | 24.9 |
| Lab 9 (5) | $TiO_2$ PC105 | 37.4 | 24.4 |
| Lab 9 (5) | $TiO_2$ NM-105 | 13.7 | 43.8 |
| Lab 9 (5) | $TiO_2$ NM-103 | 7.1 | 3.5 |
| Lab 9 (5*) | $SiO_2$ NM-203 | 4.3 | 25.5 |
| Lab 9 (5) | $SiO_2$ 244FP | 10.8 | 50.2 |
| Lab 9 (5) | $SiO_2$ NM-204 | 10.3 | 4.8 |
| Lab 5 (3) | $TiO_2$ PC105 | 34.3 | 18.1 |
| Lab 5 (3) | $TiO_2$ NM-105 | 23.3 | 5.1 |
| Lab 5 (3) | $TiO_2$ NM-103 | 10.9 | 13.2 |
| Lab 5 (3) | $SiO_2$ NM-203 | 4.4 | 12.6 |
| Lab 5 (3) | $SiO_2$ 244FP | 22.1 | 7.0 |
| Lab 5 (3) | $SiO_2$ NM-204 | 7.0 | 44.2 |

71. Data for all materials and laboratories are plotted together in Figure 21. Overall, the materials appear to be classified into similar dustiness levels by the different laboratories, with Lab 10 exhibiting the highest respirable mass dustiness index, except for $TiO_2$ NM-103, where discrepancies were also observed in other methods. For the particle number dustiness index, Lab 10 generally shows higher values, although the differences are smaller than those seen for the respirable mass index. These variations are further illustrated in Figure 22 and Figure 23 for the respirable mass and particle number-based dustiness indices. The higher respirable dustiness index reported by Lab 10 could be attributed to differences in tubing length, which is shorter for Lab 10, leading to reduced particle losses. Although the procedures were carefully harmonised, certain setup aspects, such as aerosol instrumentation and tubing length, were not standardised. This lack of standardisation means that there is a risk of unexplained slight variations, as seen in this case, while also accounting for natural variations between different laboratories.

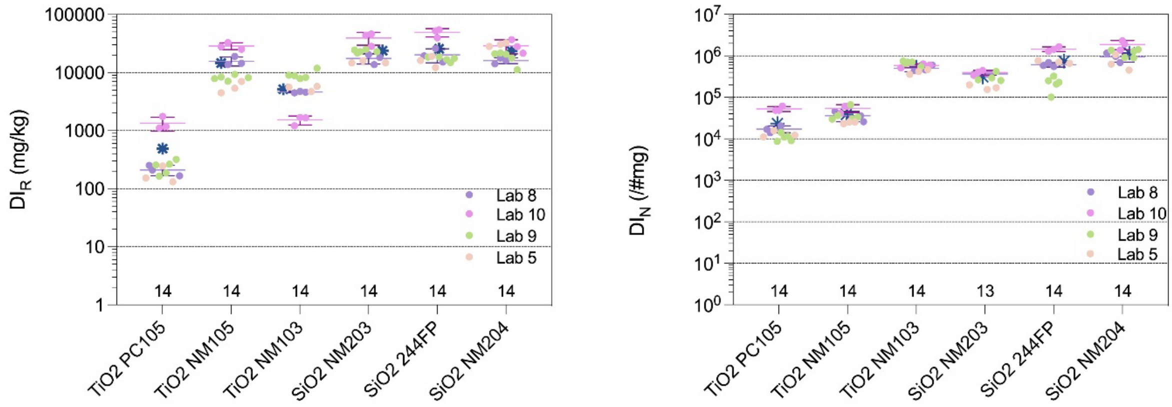


**Figure 21. Individual data points obtained per laboratory and material for each metric assessed for the Vortex Shaker. $DI_R$: respirable dustiness index; $DI_N$: number-based dustiness index. Error bars show standard deviation from all the replicates for each laboratory. Error bars show standard deviation of all the replicates for each laboratory. Note: log scale used.**

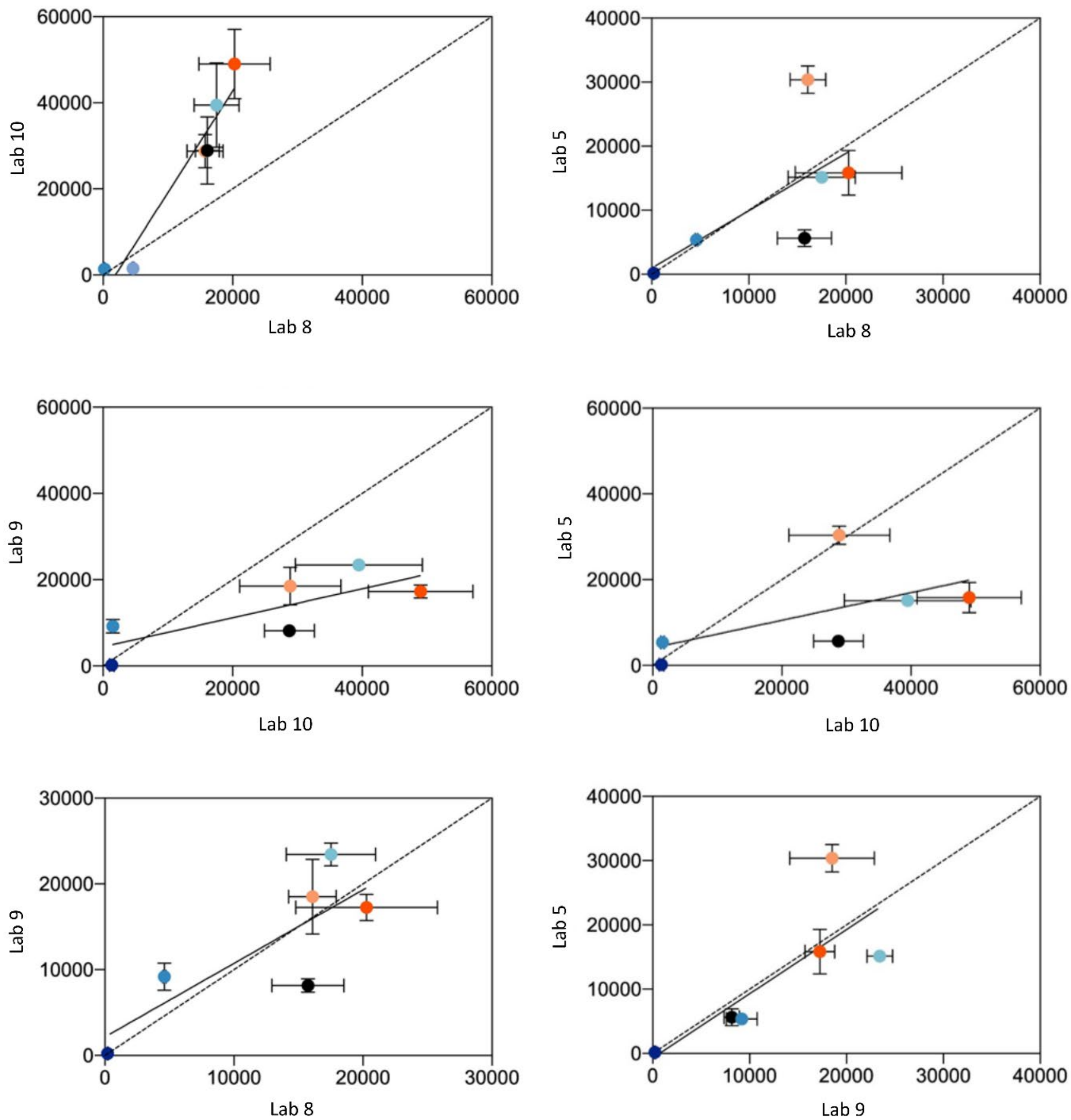


**Figure 22. Correlation between Vortex Shaker laboratories (Lab 8, Lab 9 and Lab 10) for respirable mass dustiness index. Materials are identified with colours: dark blue - $TiO_2$ PC105; black - $TiO_2$ NM105; dark turquoise - $TiO_2$ NM103; light turquoise -$SiO_2$ NM203; dark orange - $SiO_2$ 244; light orange - $SiO_2$ NM204.**

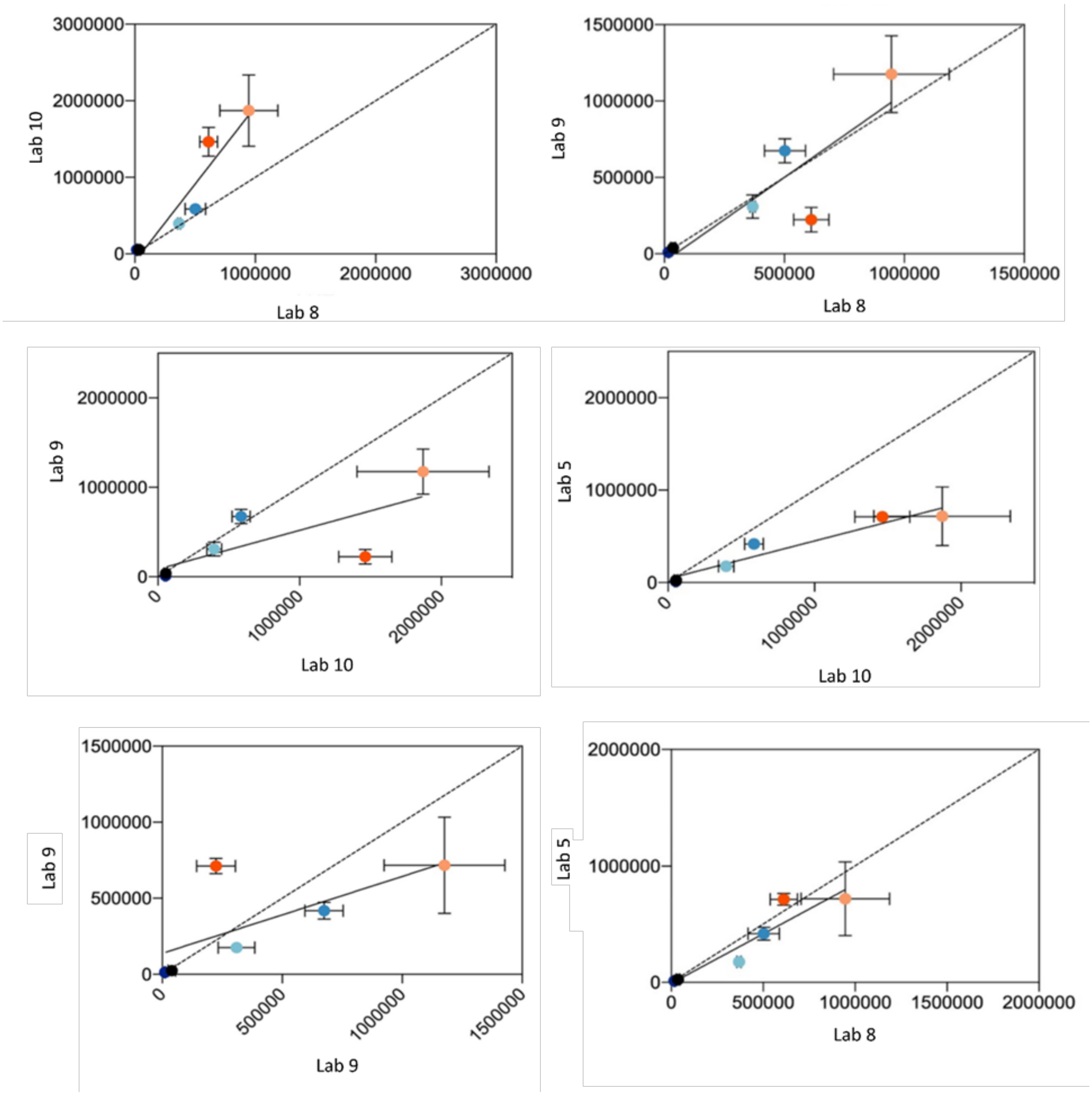


**Figure 23. Correlation between Vortex Shaker laboratories (Lab 8, Lab 9 and Lab 10) for particle number-based dustiness index. Materials are identified with colours: dark blue – $TiO_2$ PC105; black - $TiO_2$ NM105; dark turquoise - $TiO_2$ NM103; light turquoise - $SiO_2$ NM203; dark orange - $SiO_2$ 244; light orange - $SiO_2$ NM204.**

72. The z-scores calculated for the respirable and particle number-based dustiness indices are presented in

73. Table 13 and Table 14. All obtained z-scores for these indices were below 2, indicating that the results from the Vortex Shaker method are satisfactory.

**Table 13. Vortex Shaker respirable mass dustiness index calculated z-score.**

| Laboratory | $TiO_2$ PC105 | $TiO_2$ NM-105 | $TiO_2$ NM-103 | $SiO_2$ NM-203 | $SiO_2$ 244FP | $SiO_2$ NM-204 |
|---|---|---|---|---|---|---|
| Lab 8 | 0.49 | 0.23 | 0.36 | 0.63 | 0.29 | 0.89 |
| Lab 10 | 1.76 | 1.65 | 1.35 | 1.56 | 1.75 | 0.82 |
| Lab 9 | 0.43 | 0.60 | 1.10 | 0.04 | 0.51 | 0.57 |
| Lab 5 | 0.55 | 0.87 | 0.12 | 0.87 | 0.61 | 0.57 |

**Table 14. Vortex Shaker particle number-based dustiness index calculated z-score.**

| Laboratory | $TiO_2$ PC105 | $TiO_2$ NM-105 | $TiO_2$ NM-103 | $SiO_2$ NM-203 | $SiO_2$ 244FP | $SiO_2$ NM-204 |
|---|---|---|---|---|---|---|
| Lab 8 | 0.26 | 0.19 | 0.50 | 0.58 | 0.14 | 0.46 |
| Lab 10 | 1.79 | 1.08 | 0.19 | 0.88 | 1.63 | 1.39 |
| Lab 9 | 0.62 | 0.05 | 0.91 | 0.03 | 0.94 | 0.00 |
| Lab 5 | 0.50 | 0.96 | 1.20 | 1.42 | 0.07 | 0.92 |

### 3.6.4. Continuous Drop

74. Only two laboratories participated in the Continuous Drop method, and due to the material requirements for determining the dustiness index using this method, only three materials could be tested (see the combined dustiness report in Annex I). The materials tested included TiO2 PC105, SiO2 244FP (one test of three replicates), and an additional material not assessed by any other method (Micro Alumina), for which three tests of three replicates were conducted by both laboratories (Lab 1 and 2). Results for the respirable mass and number-based dustiness indices are presented in Figure 24, with laboratory variability detailed in

75. Table 15. Overall, variability was below 20%, with only three exceptions: $DI_R$ and $DI_N$ for $SiO_2$ 244FP from Lab 2 and $DI_I$ for $TiO_2$ PC105 from Lab 1.

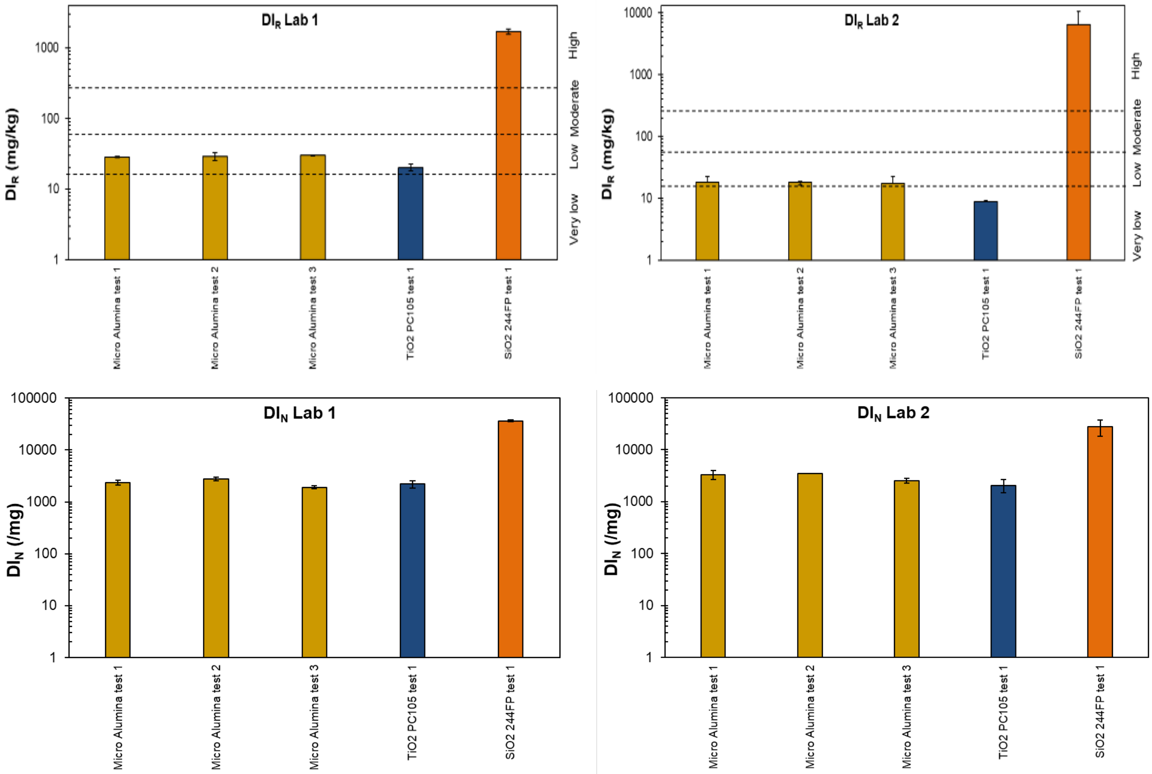


**Figure 24. Respirable mass ($DI_R$) and particle number ($DI_N$) dustiness index obtained per test (with replicates standard deviation) and material (represented in different colours) for each participant Continuous Drop laboratory. Continuous Drop ranking dustiness index values (15051-3:2025) plotted (very low, low, moderate and high). Error bars show standard deviation of the three replicates. Note: log scale used.**

74. In Figure 25, data from the two laboratories testing the Continuous Drop method is plotted for the three analysed metrics ($DI_R$, $DI_I$, and $DI_N$), along with a comparison between the laboratories. The data obtained suggests a similar classification of materials based on the three dustiness metrics, with the exception of micro alumina, which falls between two EN 15051-3:2025 [40] classification bands (as shown in Figure 24). Overall, for the respirable dustiness index, Lab 1 exhibits higher values for low-dust materials, while Lab 2 reports higher values for materials with greater dustiness, as well as for the inhalable dustiness index. Both laboratories demonstrate very similar values for the particle number dustiness index.

**Table 15. Continuous Drop method variability (%) for each laboratory and material. *$DI_R$*: respirable dustiness index; *$DI_I$*: inhalable dustiness index; $DI_N$: number-based dustiness index. Variability values >20% are indicated in italics.**

| Laboratory (n) | Material | *$DI_R$* | *$DI_N$* | *$DI_I$* |
|---|---|---|---|---|
| Lab 1 (9) | Micro Alumina | 6.9 | 17.4 | 18.9 |
| Lab 1 (3) | $TiO_2$ PC105 | 10.7 | 16.3 | 26.1 |
| Lab 1 (3) | $SiO_2$ 244FP | 9.5 | 3.6 | 19.6 |
| Lab 2 (7) | Micro Alumina | 19.0 | 18.1 | 19.7 |
| Lab 2 (2) | $TiO_2$ PC105 | 4.01 | 20.8 | 9.0 |
| Lab 2 (3) | $SiO_2$ 244FP | 62.4 | 35.1 | 16.0 |

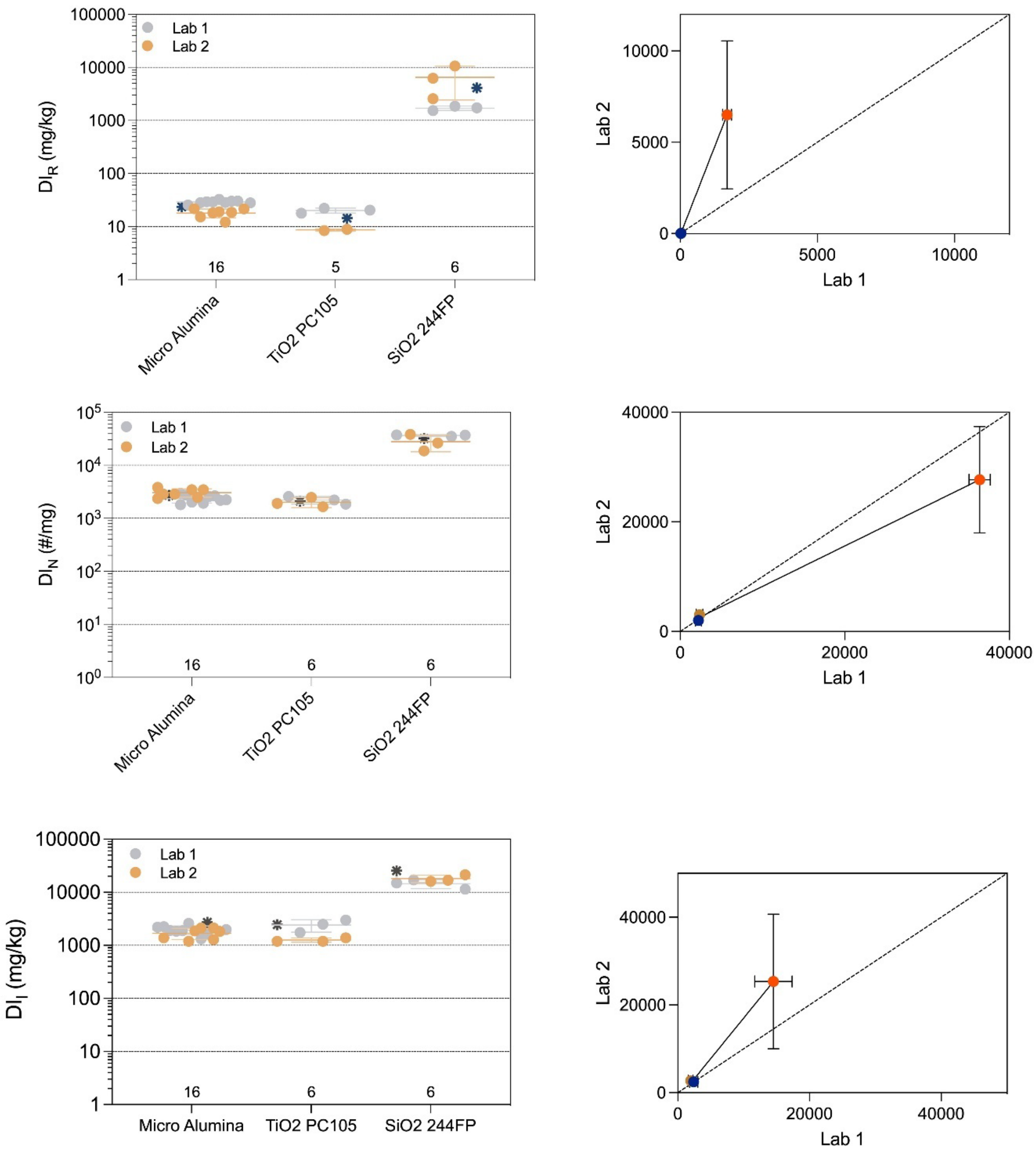

**Figure 25. Individual data points obtained per laboratory and material for each metric assessed for the Continuous Drop method and correlation between laboratories (Lab 1 and Lab 2). $DI_R$: respirable dustiness index; $DI_N$: number-based dustiness index; $DI_I$: inhalable dustiness index. Error bars show standard deviation of all the replicates for each laboratory. Note: log scale used. For correlation plots, materials are identified with colours: dark blue - $TiO_2$ PC105; black - $TiO_2$ NM105; dark turquoise - $TiO_2$ NM103; light turquoise - $SiO_2$ NM203; dark orange - $SiO_2$ 244; light orange - $SiO_2$ NM204.**

75. Materials moisture content was measured, and its effect on the respirable mass and particle number dustiness index was investigated. Considerable differences in the determined moisture content between Lab 1 and Lab 2 were observed for the three materials, ranging from 1.5% to 14.6%. A significant positive correlation (n=6) was found between moisture content and the respirable mass dustiness index for the alumina material, with a Pearson correlation coefficient of 0.99 (see Appendix Figure A11). In contrast, a negative, non-significant tendency was observed for the particle number-based dustiness index. For the other materials, only one test per laboratory was available, which was insufficient to assess any correlations. However, it is noteworthy that Lab 1 moisture levels were 4 to 14 times higher than those of Lab 2, corresponding to lower respirable dustiness indices and higher particle number-based dustiness indices, mirroring the trend observed with the alumina material.

76. The z-scores for the respirable, inhalable, and particle number-based dustiness indices are presented in Table 16. All calculated z-scores were below 2, indicating that the results obtained for the Continuous Drop method are satisfactory. However, it is important to note that these results are based on only two laboratories and three materials.

**Table 16. Continuous Drop respirable mass and particle number dustiness index calculated z-score. $DI_R$: respirable dustiness index; $DI_N$: number-based dustiness index; $DI_I$: inhalable dustiness index.**

| Metric | Laboratory | Micro Alumina | $TiO_2$ PC105 | $SiO_2$ 244FP |
|---|---|---|---|---|
| $DI_R$ | Lab 1 | 0.78 | 0.71 | 0.65 |
| | Lab 2 | 1.00 | 1.06 | 0.65 |
| $DI_I$ | Lab 1 | 0.26 | 0.77 | 0.56 |
| | Lab 2 | 0.33 | 0.77 | 0.56 |
| $DI_N$ | Lab 1 | 0.53 | 0.28 | 0.56 |
| | Lab 2 | 0.68 | 0.28 | 0.56 |

### 3.6.5. Fluidizer

77. Data from two laboratories (Lab 11 and Lab 12) were generated for the Fluidizer method (see the combined dustiness report in Annex J). The results for total mass and number-based dustiness indices from both laboratories are presented in Figure 26 and Figure 27, respectively. Laboratory variability is given in Table 17. For this dustiness method, variability exceeded 20% in many cases, particularly for total dustiness mass. Notably, gravimetric determination of total dust was incorporated into this specific ILC for the first time.

78. In addition to the high variability, the results for total dustiness mass do not classify the materials in the same order or ranges as observed with other methods. The Fluidizer method has a considerably longer testing duration of 60 minutes compared to 60 seconds for methods like the Rotating Drum or Vortex Shaker. Furthermore, it requires a relatively lower amount of material than other methods, and the energy input in the Fluidizer is determined to be low [11]. Therefore, the determination of total dustiness mass, as conducted in this ILC, needs further investigation to understand its relevance for this method.

79. For the number-based dustiness index, variability for Lab 11 was generally below 20-30%. In contrast, variability for the Lab 12 was higher, ranging from 15% to 75%. It is important to note that while Lab 11 has several years of experience with the Fluidizer setup, this was Lab 12 first time using this methodology, which could help explain the higher variability observed. The specific data points contributing to the increased variability could not be linked to any issues during testing or equipment malfunctions.

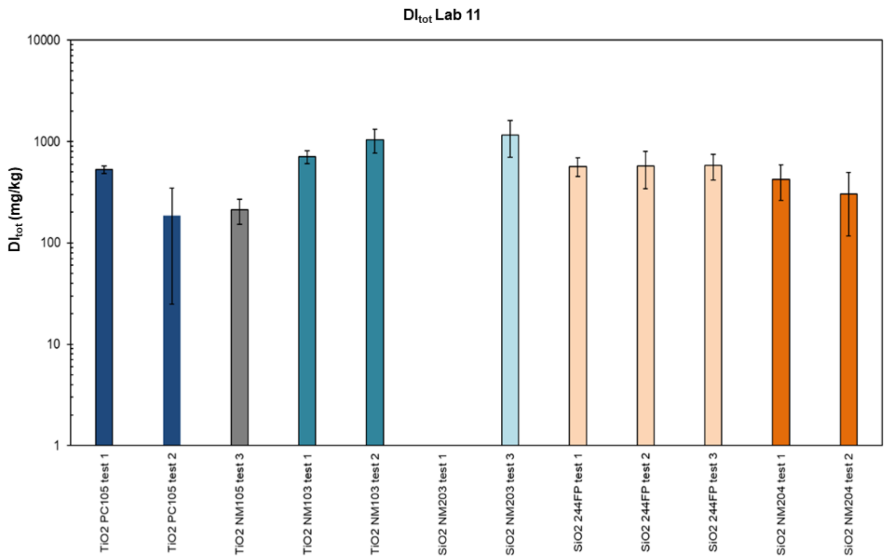


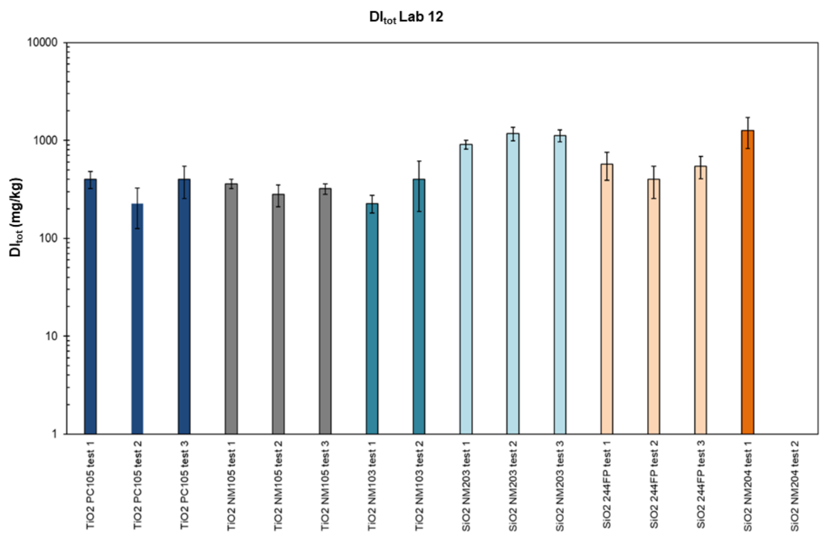


**Figure 26. Total mass ($DI_{tot}$) dustiness index obtained per test (with replicates standard deviation) and material (represented in different colours) for the Fluidizer method obtained by Lab 11 and Lab 12. Error bars show standard deviation of the three replicates. Note: log scale used.**

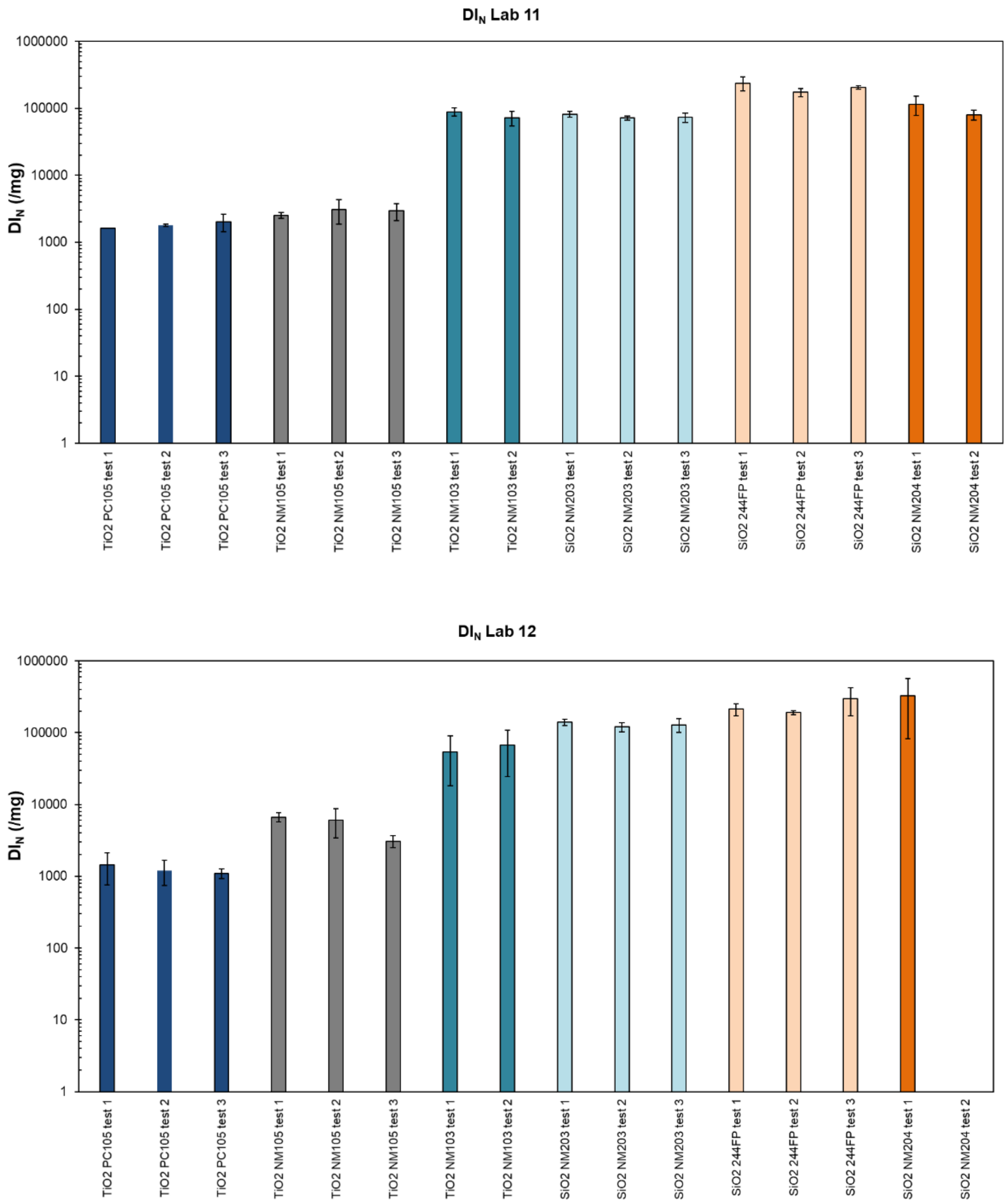


**Figure 27. Particle number-based dustiness index (*$DI_N$*) dustiness index obtained per test (with replicates standard deviation) and material (represented in different colours) for the Fluidizer method obtained by Lab 11 and Lab 12. Error bars show standard deviation of the three replicates. Note: log scale used.**

**Table 17. Variability % for particle number ($DI_N$), and total mass ($DI_{tot}$) dustiness index obtained per test (with replicates standard deviation) and material for each Vortex Shaker participant laboratory. Variability values >20% are indicated in italics.**

| Laboratory (n) | Material | $DI_{tot}$ | $DI_N$ |
|---|---|---|---|
| Lab 11 (9) | $TiO_2$ PC105 | 79.5 | 22.4 |
| Lab 11 (9) | $TiO_2$ NM-105 | 97.7 | 27.8 |
| Lab 11 (9) | $TiO_2$ NM-103 | 29.9 | 20.6 |
| Lab 11 (6) | $SiO_2$ NM-203 | 115.0 | 11.3 |
| Lab 11 (9) | $SiO_2$ 244FP | 26.9 | 20.6 |
| Lab 11 (6) | $SiO_2$ NM-204 | 46.8 | 32.4 |
| Lab 12 (9) | $TiO_2$ PC105 | 37.9 | 35.7 |
| Lab 12 (9) | $TiO_2$ NM-105 | 17.7 | 42.1 |
| Lab 12 (6) | $TiO_2$ NM-103 | 53.2 | 59.1 |
| Lab 12 (9) | $SiO_2$ NM-203 | 16.8 | 15.2 |
| Lab 12 (9) | $SiO_2$ 244FP | 31.1 | 35.0 |
| Lab 12 (3) | $SiO_2$ NM-204 | 118.1 | 74.5 |

80. Data from the two laboratories testing the Fluidizer method are plotted together for the two metrics (total dustiness index and number-based dustiness index) (Figure 28). As mentioned in the previous paragraph, total dustiness index does not seem to provide relevant information of material dustiness classification. Conversely, number-based dustiness index data obtained from both laboratories seems to consistently classify the materials in the same order. For number-based dustiness index Lab 12 data tends to be slightly higher than Lab 11, although the difference is minimal. Conversely, for $DI_{tot}$, a clear tendency was not observed. Slope and $R^2$ were 0.6220 and 0.08051 for $DI_{tot}$, and 0.5871 and 0.5497 for $DI_N$.

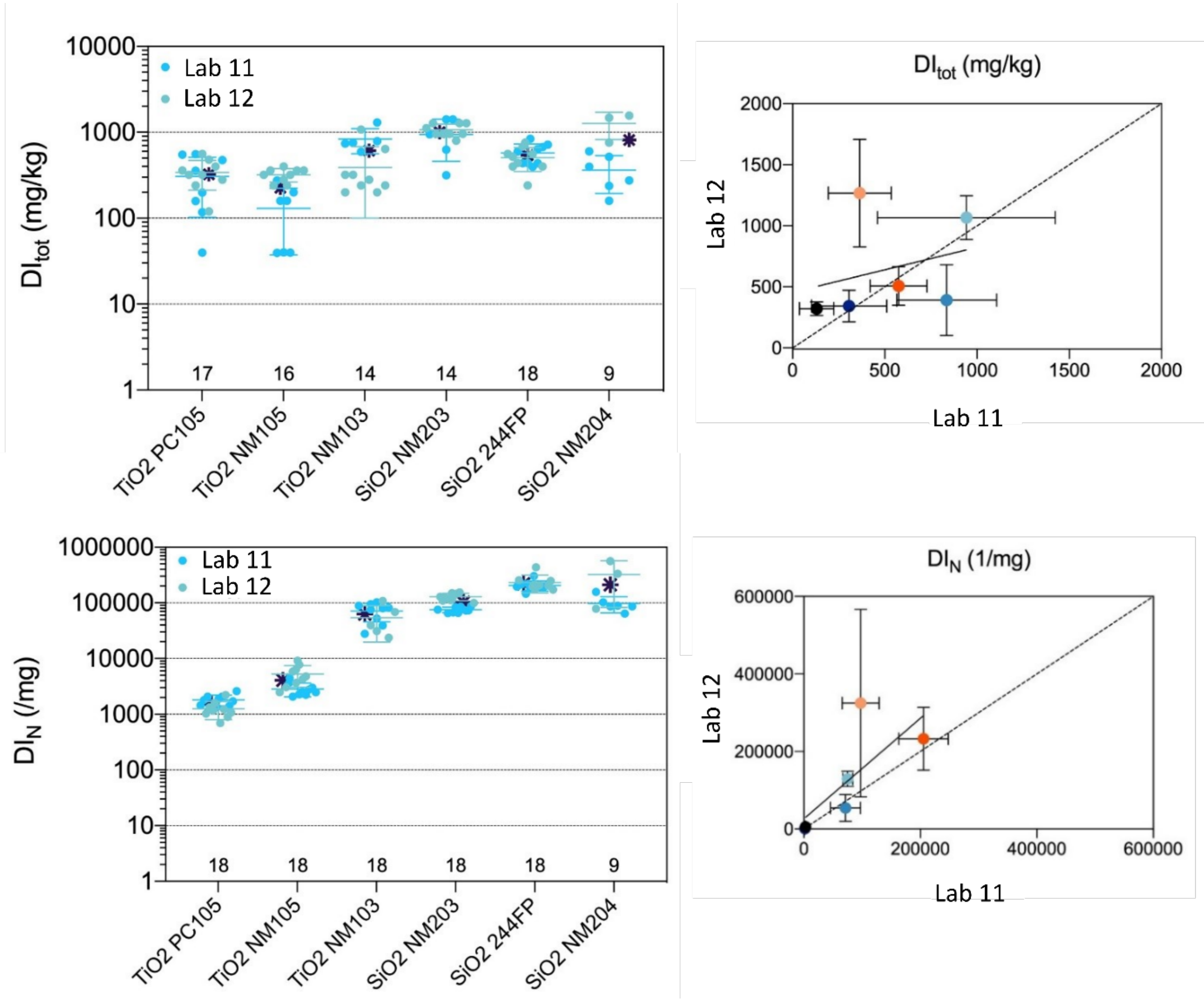


**Figure 28. Individual data points obtained per laboratory and material for each metric assessed for the Fluidizer method and correlation between laboratories (Lab 11 and Lab 12).** ***$DI_N$*****: number-based dustiness index;** ***$DI_{tot}$*****: total mass dustiness index. Error bars show standard deviation of all the replicates for each laboratory. Note: log scale used. For correlation plots, materials are identified with colours: dark blue - $TiO_2$ PC105; black - $TiO_2$ NM105; dark turquoise - $TiO_2$ NM103; light turquoise - $SiO_2$ NM203; dark orange - $SiO_2$ 244; light orange - $SiO_2$ NM204.**

81. The z-scores for total and particle number-based dustiness indices are presented in

82. Table 18. All calculated z-scores were below 2, indicating that the results obtained for the Fluidizer method are satisfactory. However, it is essential to note that these results are based on data from only two laboratories.

**Table 18. Fluidizer total mass and particle number dustiness index calculated z-score. $DI_N$: number-based dustiness index; $DI_{tot}$: total mass dustiness index.**

| Metric | Laboratory | $TiO_2$ PC105 | $TiO_2$ NM-105 | $TiO_2$ NM-103 | $SiO_2$ NM-203 | $SiO_2$ 244FP | $SiO_2$ NM-204 |
|---|---|---|---|---|---|---|---|
| $DI_{tot}$ | Lab 11 | 0.11 | 0.80 | 0.93 | 0.26 | 0.22 | 0.58 |
| | Lab 12 | 0.10 | 0.80 | 0.70 | 0.14 | 0.22 | 1.16 |
| $DI_N$ | Lab 11 | 0.56 | 0.59 | 0.51 | 0.86 | 0.21 | 0.45 |
| | Lab 12 | 0.56 | 0.59 | 0.39 | 0.86 | 0.21 | 0.90 |

## 3.6.6. Venturi

83. The Venturi method was evaluated in this ILC by one laboratory (Lab 3; see the combined dustiness report in Annex K). Results for the determined respirable and total dustiness indices per test are displayed in Figure 29. Variability for nearly all materials was under 15%, with the exception of the respirable dustiness index ($DI_R$) for $SiO_2$ NM204, which exhibited an outlier (see Table 19). Overall, the data showed low dispersion and variability (Figure 30). The outlying data point could not be attributed to any known methodological errors and could not be statistically discarded due to the limited amount of available data.

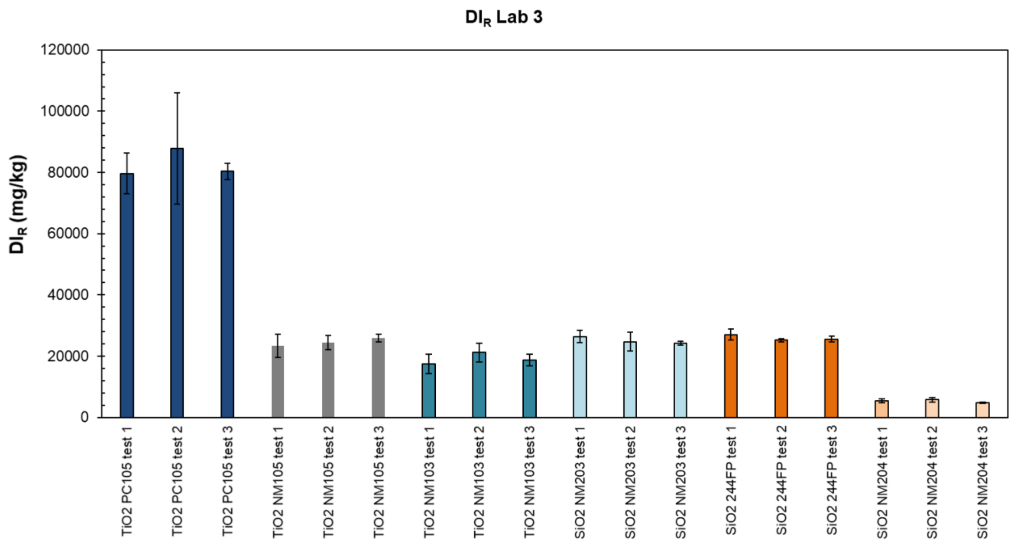

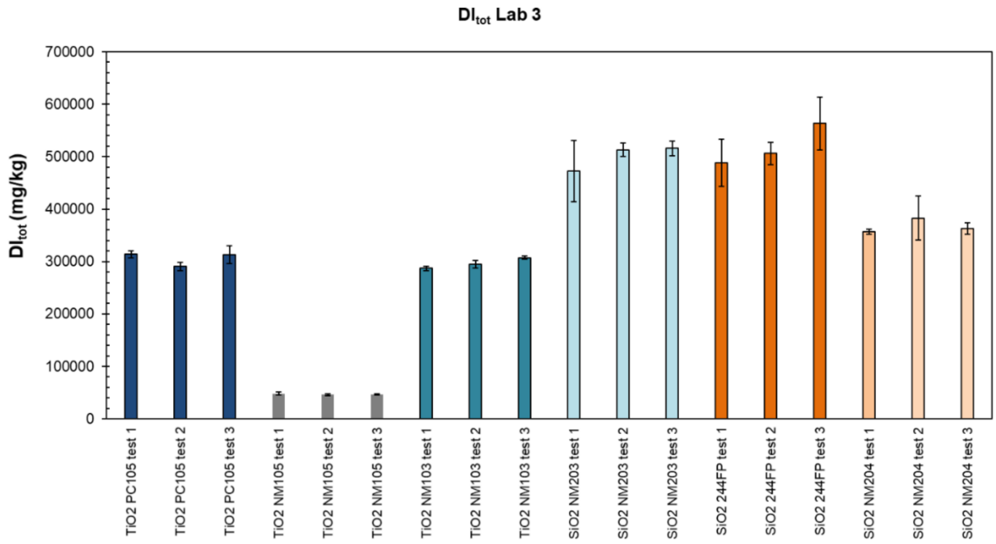


**Figure 29. Respirable ($DI_R$) and total mass ($DI_{tot}$) dustiness index obtained per test (with replicates standard deviation) and material (represented in different colours) for the Venturi method obtained by Lab 3. Error bars show standard deviation of the three replicates.**

**Table 19. Variability % of particle mass ($DI_N$) dustiness index obtained per test and material for the Venturi participant laboratory. $DI_R$: respirable mass dustiness index; $DI_{tot}$: total mass dustiness index.**

| Laboratory (n) | Material | $DI_R$ | $DI_{tot}$ |
|---|---|---|---|
| Lab 3 (9) | $TiO_2$ PC105 | 12.8 | 5.0 |
| Lab 3 (9) | $TiO_2$ NM-105 | 10.4 | 4.7 |
| Lab 3 (9) | $TiO_2$ NM-103 | 15.2 | 3.4 |
| Lab 3 (9) | $SiO_2$ NM-203 | 8.5 | 7.4 |
| Lab 3 (9) | $SiO_2$ 244FP | 5.2 | 9.4 |
| Lab 3 (9) | $SiO_2$ NM-204 | 154.7 (13.2)* | 6.7 |

*Removing the one data point showing very high variability.

84. In Figure 30, all data points from Lab 3 are plotted. Unlike the other methods, the Venturi method exhibited low variation in both respirable and total mass dustiness indices across different materials. This is likely due to the high energy applied during the test. Previous studies reported that the differences between materials in terms of dustiness indices measured with the Venturi method were generally around two orders of magnitude for fine and nanoscale materials [30]. In this study, the differences in respirable mass dustiness indices were generally between 1 and 4.

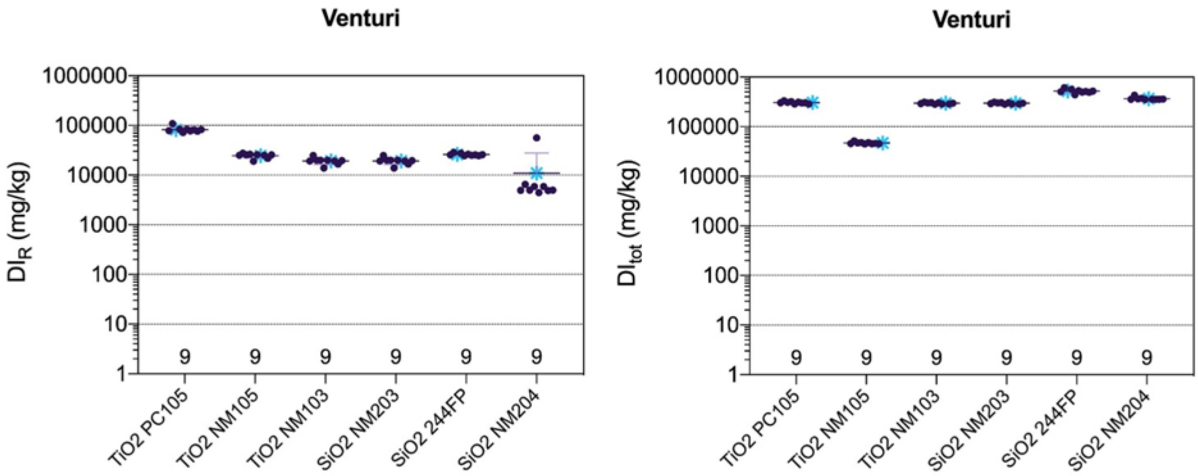


**Figure 30. Individual data points obtained per laboratory and material for each metric assessed for the Venturi method. $DI_R$: respirable dustiness index; $DI_{tot}$: total mass dustiness index. Error bars show standard deviation of all the replicates. Note: A logarithmic scale is used.**

### 3.6.7. Data comparison between dustiness methods

85. To investigate the relationships between different dustiness methods and identify potential correlations for developing ranking schemes, ratios between the Vortex Shaker method (which produced the highest values) and other methods were calculated and are shown in Figure 31 for the particle number-based dustiness index. The differences between the Vortex Shaker and other methods appear consistent across the tested materials, although some methods, such as the Small Rotating Drum, exhibit a broader ratio range (e.g., 20-50). Pearson and Spearman correlations between the methods are presented in Figure 32 as colour-gradient plots. For the respirable dustiness index, the Rotating Drum and Small Rotating Drum methods showed a strong Pearson correlation coefficient of 0.98 (Appendix Figure A12). Both methods (rotating and Small Rotating Drum) have Pearson correlation coefficients of 0.49 and 0.59, and -0.57 and -0.54 with Vortex Shaker and Venturi methods, respectively. Conversely, the Venturi and Vortex Shaker methods had a correlation coefficient of -0.69, while the Rotating Drum and Fluidizer methods exhibited a Pearson coefficient of 0.81 for the total/inhalable dustiness index (although with a non-significant p-value of 0.0508; Appendix Figure A12). Both the Rotating Drum and Fluidizer showed limited correlation with the Venturi method, with coefficients of 0.43 and 0.42, respectively. For the particle number dustiness index, the Small Rotating Drum, Vortex Shaker, and Fluidizer methods demonstrated significant Pearson correlation coefficients, ranging from 0.85 to 0.99 (Appendix Figure A12). Conversely, and opposed to what was observed for *DI* respirable, Rotating Drum Pearson coefficient correlations with Vortex, Small Rotating Drum and Fluidizer were weaker, with coefficients of 0.44, 0.40 and 0.21, respectively.

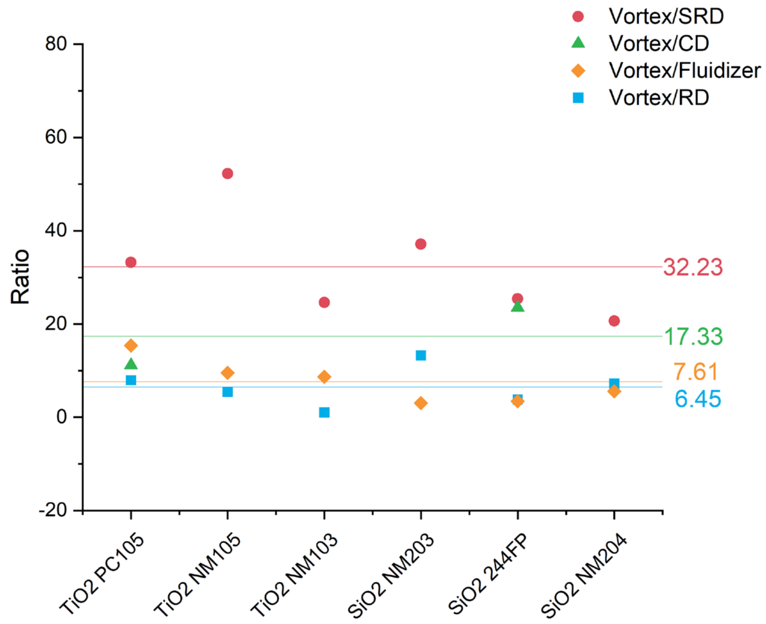


**Figure 31. Difference of particle number-based dustiness index shown as a ratio between the different methods and Vortex Shaker. Vortex is used as references as is the method showing the highest values. RD: Rotating Drum, SRD: Small Rotating Drum, and CD: Continuous Drop.**

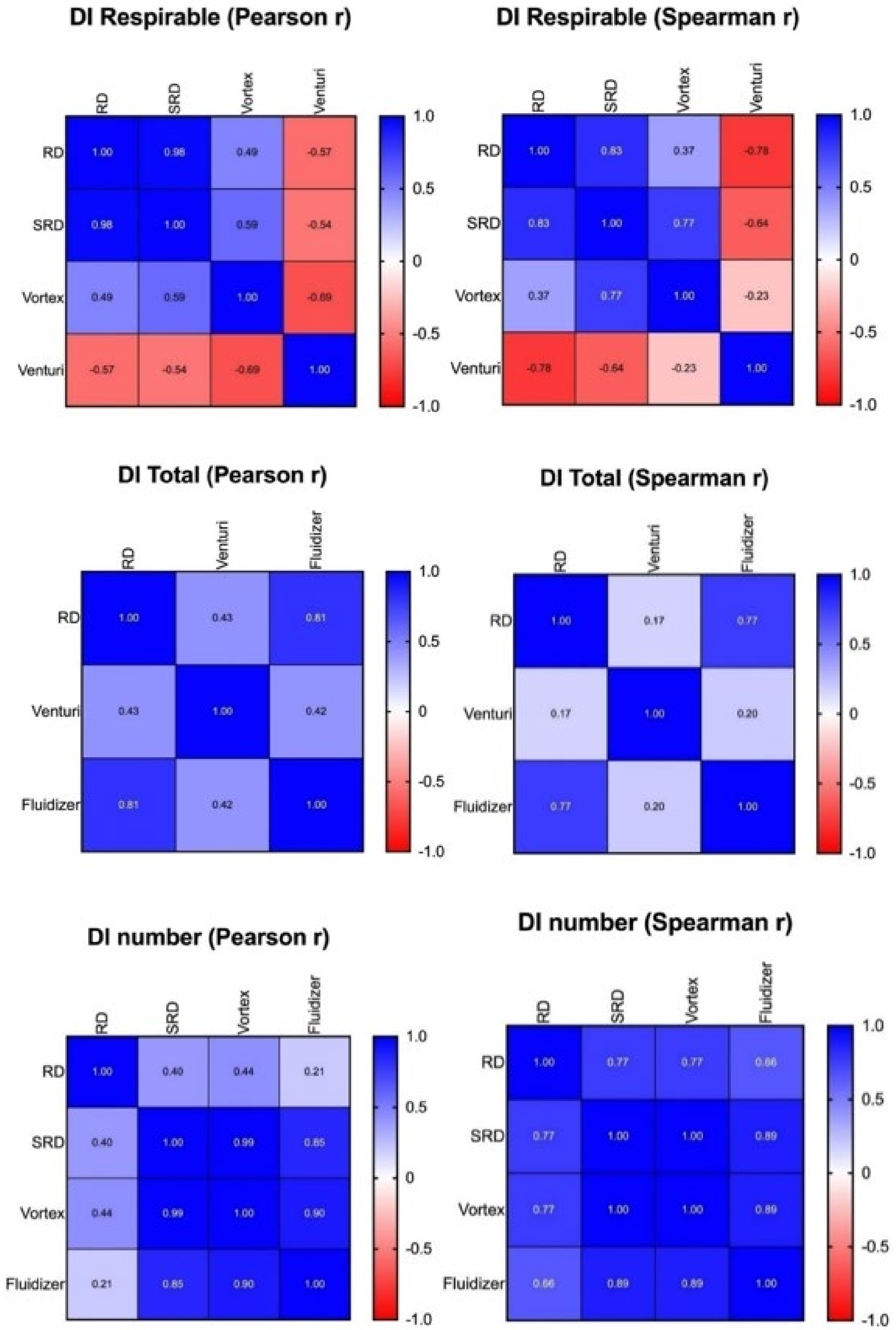


**Figure 32. Pearson and Spearman correlation coefficients between methods shown as colour-gradient plots for**

**respirable (top), total/inhalable (middle) and particle number (bottom) dustiness index. RD: Rotating Drum, and SRD: Small Rotating Drum.**

86. Repeatability and reproducibility were evaluated for the Rotating Drum and Vortex Shaker methods in accordance with ISO 5725-2:2025 [26]. The results, explored through the relationship between repeatability, reproducibility, and the mean values for each material and method, are shown in Table 20. A full assessment is available in Annexes E and H. A mostly linear relationship was observed between repeatability, reproducibility, and the mean dustiness values, with both repeatability and reproducibility being higher for the Vortex Shaker method and for particle number-based dustiness indices compared to respirable mass dustiness indices. This trend is expected, as higher values generally lead to increased repeatability and reproducibility. Other factors, such as sample size, sample homogeneity, and the precision of energy transfer during agitation, may also influence these relationships.

**Table 20. Calculated repeatability and reproducibility for Rotating Drum and Vortex Shaker for each material and dustiness index fraction (respirable mass and particle number). Best fit linear relationship and equation is also given.**

| *DI* | Material | Repeatability (r) | | Reproducibility (R) | |
|---|---|---|---|---|---|
| | | Rotating Drum | Vortex Shaker | Rotating Drum | Vortex Shaker |
| Respirable mass | $TiO_2$ PC105 | 5.6 | 188.1 | 11.3 | 591.8 |
| | $TiO_2$ NM-103 | 34.9 | 443.2 | 130.0 | 2841.5 |
| | $TiO_2$ NM-105 | 5.0 | 2,527.6 | 5.9 | 10,605.5 |
| | $SiO_2$ NM-203 | 33.0 | 5,235.6 | 177.5 | 11,761.6 |
| | $SiO_2$ NM-204 | 96.1 | 4,283.2 | 536.8 | 7,724.4 |
| | $SiO_2$ 244FP | 32.7 | 5,256.5 | 217.5 | 16,391.6 |
| | Relationship type (I-IV) | II =3.235+0.119*m | I (linear) = 0.584*m | I (linear) = 0.63*m | I (linear) = 0.66*m |
| Particle number | $TiO_2$ PC105 | 891.3 | 4502.1 | 2,075.0 | 19,997.4 |
| | $TiO_2$ NM-103 | 162,685.9 | 61,291.9 | 436,383.7 | 139,504.9 |
| | $TiO_2$ NM-105 | 483.3 | 12,465.9 | 8,130.0 | 16,348.7 |
| | $SiO_2$ NM-203 | 11,226.3 | 33,180.0 | 29,673.8 | 123,582.9 |
| | $SiO_2$ NM-204 | 68,186.9 | 30,7945.4 | 14,1461.1 | 565,644.6 |
| | $SiO_2$ 244FP | 27,507.9 | 118,278.7 | 170,548.4 | 526,456.0 |
| | Relationship type (I-IV) | I (linear) = 0.291*m | I (linear) = 0.188*m | I (linear) = 0.989*m | I (linear) = 0.51*m |

87. The PSD data for each material is presented in Figure 33. No clear relationship or pattern between PSD and the dustiness methods is evident. Instead, PSD appears to be highly material-dependent, showing similar profiles regardless of the dustiness method employed. This trend is less apparent for $SiO_2$ NM-203 and $SiO_2$ 244FP, where significant deviations, especially in smaller size ranges, are observed. Moreover, substantial differences in PSD concentrations between laboratories do not correlate with differences in dustiness indices ($DI_N$), as seen when comparing the results from different laboratories.

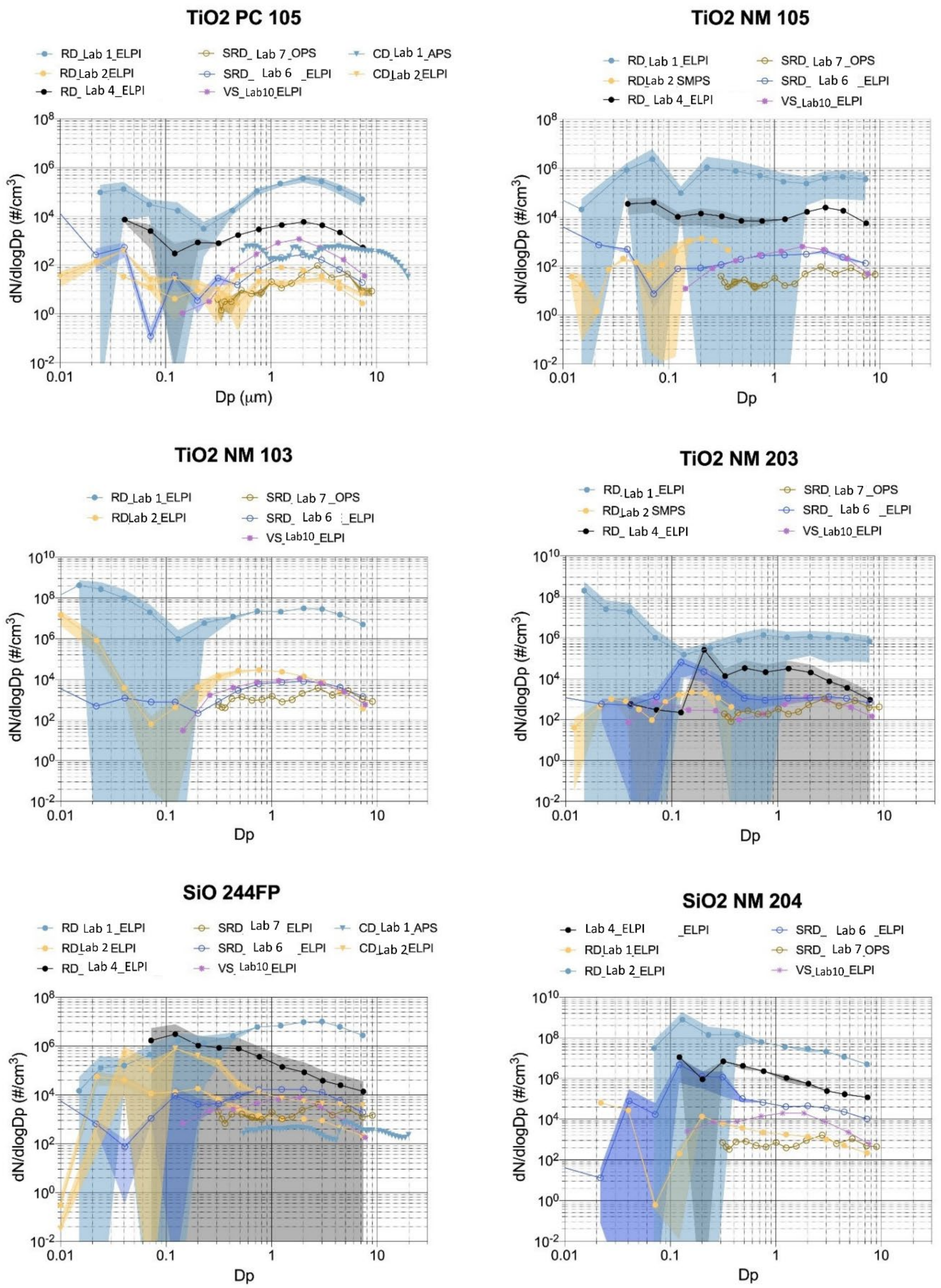
TiO2 PC 105
RD_Lab 1_ELPI
RD Lab 2ELPI
RD_ Lab 4_ELPI
SRD_ Lab 7_OPS
SRD_ Lab 6 _ELPI
VS_Lab10_ELPI
CD Lab 1_APS
CD Lab 2 ELPI
dN/dlogDp (#/cm3)
Dp (μm)
TiO2 NM 105
RD_Lab 1_ELPI
RD Lab 2 SMPS
RD_ Lab 4_ELPI
SRD_ Lab 7_OPS
SRD_ Lab 6 _ELPI
VS_Lab10_ELPI
Dp
TiO2 NM 103
RD_Lab 1_ELPI
RD Lab 2_ELPI
SRD_Lab 7_OPS
SRD_ Lab 6 _ELPI
VS_Lab10_ELPI
TiO2 NM 203
SiO 244FP
SiO2 NM 204
Lab 4_ELPI _ELPI
RD Lab 1ELPI
RD Lab 2_ELPI
SRD_ Lab 6 _ELPI
SRD_ Lab 7 OPS
VS_Lab10_ELPI

**Figure 33. d*N*/dlog*Dp* obtained for the 6 materials $TiO_2$ PC 105, $TiO_2$ NM-105, $TiO_2$ NM-103, $SiO_2$ NM-203, $SiO_2$ 244FP and $SiO_2$ NM-204. RD: Rotating Drum, SRD: Small Rotating Drum; CD: Continuous Drop; and VS: Vortex Shaker.**

### 3.6.8. Conclusions

88. The ILC was performed involved six different dustiness test methods, performed across multiple laboratories using six powders containing granular NOAA. The results of this ILC demonstrate that these methods can be reliably applied in different laboratories, yielding reproducible and acceptable results (Figure 34).

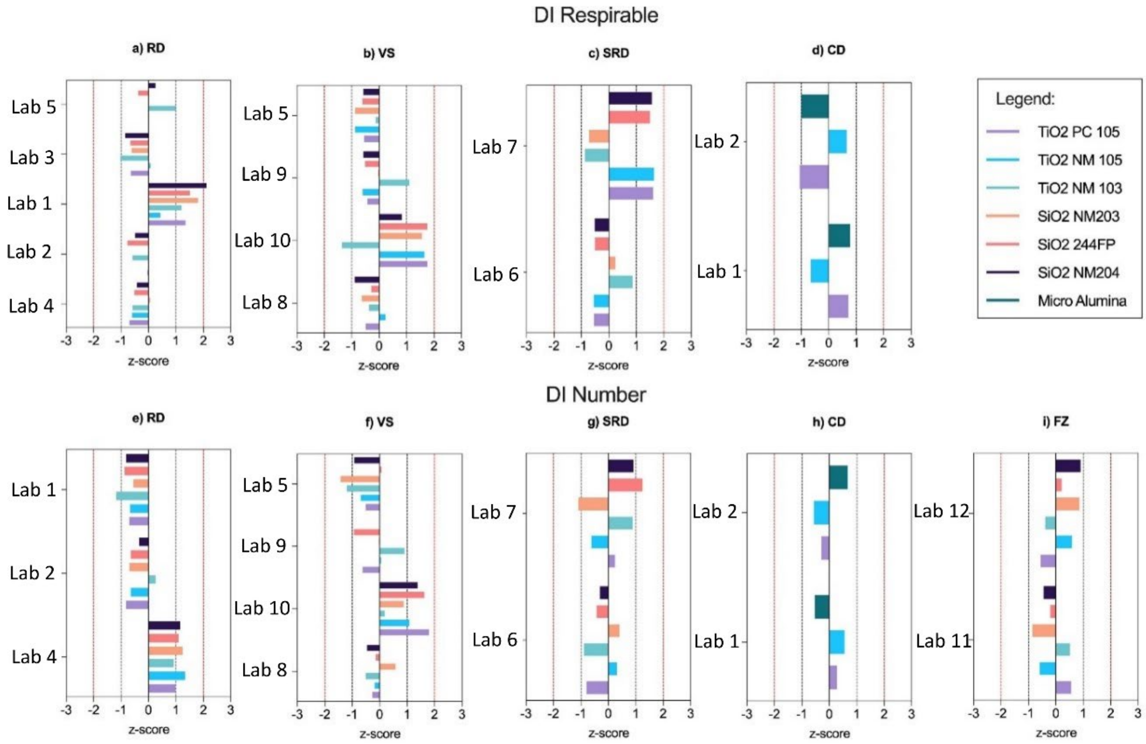


**Figure 34. Summary of z-score values obtained per laboratory and material, represented for each method and dustiness metric. Respirable dustiness index ($DI_R$) (a, b, c and d) and particle number dustiness index ($DI_N$) (e, f, g, h and i). RD: Rotating Drum, SRD: Small Rotating Drum; CD: Continuous Drop; VS: Vortex Shaker; and FZ: Fluidizer.**

89. In the study, the z-scores calculated for each method were consistently less than 2, indicating satisfactory results, with one exception: a z-score of 2.1 was recorded for the respirable dustiness index ($DI_R$) measured using the Rotating Drum, suggesting a borderline questionable result. Overall, the findings confirm that the dustiness results obtained using each method and metric, whether Rotating Drum, Vortex Shaker, Continuous Drop, Small Rotating Drum, or Fluidizer, are reliable when harmonised procedures are followed. However, due to a limited number of participants, z-scores could not be calculated for the Venturi method.

90. Variability between laboratories was generally around or below 20-30% for most methods, although in some cases it reached up to 50% (Figure 35). Statistical analysis identified a few outliers, but only those associated with clear errors or extreme variability (e.g., 100%) were removed. Further removal of outliers was avoided, given the limited dataset, to prevent overly optimistic results that might not account for natural variability. For mass-based dustiness data, greater variability between

laboratories was observed compared to particle number-based dustiness indices, which exhibited lower between-laboratory variability.

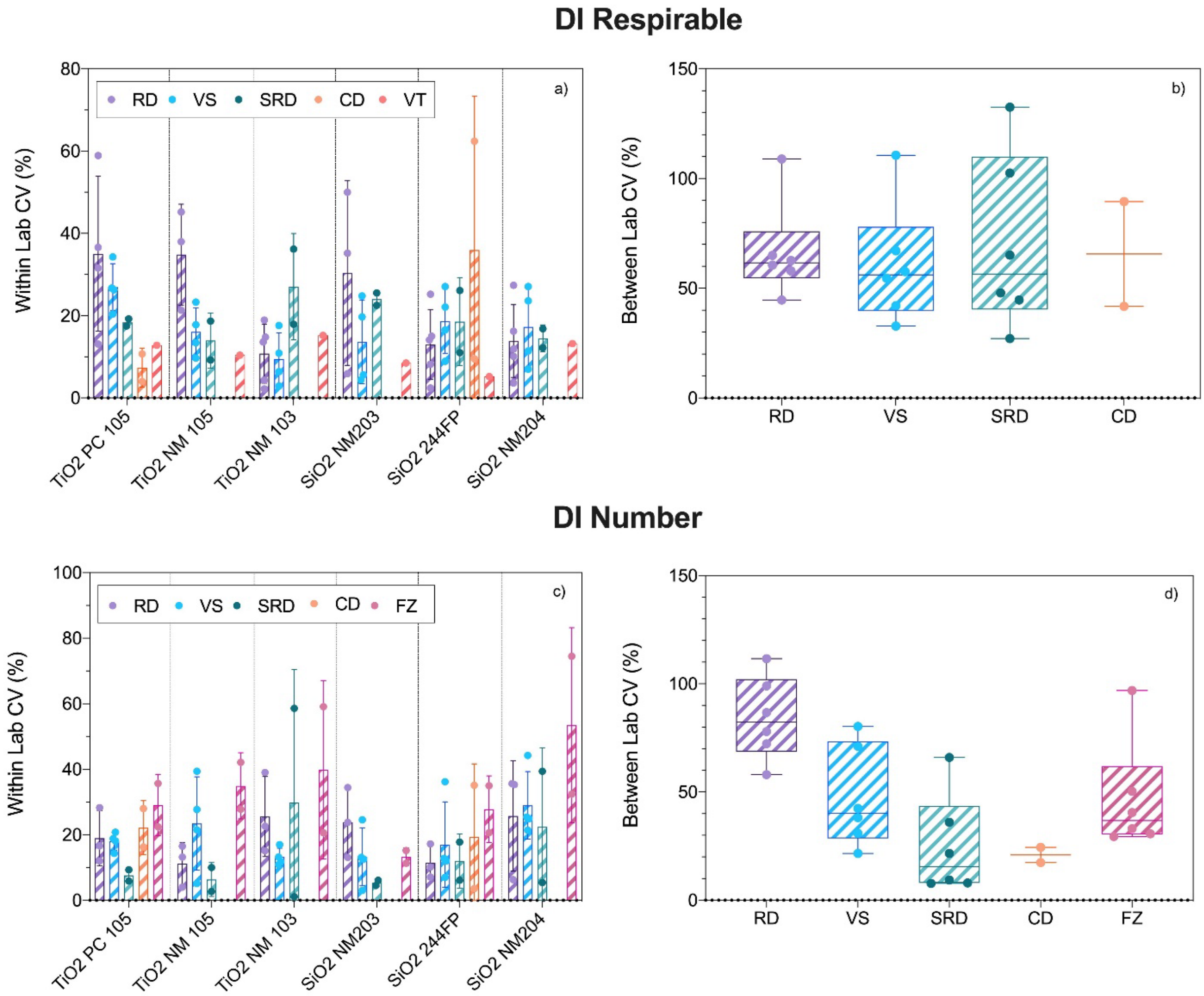


**Figure 35. Within and between laboratory coefficient of variation (CV) % per material and method, for respirable dustiness index (*DI*$_R$) (a and b, respectively), particle number dustiness index (*DI*$_N$) (c and d, respectively). Within laboratory CV % is shown for each participant lab considering all materials together with mean and standard deviation bars. Between laboratory CV % is represented for each method considering all materials using box plots with mean and min-max limits. RD: Rotating Drum, SRD: Small Rotating Drum; CD: Continuous Drop; VS: Vortex Shaker; VT: Venturi; and FZ: Fluidizer.**

91. Given the different characteristics of the dustiness test methods and the varying levels of energy impact they involve, a standardised comparison of the methods, including the development of a comparison factor, requires further investigation. This is essential for creating a decision-making framework that can guide the selection of the most appropriate dustiness test method.

92. Material ranking appeared consistent across laboratories, though slight differences were linked to variations in the experimental setup, such as tubing length or the aerosol instrumentation used, including different CPC models. One material, $TiO_2$ NM-103, presented significant discrepancies between laboratories and methods, exhibiting an unusual bimodal PSD, with a higher proportion of micron-sized particles than sub-micron particles.

93. Finally, the relationship between moisture content and dustiness index values was explored using data from the Rotating Drum, Small Rotating Drum, and Continuous Drop methods. Differences in moisture content ranged from 0.14% to 1.85% for the Rotating and Small Rotating Drum methods, while the Continuous Drop method showed larger variations, up to 14.6%. Due to limited data, the maximum number of samples used for correlation analysis ranged from four to eight. Overall, positive correlations between moisture content and respirable mass dustiness index were observed for $TiO_2$ PC 105 and $SiO_2$ 244FP (using the Rotating Drum), $TiO_2$ PC105, NM-105, and $SiO_2$ NM-204 (using the Small Rotating Drum), and alumina (using the Continuous Drop method). In contrast, negative correlations with the particle number dustiness index were found for $TiO_2$ PC 105 and $SiO_2$ 244FP (using the Rotating Drum) and alumina (using the Continuous Drop method). No significant correlations were observed for the other materials and methods. These results suggest opposing behaviours for different particle sizes, but given the limited dataset, the findings should be interpreted with caution.

# 4. ILC for powders containing fibrous NOAA

## 4.1. Time frame and instructions to participants

94. The time schedule of this ILC is shown in Table 21. After the call for participants was circulated in December 2020, the ILC activities officially started on June 2021. The ILC activities mainly consisted of two parts, the pre-tests, designed to adapt and define the procedures to be used during the ILC activities, and the actual ILC test. More details on the study design are provided in the following section. During the duration of the ILC activities, several meetings took place.

Table 21. List of main activities taking place during the ILC.

| Activities | Date |
|---|---|
| Call for contributions to the ILC | December 2020 |
| Kick-off-Meeting on ILC | June 2021 |
| Start of pre-test | February 2022 |
| Extended expert group meeting | October 2022 |
| Pre-test finalisation | December 2022 |
| Start of the ILC experiments | April 2023 |
| Finalisation of the ILC experiments | Early 2025 |
| Discussion of the ILC results | May 2023 – September 2025 |
| Joint expert group meeting | April 2024 |
| Joint expert group meeting | November 2024 |
| Finalisation of the TG and validation report | September 2025 |
| Final submission of TG and validation report | February 2026 |

95. Laboratories were requested to follow the harmonised procedures for the testing and to provide their setup details (i.e. used instrumentation, sampling times, amount of mass used and other operational details) and report dustiness data results by using a common developed template (Annex A).

## 4.2. Participating institutions and respective methods

96. About 20 international institutions from several European countries, the USA and Korea showed interest in the ILC and were involved in the ILC development providing expert opinion. The ILC experiments were performed by eight of the participating institutions, as shown in Table 22. From all the

participant laboratories, 4 partners collaborated with dustiness test performance, and 7 collaborated in the image acquisition using scanning electron microscopy (SEM) and the analysis of the obtained micrographs. The participation of additional laboratories performing SEM analysis was needed given that some of the dustiness performing laboratories do not have the capacities to perform SEM analysis.

97. In total, two dustiness methods are covered in this ILC, the Small Rotating Drum and the Fluidizer, described in detail in the TG 127 [57] with two participating laboratories, respectively. Five laboratories participated on the SEM image acquisition. Details on the participating institutions per dustiness method and SEM analysis are detailed in Table 22.

**Table 22. Name, abbreviation and country code of the participating institutions in the dustiness determination.**

| Name of participant institutions | Abbreviation | Country | Dustiness method | SEM for image acquisition | Data analysis |
|---|---|---|---|---|---|
| Federal Institute for Occupational Safety and Health | BAuA | DE | Fluidizer | Hitachi SU8230 | yes |
| The Cyprus Institute | Cyprus | CY | Fluidizer | - | - |
| The National Research Center for Work Environment | NRCWE | DK | Small Rotating Drum | - | - |
| Delft Solids Solutions | DSS | NL | Small Rotating Drum | JEOL JSM-5600 | yes |
| IBEVE Groep IDEWE | IBEVE | BE | - | JEOL JSM-IT500HR/LA | yes |
| ITGA | ITGA | FR | - | JEOL JSM 7610F | yes |
| International Iberian Nanotechnology Laboratory | INL | PT | - | - | yes |
| TÜV Nord | TÜV Nord | DE | - | - | yes |

## 4.3. Study design

98. The ILC procedure covered all parts that are needed to assess the dustiness of powders containing fibrous NOAA. A dustiness test of powders containing fibrous NOAA can be seen as a sequence of three sub-parts (see Figure 36):

– Step 1: Aerosol generation using a dustiness test method (e.g., Small Rotating Drum, Fluidizer) with sampling of aerosol on a substrate suitable for SEM and real-time instrumentation (e.g., CPC).
– Step 2: Acquisition of micrographs of the collected aerosol sample using SEM.
– Step 3: Analysis of the obtained micrographs including counting of all the identified NOAA (fibrous and non-fibrous), measuring of their dimensions, categorisation and statistical data analysis. Analysis of the real-time instrumentation results.

99. Two dustiness methods were tested, the Small Rotating Drum and the Fluidizer. Each dustiness method is described in the TG 127 [57] on dustiness determination of manufactured nanomaterials. The procedures developed for powders containing granular NOAA were further modified to be applicable for the dustiness testing of powders containing fibrous NOAA. In addition, the procedure on morphological characterisation using SEM was developed and established.

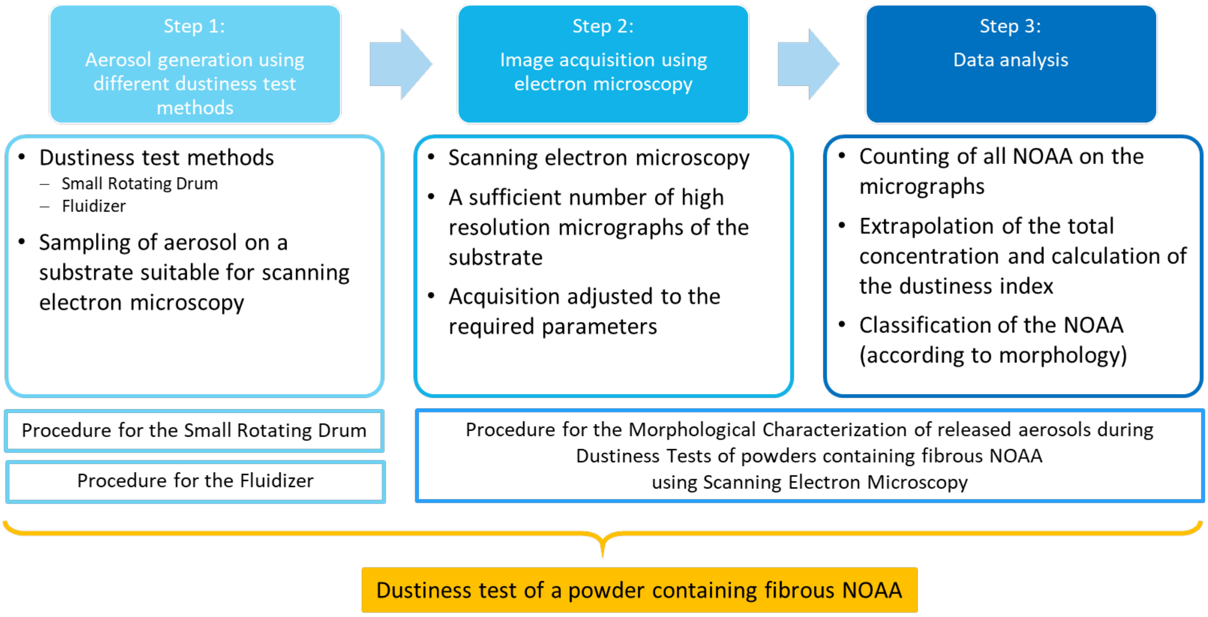


**Figure 36. Overview of the steps compulsory for a dustiness test.**

100. In order to finalize the method development, three pre-tests were performed, one for each step of the dustiness test (Figure 36) prior the actual ILC tests.

101. The 1st pre-test dealt with Step 1 of the dustiness test (Figure 36), by developing the procedures for the dustiness characterisation of powders containing fibrous NOAA using the two dustiness methods covered in this ILC. The procedures for performing the aerosol generation including the aerosol sampling on a substrate suitable for SEM were described. For this task, the pre-existing procedures developed in the ILC on powders containing granular NOAA were modified as needed to measure dustiness of powders containing fibrous NOAA and to implement aerosol sampling on a substrate suitable for SEM analysis. Parameters considered for adjustment were the amount of powder used for one run, the duration of the SEM sampling, the exclusion of aerosol measurement equipment not relevant for measuring fibrous NOAA, safety measures and adaptation of the dustiness measurands.

102. This 1st pre-test part was performed by one participating laboratory per dustiness method. The setups available at the different laboratories were harmonised as far as possible. For performing this 1st pre-test, one laboratory for each method received two powders (one with low dustiness (NC7000) and one with high dustiness (C2158)).

103. After the examination of the methods applicability to powders containing fibrous NOAA, the following parts were adjusted and modified:

– The amount of powder inserted in the dustiness test setup for one run was adjusted for powders containing fibrous NOAA due to the generally lower density when compared to powders containing granular NOAA. For the Small Rotating Drum, the amount of material required for one run was determined by using the respective mass that fills a volume of 56 $cm^3$. For the Fluidizer the amount of material required for one run was stablished to be 0.3 g except on cases in which this amount of mass fills more than 1 $cm^3$, in that case 1 $cm^3$ was used.
– The sampling procedures were modified for enabling sampling of aerosol on substrates suitable for SEM. For most of the methods, the sampling of aerosol on gravimetrical filters was replaced by the sampling on filters suitable for SEM. For this procedure, the same sampling equipment and procedures were used by all methods.
– The collection time on the filters suitable for SEM analysis was adjusted based on the observed

CPC particle number concentrations. This enabled the collection of suitably covered samples for EM avoiding substrate overload. This is of relevance to accurately quantify and characterize the collected objects. Acceptance of micrographs is based on fiber surface compared to sampler surface following the VDI 3492 specifications [28], micrographs shall be rejected due to overloading, if fibers and/or particles cover more than approximately 1/8 (12.5%) of the area of an image field. If more than 10% of the micrographs of a sample substrate are overloaded, the sample shall be rejected.

104. The 2nd pre-test dealt with parts of Step 2 (Figure 36). The goal of this pre-test was to identify image acquisition parameters and procedure that need to be pre-defined in order to minimize the experimental errors and to enable a comparison of the results obtained at the different laboratories having different SEMs. To achieve this, one sample for SEM analysis (a gold-coated nucleopore filter with fibres with a modal diameter of 10-30 nm) was shared with the partners who have access to an SEM. The partners used the sample shipped to them in order to discuss with their SEM-experts the requirements for the micrograph acquisition and the feasibilities within their SEM facilities. One important point for the harmonisation was the image acquisition at random locations. Taking micrographs at random locations on the sample is mandatory for statistical analysis of the sample. However, it is contrary to the usual procedures for taking SEM micrographs of defined objects. Example micrographs of the sample are shown in Figure 37, before and after the fine-tuning of the procedure and the discussions with the SEM-experts.

a)

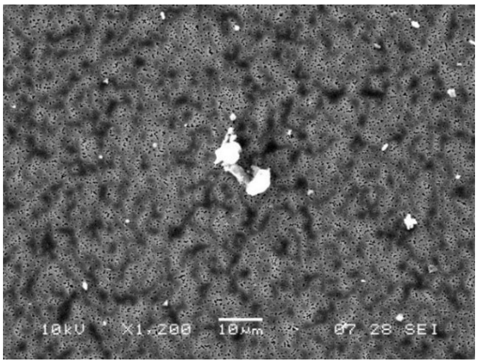


b)

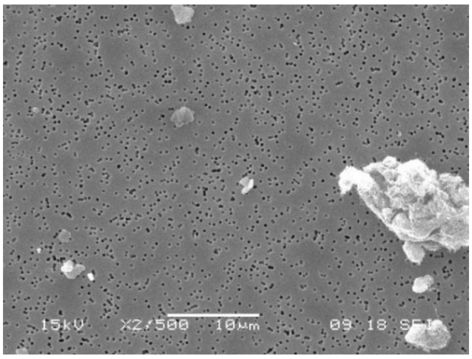


**Figure 37. SEM micrographs obtained by the same laboratory a) prior to and b) after the harmonisation efforts.**

105. The handling of aerosol samples for the SEM analysis was also discussed within the course of this pre-test and optimal procedures were established by the laboratories and implemented in the procedures. Furthermore, the 2nd pre-test helped in raising awareness of potential quality issues occurring with the gold-coated nucleopore filters (Figure 38). Holes and ruptures in the gold filter (as in the example provided in Figure 38c) cause losses in the image quality since the conducting film is not complete over the entire substrate and hinder the analysis of fibres since they are less visible and recognisable.

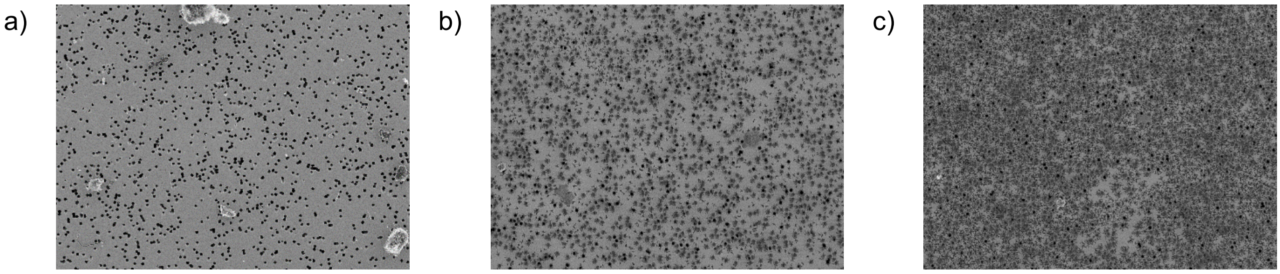


**Figure 38. Quality of the gold-coated nucleopore filters. a) shows a filter with a good quality, whereas b) and c) show a filter surface that is not entirely covered with gold and especially in the case of c) has a lot of holes and ruptures in the gold film. Note: no scale bars are shown, as the images are intended for qualitative comparison only.**

106. The goal of the 3rd pre-test was to establish the counting and classification rules and to harmonise the procedures (Step 3; Figure 36). The same data set of 10 micrographs (containing NM-401 fibres with a mean diameter of 67 nm) was shared with the partners for performing the NOAA counting. The results of the different analysers were compared. After discussions with the group of experts it was concluded that a fully manual analysis would be used for the data analysis of the ILC, supported by a software to count, categorize and measure the objects. The software FibreDetect developed by BAuA was offered and shared with the participating laboratories to help with data analysis. FibreDetect is an image analysis software that can be used for displaying and analysing images such as electron micrographs and facilitates the counting and characterisation of fibrous NOAA [41]. It offers the possibility of image viewing, determination of length, width and projected area as well as classification of NOAA into the different classes depending on their morphology. For further processing of the determined data, the data can be exported as csv file.

107. From the different possible categories, four were identified as key and selected for categorising the different objects:

- Single fibre = High aspect ratio fibre object (HARFO)
- High aspect ratio fibrous agglomerate (HARFA)
- Low aspect ratio fibrous agglomerate (LARFA)
- Low aspect ratio object (LARPO)

108. A total of six different individuals from the participating laboratories took part in the 3rd pre-test. As a first step, a written manual of the FibreDetect was shared and an online video training was held to ensure a good familiarisation with the software and the counting activities to be performed. Total objects counted by each individual (anonymised as Analyser A-F) for the different categories (*e.g.,* HARFO, HARFA) are shown in Figure 39. Mean and standard deviation of counted objects in categories total objects, HARFO, HARFA, LARFO, LARPA and WHO (= fibrous NOAA with potentially critical dimensions) were calculated considering all analysers (Figure 40). Two of the analysers (A and E) showed around double the number of objects counted in all categories. After discussing the results with all the participants, it was found that this was due to analysers counting all the objects of agglomerates consisting of more than four fibres/objects (Figure 41).

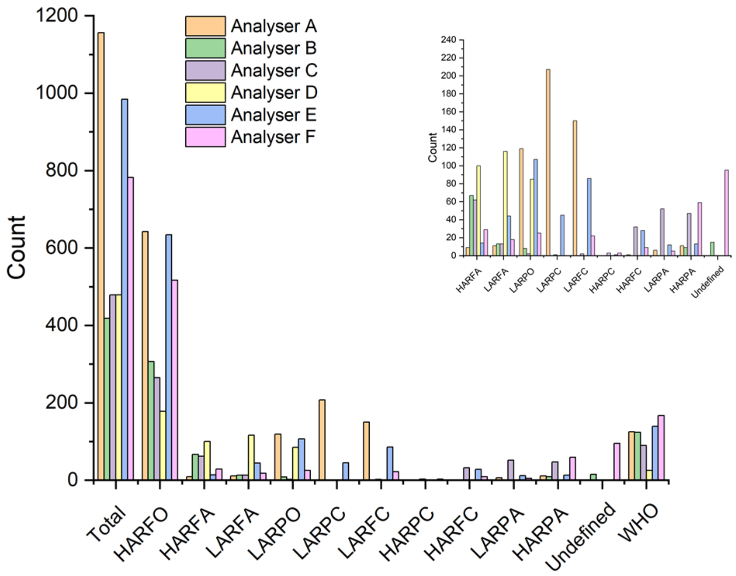


**Figure 39. Total objects counted for the different categories by each analyser. LARPC: low aspect ratio particle cluster; LARFC: low aspect ratio fibrous cluster; HARPC: high aspect ratio particle cluster; HARFC: high aspect ratio fibrous cluster; LARPA: low aspect ratio particle agglomerate; HARPA: high aspect ratio particle agglomerate. Insert: The categories HARFA to Undefined are shown with a different scale to visualise the differences.**

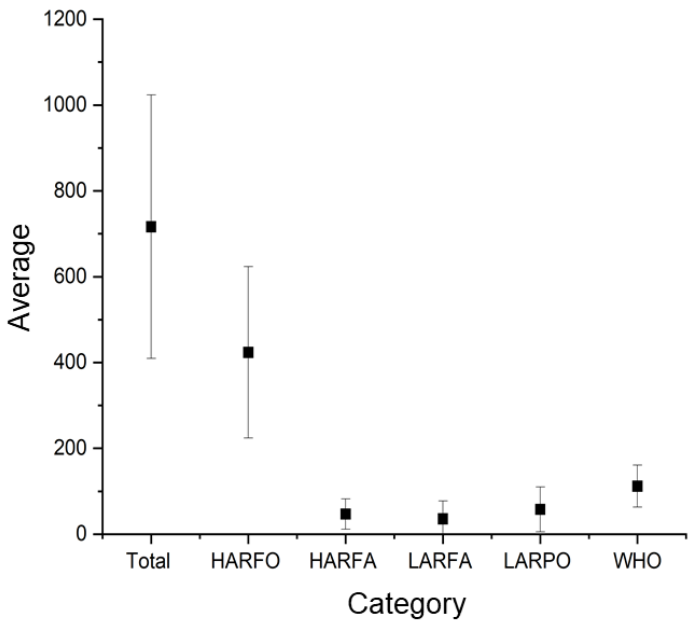


**Figure 40. Mean and standard deviation for total objects, HARFO, HARFA, LARFA, LARPO and WHO categories.**

109. The observed differences between the results in counting were mainly due to the following rules:

- All NOAA, not only fibrous NOAA, need to be counted in order to correctly assess the dustiness of powders containing fibrous NOAA.
- NOAA, which are not entirely visible in the micrograph, need to be counted as ½. NOAA, which are laying entirely on the micrograph are counted as 1.
- An agglomerate composed of 5 or more fibres is counted as 1 (see example in Figure 41). When an agglomerate is composed of 4 or less fibres, each fibre is counted as an independent object.

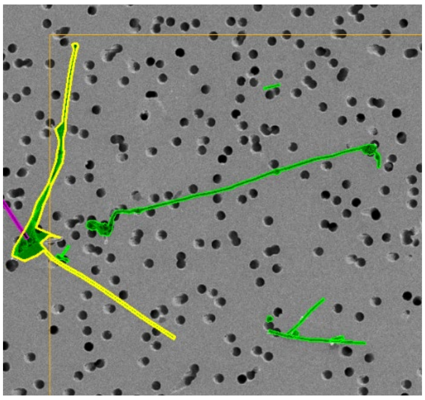

**Figure 41. Example of two different counting procedures applied during the 3rd pre-test: example of agglomerate that could be counted as individual fibres.**

110. In addition, for determining the dustiness of total fibres, the categories HARFO and HARFA are summed up. The WHO-fibres are HARFOs and HARFAs that fulfil the WHO-criteria (named in this context as fibrous NOAA with potentially critical dimensions).

111. The 3rd pre-test resulted in fine-tuned counting and categorisation rules, which were implemented in the final version of the method description for the morphological characterisation used for performing the ILC experiments and data analysis.

112. From the 2nd and 3rd pre-test, a combined procedure for Step 2 and Step 3 (Figure 36) covering the morphological characterisation of aerosols containing fibrous NOAA was developed. The combined procedure covers the image acquisition, the counting and categorisation rules, and the subsequent statistical data analysis.

113. Once the pre-tests were completed and procedure descriptions were available, the ILC tests started. The developed procedures described in the OECD TG 127 [57] for Small Rotating Drum and Fluidizer were closely followed and applied by the participants.

114. A dustiness test consists of three technically valid runs (1x3) performed on the same day. During each run, a sample for a subsequent SEM analysis is collected and real-time concentrations are recorded using an online aerosol measurement tool (e.g., CPC). Micrographs of the SEM sample are taken and analysed as defined in the procedure for morphological characterisation using SEM.

115. For the inter-laboratory comparison, all selected materials were tested once (1x3 runs) by all labs and the variations between the different labs were analysed. For the intra-laboratory comparison, each lab performed three dustiness tests (3x3 runs) for two of the powders. The within-laboratory variations between the different days were analysed.

## 4.4. Metrics and measurands

116. Both dustiness methods, Small Rotating Drum and Fluidizer, include different parameters to be measured depending on the setup and expected use of the generated data. Measurands validated in this ILC for each dustiness method are detailed in Table 23.

**Table 23. Overview of measurands validated (Yes/No) for the evaluation and characterisation of the dustiness of powders containing fibrous NOAA within this ILC.**

| Measurands | Symbol | Unit | Small Rotating Drum | Fluidizer |
|---|---|---|---|---|
| Object number (total number of counted NOAA on the respective analysed area) | $n_{NOAA}$ | # | Yes | Yes |
| | | | | |
| Mean total object number concentration | $C_{total}$ | #/cm³ | Yes | Yes |
| Standard deviation of total object number concentration | σ | #/cm³ | Yes | Yes |
| Upper confidence interval level ($\alpha = 0.05$) of total object number concentration | $H^n_{up}$ | #/cm³ | Yes | Yes |
| Total number-based dustiness index | $DI_N$ | #/mg | Yes | Yes |
| Total number-based emission rate | $E_n$ | #/mg/s | Yes | Yes |
| Fibre number (counted fibrous NOAA on the respective analysed area) | $n_{fibrousNOAA}$ | # | Yes | Yes |
| Fibrous NOAA number concentration (extrapolated) | $C_{fibrousNOAA}$ | #/cm³ | Yes | Yes |
| Fibrous NOAA fraction | $F_{fibrousNOAA}$ | % | Yes | Yes |
| Number of fibrous NOAA with potentially critical dimensions [a] (counted fibrous NOAA with potentially critical dimensions on the respective area) | $n_{criticalfibrousNOAA}$ | # | Yes | Yes |
| Number concentration of fibrous NOAA with potentially critical dimensions [a] (extrapolated) | $C_{criticalfibrousNOAA}$ | #/cm³ | Yes | Yes |
| Fraction of fibrous NOAA with potentially critical dimensions [a] | $F_{criticalfibrousNOAA}$ | % | Yes | Yes |
| Respirable mass-based dustiness index | $DI_R$ | mg/kg | Yes | No |
| Number-based initial dustiness kinetics [b] | $D_k$ | #/mg·s² | Yes | No |
| Time-based dustiness kinetics assessed as the time required to generate 50 % of the total number of particles released [b] | $n_{50}$ | s | Yes | No |

[a] Projected length is measured since in EM only a two-dimensional projection of the three-dimensional objects is shown on the micrographs. The length of fibres that are lying not entirely planar on the sample will be underestimated. [b] Only mandatory for the Small Rotating Drum dustiness method.

117. Metrics validated are the same for both dustiness methods with the exception of the dustiness kinetics, and total mass-based dustiness index, which were only validated for the Small Rotating Drum.

118. The Fluidizer is a method that was designed to disentangle fibrous agglomerates, thus generating an aerosol in which single fibres a predominant. This, together with the low energy input, low amount of powder required and materials low density made a mass-based assessment of the dustiness index of powders containing fibrous NOAA not adequate for the Fluidizer method.

119. In addition, in order to characterise the dustiness of a powder containing fibrous NOAA in detail, several measurands based on the complexity of fibrous NOAA are important to consider including the impact of large agglomerates, which are not fully represented by number-based measurements alone. Depending on the morphology, i.e., length, diameter and aspect ratio, fibrous NOAA are categorised into subclasses. The most relevant example are fibrous NOAA with potentially critical dimensions, i.e. fibrous NOAA, with length > 5 µm, diameter < 3 µm and aspect ratio > 3 (WHO 1997). This is only

achievable from micrographs analysis. For this reason, an important number of the evaluated measurands on the dustiness determination of powders containing fibrous NOAA is based on micrographs analysis. The measurands based on the micrograph analysis are particle number concentration given as total counted NOAA, total fibrous NOAA and total fibrous NOAA with potentially critical dimensions to make a characterisation of the generated aerosol as complete as possible and to support risk assessment. In addition, micrograph analysis enables detailed assessment of agglomerate morphology and cluster structure and, when performed according to the OECD TG 125: 2023 [27], allows determination of the particle size distribution, providing valuable insights into their role in dustiness.

120. For calculating the measurands from Table 23 the equations detailed in the TG 127 [57] were followed. For the calculation of number concentration based on micrograph analysis the collection efficiency onto the substrate is of relevance. The collection efficiency is the ratio of the total number of objects being found lying on the substrate versus the number of objects being sampled. This is usually a number less than 1, considering possible losses during sampling. When fibres are thin, they can enter filter pores, which form much longer channels (~ 20 µm) than the pore size (200-800 nm). Such fibres then do not contribute to the object count in the SEM micrograph and the fibre number in the dust is underestimated. Collection efficiencies vary for different combinations of filters and fibrous NOAA. If the fibre diameter is usually larger than the pore size, collection efficiency can be assumed to be near or equal to 1. If the fibre diameter is much smaller than the pore size, the collection efficiency will be reduced. Thus, a small pore size can significantly increase the collection efficiency. However, very small pore sizes can generate pressure drops at given flow rates that some pumps cannot handle. The collection efficiency of the substrate used for the determination of the concentration was estimated to be 99%.

121. The effective substrate area used was 23 mm corresponding to the 25 mm filter diameter minus the not effective area due to clamping in the sampler, which had a thickness of 1 mm.

122. Real-time aerosol measurement devices like CPC, SMPS, ELPI ® or APS ® used for the dustiness index determination of granular NOAA are not calibrated for fibres and the extent of their use for the quantification of fibrous aerosols is still under investigation (e.g., multiple charging due to the length of fibres). However, since CPC is widely used for aerosol characterisation, and was included in the ILC with powders containing granular NOAA, it was decided, that measuring the total particle number concentration with a CPC would be mandatory on this ILC as well as the determination of the CPC number-based dustiness index and emission rate for comparison reasons.

123. In addition, for the Small Rotating Drum, the number-based ($D_k$) and time-based dustiness kinetics ($n_{50}$) were calculated (Table 23). The purpose of this is to 1) obtain comparable data between the two ILC (powders containing granular and fibrous NOAA), 2) generate results that can provide additional insights in the usability of such instrumentation for powders containing fibrous NOAA, and 3) quality assurance.

## 4.5. Instruments and samplers

124. The online aerosol instrumentation, filters and samplers' details for the gravimetrical and microscopy determination of the dustiness measurands by the different participant laboratories, and for each method is detailed in Table 24.

**Table 24. Details on samplers, filters and aerosol measuring devices used.**

| Method | Laboratory | Gravimetrical mass fraction | Real-time number-based (CPC) | Sampling collection for microscopy |
|---|---|---|---|---|
| Small Rotating Drum | Lab 1 | Sensidyne GK2.69 (PTFE filter 37 mm) at 4.2 L/min | CPC 3007, TSI | VDI 3492 sampling head + nuclepore filters gold-coated with 40/20 nm layer thickness, diameter of 25 mm and pore size of 0.4 µm |
| | Lab 2 | Not applicable | CPC 3750, TSI | |
| Fluidizer | Lab 3 | Not applicable | CPC 5.403, GRIMM Aerosol Technik | |
| | Lab 4 | Not applicable | CPC 3022A, TSI | |

## 4.6. Test materials

125. The ILC intended to cover powders containing fibrous NOAA with different properties within the scope of the TG (powders containing fibres with a diameter <100 nm). For the powder selection, several criteria were considered. Main aspects considered were the inclusion of powders with different 1) chemical composition, 2) characteristics and properties (rigid/flexible, diameter and length), 3) amount of fibrous NOAA with potentially critical dimensions, 4) dustiness level, and 5) manufactured and available in large quantities. The selected powders and their properties are detailed in Table 25. The selection of powders with different dustiness levels was essential to obtain data spanning a broad range allowing dustiness ranking and evaluation of the methods for both, low and high dusty materials. In terms of the fibrous NOAA with potentially critical dimensions content, the selected materials also covered the possible range from low to high. In addition, the selected powders covered the whole nano-range with mean diameters from ranging from 9.5 nm (NC7000) up to 100 nm (ACM-SiC6). From the five powders containing fibrous NOAA, three are considered potentially flexible and two potentially rigid. Currently, there are not exact measurands available for fibre rigidity and an exact threshold is not defined since it is complex and depends on the fibre diameter but also the bending modulus which is material specific [42]. Here we consider materials with diameter > 30 nm to be rigid adopting the cut-off value of 30 nm as in the CLH report for multi-walled carbon nanotubes [43].

**Table 25. Powder selection and detailed information. Diameter, length and specific surface area data: provided by the supplier/manufacturer. Dustiness level and fibrous NOAA with potentially critical dimensions content data: previously partially tested at BAuA using the Fluidizer [11].**

| Material code / ID | Abbreviation | Manufacturer / provider | Composition | Rigidity (according to the diameter)[a] | Mean diameter (nm) | Mean length (nm) | Specific surface area ($m^2/g$) | Fibrous NOAA with potentially critical dimensions content | Dustiness level |
|---|---|---|---|---|---|---|---|---|---|
| Nanocyl NC7000 | NC7000 | Nanocyl | MWCNT | Flexible | 9.5 | 1500 | 250-300 | Moderate | Low |
| JRCNM04000a | NM-400 | JRC | MWCNT | Flexible | 11 | 846 | 254 | Moderate | Low |
| JRCNM40001a | NM-4001 | JRC | MWCNT | Flexible | 15 | ~50000 | >233 | Unknown | Unknown |
| ACM409212 | ACM-SiC6 | Alfa-Chemistry Materials | SiC nanowire | Rigid | 100-500 | 50000-100000 | Unknown | High | Unknown |
| C2158 | C2158 | TCI Chemicals | MWCNT | Rigid | 60-100 | >5000 | Unknown | High | High |

[a] Flexible: mean diameter >30 nm. Rigid: mean diameter <30 nm [43].

126. In order to ensure maximal homogeneity of the powder samples distributed among the different participants, subsamples from the same batch were distributed. The subsampling was performed either by the JRC (i.e., NM-400 and NM-4001) or the respective supplier according to standardised methodologies. Each participant laboratory received the quantity needed for performing the respective tests plus extra runs.

## 4.7. Validation and evaluation of the ILC results

127. In this section, the procedure and data analysis performed to evaluate the data generated in the ILC for powders containing fibrous NOAA is detailed. It is important to note that since the number of laboratories per method was limited to two, certain statistical tests generally used to assess ILC data as detailed in ISO 5725-2:2025 [26] (e.g., Mendel's' h and k statistics and Grubb's test) could not be applied. Moreover, some tests, although applicable, present certain limitations and risk of wrong interpretation when applied to small samples sizes. Thus, when applied, interpretation should be carefully conducted.

## 4.8. Reporting of mean, standard deviation and coefficient of variation (%)

128. When analysing ILC data of small samples, robust statistics for e.g., outlier identification, are not often recommended [22,44]. In those cases, it is preferable to relay on mean and standard deviation evaluation (ISO 13528:2022 [22]) or define arbitrary criteria based on the laboratories experience [44]. Therefore, mean, standard deviation (SD) and coefficient of variation (CV) were determined per test as well as between laboratories. The CV in % was calculated as:

$$\boldsymbol{CV = \frac{\sigma}{\mu} \times 100} \qquad \text{Equation 1}$$

σ Standard deviation

μ Mean of the considered data.

129. The evaluation of these data together with their graphical visualisation by using different bar and box plots served for a first inspection and interpretation.

130. CV% where compared to those obtained for powders containing granular NOAA for which a more robust statistical analysis could be performed.

131. In addition, the Pearson correlation between laboratories was studied.

### 4.8.1. Cochran C test and Dixon's Q test

132. Two statistical tests where applied. The Cochran C statistic, as recommended in the ISO 5725-2:2025 [26], and Dixon's Q-test were used to examine the within laboratories consistency and detection of outliers.

133. The Cochran test was used to assess the within laboratory consistency. Cochran statistic *C* is defined as

$$\boldsymbol{C = \frac{\sigma_{max}^2}{\sum_{i=1}^{p} \sigma_i^2}} \qquad \text{Equation 2}$$

$\sigma^2$ Standard deviation

$\sigma_{max}^2$ Highest standard deviation in the set of standard deviations tested.

134. Cochran test was applied first to test the homogeneity of variances of both participants. In case an outlier was detected for one laboratory, if repeated measurements were available (i.e. three tests of three replicates for materials NM-4001 and C2158) they were used to investigate the laboratory consistency [45]. It is important to note that the Cochran test, is a one-sided upper limit variance outlier statistical test in which the within laboratory consistency is analysed only based on whether the highest standard deviation of the group deviates significantly from the rest.

135. In addition, the Dixon's Q-test was used to further examine data outliers. The Dixon's Q-test is an alternative test useful to detect outliers in small sample sizes 3 < 30 [46,47]. This test has been previously used in some interlaboratory comparisons with limited sample sizes [48]. The test statistics are calculated as defined in $PW_{min} = x\mathbf{2} - x_1 x_n \text{-} x_1$ Equation 3 and $PW_{max} = \frac{x_n - x_{n-1}}{x_n - x_1}$ Equation 4 for n = 3-7 and $PW_{min} = \frac{x_2 - x_1}{x_{n-1} - x_1}$ Equation 5 and $PW_{max} = \frac{x_n - x_{n-1}}{x_n - x_2}$ Equation 6 for n = 8-10.

$$PW_{min} = \frac{x_2 - x_1}{x_n - x_1} \qquad \text{Equation 3}$$

$$PW_{max} = \frac{x_n - x_{n-1}}{x_n - x_1} \qquad \text{Equation 4}$$

$$PW_{min} = \frac{x_2 - x_1}{x_{n-1} - x_1} \qquad \text{Equation 5}$$

$$PW_{max} = \frac{x_n - x_{n-1}}{x_n - x_2} \qquad \text{Equation 6}$$

136. In sum, Cochran and Dixon's Q-test were applied to analyse the within- and between-laboratories differences, and results were carefully interpreted together with the descriptive statistics to detect possible outliers and perform a data assessment. When an outlier was detected, possible reasons were discussed with the expert group, results were only discarded if non-solvable issues where detected. No values were removed.

### 4.8.2. z- score

137. The ISO 13528:2022 [22] recommends the use of the z-score to assess the consistency of the data from the different laboratories. The z-score is defined as:

$$z_i = \frac{x_i - X}{\sigma} \qquad \text{Equation 7}$$

| | |
|---|---|
| $x_i$ | Test results from the i-th laboratory |
| $X$ | Robust estimate of the group average |
| $\sigma$ | Robust estimate of the group standard deviation. |

For the calculation of the z-score, it is important to have excluded significant outliers prior calculation. Results interpretation is as follows:

if $|z| \leq 2$; the performance is satisfactory/acceptable;

if $2 < |z| \leq 3$; the performance is questionable/warning signal;

if $|z| > 3$; the performance is unsatisfactory/unacceptable.

138. The robust estimation of $X$ and $s$ where conducted following Algorithm A detailed in ISO 13528:2022-08 Annex C.3 [22] with the variation for small number of participants (2 participants) introduced in Szewczak & Bondarzewski (2016) [44] as follows:

$X = median\ of\ x_{ij}$ (ij= 1,2, …, p)

$\sigma = 1.483 \times median\ of\ |x_{ij} - X|$

$\delta = 1.5 \times \sigma$

$x_{ij}$ Results for all tests performed by the two laboratories.

139. For each $x_{ij}$ the following calculation is performed:

$$x^*_{ij} = \begin{cases} X - \delta & \text{when} \quad x_{ij} < X - \delta \\ X + \delta & \text{when} \quad x_{ij} > X + \delta \\ x_{ij} & \text{otherwise} \end{cases}$$

and new values of $X$ and s are calculated as:

$$\boldsymbol{X = \sum_{ij=1}^{p} x^*_{ij}/p} \qquad \text{Equation 8}$$

$$\boldsymbol{s = 1.134 \times \sqrt{\sum_{ij=1}^{p} (x^*_{ij} - X)^2 / (p-1)}} \qquad \text{Equation 9}$$

The robust estimates of $X$ and s are then derived from an iterative calculation until the process converges (i.e., no changes from one iteration to the next).

## 4.9. Results

### 4.9.1. Small Rotating Drum intra- and interlaboratory comparison ($DI_{N\text{-}SEM}$ and $DI_{N\text{-}CPC}$)

Data generated for total number-based dustiness index obtained from micrograph analysis ($DI_{N\text{-}SEM}$) and CPC data ($DI_{N\text{-}CPC}$) by the two participant laboratories (Lab 1 and Lab 2) is shown in Figure 42 together with between laboratories correlation (see Annex F for detailed results). For $DI_{N\text{-}CPC}$ both laboratories showed comparable dustiness values, with a Pearson coefficient of 0.96 and test CV lower than 27% (Table 26). For all materials Lab 2 showed consistently slightly higher $DI_{N\text{-}CPC}$ values than Lab 1 (1.3-3.8-fold). On the contrary, for $DI_{N\text{-}SEM}$, higher differences between laboratories were observed (Pearson coefficient of less than 0.1), with Lab 2 values being in average 25-fold higher than Lab 1. For $DI_{N\text{-}SEM}$, the test CV was between 10-73% for Lab 1, and 3-64% for Lab 2 (

140. Table 26), which is comparable to what was obtained for powders containing granular NOAA (1.1-58.6%; Table 10).

After discussing with the two laboratories possible reasons for the big discrepancy on the $DI_{N\text{-}SEM}$ generated values, it was detected that Lab 1 had used a sampling flow of 0.3 L/min instead of the 4.2 L/min stablished in the procedure, and used by Lab 2. Although in the dustiness calculation one takes into consideration the sampling flow and time, the 10-fold difference in the sampling flow was most likely the cause of this discrepancy. The number of objects visible in the obtained micrographs from Lab 1 were lower than 5 with several images containing no objects at all. This low number of objects count, below what is considered adequate for optimal counting, has a bias to lower estimated concentrations. Other possible effects causing the lower $DI_{N\text{-}SEM}$ values in Lab 1 are that at lower sampling flows there are higher losses due to longer residence time in the tubbing [49], and that due to lower face velocity there are higher losses on bigger objects and agglomerates collected [50].

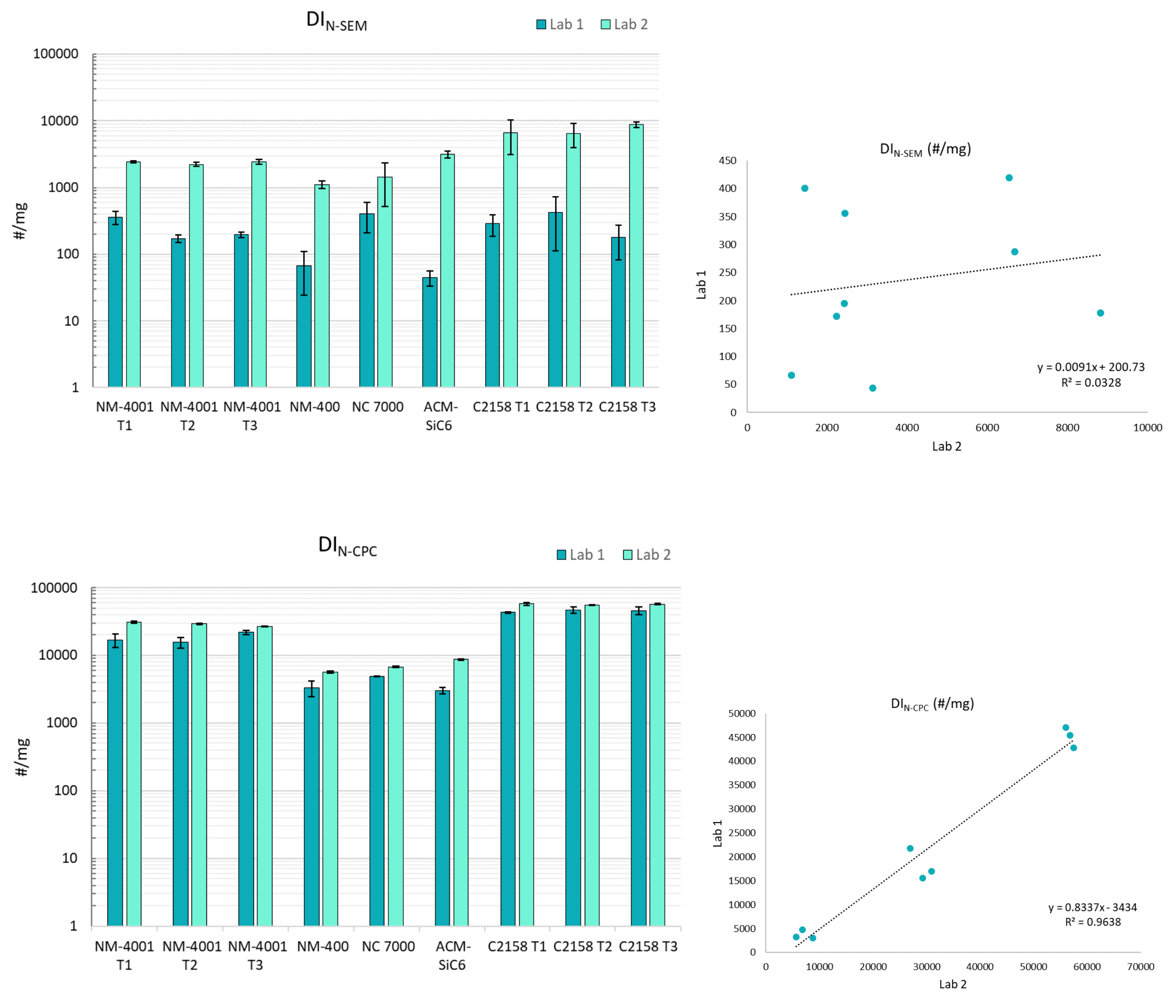


**Figure 42. Small Rotating Drum Lab 1 and 2 results of total number-based dustiness index calculated based on the micrographs analysis ($DI_{N\text{-}SEM}$) and CPC data ($DI_{N\text{-}CPC}$). Each bar corresponds to one test of three replicates and standard deviation. Three tests are available for NM-40001 and C2158. Note: log scale used.**

**Table 26. Small Rotating Drum test coefficient of variation (%) per material and metric. For NM-4001 and C2158 the CV for each individual test (3 tests) are presented as a range (min-max), the value in parentheses corresponds to the combined CV from all three tests.. N/A: not available. $DI_{N\text{-}SEM}$: SEM-based total number dustiness index; $DI_{N\text{-}CPC}$: CPC-based total number dustiness index; $DI_{fibrousNOAA}$: fibrous NOAA with potentially critical dimensions dustiness index.**

| Laboratory (n) | Material | $DI_{N\text{-}SEM}$ | $DI_{N\text{-}CPC}$ | $DI_{fibrousNOAA}$ |
|---|---|---|---|---|
| Lab 1 (3) | NM-400 | 64.0 | 27.0 | 96.0 |
| Lab 1 (3) | NC7000 | 48.0 | 1.0 | 118.0 |
| Lab 1 (3) | ACM-SiC6 | 26.0 | 11.5 | 67.0 |
| Lab 1 (3x3) | NM-4001 | 10.0-22.0 (40.2) | 8.1-22.5 (20.9) | 27.0-54.0 (71.3) |
| Lab 1 (3x3) | C2158 | 36.0-73.0 (67.2) | 2.2-13.3 (10.0) | 64.0-87.0 (93.5) |
| Lab 2 (3) | NM-400 | 13.0 | 4.0 | 30.0 |
| Lab 2 (3) | NC7000 | 64.0 | 2.0 | 49.0 |
| Lab 2 (3) | ACM-SiC6 | 11.0 | 2.4 | 7.0 |
| Lab 2 (3x3) | NM-4001 | 3.0-9.0 (7.3) | 1.7-3.9 (6.4) | 8.0-27.0 (22.1) |
| Lab 2 (3x3) | C2158 | 10.0-53.0 (34.1) | 1.2-3.9 (2.6) | 16.0-56.0 (36.1) |

141. Intra-laboratory outliers’ analysis was conducted using Cochran (Figure 43) and Dixon’s Q-test (

142. Table 27 and Annex L). The calculated Cochran C statistic was below the critical value for all material groups indicating no significant differences between the higher standard deviation and the rest of the group. With the Dixon's Q-test, one outlier was identified (α 1%) for Lab 1, C2158 material and SEM dustiness index ($DI_{N\text{-}SEM}$). The outlier was not identified at α of 5%. No data was removed as there were no indications for a wrong image analysis or any issues during the dustiness test.

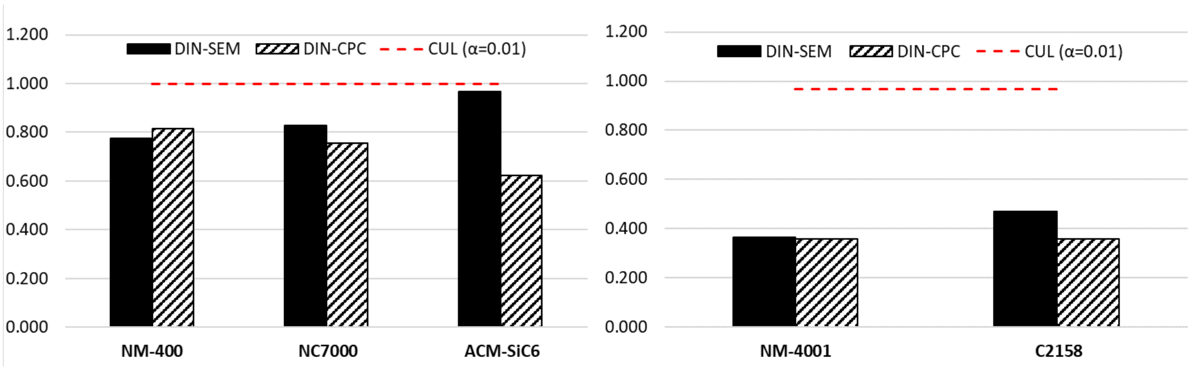


**Figure 43. Cochran C test results for the Small Rotating Drum. $DI_{N\text{-}SEM}$: SEM-based total number dustiness index; $DI_{N\text{-}CPC}$: CPC-based total number dustiness index.**

**Table 27. Dixon's Q test results for Lab 1 and 2 and for SEM-based total number dustiness index *($DI_{N\text{-}SEM}$)* and CPC-based total number dustiness index *($DI_{N\text{-}CPC}$)*. Outlier highlighted in red.**

| Material | Q (5%) | Q (1%) | Lab 1 | | | | Lab 2 | | | |
|---|---|---|---|---|---|---|---|---|---|---|
| | | | $DI_{N\text{-}SEM}$ | | $DI_{N\text{-}CPC}$ | | $DI_{N\text{-}SEM}$ | | $DI_{N\text{-}CPC}$ | |
| | | | Min | Max | Min | Max | Min | Max | Min | Max |
| NM-400 | 0.941 | 0.988 | 0.446 | 0.554 | 0.256 | 0.744 | 0.071 | 0.929 | 0.175 | 0.825 |
| NC7000 | 0.941 | 0.988 | 0.381 | 0.619 | 0.025 | 0.975 | 0.526 | 0.474 | 0.369 | 0.631 |
| ACM-SiC6 | 0.941 | 0.988 | 0.323 | 0.677 | 0.760 | 0.240 | 0.410 | 0.590 | 0.527 | 0.473 |
| NM-4001 | 0.512 | 0.635 | 0.106 | 0.378 | 0.059 | 0.104 | 0.205 | 0.137 | 0.088 | 0.069 |
| C2158 | 0.512 | 0.635 | 0.296 | *0.655* | 0.210 | 0.148 | 0.135 | 0.059 | 0.104 | 0.023 |

143. The z-score was calculated for both, SEM and CPC number-based dustiness index (Figure 44 and Annex L). Although, for SEM high differences were observed between both laboratories, the z-score was under 2, indicating satisfying or acceptable results. It is important to note that the z-score is designed to be applied for 3 or more laboratories. Although here a modification to be used on two laboratories was applied, results should be interpreted with care.

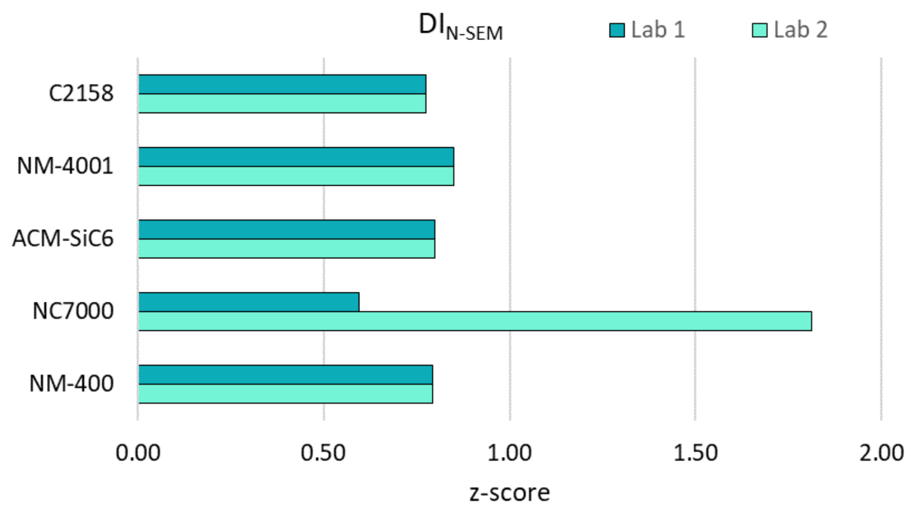

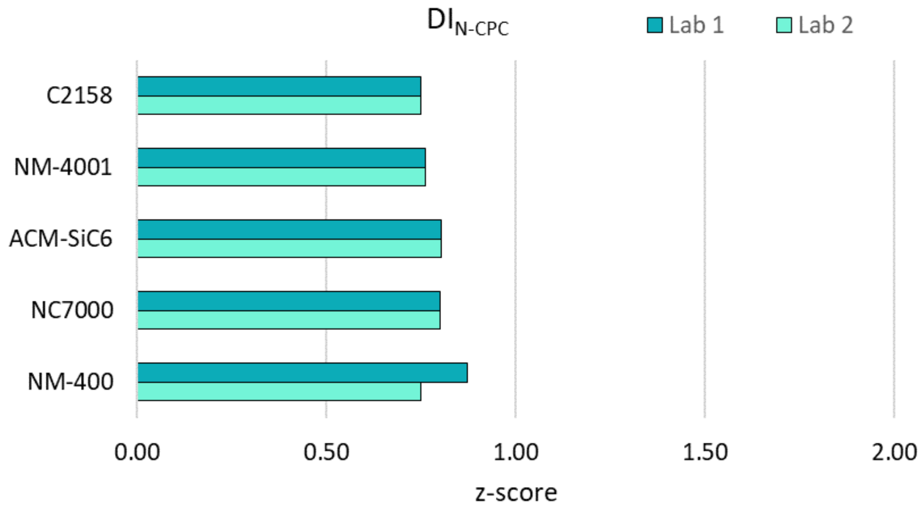


**Figure 44. Z-score for Small Rotating Drum SEM-based total number dustiness index *($DI_{N-SEM}$)* and CPC-based total number dustiness index *($DI_{N-CPC}$)*.**

## 4.9.2. Fluidizer intra- and interlaboratory comparison ($DI_{N-SEM}$ and $DI_{N-CPC}$)

144. Total number-based dustiness index calculated from micrograph analysis ($DI_{N-SEM}$) and CPC data ($DI_{N-CPC}$) for Lab 3 and 4 are shown in Figure 45 together with the correlation between the two laboratories (see Annex J for detailed results). Results showed comparable dustiness index ($DI_{N-SEM}$ and $DI_{N-CPC}$) for both laboratories, with Lab 4 showing consistently slightly higher values than Lab 3. This difference was more pronounced for ACM-SiC6 and NM-400 with Lab 4 showing 4-5 times higher values than Lab 3 for both $DI_{N-SEM}$ *and* $DI_{N-CPC}$. Overall, the good Pearson coefficient between the two laboratories for both, $DI_{N-SEM}$ *and* $DI_{N-CPC}$ of 0.88 and 0.91 showed the good agreement between the data generated by both laboratories.

145. The test CV percentage for $DI_{N-SEM}$ and $DI_{N-CPC}$ ranged from 1.0 to 35.0% for Lab 3 (

146. Table 28), which is comparable to what was obtained for powders containing granular NOAA (Table 17). For Lab 4 CV percentage for $DI_{N\text{-}CPC}$ was similar to Lab 3 (5.0 to 36.0%). Conversely, slightly higher values were obtained for $DI_{N\text{-}SEM}$ (up to 56%) for ACM-SiC6 and NM-400.

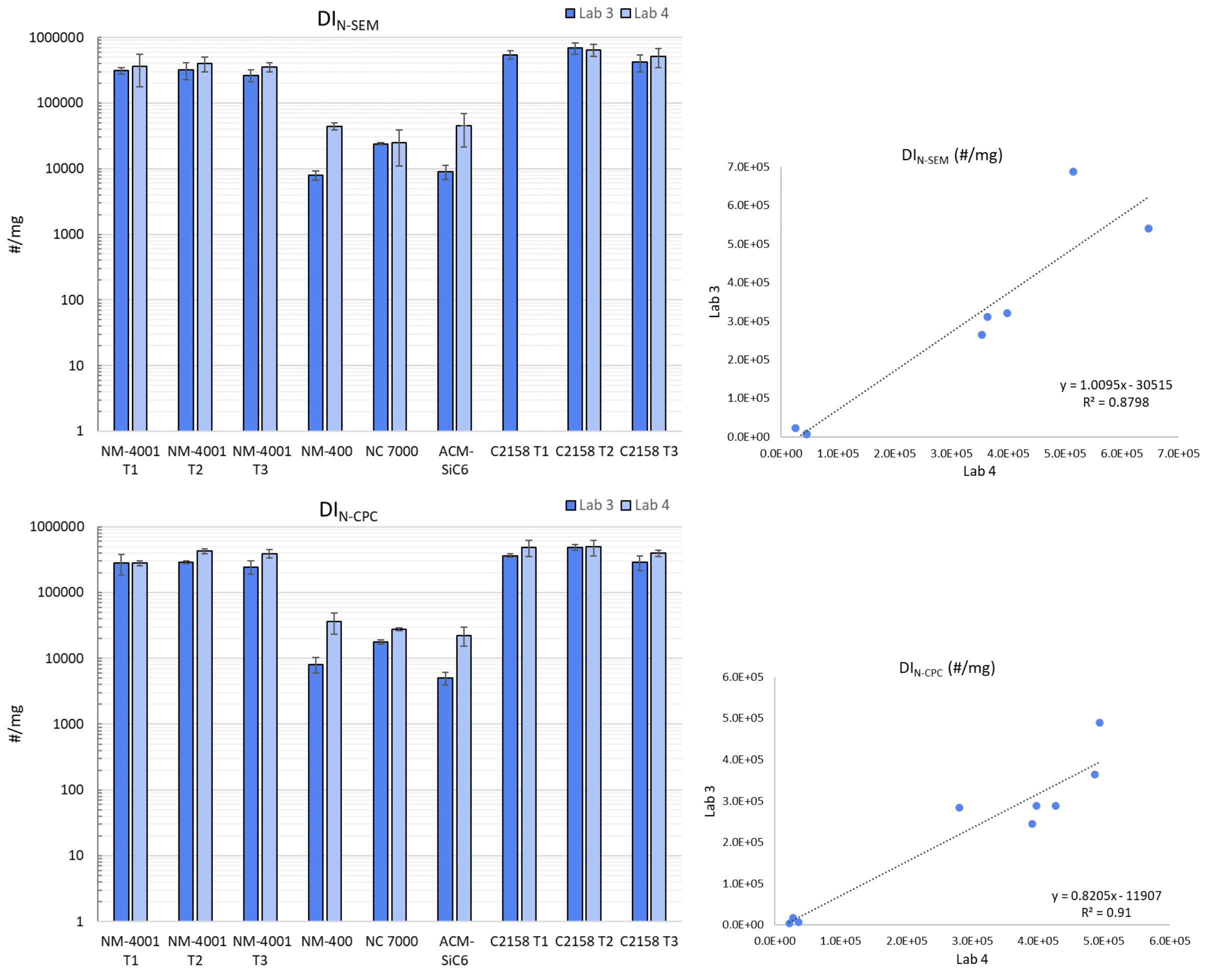


**Figure 45. Fluidizer Lab 3 and 4 results of total number-based dustiness index calculated based on the micrographs analysis and CPC data. Each bar corresponds to one test of three replicates and standard deviation. Three tests are available for NM-40001 and C2158. Note: log scale used. SEM-based total number dustiness index *($DI_{N\text{-}SEM}$)* and CPC-based total number dustiness index *($DI_{N\text{-}CPC}$)*.**

**Table 28. Fluidizer test variability (%) per material. For NM-4001 and C2158 the CV for each individual test (3 tests) are presented as a range (min-max), the value in parentheses corresponds to the combined CV from all three tests. N/A: not available. SEM-based total number dustiness index *($DI_{N-SEM}$)* and CPC-based total number dustiness index *($DI_{N-CPC}$)*; *$DI_{fibrousNOAA}$*: fibrous NOAA with potentially critical dimensions dustiness index.**

| Laboratory (n) | Material | $DI_{N-SEM}$ | $DI_{N-CPC}$ | $DI_{fibrousNOAA}$ |
|---|---|---|---|---|
| Lab 3 (3) | NM-400 | 16.0 | 26.8 | 36.0 |
| Lab 3 (3) | NC7000 | 4.0 | 7.1 | 1.0 |
| Lab 3 (3) | ACM-SiC6 | 24.0 | 22.9 | 28.0 |
| Lab 3 (3x3) | NM-4001 | 12.0-29.0 (21.1) | 5.7-34.5 (22.2) | 18.0-30.0 (21.8) |
| Lab 3 (3x3) | C2158 | 15.0-29.0 (28.2) | 6.0-24.8 (25.9) | 15.0-28.0 (27.2) |
| Lab 4 (3) | NM-400 | 12.0 | 35.6 | 12.0 |
| Lab 4 (3) | NC7000 | 56.0 | 5.0 | 82.0 |
| Lab 4 (3) | ACM-SiC6 | 53.0 | 32.1 | 55.0 |
| Lab 4 (3x3) | NM-4001 | 16.0-52.0 (30.3) | 8.9-14.3 (20.6) | 4.0-60.0 (42.7) |
| Lab 4 (3x2) | C2158 | 20.0-32.0 (23.9) | 10.6-27.5 (23.0) | 23.0-31.0 (25.3) |

147. Intra- and inter- laboratory outliers' analysis was conducted using Cochran (Figure 46) and Dixon's Q-test (

148. Table 29 and Annex L). In both cases, no outliers were identified, which is consistent with the good correlations observed between the two laboratories. The calculate Cochran C static for each material group was below the critical value for α of 1%, indicating that the highest standard deviation of the group does not deviate significantly from the rest. For Dixon's Q test, min and max calculated statistics were also below the critical Q values at α of 5 and 1% indicating no significantly deviations between the calculated dustiness index values between laboratories and test replicates.

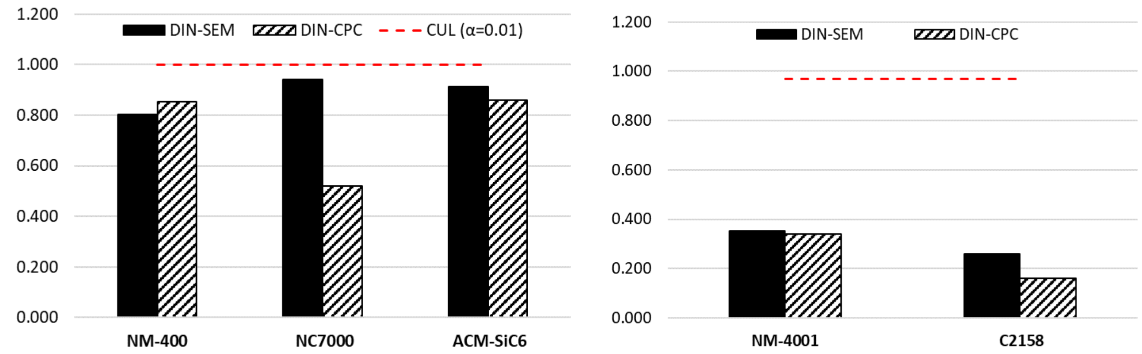


**Figure 46. Cochran C test results for the Fluidizer SEM-based total number dustiness index *($DI_{N\text{-}SEM}$)* and CPC-based total number dustiness index *($DI_{N\text{-}CPC}$)*.**

**Table 29.Dixon's Q test results for Lab 3 and 4 and for SEM-based total number dustiness index *($DI_{N\text{-}SEM}$)* and CPC-based total number dustiness index *($DI_{N\text{-}CPC}$)*.**

| Material | Q (5%) | Q (1%) | Lab 3 | | | | Lab 4 | | | |
|---|---|---|---|---|---|---|---|---|---|---|
| | | | $DI_{N\text{-}SEM}$ | | $DI_{N\text{-}CPC}$ | | $DI_{N\text{-}SEM}$ | | $DI_{N\text{-}CPC}$ | |
| | | | Min | Max | Min | Max | Min | Max | Min | Max |
| NM-400 | 0.941 | 0.988 | 0.776 | 0.224 | 0.075 | 0.925 | 0.883 | 0.117 | 0.177 | 0.823 |
| NC7000 | 0.941 | 0.988 | 0.297 | 0.703 | 0.140 | 0.860 | 0.538 | 0.462 | 0.742 | 0.258 |
| ACM-SiC6 | 0.941 | 0.988 | 0.714 | 0.286 | 0.834 | 0.166 | 0.350 | 0.650 | 0.613 | 0.387 |
| NM-4001 | 0.512 | 0.635 | 0.379 | 0.443 | 0.118 | 0.482 | 0.339 | 0.245 | 0.156 | 0.083 |
| C2158 | 0.512 | 0.635 | 0.196 | 0.146 | 0.360 | 0.035 | 0.512 | 0.373 | 0.026 | 0.067 |

149. Finally, the z-score (Figure 47 and Annex L) was calculated and found to be under 2 for $DI_{N\text{-}CPC}$ and $DI_{N\text{-}SEM}$ and all materials, indicating satisfying or acceptable results.

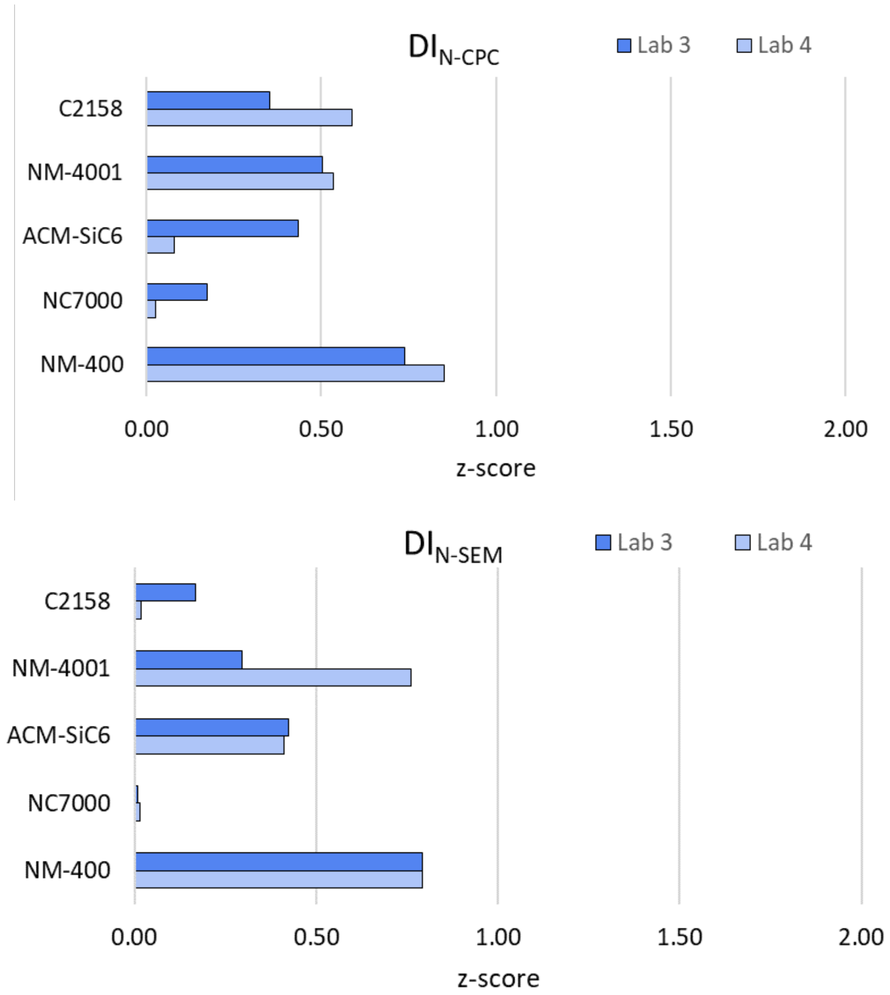

**Figure 47. Calculated Z-score for Fluidizer SEM-based total number dustiness index ($DI_{N-SEM}$) and CPC-based total number dustiness index ($DI_{N-CPC}$) for Lab 3 and 4.**

### 4.9.3. Micrograph analysis dustiness index vs. CPC-based dustiness index

150. The use of real-time instrumentation such as CPC or SMPS to measure particle number concentration of aerosols containing fibrous NOAA is still under investigation. In this ILC, the use of CPC was made mandatory due to its importance in aerosol measurements as well as to ensure comparability with results obtained for powders containing granular NOAA. Therefore, here we explore the obtained correlation between dustiness index calculated from CPC data and micrograph analysis obtained for Small Rotating Drum (Figure 48) and Fluidizer (Figure 49) dustiness methods.

151. Results showed that dustiness index obtained from CPC ($DI_{N-CPC}$) and from the micrograph counting ($DI_{N-SEM}$) were in general comparable to each other with Pearson coefficients >0.6. Specifically, for the Fluidizer, very high correlations were obtained, with Pearson coefficients of 0.91 for Lab 3 and 0.77 for Lab 4. Only for the Lab 1 (Small Rotating Drum), a correlation <0.6 was obtained. This lower correlation degree for Lab 1 was likely due to the low flow used for sampling (0.3 L/min instead of 4.2 L/min) which yielded $DI_{N-SEM}$ values much lower than the CPC and the Lab 2. These results show that CPC data, although not able to fully represent the complexity of aerosols generated from materials containing fibrous NOAA, and thus not applicable as a stand-alone measurand, can be used to determine a realistic value of total number-based dustiness index.

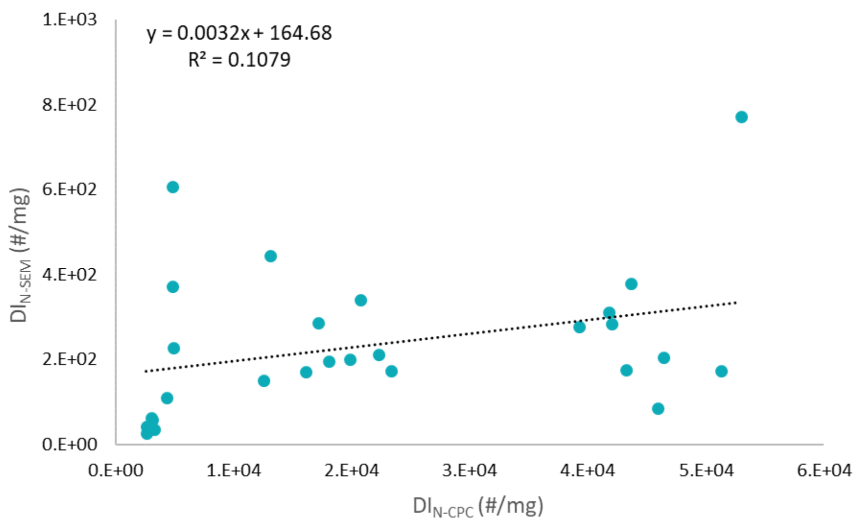

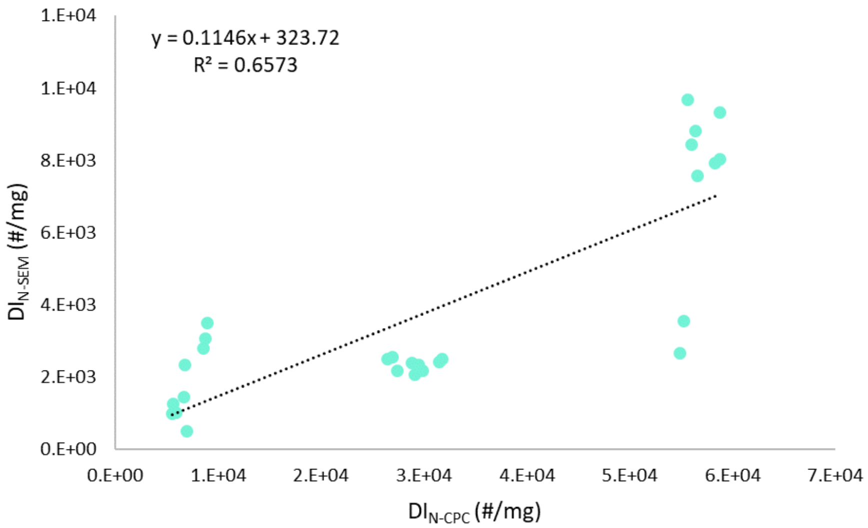


**Figure 48. SEM vs CPC dustiness index for Lab 1 (top) and 2 (bottom) obtained with the Small Rotating Drum. *$DI_{N\text{-}SEM}$*: SEM-based total number dustiness index; *$DI_{N\text{-}CPC}$*: CPC-based total number dustiness index.**

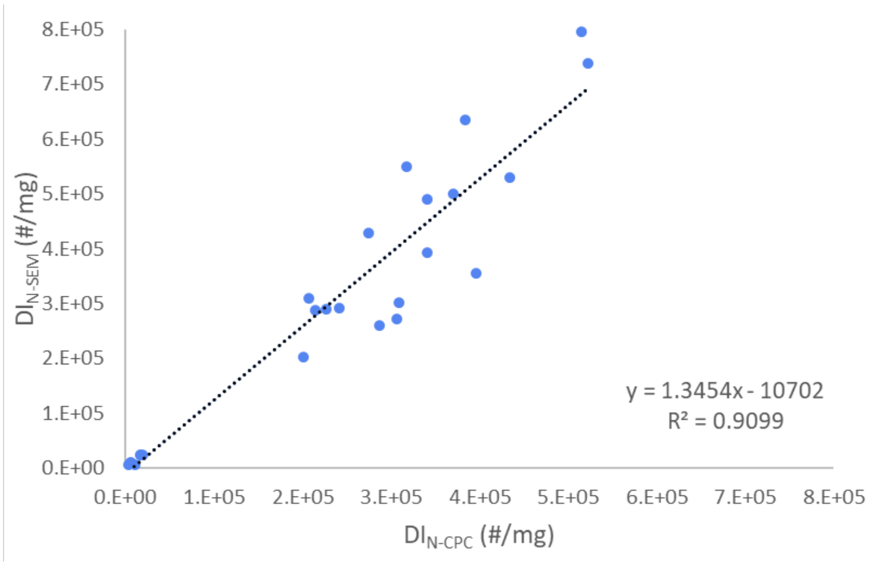

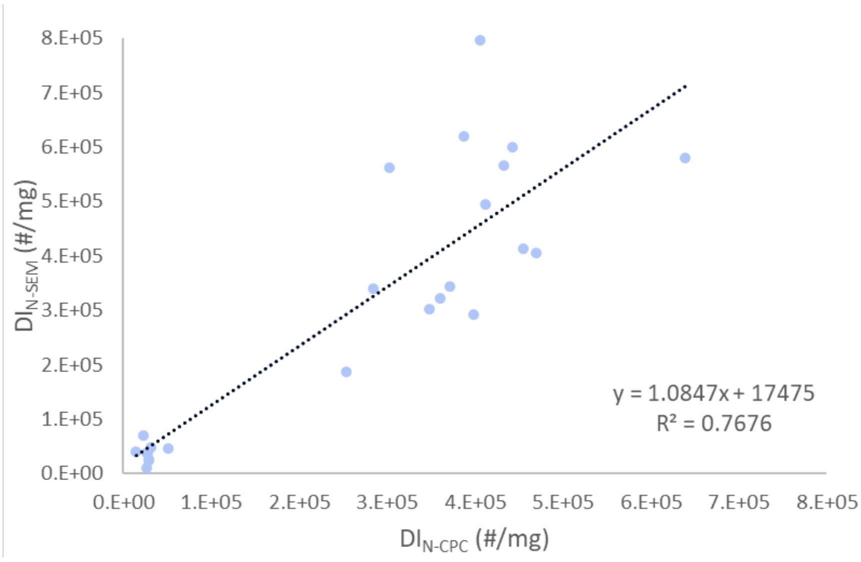


**Figure 49. SEM vs CPC dustiness index for Lab 3 (top) and 4 (bottom) obtained with the Fluidizer. $DI_{N\text{-}SEM}$: SEM-based total number dustiness index; $DI_{N\text{-}CPC}$: CPC-based total number dustiness index**

### 4.9.4. Dustiness time-series analysis

152. Time series obtained with the CPC during the dustiness experiments are shown in and Figure 50 and Figure 51, for Small Rotating Drum Lab 1 and Lab 2. For both laboratories, time-series were reproducible and followed the same trend in each replicate for all materials assessed. In addition, the time-series were comparable between laboratories and no pattern differences were observed between materials. Small rotating drum time-series were always characterised by a constant and sharp increase of the concentration during the first 30 seconds, and an exponential decay after the 60 seconds, once the drum is stopped.

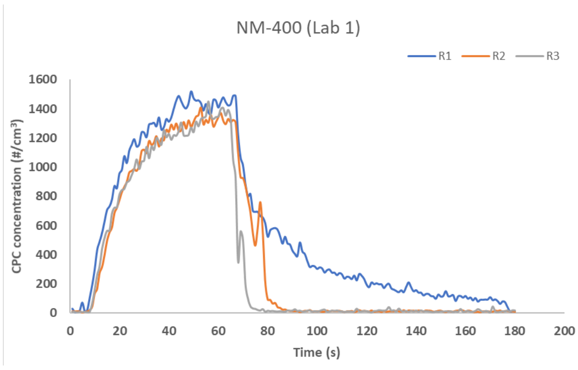


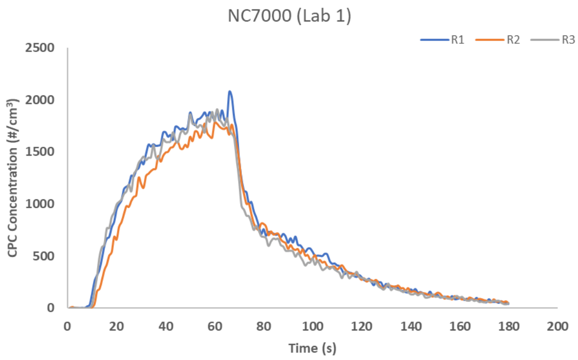

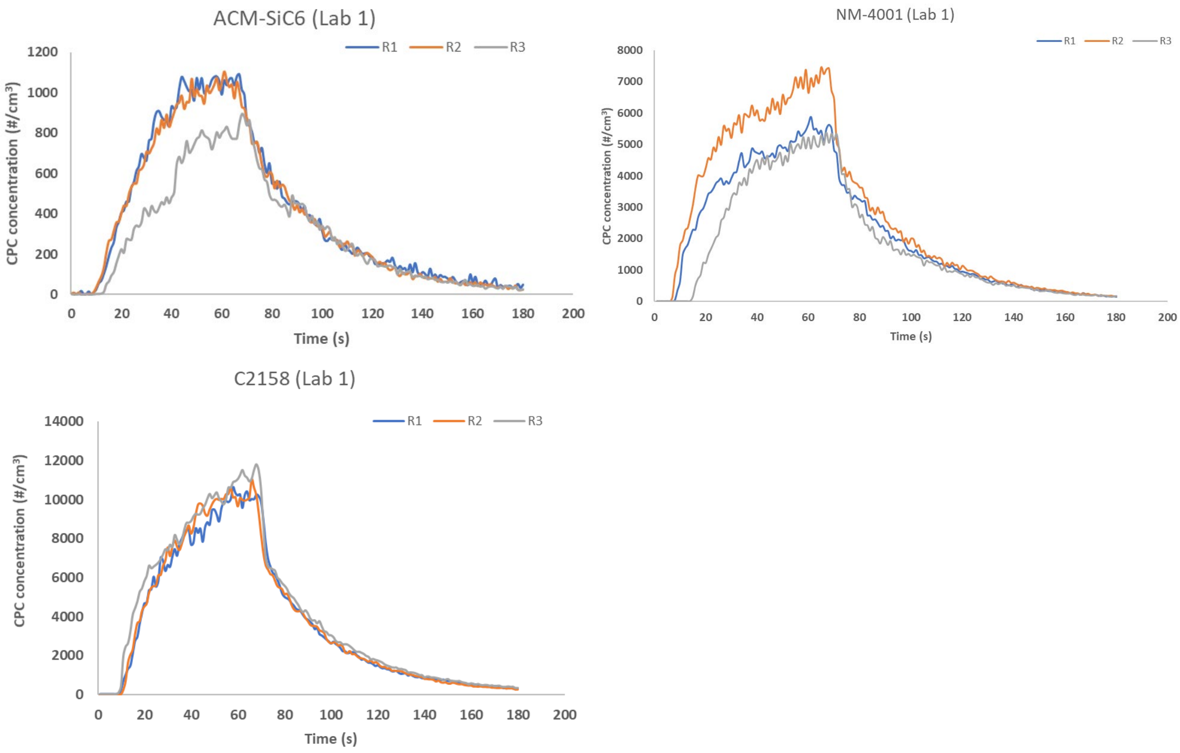


**Figure 50. Small Rotating Drum Lab 1 particle number concentration time series during each test and material. For NM-4001 and C2158 only test 1 data is shown as example.**

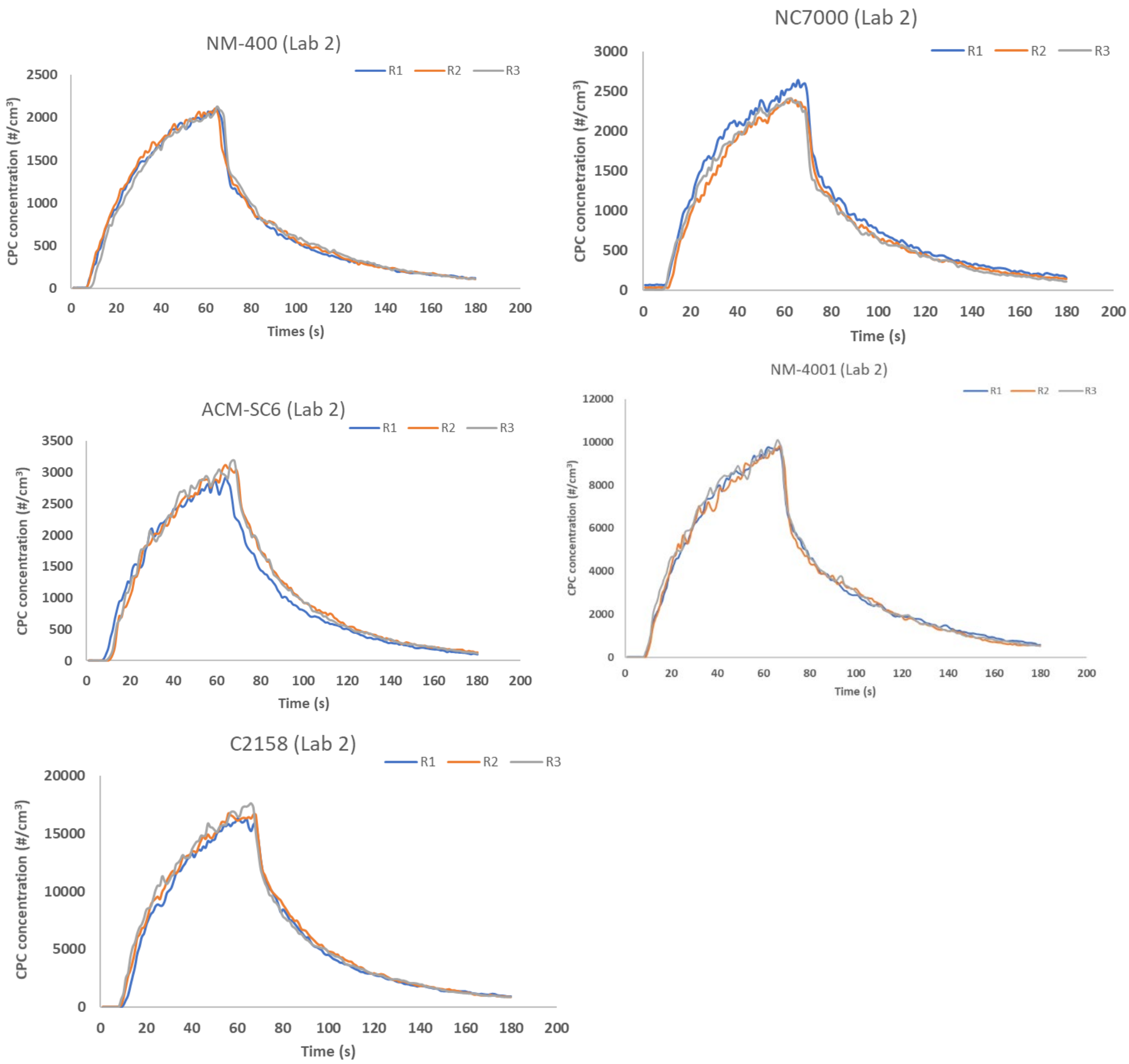


**Figure 51. Small Rotating Drum Lab 2 particle number concentration time series during each test and material. For NM-4001 and C2158 only test 1 data is shown as example.**

153. Time-series obtained with the CPC during Fluidizer dustiness tests and for all materials are plotted in Figure 52 (Lab 3) and Figure 53 (Lab 4). For Lab 3 data (Figure 52), reproducible time series concentration was obtained for the five materials studied with slight variations between replicates. The only exception to this was the first replicate for NM-400, which showed the same trend but concentrations were 1.5 times higher than during replicate 2 and 3. Similarly, for NM-4001, the first replicate showed higher concentration than replicate 2 and 3, and concentrations were more stable through the test. As opposed to the Small Rotating drum obtained time-series, different emission patterns were observed for the different materials. For NM-400 and NM-4001 a progressive increase of the concentrations occurs during the first approximately 20 minutes until a plateau is reached. For NC7000 and C2158 this occurs in less than 10 minutes. Conversely, for ACM-SiC6 a first concentration burst is observed during the first few minutes, followed by a decrease of concentrations until a plateau is reached. This behaviour resembles the behaviour observed for the powders containing granular NOAA. Patterns observed for Lab 4 data (Figure 53) were in general comparable to those observed for Lab 3 in the sense that an initial burst was observed and the concentrations reached a plateau. However,

Lab 4 showed a faster increase than Lab 3 on concentration at the beginning of the test. This was slightly different for ACM-SiC6 and C2158, in which two replicates showed a slight decrease after the first burst and before reaching stable concentrations.

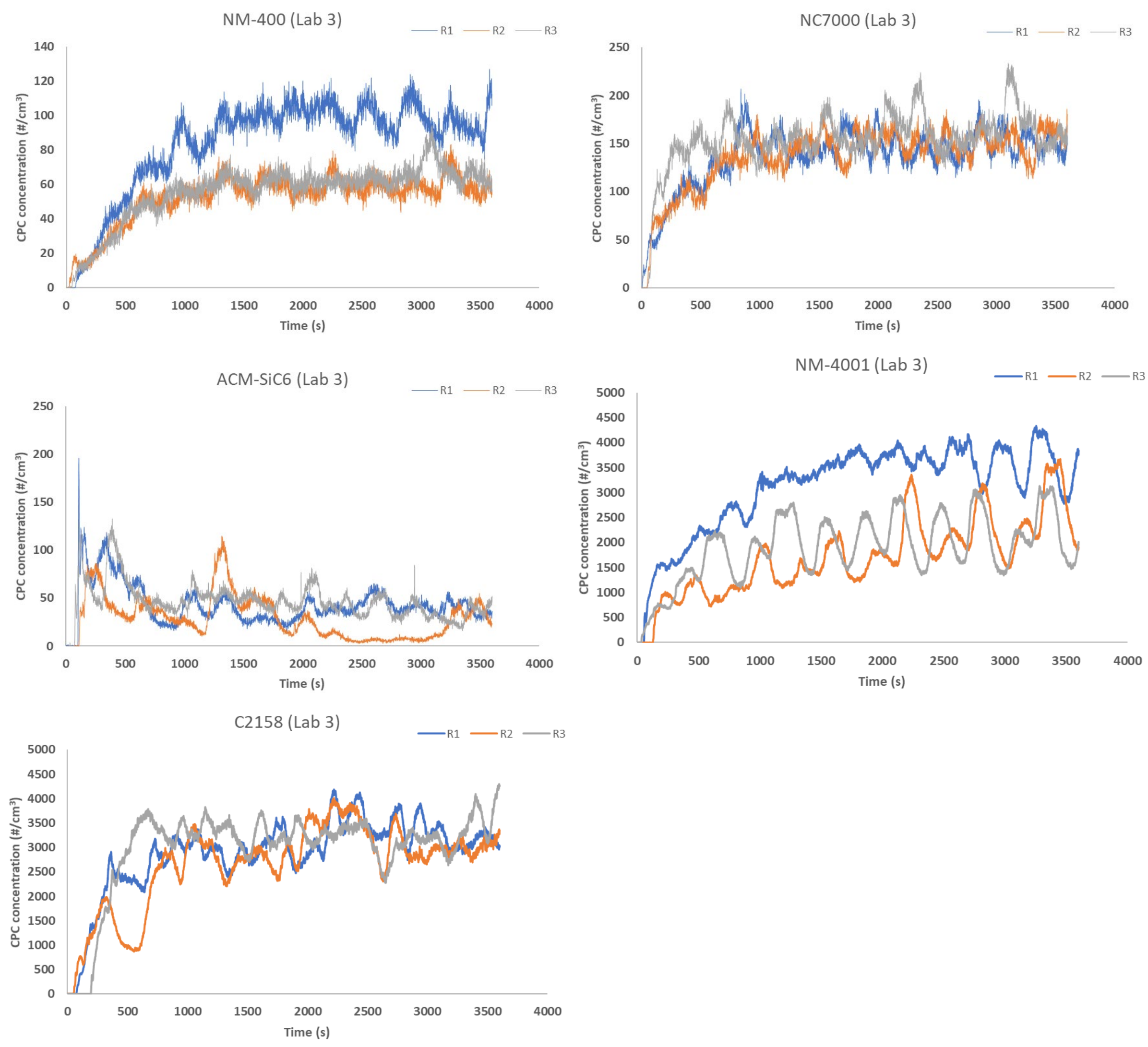


**Figure 52. Fluidizer Lab 3 CPC particle number concentration time series during each test and material. For NM-4001 and C2158 only data of one representative test is shown.**

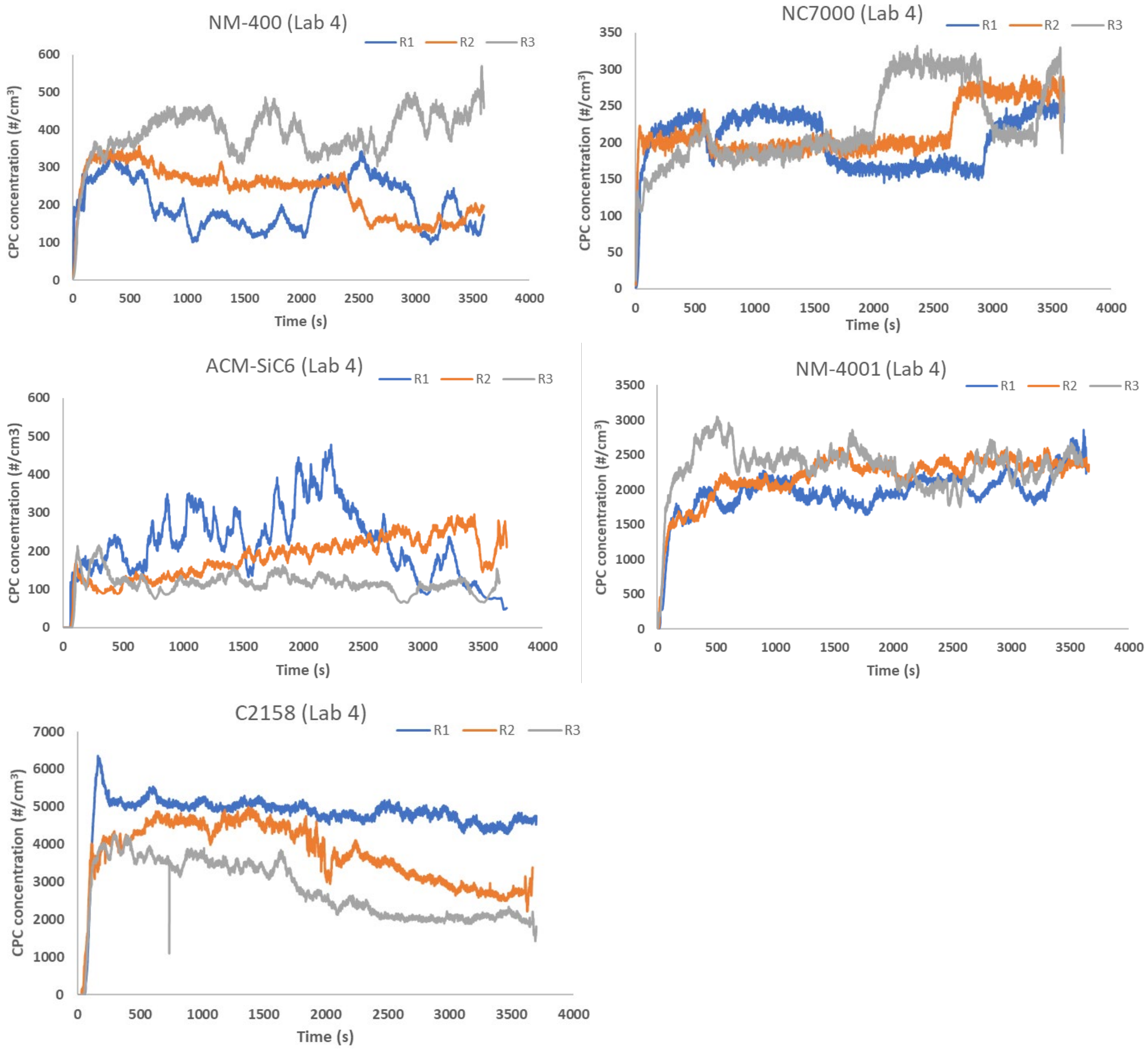


**Figure 53. Fluidizer Lab 4 CPC particle number concentration time series during each test and material. For NM-4001 and C2158 only data of one representative test is shown.**

### 4.9.5. Type of objects released and mass-based dustiness index

154. One of the main differences between the dustiness ILC for powders containing granular and fibrous NOAA is the fact that for fibrous NOAA, the dustiness index is also calculated from the analysis of EM micrographs. From this analysis, the total number-based dustiness index is determined, but also fibre-specific measurands that provide risk-relevant information. This is the case of $DI_{fibrousNOAA}$ and $DI_{criticalfibrousNOAA}$, representing the dustiness index of the total identified fibrous NOAA including agglomerates as well as the fibrous NOAA with potentially critical dimensions.

155. For fibrous NOAA dustiness index, CV (

156. Table 26,

157. Table 28) is comparable to what was obtained for total number dustiness index ($DI_{N\text{-}SEM}$), with values 27-118% for Lab 1, 7- 56% for Lab 2, 1-36% for Lab 3, and 4-82% for Lab 4.

158. For the Small Rotating Drum dustiness method, the calculated $DI_{fibrousNOAA}$ and $DI_{criticalfibrousNOAA}$ fractions for each material and laboratory are shown in Figure 54. Overall, $DI_{fibrousNOAA}$ and $DI_{criticalfibrousNOAA}$ fractions were somehow comparable between laboratories (10-20% differences) for flexible materials such as NM-400, NC7000 and NM-4001. However, for rigid and long materials (ACM-SiC6 and C2158), Lab 1 showed much lower percentage than Lab 2 of fibrous NOAA and values close to 0% for fibrous NOAA with potentially critical dimensions, whereas Lab 2 had values of 40% for ACM-SiC6 and 6.2% for C2158 materials. These differences were likely due to the lower flow used for sampling. As already pointed out earlier, due to the lower sampling flow used by Lab 1, and thus lower face velocity, there is a loss on the collection of bigger fibres and agglomerates.

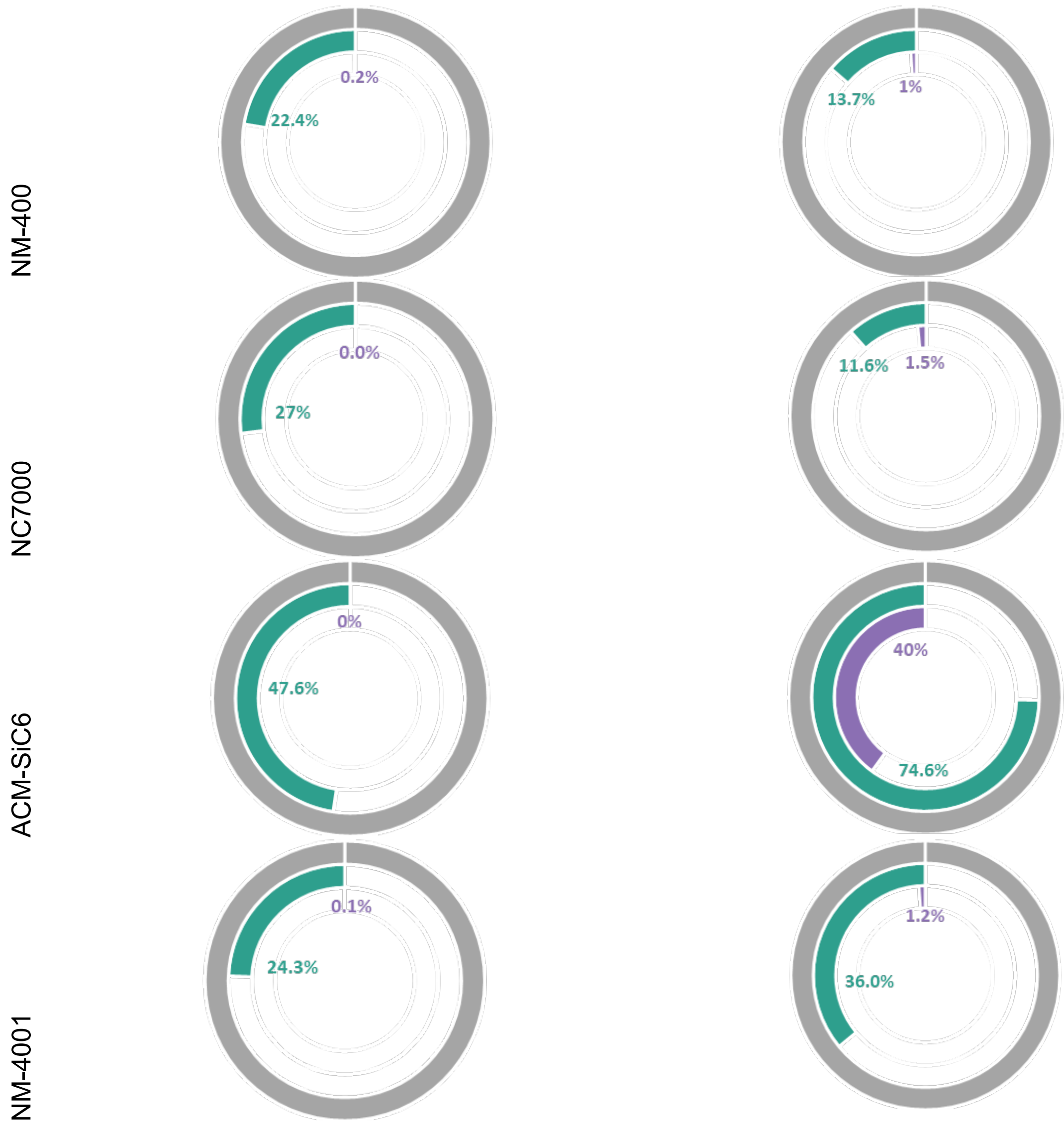

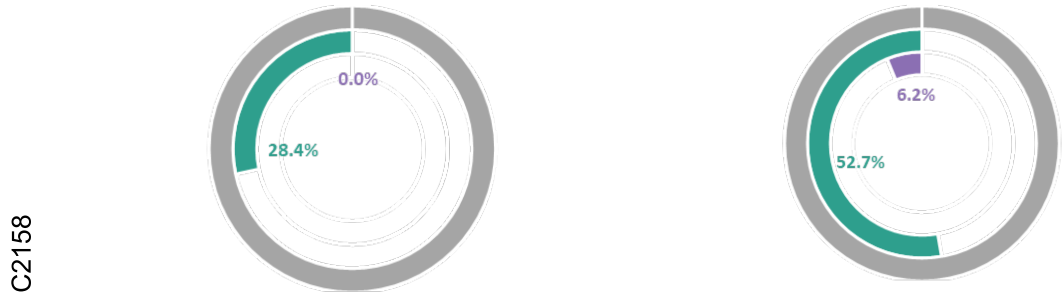


**Figure 54. Type of objects released during Small Rotating Drum dustiness tests by defined categories, SEM-based total number dustiness index (*$DI_{N\text{-}SEM}$*; grey), total fibrous NOAA dustiness index (*$DI_{fibrousNOAA}$*; green) and total fibrous NOAA with potentially critical dimensions (*$DI_{criticalfibrousNOAA}$*; purple) for Lab 1 (left) and Lab 2 (right).**

159. For the Fluidizer dustiness method, the calculated $DI_{fibrousNOAA}$ and $DI_{criticalfibrousNOAA}$ fractions for each material and laboratory are shown in Figure 55. Overall, the fractions were highly comparable between the two laboratories, especially for the three materials presenting higher rigidity (ACM-SiC6, NM-4001 and C2158). For materials with lower rigidity and higher agglomerate formation, as in the Small Rotating Drum, fraction for $DI_{fibrousNOAA}$ showed slight differences of 10-20% between laboratories due to the materials characteristics. This showed that $DI_{fibrousNOAA}$ and $DI_{criticalfibrousNOAA}$ calculated from the micrograph analysis can provide robust and relevant information when dealing with powders containing fibrous NOAA.

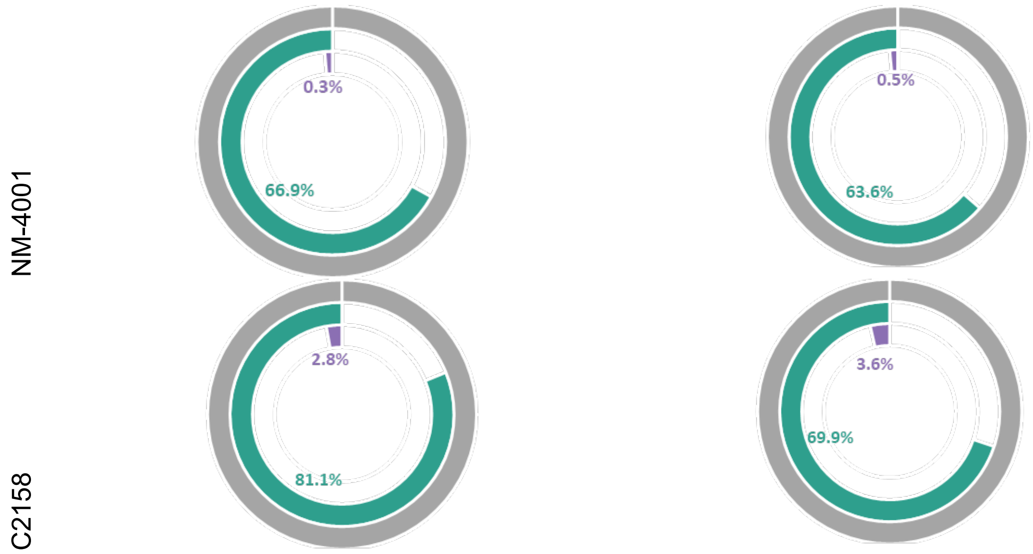


**Figure 55. Type of objects released during Fluidizer dustiness tests by defined categories, , SEM-based total number dustiness index (*$DI_{N\text{-}SEM}$*; grey), total fibrous NOAA dustiness index (*$DI_{fibrousNOAA}$*; green) and total fibrous NOAA with potentially critical dimensions (*$DI_{criticalfibrousNOAA}$*; purple) for Lab 3 (left) and Lab 4 (right).**

160. Respirable mass-based dustiness index was determined by Lab 1 with the Small Rotating Drum and only for two materials, NM-400 and NM-4001. Results are shown in Figure 56. Interestingly, mass-based dustiness index was higher for NM-400 than NM-4001 as opposed to number-based dustiness index (both CPC and SEM based). This may be explained, among other factors, by the type of objects released during agitation. For NM-4001 a higher proportion of the released NOAA during a Small Rotating Drum test consisted of single fibres compared with NM-400. In contrast, NM-400, was observed to release mainly agglomerates, some bigger than 20 µm, and particulate objects. The presence of these big agglomerates have a larger effect on mass than on number. See section below “Between methods comparison” for micrographs and further discussion on agglomeration effects due to the dustiness methods agitation mechanisms.

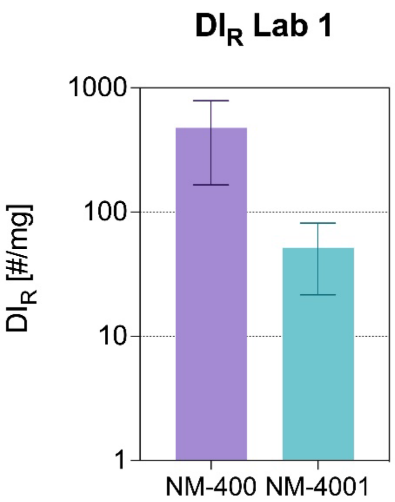

**Figure 56. Small Rotating Drum mass-based dustiness index ($DI_R$) given for NM-400 and NM-4001 and determined by Lab 1. One test of three replicates and standard deviation is given. Note: log-scale used.**

## 4.9.6. Between methods comparison

161. Since the different dustiness methods use different agitation mechanisms and energy inputs, dustiness indexes obtained and classification might be different between methods. Results from the Fluidizer experiments and Small Rotating Drum are shown in Figure 57. Both methods showed comparable $DI_{N\text{-}CPC}$ results in terms of material ranking, with Small Rotating Drum showing lower dustiness index. For $DI_{N\text{-}SEM}$, a similar tendency was observed although differences between Small Rotating Drum and Fluidizer in absolute values was higher than for $DI_{N\text{-}CPC}$, and differences between materials with the Small Rotating Drum were less marked.

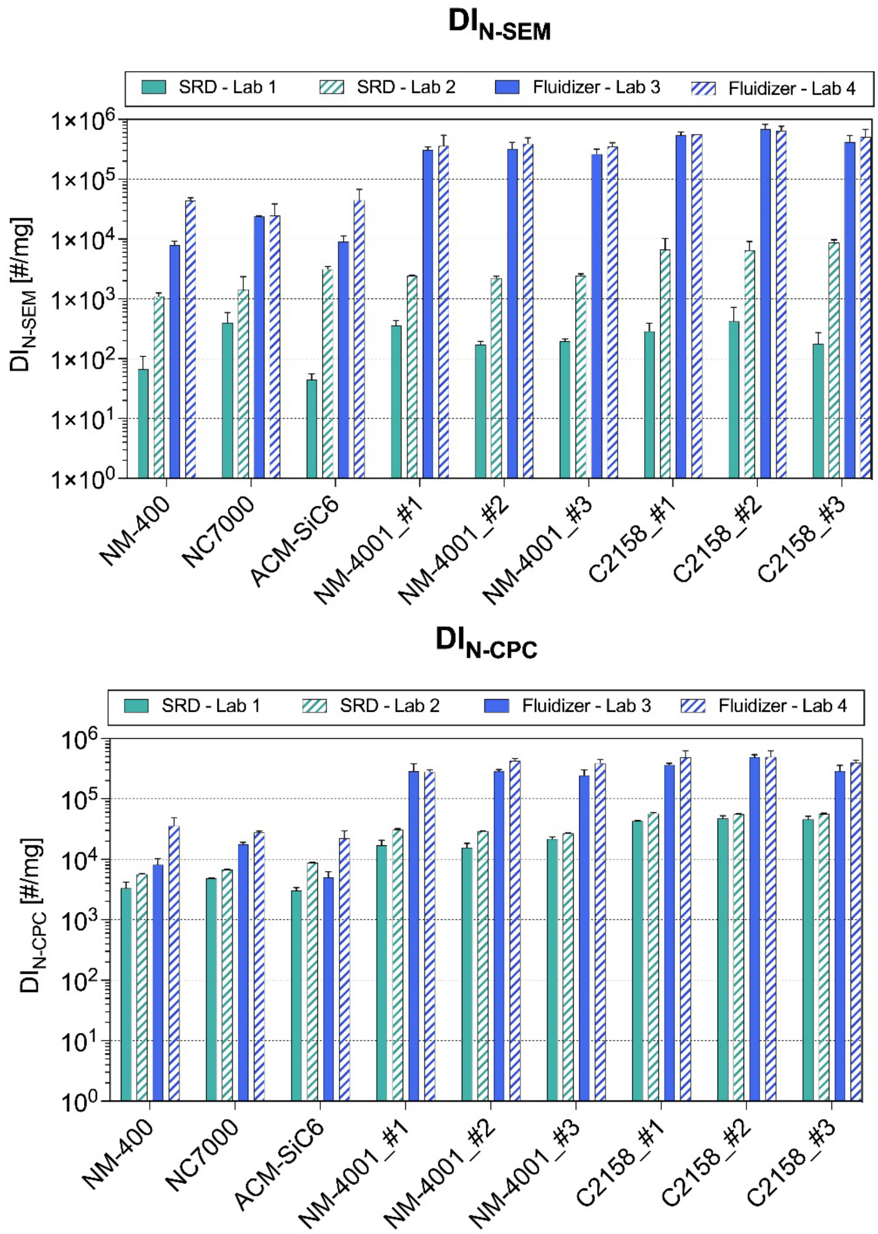

**Figure 57. SEM micrograph analysis dustiness index ($DI_{N\text{-}SEM}$) and CPC number-based dustiness index ($DI_{N\text{-}CPC}$) results Small Rotating Drum (SRD) Lab 1 and Lab 2 and Fluidizer Lab 3 and Lab 4. One test of three replicates and standard deviation is given. Note: log-scale used.**

162. In addition to the total number of objects released, their shape and agglomeration state was observed to be different between methods likely due to the differences in the methods dust generation processes.

163. Exemplary obtained micrographs are shown in Figure 58, Figure 59, Figure 60 and Figure 61. A quantitative comparison between type of objects released for both dustiness methods, Small Rotating Drum and Fluidizer is shown in Figure 62.

164. For the Small Rotating Drum method large fibrous agglomerates were released, and single fibres were scarce. Conversely, for the Fluidizer, smaller agglomerates were found in the micrographs and single fibres were more abundant. In Figure 58a and b, >20 µm low aspect ratio agglomerates composed of fibres released during a Small Rotating Drum test with NC7000 (flexible material) are shown. Such agglomerates were not observed in Fluidizer samples for the same material. Smaller (few microns) low aspect ratio agglomerates composed of fibres were observed in NC7000 samples of both, Small Rotating Drum and Fluidizer (Figure 58c and d and Figure 59). This tendency can also be observed from the quantitative object classification, in which the Small Rotating Drum was seen to have a higher proportion of LARFA than the Fluidizer (26% vs. 6%), whereas a slightly higher proportion of single fibres was observed for the Fluidizer (31% vs. 16%).

165. The difference in the proportion of single fibres is not only true for flexible materials (which tend to form more agglomerates), but also for more rigid materials (NM-4001, C2158 and ACM-SiC6). For example, for NM-4001 agglomerates composed of fibres of comparable sizes were observed in samples from Small Rotating Drum and Fluidizer (Figure 60 and Figure 61). However, a higher proportion of single fibres was observed in the Fluidizer samples (58%) compared to the Small Rotating Drum (29%) (Figure 62). Interestingly, nearly no HARFA were found in the Small Rotating Drum samples (1%) whereas a small proportion was found in Fluidizer samples (7%).

166. This behaviour can be explained and is somehow expected since the Fluidizer method involves high energy input and it is designed to break fibrous agglomerates and generate aerosols with high proportion of single fibres [11]. Conversely, the Small Rotating drum generates an aerosol by rotation (lifting and dropping the material) being less effective on fibre disentanglement.

a)

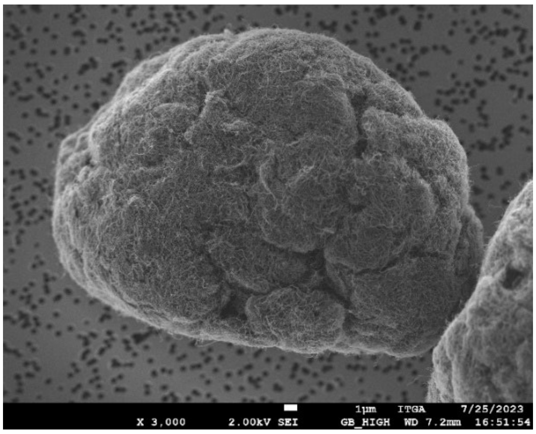


b)

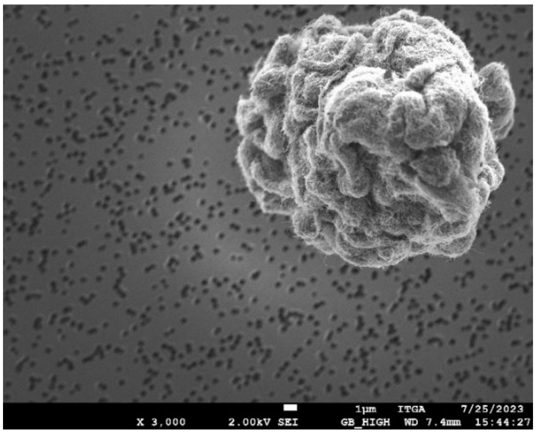

c)

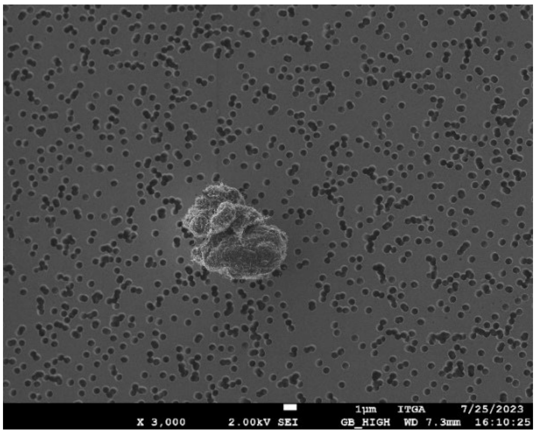


d)

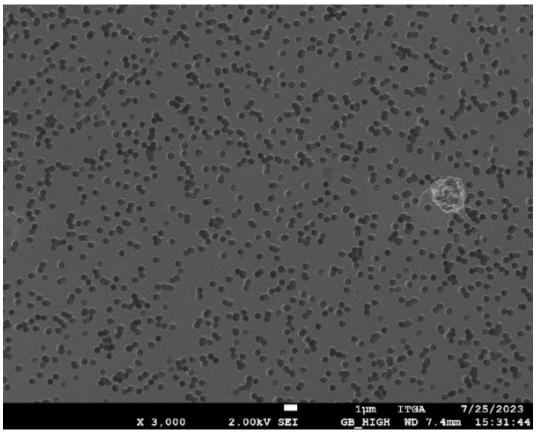


**Figure 58. Example micrographs obtained during a dustiness test of NC7000 using the Small Rotating Drum.**

a)

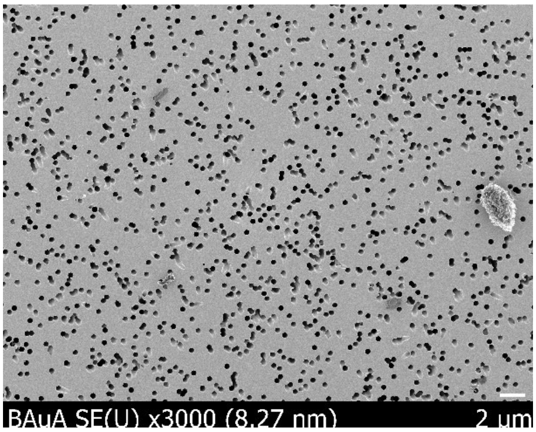


b)

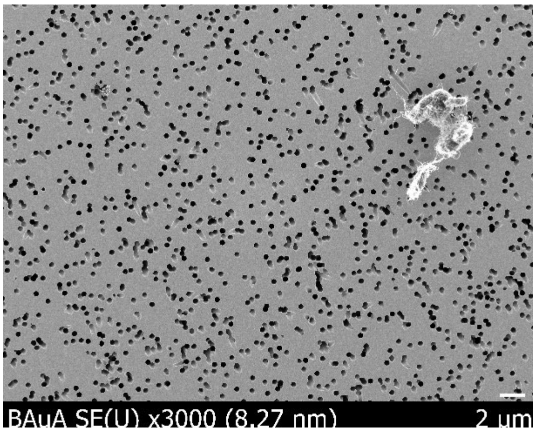


**Figure 59. Example micrographs obtained during a dustiness test of NC7000 using the Fluidizer.**

a)

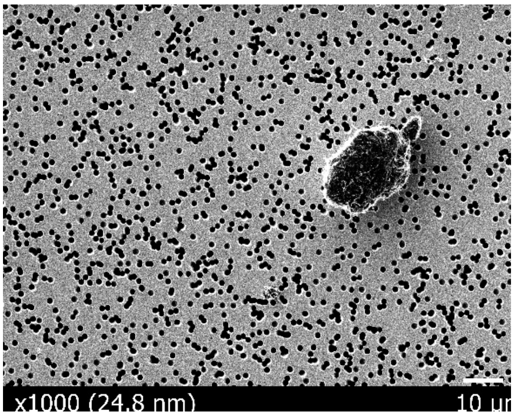


b)

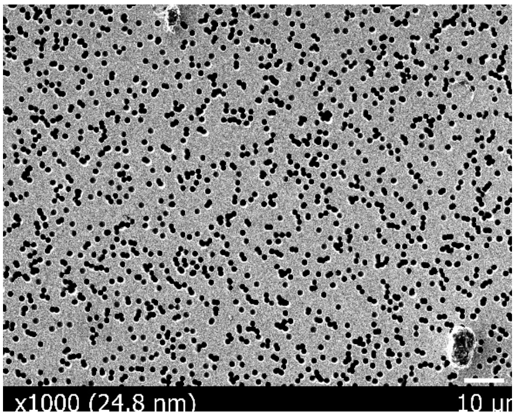

Figure 60. Example micrographs obtained during a dustiness test of the material NM-4001 using the Small Rotating Drum.

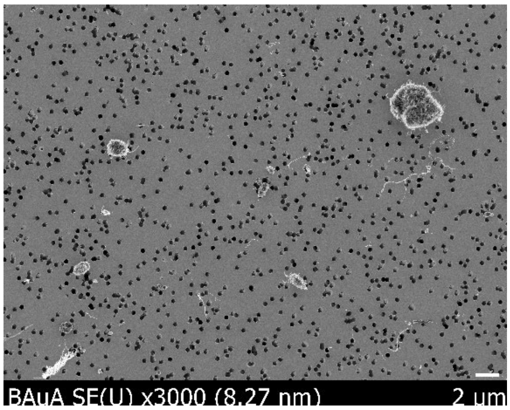


Figure 61. Example micrograph obtained during a dustiness test of the material NM-4001 using the Fluidizer.

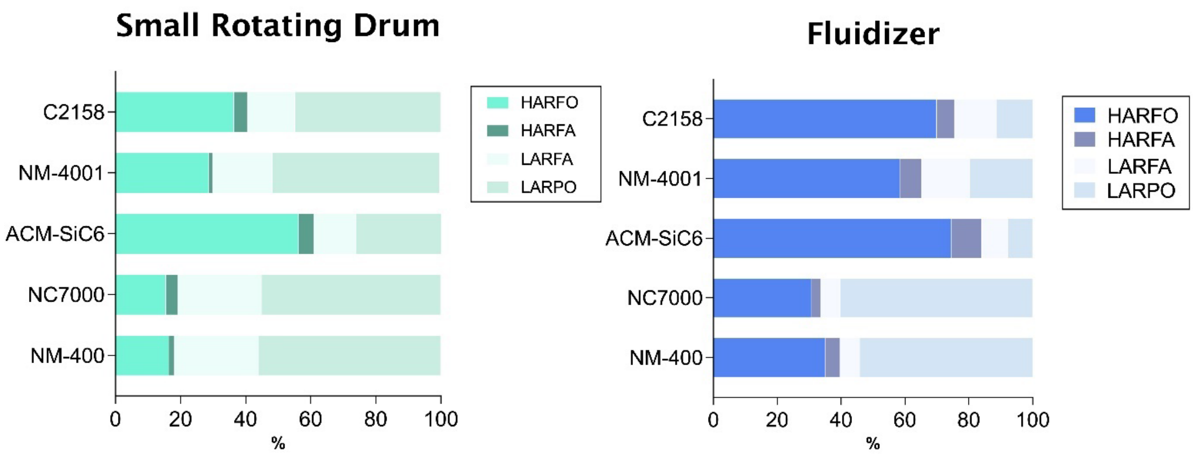


Figure 62. Object classification results obtained for Small Rotating Drum and Fluidizer considering all participating laboratories. Standard deviation not shown.

## 4.10. Conclusions

167. Despite high efforts to find additional participants for this ILC, it was only possible to obtain data from two laboratories per method and for only two dustiness test methods (Small Rotating Drum and Fluidizer). Especially the analysis using SEM and the high-resolution acquisition of micrographs is quite time- and resource- consuming.

168. When comparing the CPC data measured for powders containing fibrous NOAA and powders containing granular NOAA, the dustiness test itself worked in a comparable way. The data obtained in the ILC for powders containing fibrous NOAA, showed a CV for both, the CPC ($DI_{N\text{-}CPC}$) and the micrograph analysis ($DI_{N\text{-}SEM}$) dustiness index, in the same range as the one of the CPC data obtained for the powders containing granular NOAA. The analysis of the obtained results showed that the descriptions of the dustiness test methods are well established and can be used for obtaining

reproducible and repeatable results. Furthermore, it showed that the Small Rotating Drum and the Fluidizer can be used for powders containing granular NOAA as well as for powders containing fibrous NOAA. This is of importance given that dustiness of powders containing fibrous NOAA is not yet specifically covered in any existing standards.

169. The results obtained for the analysed powders within this ILC, showed that the CPC data can be of use for a qualitative and potentially a quantitative determination of total number-based dustiness index and thus can be useful for a first screening of powders containing fibrous NOAA and for determining the parameters under which the sample is collected (time and flow). However, since no fibrous NOAA and fibrous NOAA with potentially dimensions can be quantified nor characterised from real-time data, the potential of exposure and relevant hazard data of the powder would be incomplete without micrograph analysis and quantification. CPC and micrograph analysis data was found to correlate well in this ILC. However, CPC data should be subject of further scientific investigations as well as the material-dependency of the discrepancy of CPC and counting data. Especially since the collection efficiency of the filters used for collecting the sample for SEM analysis is not known for the different materials, the data interpretation needs to be done in a careful way.

170. When performing the analysis of fibrous NOAA with very small diameters, high-resolution SEMs are needed to fulfil the criterium of a pixel size of ¼ of the minimum diameter. Especially the high-resolution micrographs have a very long acquisition time, which is challenging for many of the laboratories performing SEM analyses, requiring many resources. In this regard, an automated image acquisition would facilitate this procedure.

171. This validation study showed that counting and categorisation of objects on the micrographs was one of the main challenges during the dustiness determination. The fine-tuning of the description of the rules was performed with the help of the participating laboratories and their experiences. Furthermore, the manual analysis of the large amount of SEM micrographs that is required to fulfil the statistical requirements for the analysis is very labour intensive and time consuming. Computer-assisted analysis procedures could potentially help with both: Automated NOAA recognition tools could facilitate the counting and the categorisation of NOAA and at the same time reduce the time needed for the analysis of the micrographs.

172. The software FibreDetect, which is developed by BAuA and which was already used for the ILC in the “manual analysis” mode, has also functions that are further advanced [41]. It supports image acquisition and can perform automated object recognition and classification. The automated object recognition was on purpose excluded from this ILC to assess the reproducibility and repeatability of the manual analysis and to develop a method that can be used independently from a specific software. In the future, the analysis of micrographs could be facilitated by using the software FibreDetect or a similar software with the additional functions.

# 5. Development of the dustiness ranking

173. An additional use of the generated data during the two ILCs is the development of a comprehensive dustiness ranking scheme for powders containing granular and/or fibrous NOAA. This ranking is based on consistent comparisons across the various methodologies tested in these ILCs. Dustiness data from all methods and laboratories were analysed, comparing respirable and total/inhalable mass dustiness indices, as well as particle number-based dustiness indices for each method.

174. The dustiness ranking for powders containing granular NOAA is presented in Figure 63, Figure 64, and Figure 65. Notably, the particle number-based dustiness index showed lower variability across methods, providing a more consistent ranking of materials. However, for $TiO_2$ NM-103, significant

discrepancies were observed between laboratories and methods. For both number- and mass-based dustiness indices, the Vortex Shaker and Venturi methods produced higher dustiness values compared to other techniques, including the Rotating Drum, Small Rotating Drum, Continuous Drop, and Fluidizer method. The Rotating Drum, Small Rotating Drum, and Fluidizer method yielded similar material rankings, with the Rotating Drum and Fluidizer typically generating slightly higher particle number dustiness values than the Small Rotating Drum. This discrepancy may be attributed to the greater height from which the powder falls during testing. Although only two materials were tested using the Continuous Drop method, the resulting ranking trends for both number and respirable mass dustiness indices were consistent with those observed for the Rotating Drum, Small Rotating Drum, and Fluidizer method. Regarding the respirable mass dustiness index, the Vortex Shaker test classifies $TiO_2$ PC105 as having the lowest dustiness. In this context, $TiO_2$ NM-103 exhibits a lower dustiness index than NM-105, with minimal differences observed among NM-105, NM-103, NM-203, NM-204, and NM-244FP. The Venturi method, while showing smaller differences in mass-based dustiness indices between materials, provided a ranking inconsistent with the other methods. For instance, it ranked $TiO_2$ PC105 with the highest respirable dustiness index, while $SiO_2$ NM-204 had the lowest.

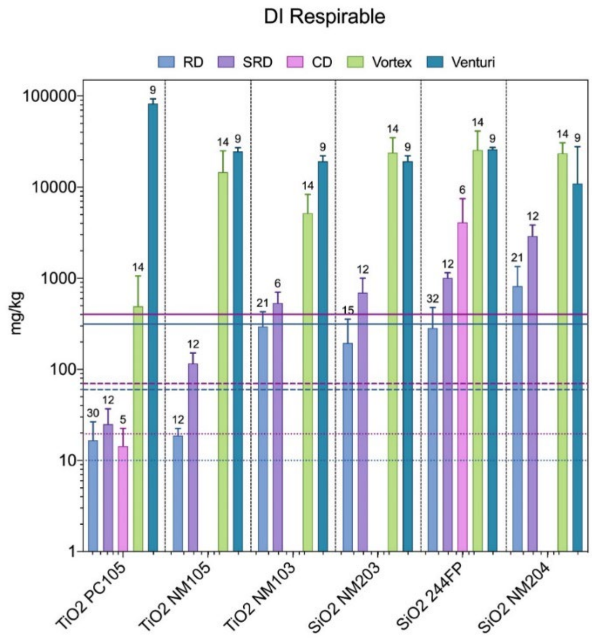


**Figure 63. Average and standard deviation for respirable mass-based dustiness index ($DI_R$) for material and method. Number of data points included per method are indicated above the bars. Existing ranking schemes (EN 15051-series) are shown in the corresponding method colour (very low-low dotted lines; low-moderate dashed lines; moderate-high solid lines). Error bars show standard deviation of all replicates. Note: log scale used.**

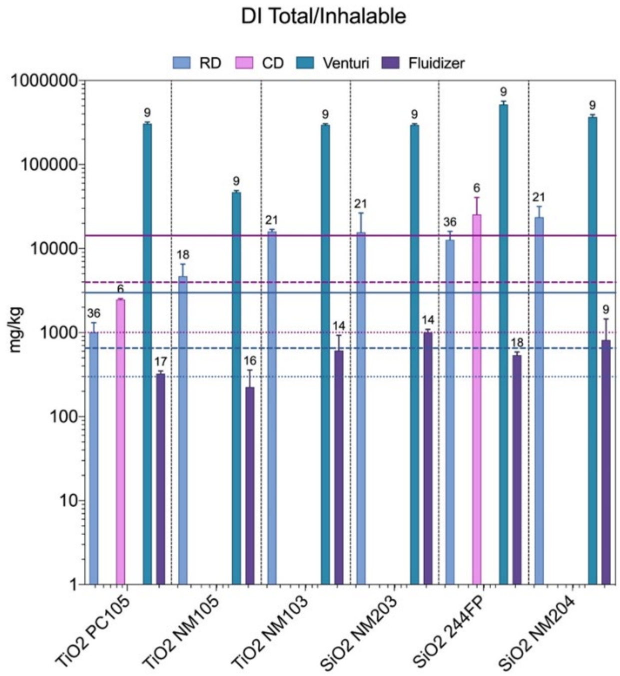


**Figure 64. Average and standard deviation for inhalable ($DI_I$) or total ($DI_{tot}$) mass-based dustiness index for material and method. Number of data points included per method are indicated above the bars. Existing ranking schemes (EN 15051-series) are showed in the corresponding method colour (very low-low dotted lines; low-moderate dashed lines; moderate-high solid lines). Error bars show standard deviation of all replicates. Note: log scale used.**

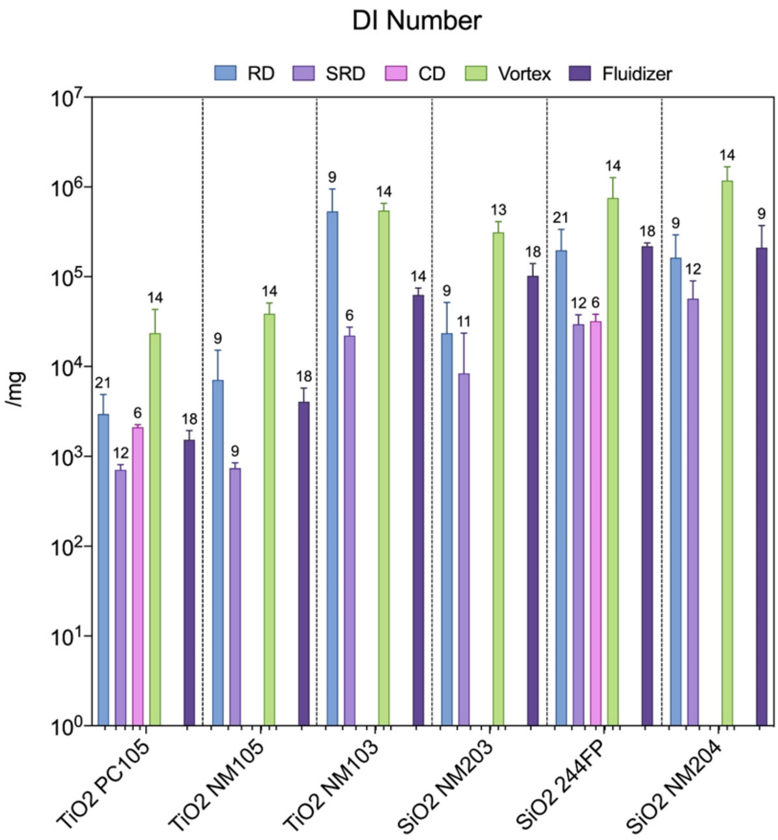


**Figure 65. Average and standard deviation for particle number-based dustiness index ($DI_N$) for material and method. Number of data points included per method are indicated above the bars. Error bars show standard deviation of all replicates. Note: log scale used.**

175. Dustiness ranking is complex because different methods yield different values due to variations in agitation mechanisms and energy input. Currently, dustiness rankings are only available for mass-based data from the Rotating Drum and Continuous Drop methods, as defined by EN 15051-series and EN 17199-series (highlighted as horizontal lines in Figure 63 and Figure 64). Dustiness rankings for particle number-based indices are not yet defined for any method. In Table 30 existing ranking as defined in EN 15051-series has been used for the granular materials assessed. While some methods, such as the Rotating Drum and Small Rotating Drum, show similar dustiness trends, the current results cover a relatively limited range of dustiness levels, making it difficult to establish a harmonised method-specific ranking. In some cases, materials fall into the same ranking category across methods (e.g., $TiO_2$ PC105 and $SiO_2$ 244FP). However, discrepancies occur where materials may rank one level higher or lower between methods, especially when the dustiness value falls between categories (e.g., $TiO_2$ NM-103 and $SiO_2$ NM-203). Furthermore, differences between laboratories also contribute to ranking discrepancies, as reflected in the standard deviations.

**Table 30. Material classification according to existing ranking for respirable dustiness index (EN 15051-series). N/A: not available.**

| Material | Rotating Drum | Small Rotating Drum | Continuous Drop |
|---|---|---|---|
| $TiO_2$ PC105 | Low | Low | Very low |

| | | | |
|---|---|---|---|
| $TiO_2$ NM-105 | Low | Moderate | N/A |
| $TiO_2$ NM-103 | Moderate | High | N/A |
| $SiO_2$ NM-203 | Moderate | High | N/A |
| $SiO_2$ NM-204 | Moderate | High | High |
| $SiO_2$ 244FP | High | High | N/A |

Note: The Small Rotating Drum ranking is based on the Rotating Drum rankings (EN 15051-2:2025).

176. In general, the Vortex Shaker and Venturi methods produce higher dustiness levels due to their higher energy input. This highlights the importance of reporting the method used when dustiness indices and rankings are provided, and considering the applicability of each method based on the energy input and the type of process they mimic.

177. Figure 66 provides an overview of CPC number-based dustiness index for powders containing granular and fibrous NOAA tested in the two ILCs using the Fluidizer and Small Rotating Drum methods. Combining the datasets from both ILCs provides a more comprehensive dataset covering different dustiness levels for both powders containing granular and fibrous NOAA. With this combined dataset (Figure 66), the particle number-based dustiness index ranges from 700 #/mg ($TiO_2$ PC105 and NM-105) to around 57000 #/mg ($SiO_2$ NM-204 and C2158) for the Small Rotating Drum, and from 1500 #/mg ($TiO_2$ PC105) to 234000 #/mg (NM-4001) for the Fluidizer. Thus, a large range of dustiness levels seems to be covered. While these methods generally rank materials similarly, some discrepancies remain (e.g., $SiO_2$ NM-203).

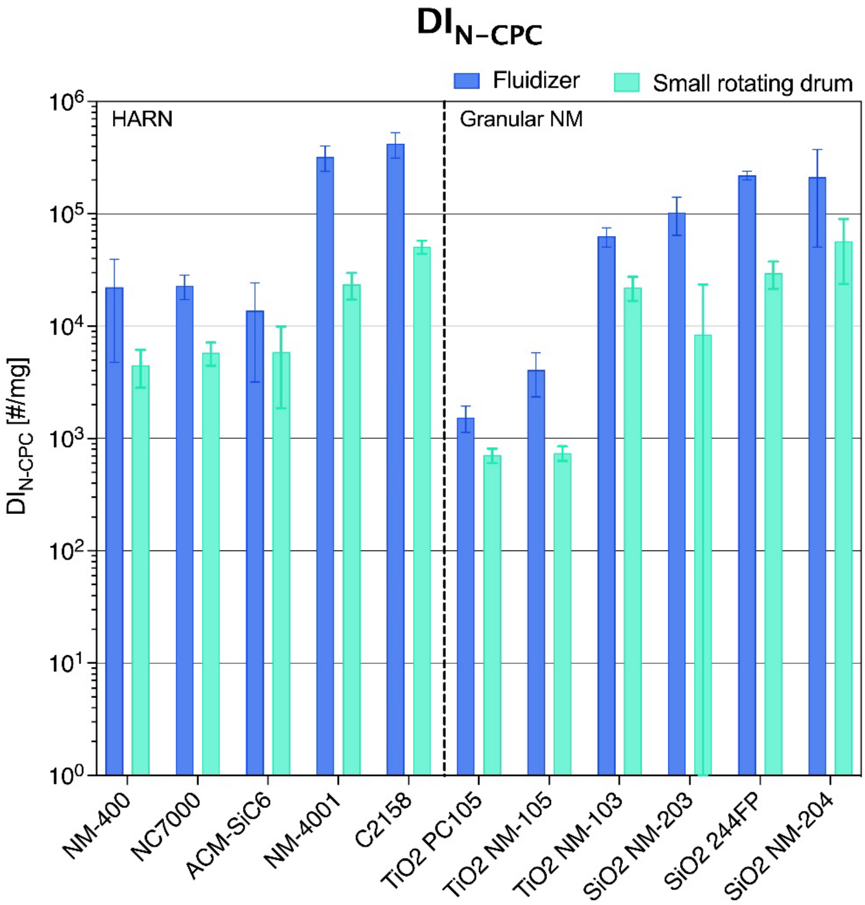

**Figure 66. Average and standard deviation for CPC particle number-based dustiness index ($DI_{N-CPC}$) for material and method (Fluidizer and Small Rotating Drum) for the powders containing fibrous NOAA assessed in this ILC and the powders containing granular NOAA assessed in the Gov4Nano ILC. Note: log scale used.**

178. The dustiness levels of the materials tested in the ILCs spanned a broad range, and similarities were observed across the methods. However, to establish a reliable material ranking scheme, additional measurements with a wider variety of materials at different dustiness levels are needed. Methods such as Rotating Drum, Small Rotating Drum, Fluidizer, and Continuous Drop produced similar classification trends, while the Vortex Shaker, though showing comparable trends in terms of particle number, yielded higher dustiness values with less variability between laboratories. The Venturi method, known for its strong agitation and maximum dispersibility, showed minimal differences between materials and a ranking that appeared inconsistent with the other methods.

# References

[1] Lidén G. Dustiness Testing of Materials Handled at Workplaces. Ann Occup Hyg 2006;50:437–9. https://doi.org/10.1093/annhyg/mel042.

[2] Klippel A, Scheid M, Krause U. 04 Journal of Loss Prevention in the Process Industries Investigations into the in fl uence of dustiness on dust explosions. J Loss Prev Process Ind 2013.

[3] Klippel A, Schmidt M, Krause U. Dustiness in workplace safety and explosion protection - Review and outlook. J Loss Prev Process Ind 2015. https://doi.org/10.1016/j.jlp.2015.01.011.

[4] Schneider T, Jensen KA. Combined single-drop and rotating drum dustiness test of fine to nanosize powders using a small drum. Ann Occup Hyg 2008. https://doi.org/10.1093/annhyg/mem059.

[5] Brouwer DH, Links IHM, De Vreede SAF, Christopher Y. Size selective dustiness and exposure; simulated workplace comparisons. Ann Occup Hyg 2006. https://doi.org/10.1093/annhyg/mel015.

[6] Madsen AM, Kruse P, Schneider T. Characterization of microbial particle release from biomass and building material surfaces for inhalation exposure risk assessment. Ann Occup Hyg 2006. https://doi.org/10.1093/annhyg/mei057.

[7] Shandilya N, Kuijpers E, Tuinman I, Fransman W. Powder Intrinsic Properties as Dustiness Predictor for an Efficient Exposure Assessment? Ann Work Expo Heal 2019;63:1029–45. https://doi.org/10.1093/annweh/wxz065.

[8] Liguori B, Hansen SF, Baun A, Jensen KA. Control banding tools for occupational exposure assessment of nanomaterials - Ready for use in a regulatory context? NanoImpact 2016;2:1–17. https://doi.org/10.1016/j.impact.2016.04.002.

[9] Fonseca AS, Ribalta C, Shandilya N, Fransman W, Alstrup Jensen K. Development of handling energy factors for use of dustiness data in exposure assessment modelling. Ann Work Expo Heal 2024;68:295–311. https://doi.org/10.1093/annweh/wxae009.

[10] Ribalta C, Jensen ACØ, Shandilya N, Delpivo C, Jensen KA, Fonseca AS. Use of the dustiness index in combination with the handling energy factor for exposure modelling of nanomaterials. NanoImpact 2024;33:100493. https://doi.org/https://doi.org/10.1016/j.impact.2024.100493.

[11] Broßell D, Heunisch E, Meyer-Plath A, Bäger D, Bachmann V, Kämpf K, Dziurowitz N, Thim C, Wenzlaff D, Schumann J, Plitzko S. Assessment of nanofibre dustiness by means of vibro-fluidization. Powder Technol 2019;342:491–508. https://doi.org/10.1016/j.powtec.2018.10.013.

[12] Bach S, Schmidt E. Determining the dustiness of powders - A comparison of three measuring devices. Ann Occup Hyg 2008. https://doi.org/10.1093/annhyg/men062.

[13] Jensen KA, Koponen IK, Clausen PA, Schneider T. Dustiness behaviour of loose and compacted Bentonite and organoclay powders: What is the difference in exposure risk? J Nanoparticle Res 2009;11:133–46. https://doi.org/10.1007/s11051-008-9420-1.

[14] EN 17199-1:2019: Workplace exposure - Measurement of dustiness of bulk materials that contain or release nano-objects or release respirable NOAA and other respirable particles - Part 1: requirements and choice of test methods 2019.

[15] EN 17199-2:2019, Workplace exposure - Measurement of dustiness of bulk materials that contain or release respirable NOAA and other respirable particles - Part 2: Rotating drum method 2019.

[16] EN 17199-3:2019, Workplace exposure - Measurement of dustiness of bulk materials that contain or release respirable NOAA and other respirable particles - Part 3: Continuous drop method 2019.

[17] EN 17199-4:2019, Workplace exposure - Measurement of dustiness of bulk materials that contain or release respirable NOAA and other respirable particles - Part 4: Small rotating drum method 2019.

[18] EN 17199-5:2025, Workplace exposure - Measurement of dustiness of bulk materials that contain or release respirable NOAA and other respirable particles - Part 5: Vortex shaker method 2025.

[19] ISO/TS 12025:2021, Nanomaterials: Quantification of nano-object release from powders by generation of aerosols. Technical specification. Geneva, Switzerland: International Organization for Standardization. 2021.

[20] CEN/TC 137 C 13/2023 Workplace exposure — Detection and characterization of airborne NOAA using electron microscopy — Rules for sampling and analysis (Draft Document) 2023.

[21] EN 16897:2017, Workplace exposure - Characterization of ultrafine aerosols/nanoaerosols - Determination of number concentration using condensation particle counters 2017.

[22] ISO 13528:2022. Statistical methods for use in proficiency testing by interlaboratory comparison.Technical Committee : ISO/TC 69/SC 6. ICS : 03.120.30 2022.

[23] ISO 14966:2019, Ambient air - Determination of numerical concentration of inorganic fibrous particles - Scanning electron microscopy method 2019.

[24] ISO 15900:2020, Determination of particle size distribution - Differential electrical mobility analysis for aerosol particles 2020.

[25] ISO 27891:2015, Aerosol particle number concentration - Calibration of condensation particle counters 2015.

[26] ISO 5725-2:2025. Accuracy (trueness and precision) of measurement methods and results. Part 2: Basic method for the determination of repeatability and reproducibility of a standard measurement method. Technical Committee : ISO/TC 69/SC 6. ICS : 17.020 03. 2025.

[27] OECD TG 125:2023. Test Guideline N°125. Nanomaterial Particle Size and Size Distribution of Nanomaterials. 2023.

[28] VDI 3492:2013-06, Indoor air measurement - Ambient air measurement - Measurement of inorganic fibrous particles - Scanning electron microscopy method. 2013.

[29] Boundy M, Leith D, Polton T. Method to evaluate the dustiness of pharmaceutical powders. Ann Occup Hyg 2006. https://doi.org/10.1093/annhyg/mel004.

[30] Evans DE, Turkevich LA, Roettgers CT, Deye GJ, Baron PA. Dustiness of fine and nanoscale powders. Ann Occup Hyg 2013. https://doi.org/10.1093/annhyg/mes060.

[31] Visser M, Gosens I, Bard D, van Broekhuizen P, Janer G, Kuempel E, Riediker M, Vogel U, Dekkers S. Towards health-based nano reference values (HNRVs) for occupational exposure: Recommendations from an expert panel. NanoImpact 2022. https://doi.org/10.1016/j.impact.2022.100396.

[32] Levin M, Koponen IK, Jensen KA. Exposure assessment of four pharmaceutical powders based on dustiness and evaluation of damaged HEPA filters. J Occup Environ Hyg 2014. https://doi.org/10.1080/15459624.2013.848038.

[33] EN 15051-1:2025, Workplace exposure - Measurement of the dustiness of bulk materials - Part 1: Requirements and choice of test methods 2025.

[34] ISO 15767:2009, Workplace atmospheres - Controlling and characterizing uncertainty in weighing collected aerosols 2009.

[35] EN 15051-2:2025, Workplace exposure - Measurement of the dustiness of bulk materials - Part 2: Rotating drum method 2025.

[36] OECD (2005), *Guidance Document on the Validation and International Acceptance of New or Updated Test Methods for Hazard Assessment*, OECD Series on Testing and Assessment, No. 34, OECD Publishing, Paris, https://doi.org/10.1787/e1f1244b-en.

[37] OECD (2019), *Physical-Chemical Decision Framework to inform Decisions for Risk Assessment of Manufactured Nanomaterials*, OECD Series on the Safety of Manufactured Nanomaterials and other Advanced Materials, OECD Publishing, Paris, https://doi.org/10.1787/1fbbaf8c-en.

[38] OECD (2019), *Guiding Principles for Measurements and Reporting for Nanomaterials: Physical Chemical Parameters*, OECD Series on the Safety of Manufactured Nanomaterials and other Advanced Materials, OECD Publishing, Paris, https://doi.org/10.1787/70c84148-en.

[39] ISO 5725-1:2023. Accuracy (trueness and precision) of measurement methods and results Part 1: General principles and definitions. Technical Committee : ISO/TC 69/SC 6. ICS : 17.020 03.120.30 2023.

[40] EN 15051-3:2025, Workplace exposure - Measurement of the dustiness of bulk materials - Part 3: Continuous drop method 2025.

[41] Peters T, Schumann J, Kämpf K, Meyer-Plath A. AI-assisted recognition of fibre instances in scanning electron microscope images for aerosol characterization and exposure assessment. Powder Technol 2026;469:121909. https://doi.org/https://doi.org/10.1016/j.powtec.2025.121909.

[42] Broßell D, Meyer-Plath A, Heunisch E, Kämpf K, Haase A, Wiemann M. Macrophages bend long fibres with flexural rigidity lower than 3 mN·nm$^2$ to avoid frustrated phagocytosis. Prepr (Version 1) Available Res Sq 2025. https://doi.org/https://doi.org/10.21203/rs.3.rs-8317185/v1.

[43] BAuA. CLH report. Proposal for Harmonised Classification and Labelling. International Chemical Identification : Multi-Walled Carbon Tubes ( synthetic graphite in tubular shape ) with a geometric tube diameter range ≥ 30 nm to < 3 μm and a length ≥ 5 μm and aspe 2021.

[44] Szewczak E, Bondarzewski A. Is the assessment of interlaboratory comparison results for a small number of tests and limited number of participants reliable and rational? Accredit Qual Assur 2016. https://doi.org/10.1007/s00769-016-1195-y.

[45] Allard A, Amarouche S. Analysis of interlaboratory comparison when the measurements are not normally distributed, 2017. https://doi.org/10.1051/metrology/201712003.

[46] Dean RB, Dixon WJ. Simplified Statistics for Small Numbers of Observations. Anal Chem 1951. https://doi.org/10.1021/ac60052a025.

[47] Efstathiou CE. Estimation of type I error probability from experimental Dixon's "Q" parameter on testing for outliers within small size data sets. Talanta 2006. https://doi.org/10.1016/j.talanta.2005.12.031.

[48] Hall MB, Mertens DR. A ring test of in vitro neutral detergent fiber digestibility: Analytical variability and sample ranking. J Dairy Sci 2012. https://doi.org/10.3168/jds.2011-4802.

[49] Zoller J, Gulden J, Meyer J, Dittler A. Loss of Nanoparticles in a Particulate Matter Sampling System Applied for Environmental Ultrafine Particle Measurements. Aerosol Sci Eng 2020. https://doi.org/10.1007/s41810-020-00054-6.

[50] Chen SC, Wang J, Fissan H, Pui DYH. Exposure assessment of nanosized engineered agglomerates and aggregates using Nuclepore filter. J Nanoparticle Res 2013. https://doi.org/10.1007/s11051-013-1955-0.

[51] ISO 26824:2022, Particle characterization of particulate systems - Vocabulary. 2022.

[52] OECD (2018), *Guidance Document on Inhalation Toxicity Studies - Second edition*, OECD Series on Testing and Assessment, No. 39, OECD Publishing, Paris, https://doi.org/10.1787/fba59116-en.

[53] CEN ISO/TS 80004-1:2023, Nanotechnologies -- Vocabulary -- Part 1: Core terms 2023.

[54] ISO 12640-2:2004, Graphic technology — Prepress digital data exchange. Part 2: XYZ/sRGB encoded standard colour image data (XYZ/SCID). 2004.

[55] World Health Organization (WHO). Determination of airborne fiber number concentrations: A recommended method, by phase-contrast optical microscopy (membrane filter method). https://iris.who.int/handle/10665/41904. World Heal Organ Geneva 1997:1–53.

[56] EN 481:1993, Workplaces atmospheres-Size fraction definitions for measurement of airborne particles 1993.

[57] OECD (2023), *Test No. 125: Nanomaterial Particle Size and Size Distribution of Nanomaterials*, OECD Guidelines for the Testing of Chemicals, Section 1, OECD Publishing, Paris, https://doi.org/10.1787/af5f9bda-en.

# Appendix

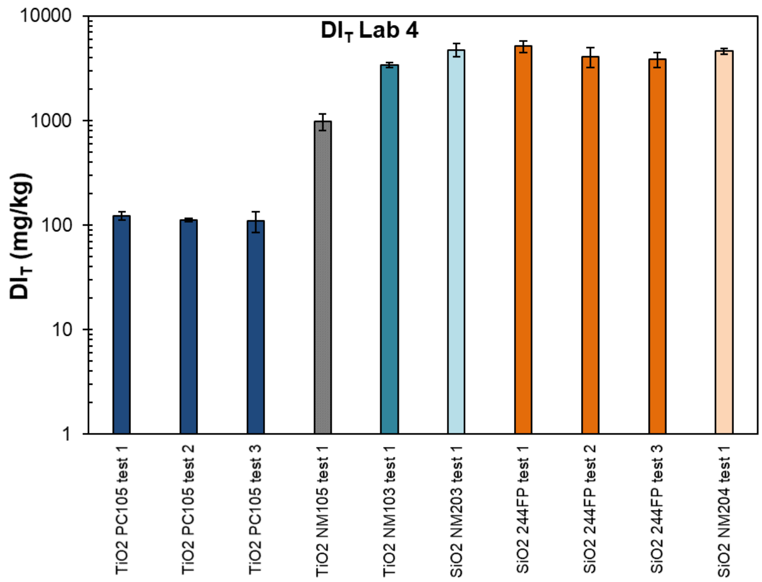


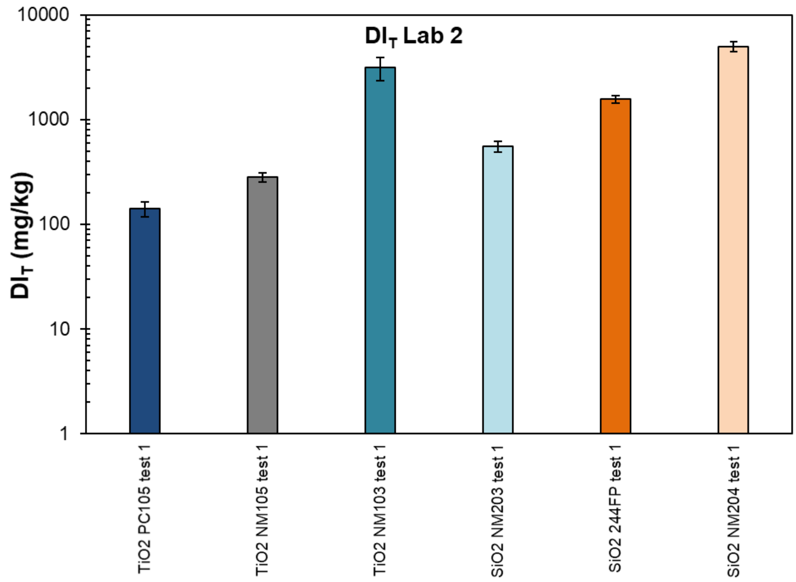

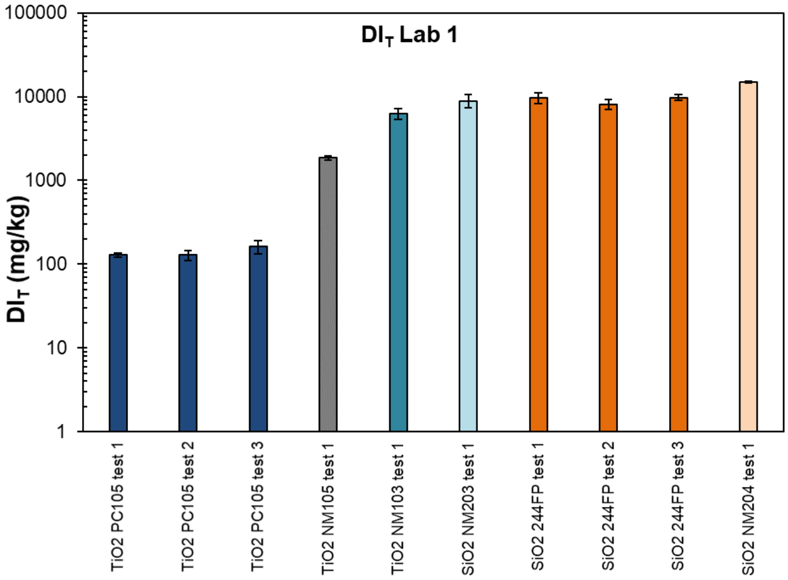
DI$_T$ Lab 1
DI$_T$ (mg/kg)
100000
10000
1000
100
10
1
TiO2 PC105 test 1
TiO2 PC105 test 2
TiO2 PC105 test 3
TiO2 NM105 test 1
TiO2 NM103 test 1
SiO2 NM203 test 1
SiO2 244FP test 1
SiO2 244FP test 2
SiO2 244FP test 3
SiO2 NM204 test 1

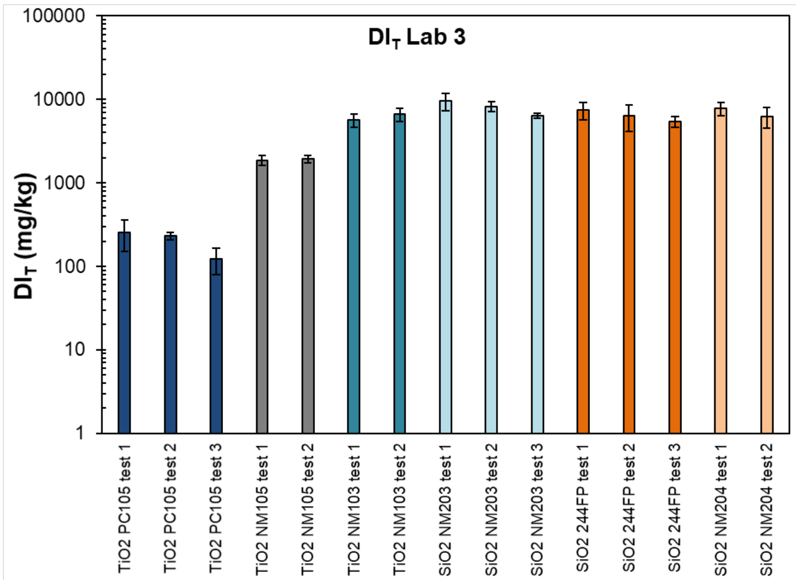
DI$_T$ Lab 3
DI$_T$ (mg/kg)
100000
10000
1000
100
10
1
TiO2 PC105 test 1
TiO2 PC105 test 2
TiO2 PC105 test 3
TiO2 NM105 test 1
TiO2 NM105 test 2
TiO2 NM103 test 1
TiO2 NM103 test 2
SiO2 NM203 test 1
SiO2 NM203 test 2
SiO2 NM203 test 3
SiO2 244FP test 1
SiO2 244FP test 2
SiO2 244FP test 3
SiO2 NM204 test 1
SiO2 NM204 test 2

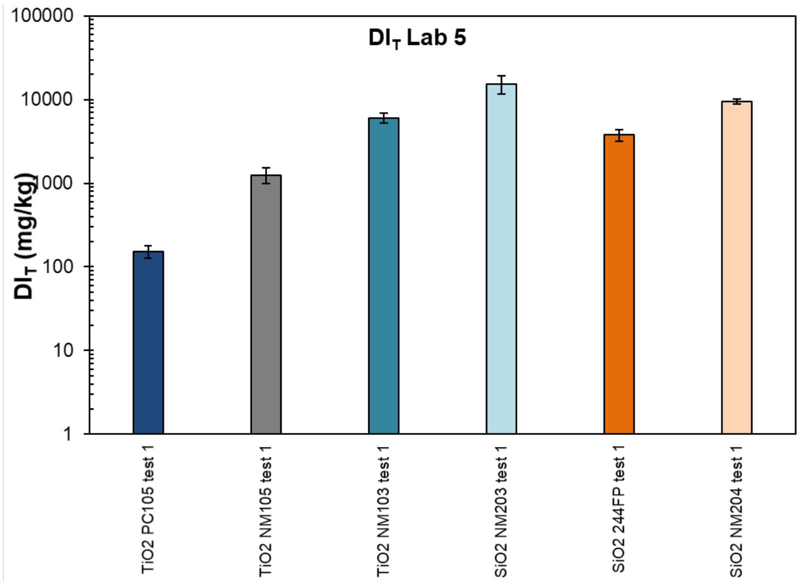


**Figure A1. Thoracic mass dustiness index obtained per test (with replicates standard deviation) and material for each participating Rotating Drum laboratories.**

179.

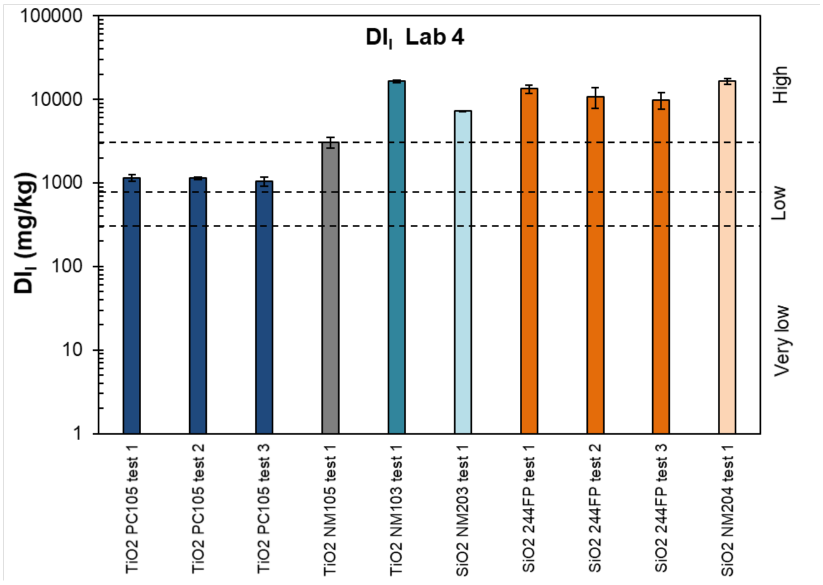

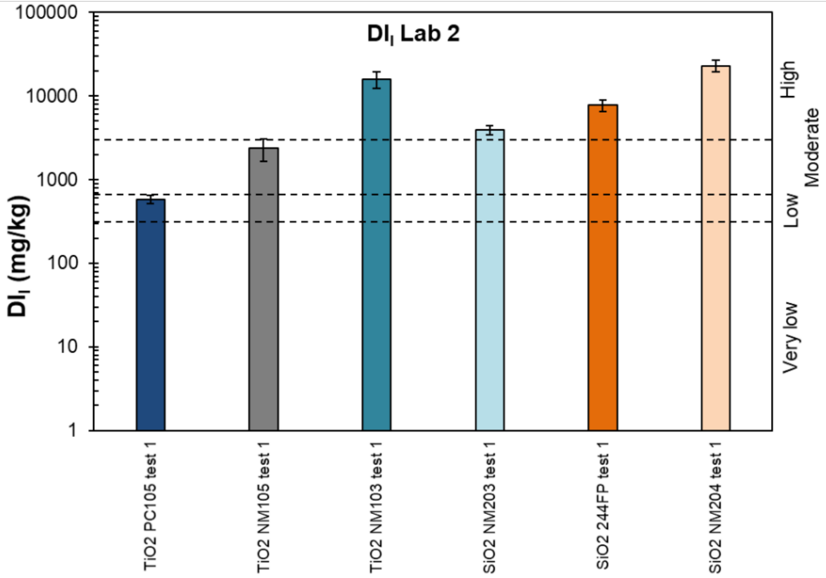
DI$_l$ Lab 2
100000
10000
1000
100
10
1
DI$_l$ (mg/kg)
High
Moderate
Low
Very low
TiO2 PC105 test 1
TiO2 NM105 test 1
TiO2 NM103 test 1
SiO2 NM203 test 1
SiO2 244FP test 1
SiO2 NM204 test 1

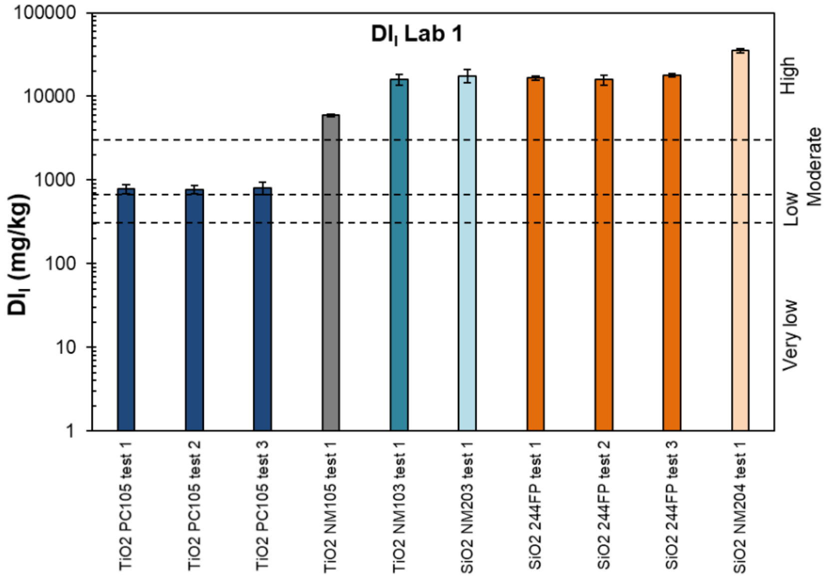
DI$_l$ Lab 1
100000
10000
1000
100
10
1
DI$_l$ (mg/kg)
High
Moderate
Low
Very low
TiO2 PC105 test 1
TiO2 PC105 test 2
TiO2 PC105 test 3
TiO2 NM105 test 1
TiO2 NM103 test 1
SiO2 NM203 test 1
SiO2 244FP test 1
SiO2 244FP test 2
SiO2 244FP test 3
SiO2 NM204 test 1

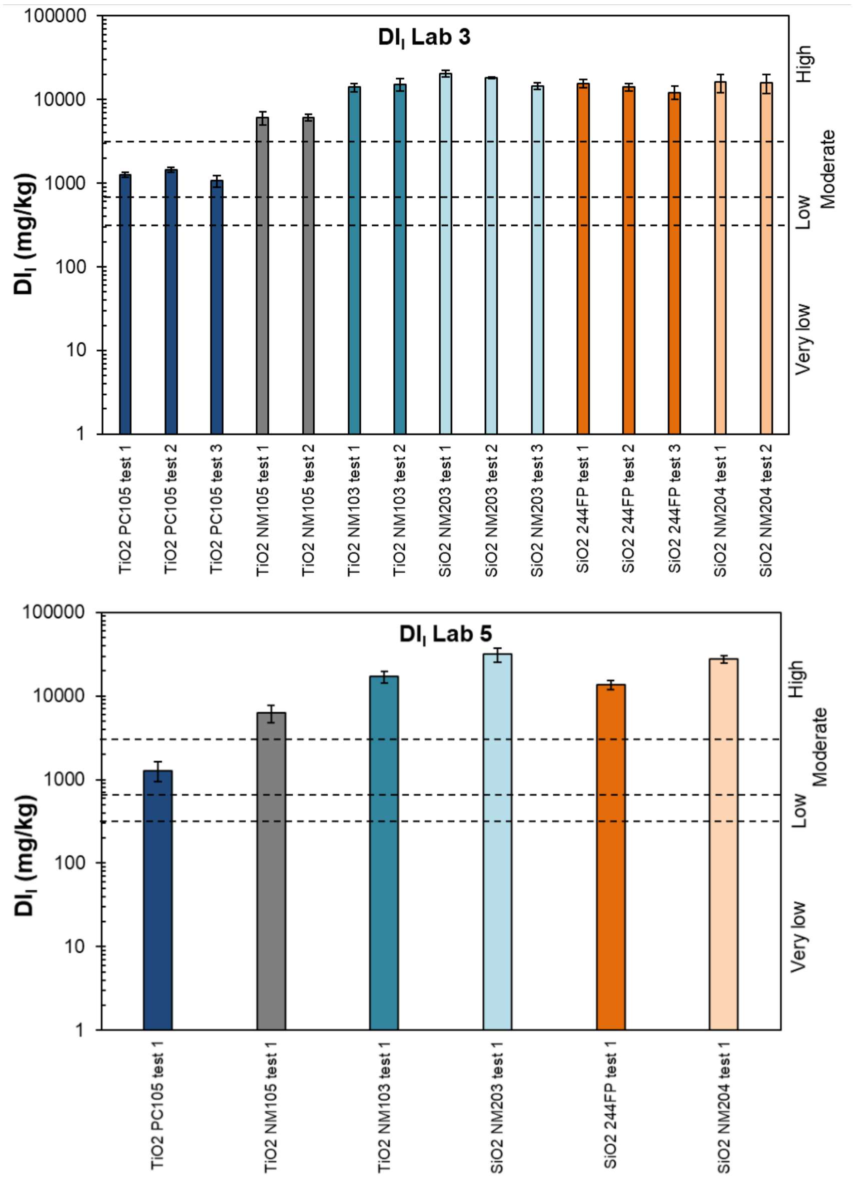


**Figure A2. Inhalable mass dustiness index obtained per test (with replicates standard deviation) and material for each participant Rotating Drum laboratory.**

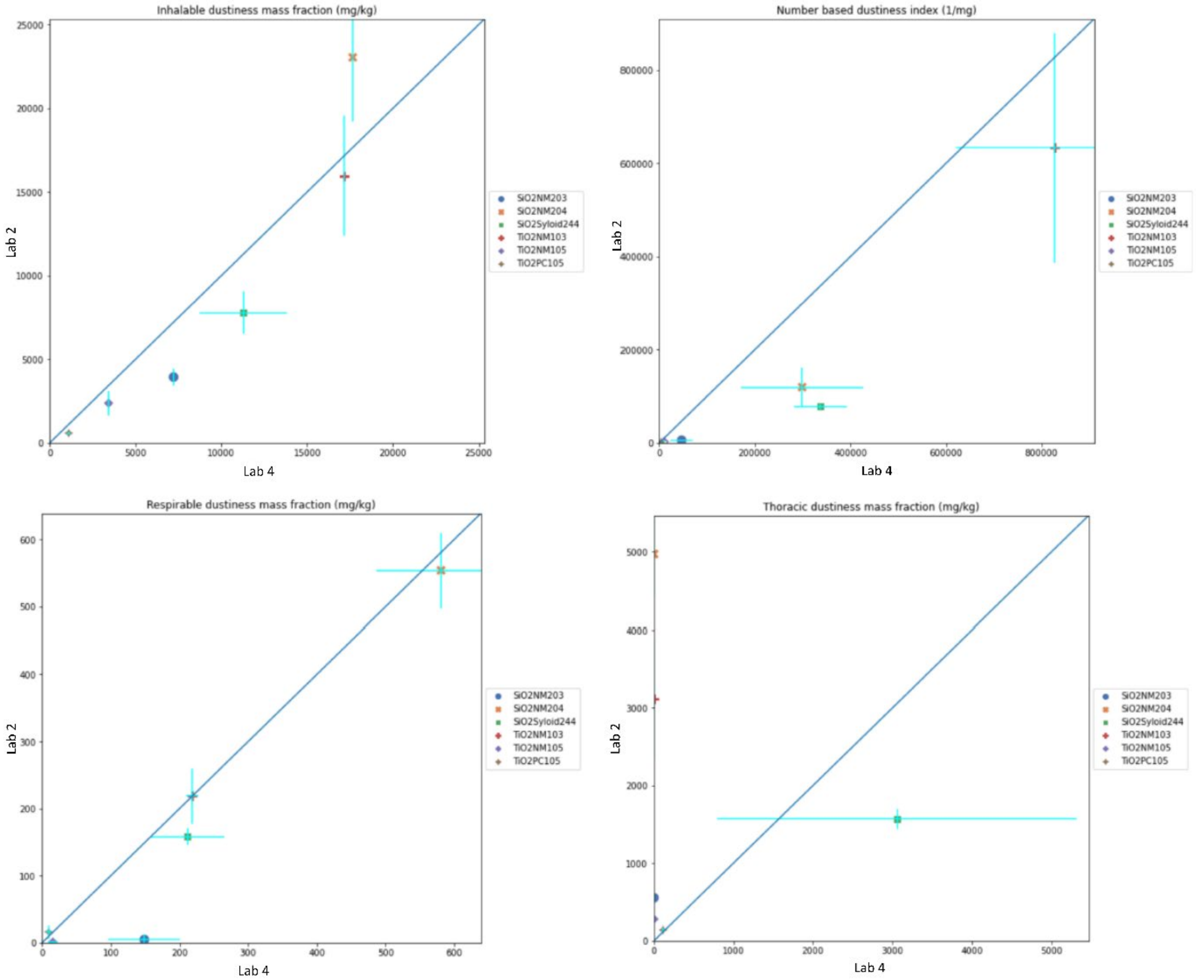


**Figure A3. Comparison and correlation between Lab 4 and Lab 2 for inhalable, respirable, thoracic and number-based dustiness index.**

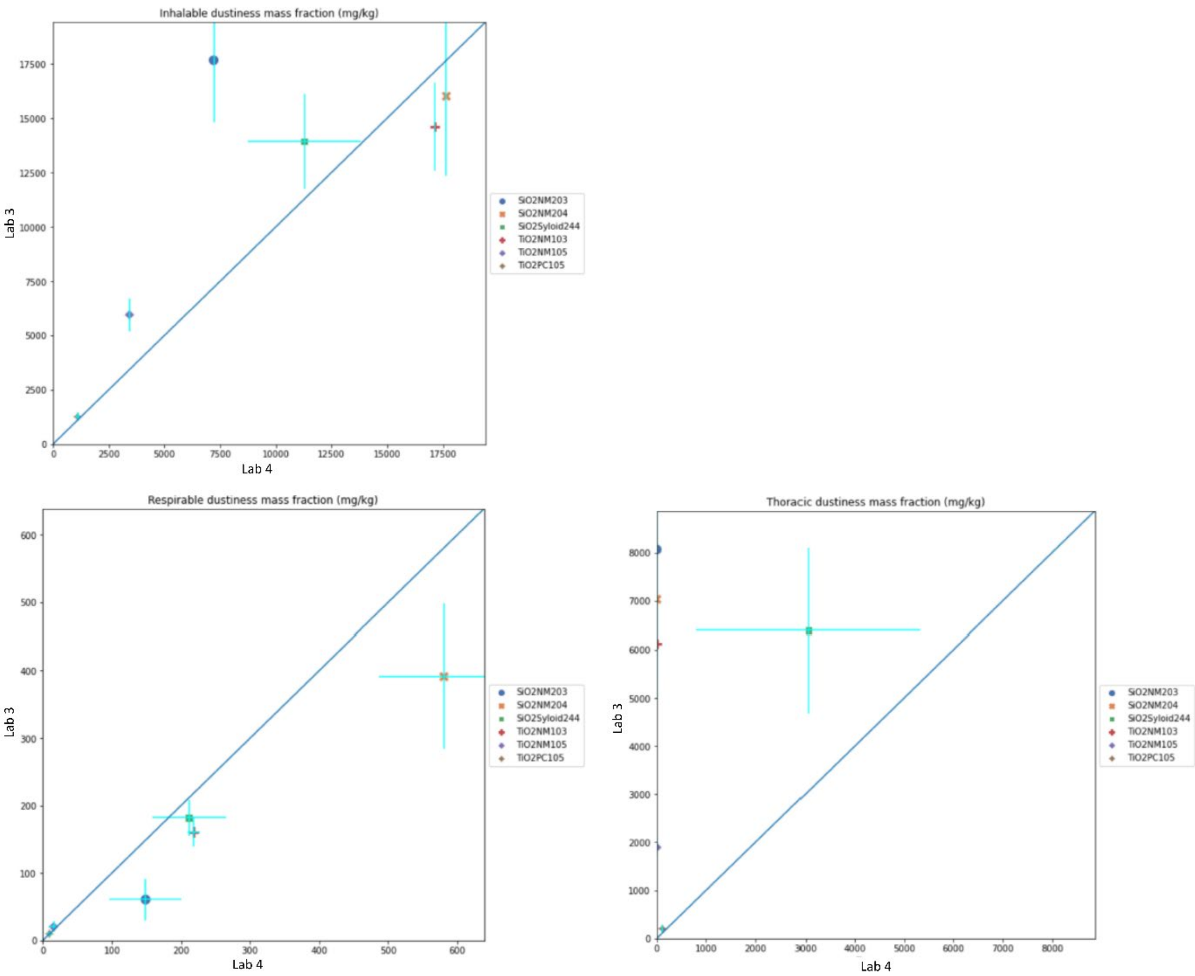


**Figure A4. Comparison and correlation between Lab 4 and Lab 3 for inhalable, respirable, and thoracic dustiness index.**

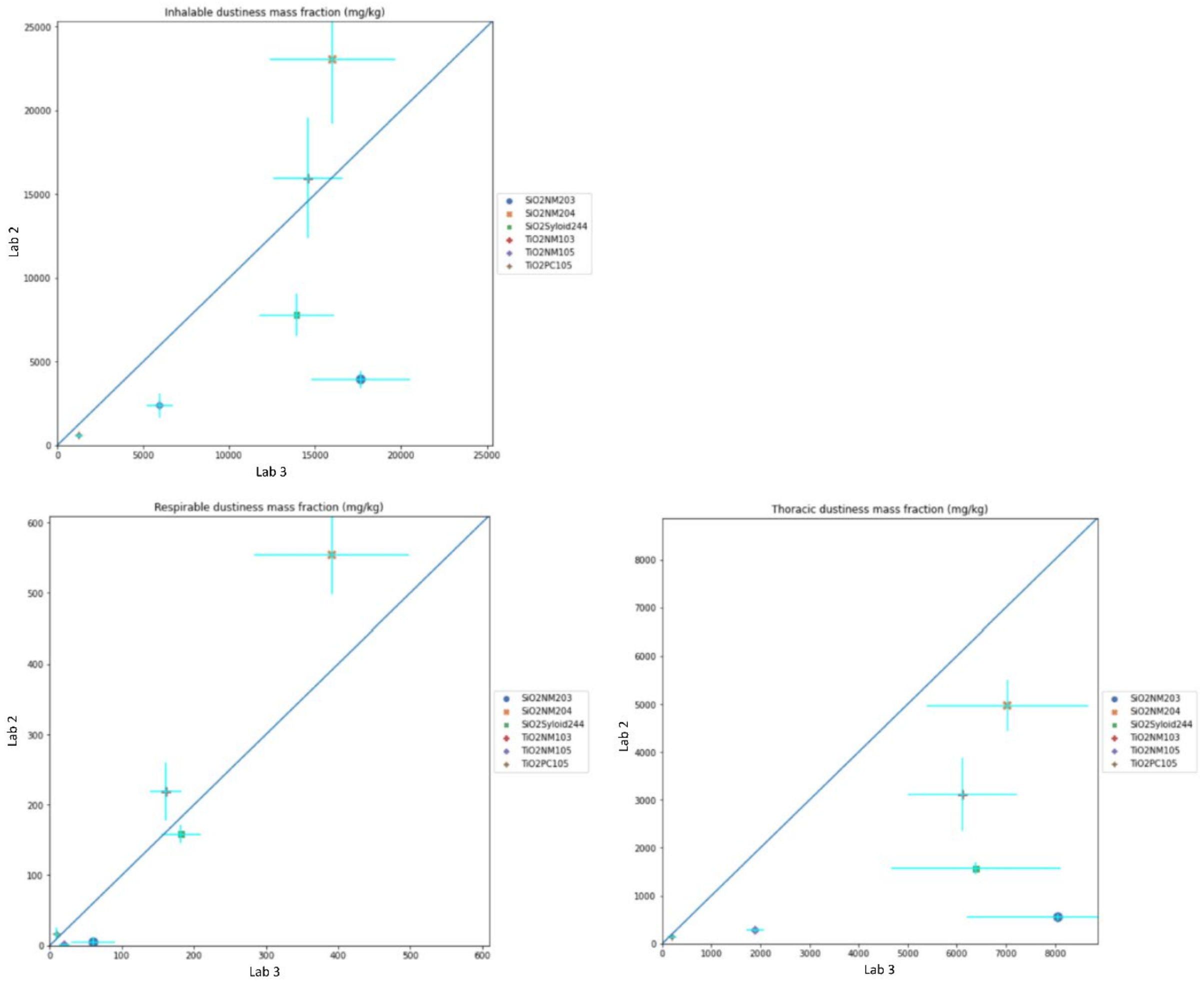


**Figure A5. Comparison and correlation between Lab 3 and Lab 2 for inhalable, respirable, and thoracic dustiness index.**

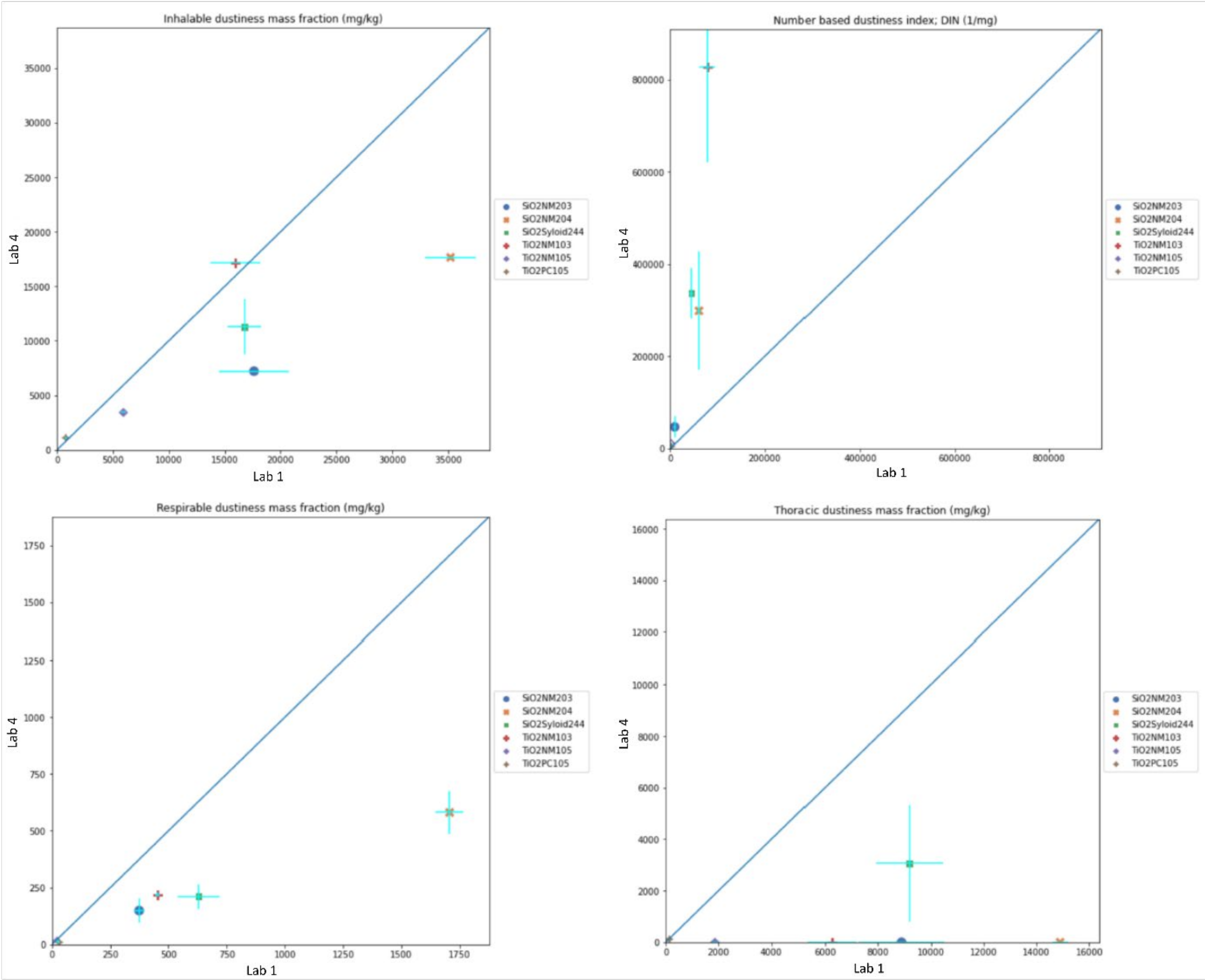


**Figure A6. Comparison and correlation between Lab 1 and Lab 4 for inhalable, respirable, thoracic and number-based dustiness index.**

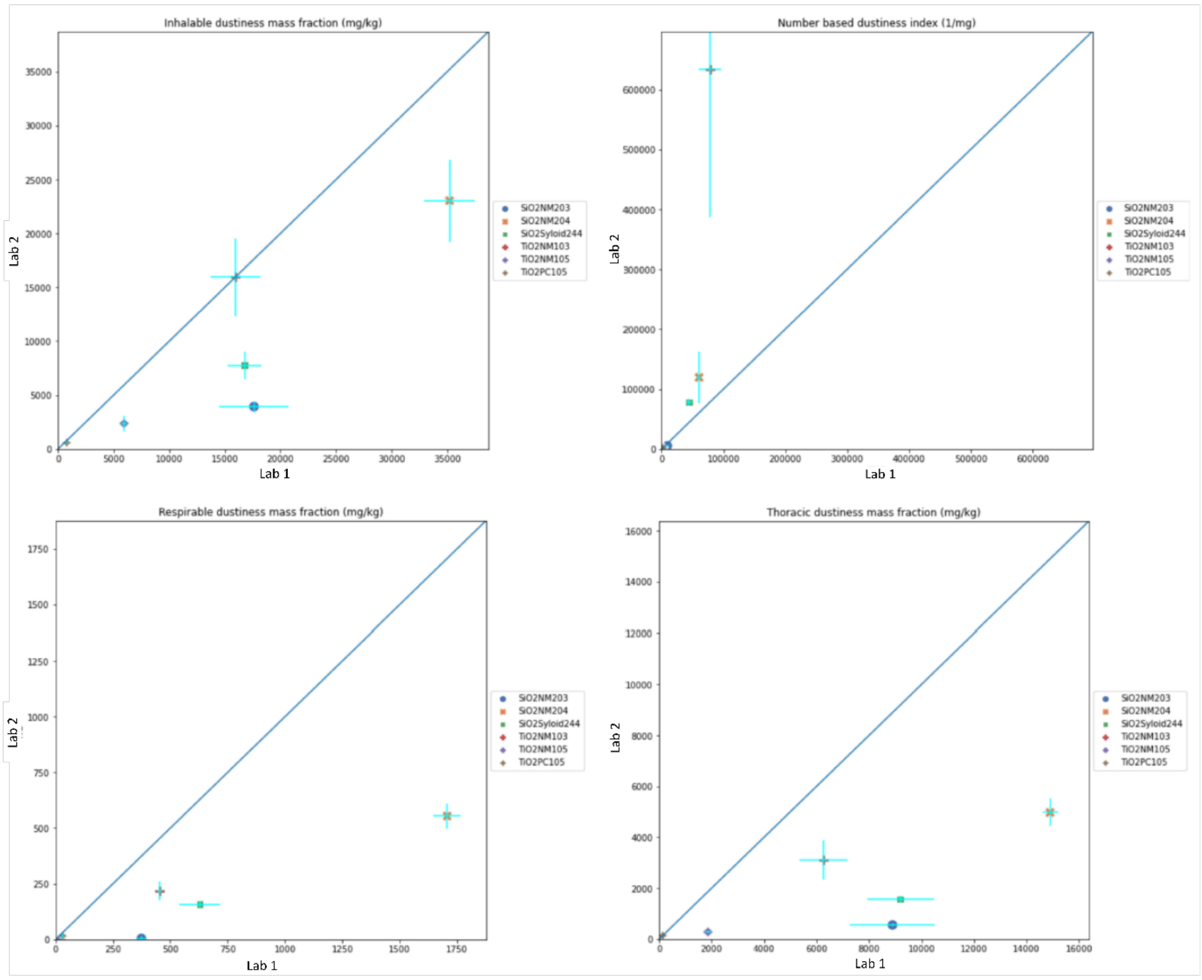


**Figure A7. Comparison and correlation between Lab 1 and Lab 2 for inhalable, respirable, thoracic and number-based dustiness index.**

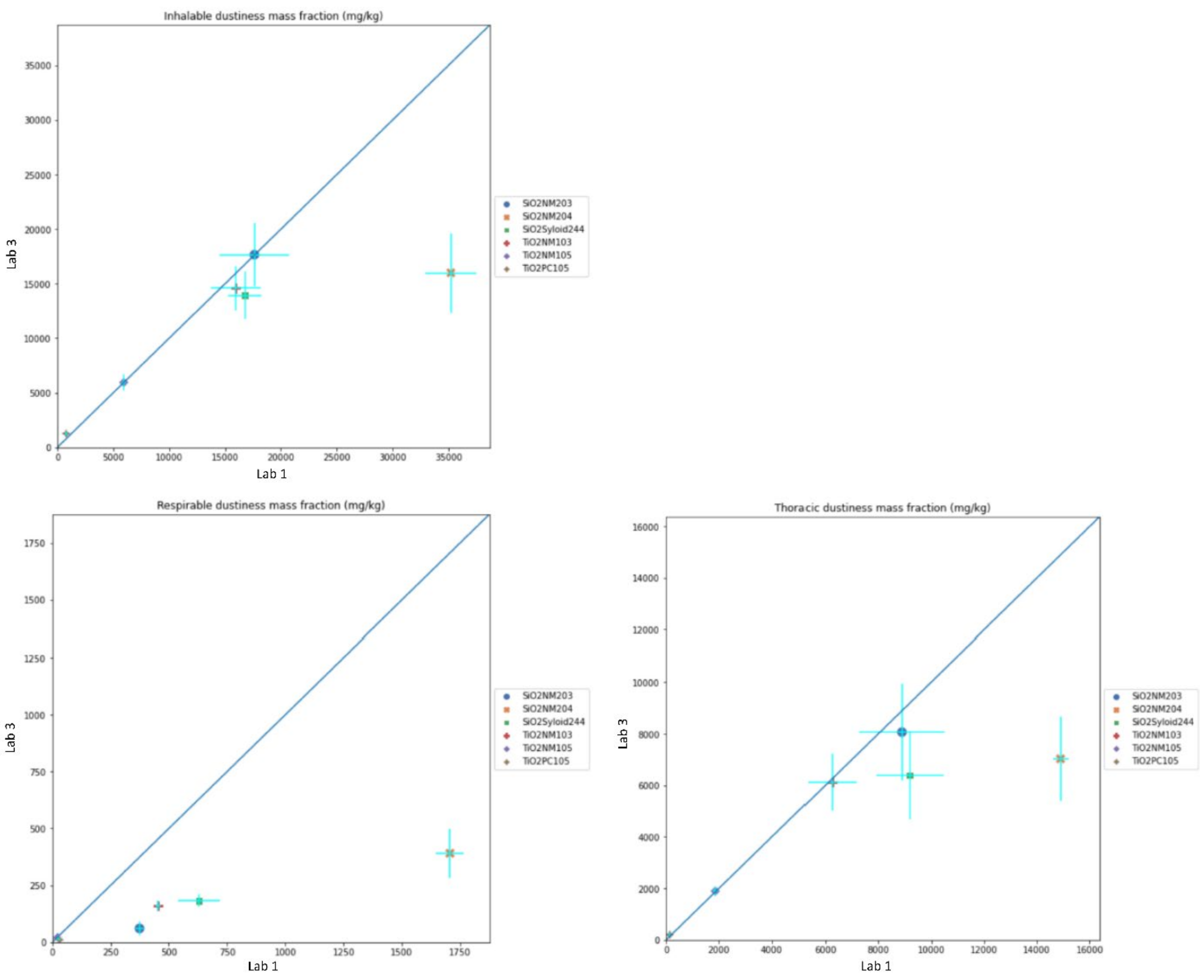


**Figure A8. Comparison and correlation between Lab 1 and Lab 3 for inhalable, respirable, and thoracic dustiness index.**

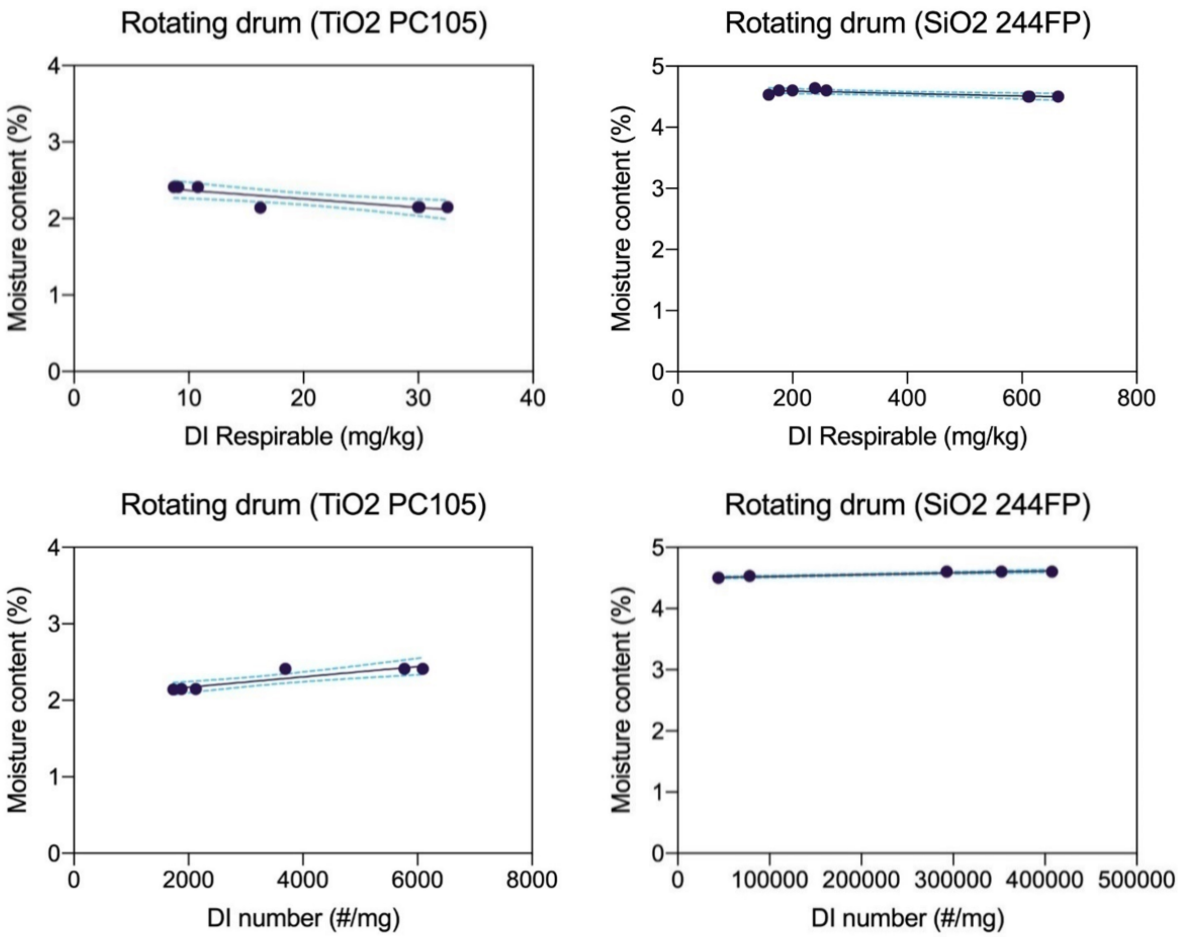


**Figure A9. Correlation between moisture content and respirable mass and particle number dustiness index for materials $TiO_2$ PC105 and $SiO_2$ 244FP with the Rotating Drum method.**

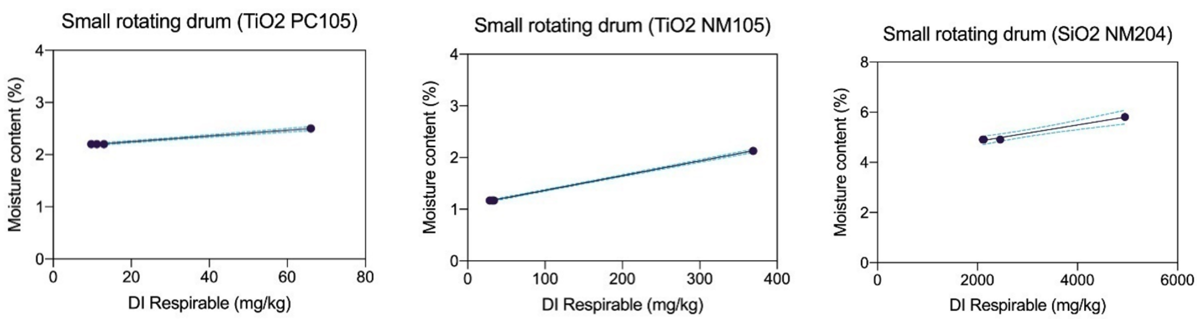


**Figure A10. Correlation between moisture content and respirable mass dustiness index for $TiO_2$ PC105, $TiO_2$ NM105 and $SiO_2$ NM204 with the Small Rotating Drum method.**

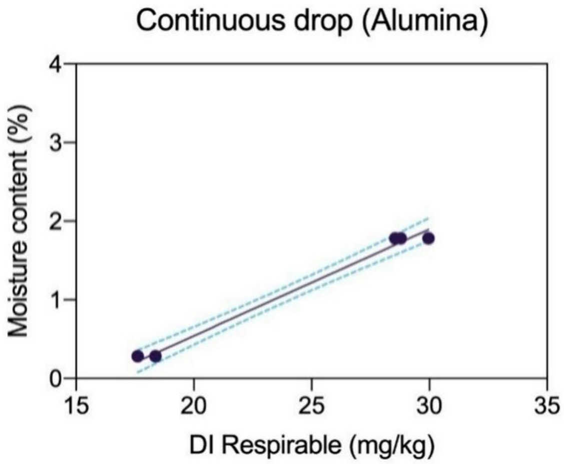


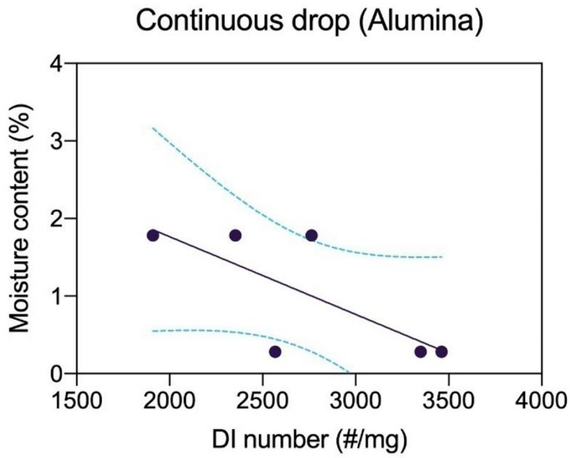


**Figure A11. Correlation between moisture content and respirable mass and particle number dustiness index for alumina material with the Continuous Drop method.**

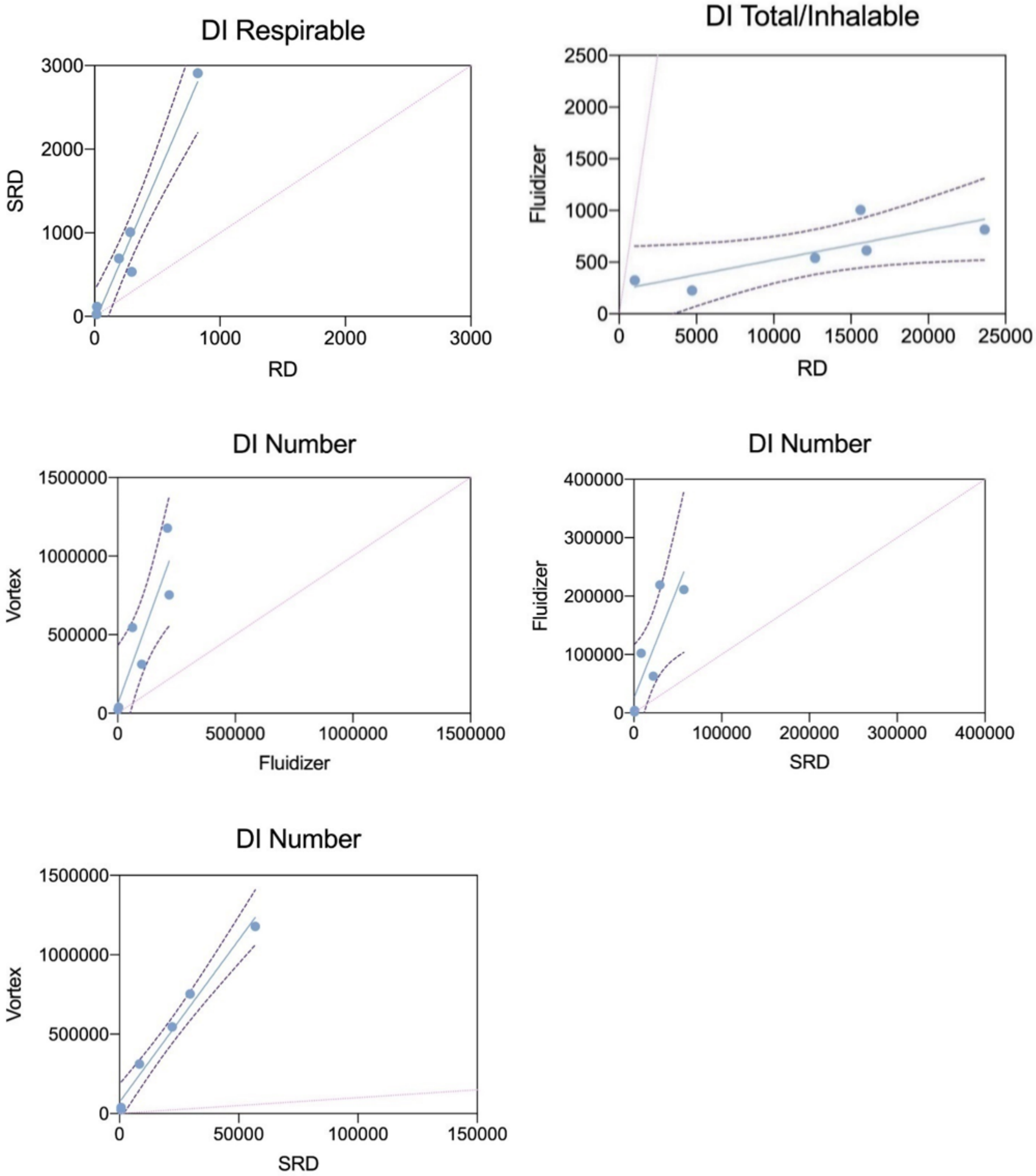
DI Respirable
SRD
RD
0
1000
2000
3000
DI Total/Inhalable
Fluidizer
RD
0
500
1000
1500
2000
2500
5000
10000
15000
20000
25000
DI Number
Vortex
Fluidizer
0
500000
1000000
1500000
DI Number
Fluidizer
SRD
0
100000
200000
300000
400000
DI Number
Vortex
SRD
0
50000
100000
150000
500000
1000000
1500000

**Figure A12. Comparison and correlation between SRD and RD respirable dustiness index (top left), RD and Fluidizer total/inhalable dustiness index (top right), and Fluidizer and vortex (middle left), SRD and Fluidizer (middle right), and SRD and Vortex (bottom left) particle number dustiness index. RD: Rotating Drum, and SRD: Small Rotating Drum.**

**Table A1. Rotating drum inhalable dustiness index calculated z-score.**

| Lab | $TiO_2$ PC105 | $TiO_2$ NM-105 | $TiO_2$ NM-103 | $SiO_2$ NM-203 | $SiO_2$ 244FP | $SiO_2$ NM-204 |
|---|---|---|---|---|---|---|
| Lab 4 | 0.37 | 1.19 | 0.23 | 1.08 | 0.61 | 0.90 |
| Lab 2 | 1.56 | 1.57 | 0.00 | 1.41 | 1.63 | 0.01 |
| Lab 1 | 0.80 | 0.45 | 0.01 | 0.05 | 1.00 | 1.59 |
| Lab 3 | 0.95 | 0.46 | 0.58 | 0.05 | 0.17 | 0.94 |
| Lab 5 | 1.05 | 0.62 | 0.46 | 1.34 | 0.08 | 0.60 |

**Table A2. Rotating drum thoracic dustiness index calculated z-score.**

| Lab | $TiO_2$ PC105 | $TiO_2$ NM-105 | $TiO_2$ NM-103 | $SiO_2$ NM-203 | $SiO_2$ 244FP | $SiO_2$ NM-204 |
|---|---|---|---|---|---|---|
| Lab 4 | 0.61 | 0.66 | 1.24 | 0.75 | 0.61 | 1.04 |
| Lab 2 | 0.19 | 1.84 | 1.41 | 1.56 | 1.64 | 0.94 |
| Lab 1 | 0.19 | 0.83 | 0.62 | 0.05 | 1.18 | 1.93 |
| Lab 3 | 0.87 | 0.88 | 0.53 | 0.11 | 0.14 | 0.34 |
| Lab 5 | 0.03 | 0.19 | 0.49 | 1.30 | 0.81 | 0.37 |

# Definitions

180. This chapter provides definitions of key terms used in this report.

**Accuracy** (ISO 5725-1:2023 [39])

The closeness of agreement between a measured value and the true or accepted reference value. It includes both trueness (how close the measurement is to the true value) and precision (how close repeated measurements are to each other).

**Agglomerate** (ISO 26824:2022 [51]; OECD TG 125:2023 [27])

Collection of weakly or medium strongly bound particles where the resulting external surface area is similar to the sum of the surface areas of the individual components.

**Aggregate** (ISO 26824:2022 [51]; OECD TG 125:2023 [27])

Particle comprising strongly bonded or fused particles where the resulting external surface area may be significantly smaller than the sum of calculated surface areas of the individual components.

**Aspect ratio** (OECD TG 125:2023 [27])

Ratio of length of a particle (the longest dimension) to its width (the shortest dimension).

**Dustiness index** (EN 17199-1:2019 [14])

The dustiness index quantifies the tendency of a material to release airborne particles when subjected to mechanical forces. It is measured either as a mass-based index, which represents the mass of released (dust) particles generated per unit mass of the material, or as a number-based index, which counts the number of released (dust) particles generated per unit mass of material. *Note: the number of particles refers to the total count of airborne individual constituent particles, as well as agglomerates and aggregates (with each agglomerate and each aggregate counted as one individual particle).*

**Fibre** (OECD TG 125:2023 [27])

Unbound, individual object or nano-object with two approximately equal lateral dimensions D $= x1 \cong x2$ (i.e. the diameters of the fibre) and a third longitudinal extension L (i.e. the length of the fibre) which exceeds D by at least a factor of 3. In other words, a fibre is an object with an aspect ratio of $L / D \geq 3$.

**Fibrous NOAA with potentially critical dimensions**

Fibrous NOAA with a length L longer than 5 µm, a diameter D smaller than 3 µm and an aspect ratio equal to or greater than 3 based on the counting convention for mineral fibres that pose health risks [55].

**Inhalable fraction** (OECD GD 39:2018 [52])

Fraction of an aerosol that can enter the human respiratory system through the nose and mouth.

**Inter-laboratory comparison** (ISO 5725:2019)

A comparison of test results obtained by different laboratories, used to assess the reproducibility of a test method.

**Intra-laboratory comparison** (ISO 5725:2019)

A comparison of test results obtained within the same laboratory, often used to assess repeatability and accuracy.

**Nano-object** (CEN ISO/TS 80004-1:2023 [53]; OECD TG 125:2023 [27])

Discrete piece of material with one, two or three external dimensions in the nanoscale.

**Nano-objects and their aggregates and agglomerates (NOAA)** (CEN ISO/TS 80004-1:2023; [53])

Material comprising nano-objects, and their aggregates and agglomerates. Note 1 to entry: NOAA include structures with one, two or three external dimensions in the nanoscale, which can be spheres, fibres, tubes and others as primary structures. NOAA can consist of individual primary structures in the nanoscale and aggregated or agglomerated structures, including those with sizes larger than 100 nm.

**Nanoscale** (OECD TG 125:2023 [27])

Length range defined e.g. by legislation or standardisation bodies for their specific uses.

**Number-based dustiness kinetics** (EN 17199-1:2019 [14])

The number-based dustiness kinetics describes the rate at which the number of respirable particles is released during the initial stages of the dustiness test. It is measured in particles per milligram per second squared and helps assess the dynamics of particle release over time.

**Number-based emission rate** (EN 17199-1:2019 [14])

The number-based emission rate refers to the quantity of particles released per unit mass of the tested material over time. It is measured in particles per milligram per second, and it provides an indication of how quickly these particles are emitted during a dustiness test.

**Outlier** (ISO 5725-2:2025 [26])

A data point that significantly deviates from the rest of the dataset, potentially due to measurement errors, instrument malfunction, or other anomalies. Outliers can skew results and are typically removed after verification of their source.

**Particle** (OECD TG 125:2023 [27])

Minute piece of matter with defined physical boundaries

**Particle size** (OECD TG 125:2023 [27])

Size of the particles, aggregates or agglomerates is given in micrometres (µm) or nanometres (nm). The measured particle size depends on the measurement method used.

**Particle size distribution** (OECD TG 125:2023 [27])

Distribution of the quantity of particles (for example, number, mass or volume based) as a function of particle size. Note: In particle size measurements for dustiness, each agglomerate and each aggregate is measured as one individual particle.

**Pixel** (ISO 12640-2:2004 [54])

Smallest element of an image that can be uniquely processed, and is defined by its spatial coordinates and encoded with colour values.

**Repeatability** (ISO 5725-2:2025 [26])

The degree of agreement between successive measurements of the same sample under the same conditions (e.g., same laboratory, operator, equipment, and test procedure). It reflects the consistency of results when tests are repeated within a short time interval.

**Reproducibility** (ISO 5725-2:2025 [26])

The degree of agreement between measurements of the same sample made under different conditions, such as in different laboratories, by different operators, or with different equipment. It is a measure of how well a method or procedure can produce consistent results across different environments.

**Resolution** (OECD TG 125:2023 [27])

Refers to pixel size in the digital electron micrographs.

**Respirable fraction** (OECD GD 39:2018 [52])

Fraction of aerosol that can reach the gas exchange region of the respiratory system (i.e., the alveoli). For details see EN 481:1993 [56].

**Straggler** (ISO 5725-2:2025 [26])

A data point that is slightly unusual or inconsistent but does not deviate as drastically as an outlier. Stragglers are often identified by statistical tests but may not be removed unless there is a clear technical justification.

**Time-based dustiness kinetics** (EN 17199-1:2019 [14])

Time-based dustiness kinetics refers to the time required for a dustiness test to generate 50% of the total number of particles released during the test. It is measured in seconds and provides insight into how quickly the particle generation reaches half of the total amount produced.

**Thoracic fraction** (OECD GD 39:2018 [52])

Fraction of aerosol that can reach the lung airways and the gas-exchange region. See also Respirable fraction, Inhalable aerosol.

# Annex A. Template for dustiness results reporting

Annex A consists of an Excel file containing a standardised template for reporting ILC results. Each participating laboratory completes this template for each dustiness method tested. The template includes six worksheets, each requiring specific information:

- **Powder characteristics and test**: Details the physical properties of the powder and the conditions under which the test was conducted.
- **Instruments and samplers**: Specifies the instruments and samplers used during the dustiness testing to ensure consistent methodology across laboratories.
- **Moisture content**: Records the moisture content of the powder, a key factor influencing dustiness behavior.
- **Bulk density**: Captures the bulk density of the material, which can affect the dust generation during testing.
- **Dustiness data**: This worksheet is used to report the dustiness test results, ensuring all relevant data points are consistently documented.
- **Morphological and chemical analysis**: Summarizes any morphological and chemical analyses of the powder, including particle size, shape, and composition, where applicable.

# Annex B. Macro script – guidance document

*Version 2.00*

**Intention of this document**: To help dustiness testers to automatically derive relevant dustiness parameters (sections 1-5) from the condensation particle counter (CPC) data recorded with a time resolution of 1 s.

Before any use of the CPC data, the concentrations measured shall be corrected for background and noise using the measurement data obtained during the first 5 min before the 1 minute drum rotating part of the Small Rotating Drum and Rotating Drum testing.

**1-Average number concentration measured by CPC [#/cm³]**

The average number concentration is calculated according to eq. 1.

$$\overline{C}_{CPC}=\frac{\sum_{t_0}^{t_0+60} C(t)}{60} \qquad \text{Eq. 1}$$

Where *C(t)* is the particle number concentration at time *t* in number of particles per cubic centimeter [#/cm³];

**2-Number-based average emission rate ($E_i$) [#/s] and Number-based average emission rate per mg powder ($PNE_i$) [#/mg·s]**

The particle number emission rate, $E_i$ [1#/s], is calculated based on the governing mass balance equation (eq. 2 and 3) which is similar as the equation previously described by Schneider & Jensen (2008) [4] and Jensen et al. (2009) [13] stated on the Small Rotating Drum standard EN 17199-4.

$$V_d \cdot \frac{dC}{dt}=E_i-QC \qquad \text{Eq. 2}$$

$$E_i=V_d\frac{dC}{dt}+QC \qquad \text{Eq. 3}$$

where $\frac{dC}{dt}$ is the change in background-corrected particle number concentration [#/cm$^3$·s], recorded by the CPC, $V_d$ is the volume of the drum e.g. 5675 cm$^3$, and Q [cm$^3$/s] is the volume flow rate through the drum.

$V_d$ is related to the exponential decay rate, $\lambda$, [1#/s] by eq. 4.

$V_d = \frac{Q}{\lambda}$ Eq. 4 (use determined $V_d$ In Eq. 3)

The time constant of the system, $\tau$ [s], is calculated according to eq. 5.

$\tau = \frac{1}{\lambda}$ Eq. 5

To calculate the average powder-normalised particle number emission rate $PNE_i$, [#/mg·s] is calculated according to eq. 6.

$PNE_i = \frac{\overline{E_i}}{m_{drum}}$ Eq. 6

Where $m_{drum}$ [mg], is the powder mass loaded into the drum, and $\overline{E_i}$ is the average emission rate during the 60 s rotation.

Because of the exponential particle decay rate, $\lambda$, is representing the overall loss rate of the system, including e.g. deposition losses in tubing and on surfaces, etc. The losses are calculated on a fit from the recorded particle number concentration. This fit needs to be done for each testing run, as it may be depending on the mixing state of the drum and the characteristics of the powder, as powder with larger particles will have a higher gravimetric deposition rate. The loss rate and thereby the time constant, $\tau$, may likely be different from the theoretically calculated values from eq. 4 and 5.

In reality, in a system such as the considered here, the mixing state of the powder in the drum is depending on the physical dust dispersion and behavior in the drum. If we consider the figure below, the powder is put in the middle of the drum and then we can conceptually think of the dust being generated during falling and to some extent the impact. If we simplify it into 3 conceptual scenarios (Fig 1):

1) Powder disperses from half-depth effectively in the entire drum before entering the sampling line, the theoretical time constant in the system $\tau$ is calculated using the full drum volume. E.g. theoretical $\tau$ = 31 s.
2) Powder disperses from half-depth effectively in the downstream half of the drum before it enters the sampling line, therefore only 50% of the drum volume is used to calculate the theoretical $\tau$. E.g. theoretical $\tau$ = 15.5 s.
3) Powder disperses from half-depth effectively in the downstream quarter of the drum before it enters the sampling line, therefore only 25% of the drum volume is used to calculate the theoretical $\tau$. E.g. theoretical $\tau$ = 7.74 s.

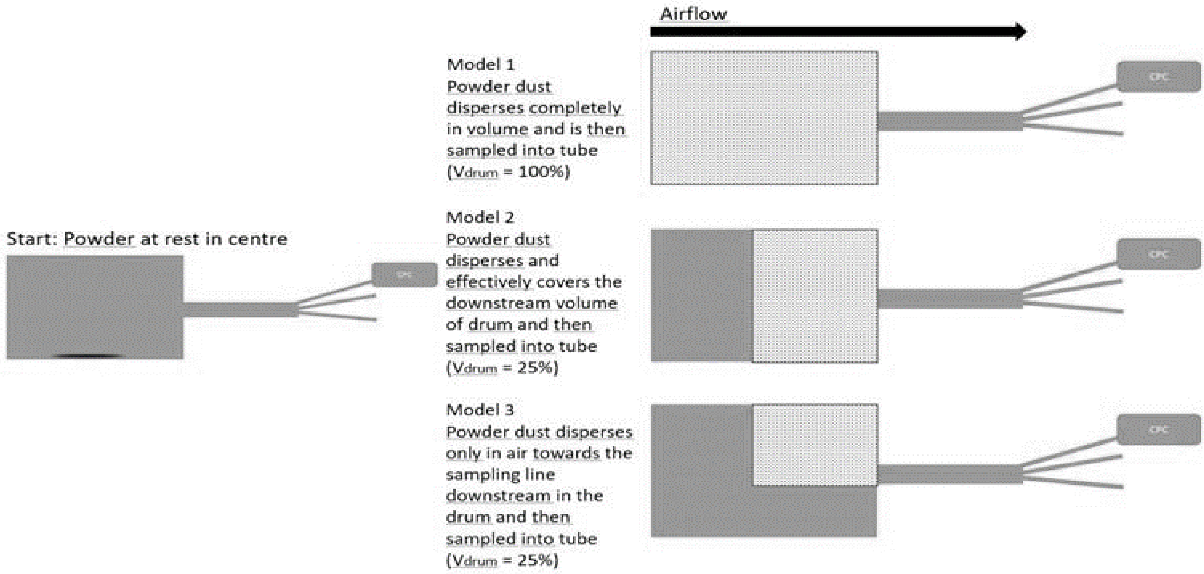


*Figure 1. Three conceptual scenarios of powder behaviour in the dustiness drum.*

**3- Number based dustiness index [#/mg]**

The number-based dustiness index, $DI_N$ [#/mg], is calculated according to eq 7.

$$DI_N = PNE_i \cdot 60s \quad \text{Eq. 7}$$

**4-Number-based initial dustiness kinetics, $D_{k,X}$ [#/mg·s²]**

The number-based initial dustiness kinetic, $D_{k,X}\left[\frac{1}{mg.s^2}\right]$, s is calculated as the maximum rate of increase in emission rate (Eq 8.). This is usually occurring in within the first 30 s of the rotation time.

$$D_{k,X} = \frac{E_{max}-E_0}{t_{max}-t_0}\frac{1}{m_{drum}} \quad \text{Eq. 8}$$

**5- Time-based dustiness kinetics, $D_{n50}$ [s], assessed as the time required to generate 50 % of the total number of particles released during the test**

The characteristic time, $D_{n50}$ [s], i.e., the time needed to reach 50 % of the released number of particles during the test is determined from the cumulative sum vector of the particle number concentration time series from $t_0$ when the rotation starts to $t_{360}$ 5 min after rotation ends.

**6- The Macro**

The created excel macro script covers all the parameters needed to be derived from the concentration data recorded with the CPC. It calculates the fitted loss rates and time constant, $\tau$ (named as fitted tau in the macro output) and use this value to calculate the emission/generation rates, the generation rate per mg from the background-corrected CPC data, the number-based dustiness index and the dustiness kinetics. It is therefore not needed to correct the CPC data prior to running the script as it is already taken into consideration the 5 min average concentrations before the 60 s of the actual dustiness testing (e.g. rotation). In addition, it gives the emission rate time series [in particles/s] in case you would like to plot.

Below there is a step-by-step guide on how to use the Excel macro script on a CPC data file exported to txt. Format and represented in two columns, time and concentration, respectively.

1. Please convert the file circulated by email "*dustines.txt* " to "*dustiness.bas*"
    a. Open the .txt file and click **File** > **save as** > replace **File name as "*dustiness.bas*" > Save**

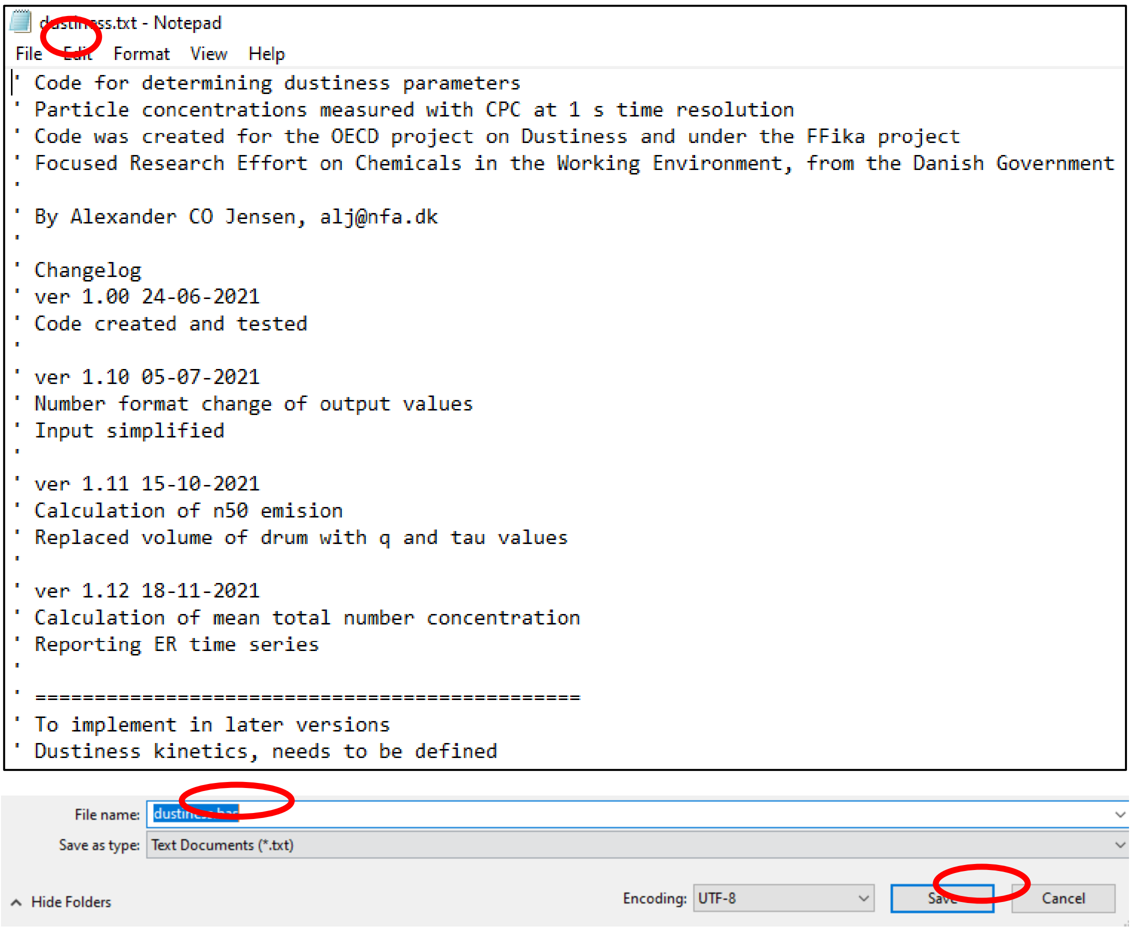

```
' Code for determining dustiness parameters
' Particle concentrations measured with CPC at 1 s time resolution
' Code was created for the OECD project on Dustiness and under the FFika project
' Focused Research Effort on Chemicals in the Working Environment, from the Danish Government
'
' By Alexander CO Jensen, alj@nfa.dk
'
' Changelog
' ver 1.00 24-06-2021
' Code created and tested
'
' ver 1.10 05-07-2021
' Number format change of output values
' Input simplified
'
' ver 1.11 15-10-2021
' Calculation of n50 emision
' Replaced volume of drum with q and tau values
'
' ver 1.12 18-11-2021
' Calculation of mean total number concentration
' Reporting ER time series
'
' ==============================================
' To implement in later versions
' Dustiness kinetics, needs to be defined
```



2. To load the data from .txt or .csv format into excel press the **data** ribbon on top

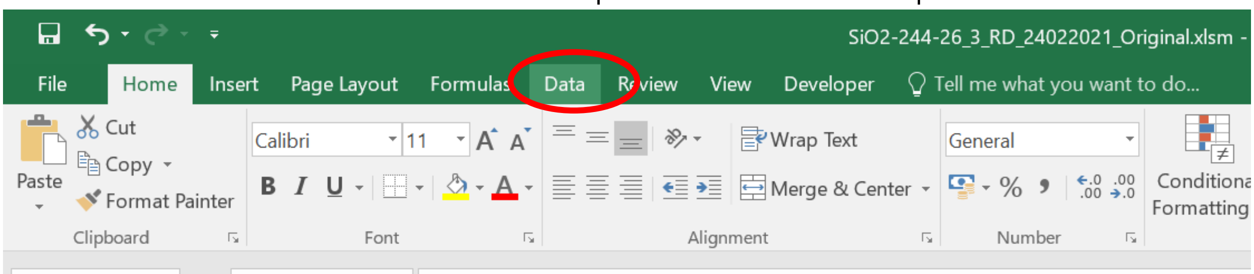


3. Import data from text file

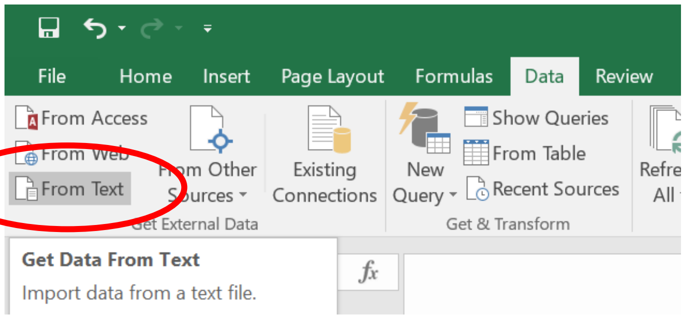


4. Choose the relevant CPC datafile in the dialogue and press **Open**
5. In the dialogue that comes up choose a **delimited** file and click **Next**

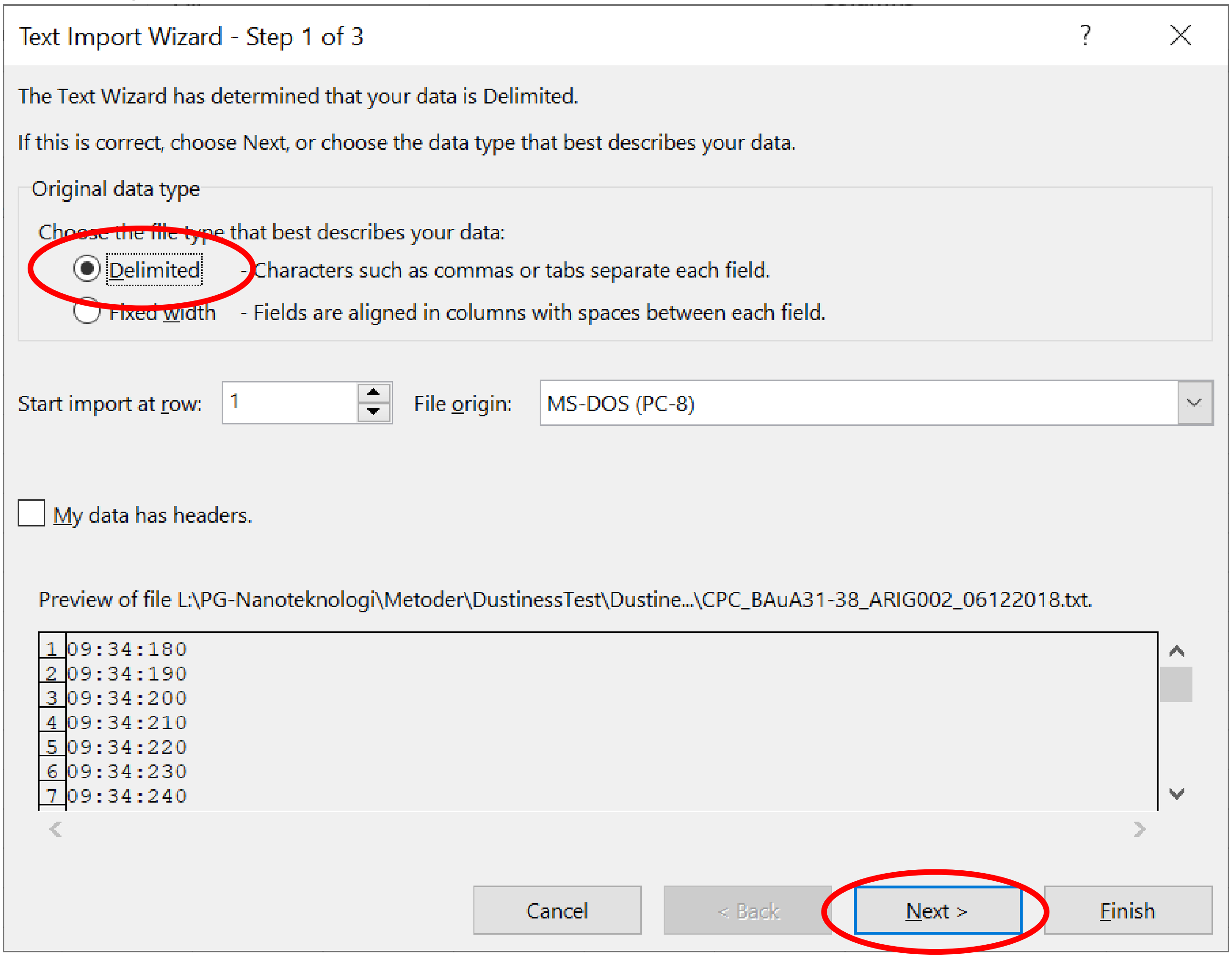


6. Select **Tab**, **Comma** and **Space** and press **Finish**. Ensure that the starting cell is '=$A$1' and click **OK**

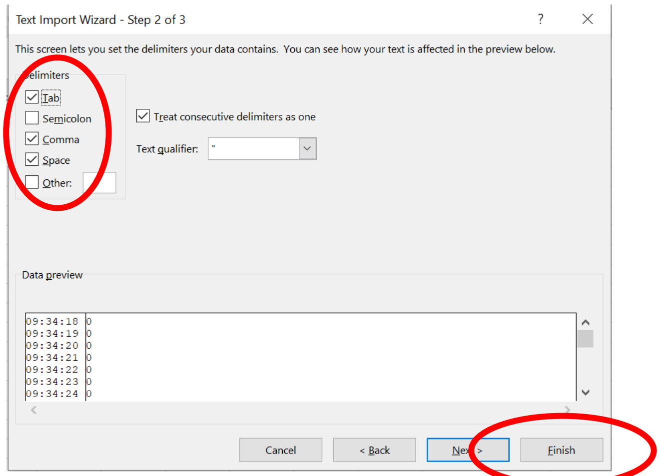


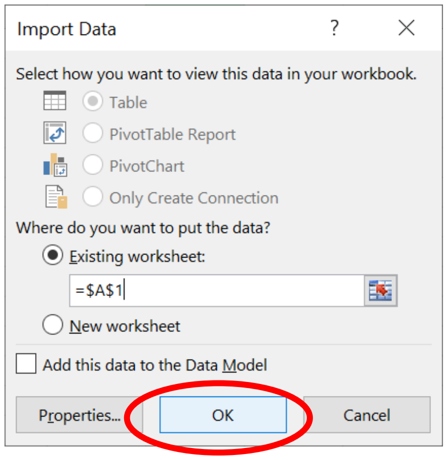


7. Press **save as** and save the file as an **.XLSM** file

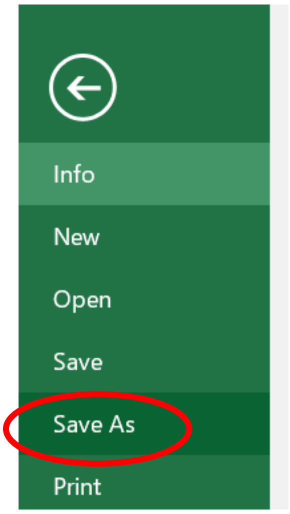

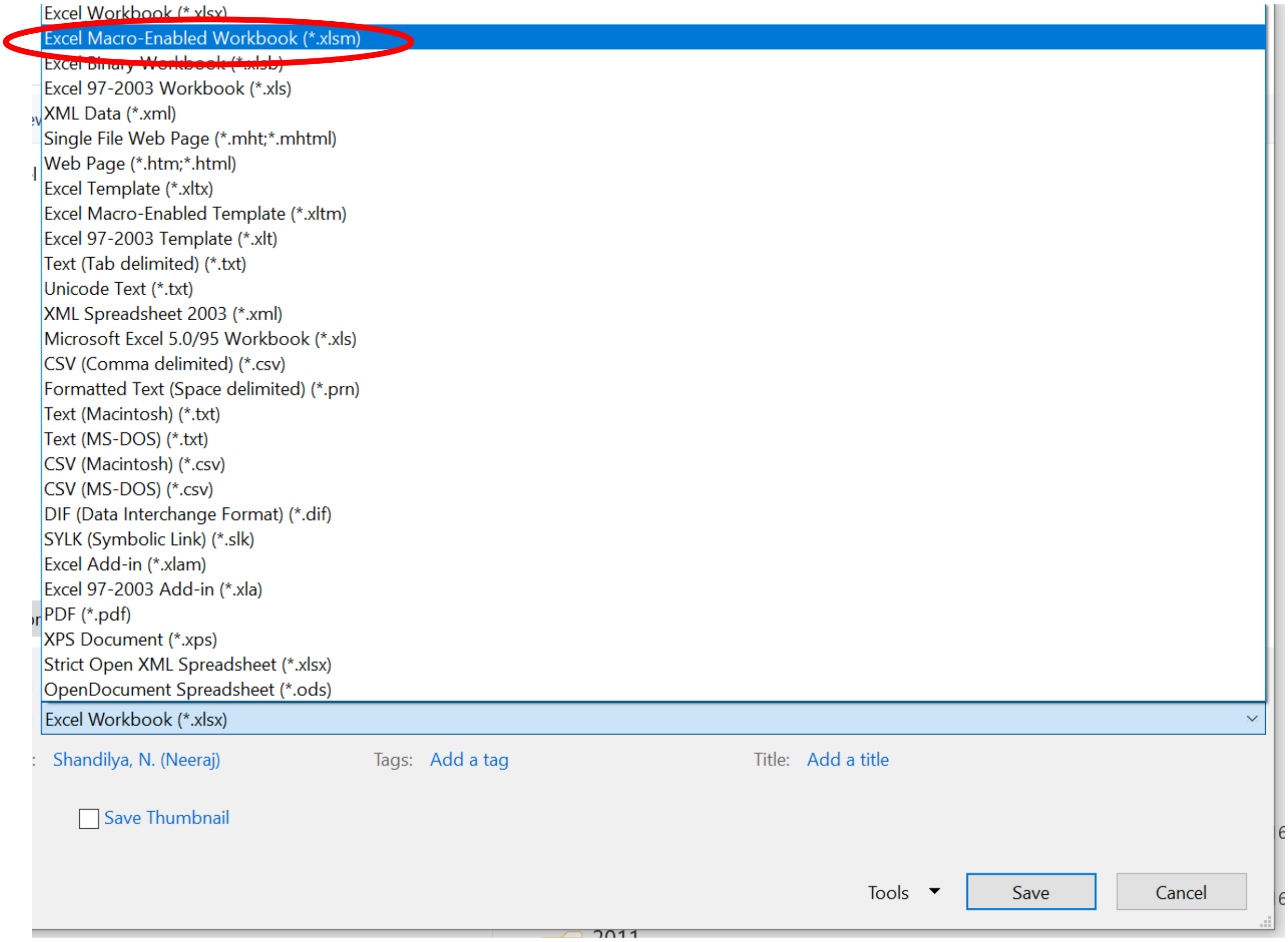


8. In case the **Developer tab** does not show in your Excel (please skip this step in case it shows):
    a. On the **File tab**, go to **Options** and click **Customize Ribbon**.
    b. Under Customize the Ribbon and under Main Tabs, select the **Developer** check box:

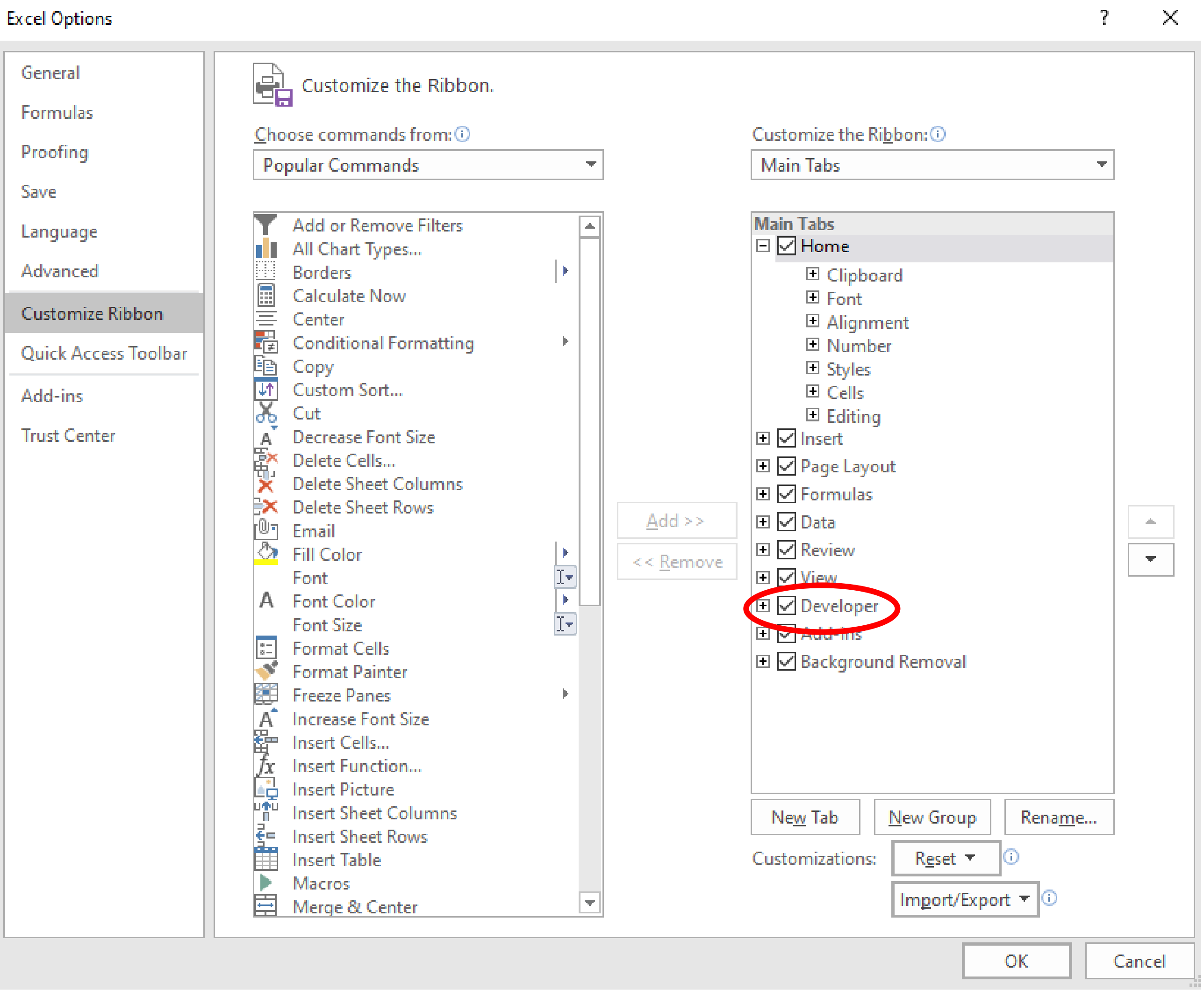


9. Go to the developer ribbon

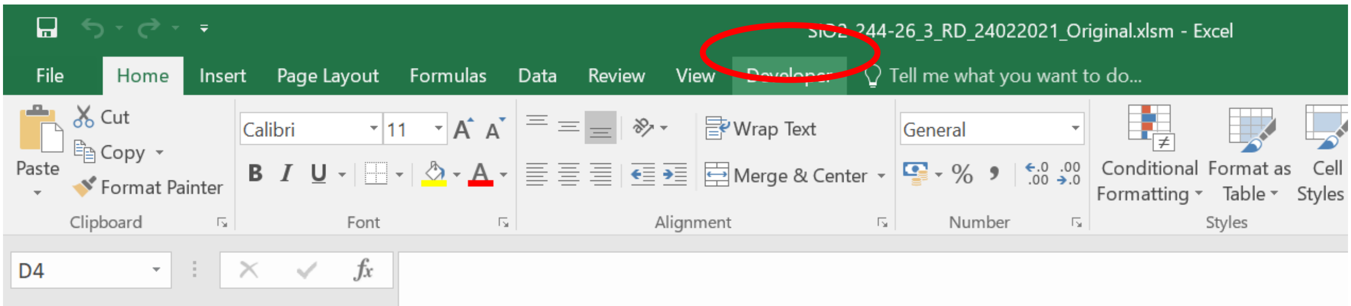

10. Press visual basic (alt + F11)

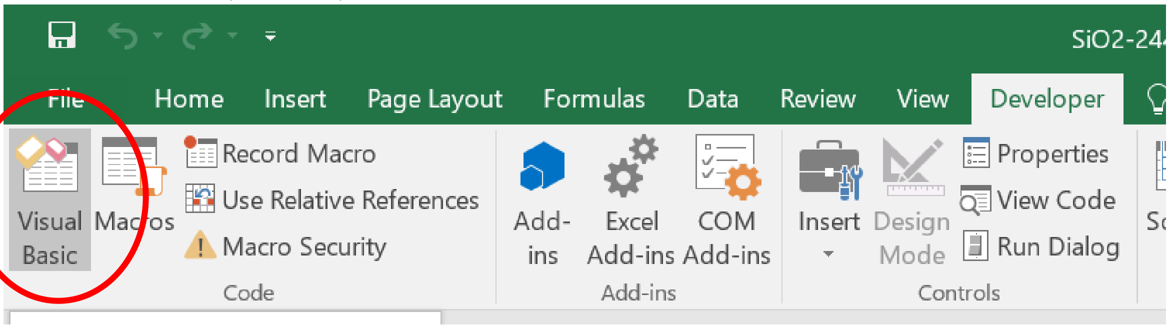


11. Press **file** -> **import** (ctrl + m)

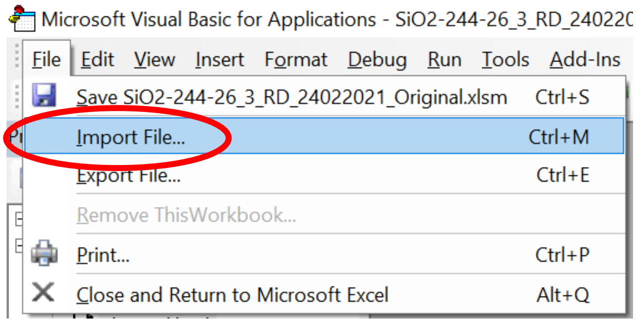


12. Locate and select the visual basic macro file **dustiness.bas** in the dialogue and press **import** (for the first use the .bas file should be extracted from the circulated zip file to a known folder on the C:\drive)

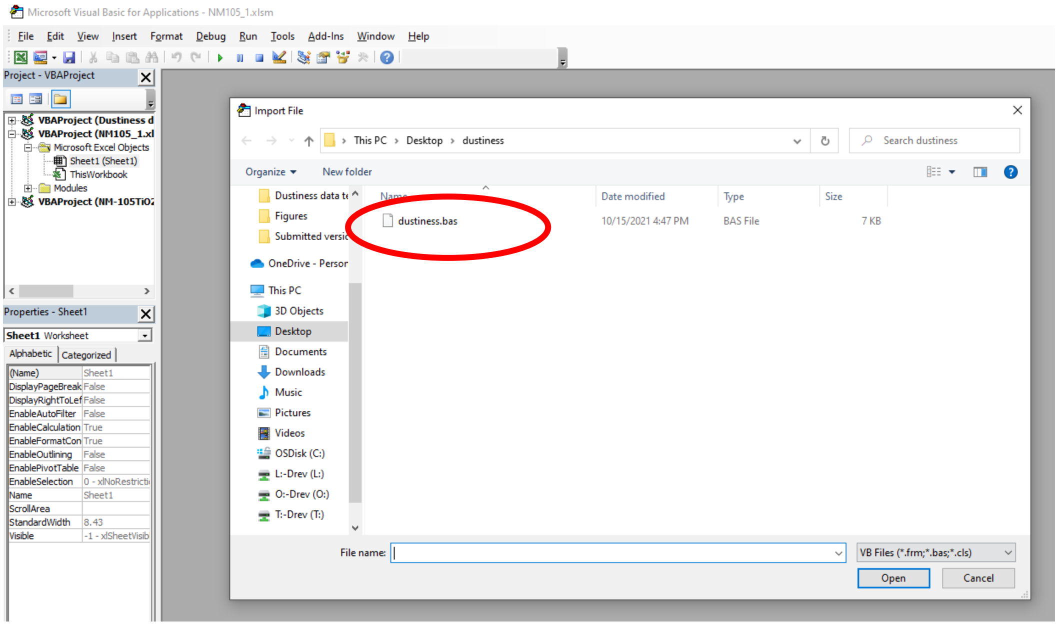


13. Close the developer window

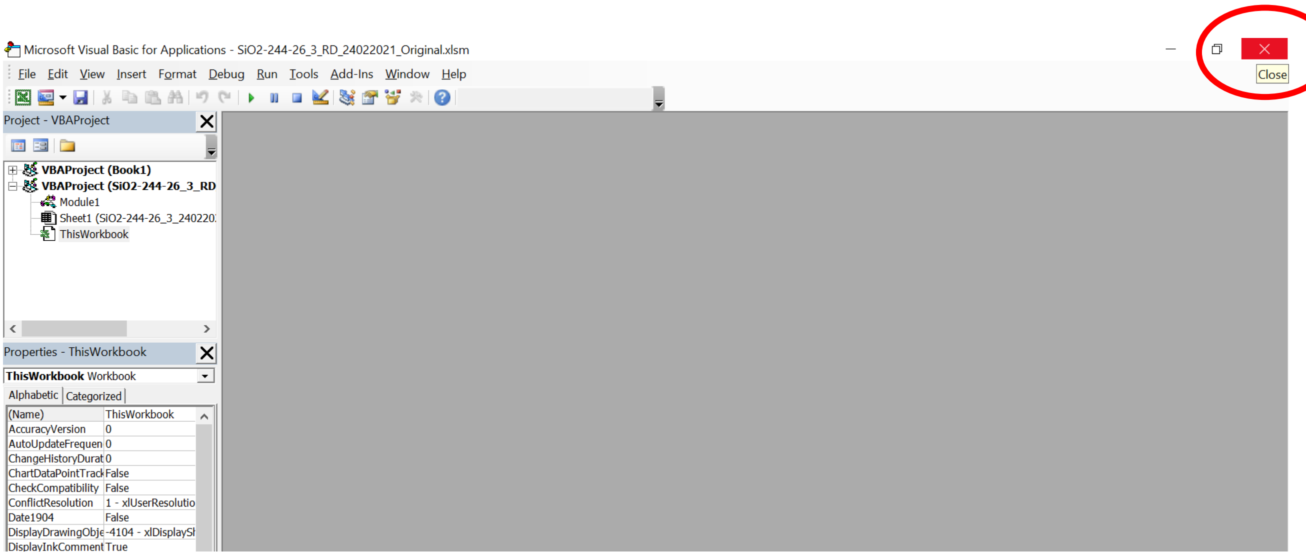


14. Start the macro by clicking **macro** (alt + F8) in the **developer ribbon** and selecting **Dustiness_Particle_generation_rate_CPC** and press **Run**

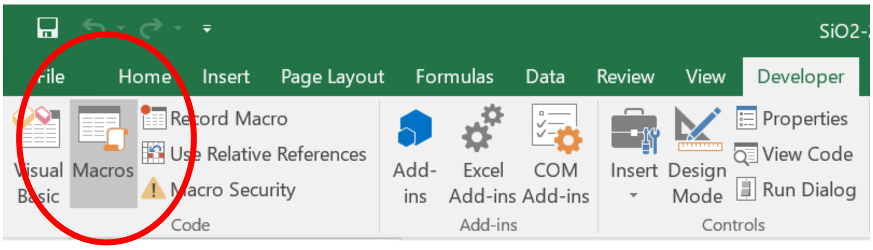


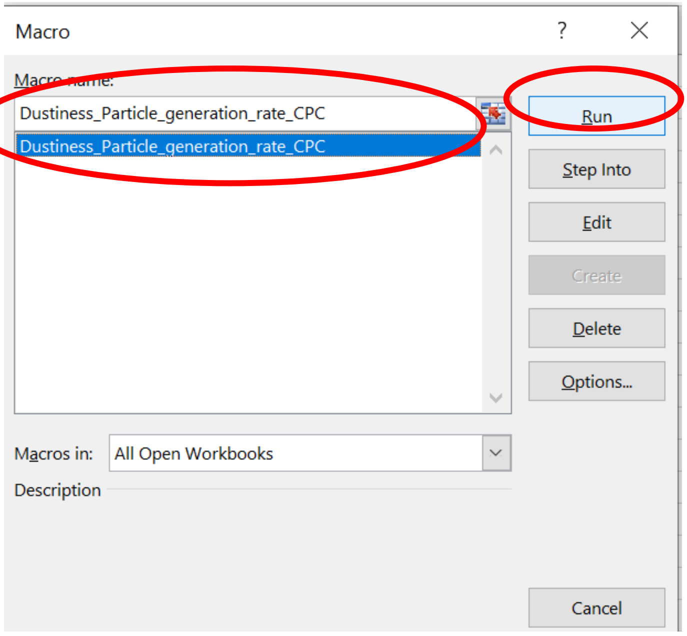

15. Add duration of the test without considering the dead time (e.g. 60s)

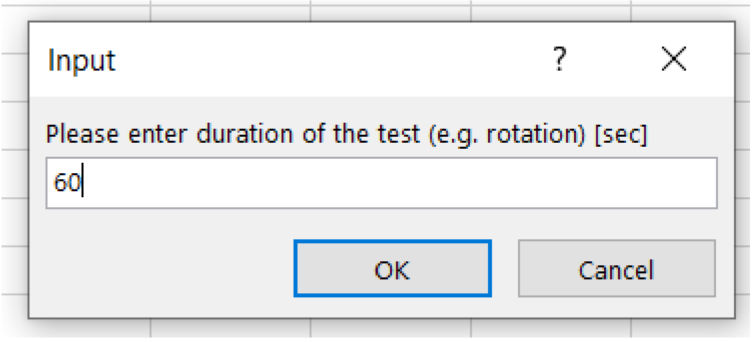


16. Add the dead time of the system (time needed to suspend the material; e.g. 5 sec)

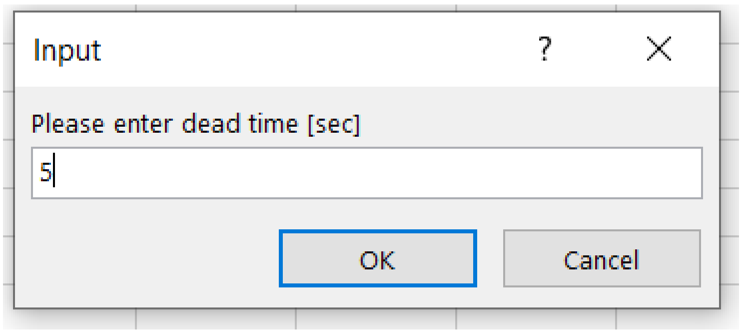


17. Select cells with **data** corresponding to times reported in the dustiness sheet (time of the rotation start)

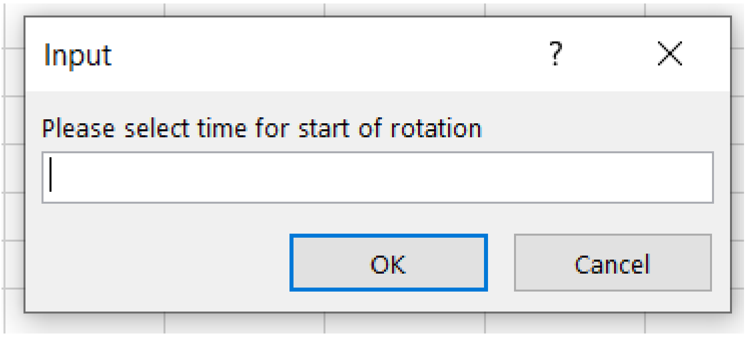


Rotation start

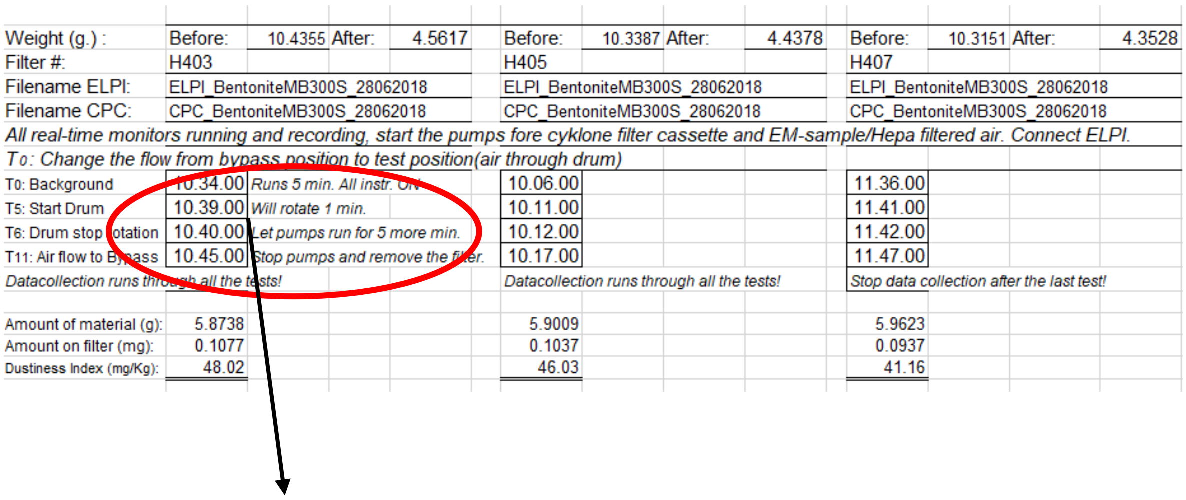

| | | | | | | | | | | | | |
|---|---|---|---|---|---|---|---|---|---|---|---|---|
| Weight (g.) : | Before: | 10.4355 | After: | 4.5617 | Before: | 10.3387 | After: | 4.4378 | Before: | 10.3151 | After: | 4.3528 |
| Filter #: | H403 | | | | H405 | | | | H407 | | | |
| Filename ELPI: | ELPI_BentoniteMB300S_28062018 | | | | ELPI_BentoniteMB300S_28062018 | | | | ELPI_BentoniteMB300S_28062018 | | | |
| Filename CPC: | CPC_BentoniteMB300S_28062018 | | | | CPC_BentoniteMB300S_28062018 | | | | CPC_BentoniteMB300S_28062018 | | | |
| *All real-time monitors running and recording, start the pumps fore cyklone filter cassette and EM-sample/Hepa filtered air. Connect ELPI.* | | | | | | | | | | | | |
| *T0: Change the flow from bypass position to test position(air through drum)* | | | | | | | | | | | | |
| T0: Background | 10.34.00 | *Runs 5 min. All instr. ON* | | | 10.06.00 | | | | 11.36.00 | | | |
| T5: Start Drum | 10.39.00 | *Will rotate 1 min.* | | | 10.11.00 | | | | 11.41.00 | | | |
| T6: Drum stop rotation | 10.40.00 | *Let pumps run for 5 more min.* | | | 10.12.00 | | | | 11.42.00 | | | |
| T11: Air flow to Bypass | 10.45.00 | *Stop pumps and remove the filter.* | | | 10.17.00 | | | | 11.47.00 | | | |
| *Datacollection runs through all the tests!* | | | | | *Datacollection runs through all the tests!* | | | | *Stop data collection after the last test!* | | | |
| Amount of material (g): | 5.8738 | | | | 5.9009 | | | | 5.9623 | | | |
| Amount on filter (mg): | 0.1077 | | | | 0.1037 | | | | 0.0937 | | | |
| Dustiness Index (mg/Kg): | 48.02 | | | | 46.03 | | | | 41.16 | | | |

| | |
|---|---|
| 10.38.58 | 0 |
| 10.38.59 | 0 |
| 10.39.00 | 0 |
| 10.39.01 | 0 |
| 10.39.02 | 0 |

18. Enter the airflow through drum (e.g 11L/min for the Small Rotating Drum))

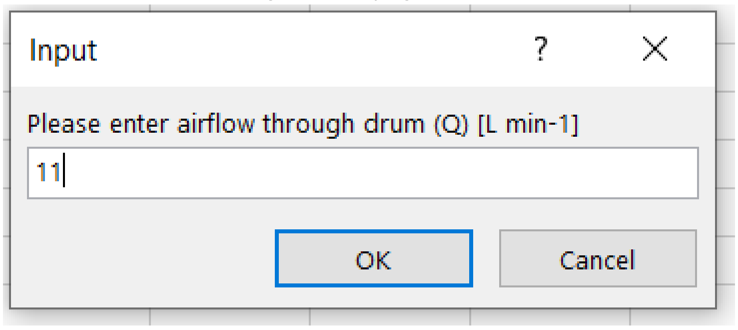


19. Enter the mass of the powder used for the test

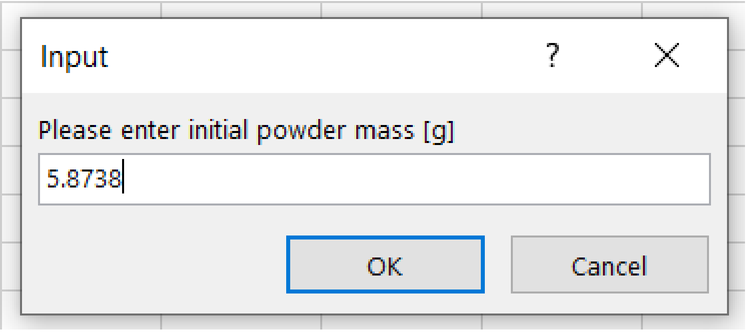


| | | | | | | | | | | | | |
|---|---|---|---|---|---|---|---|---|---|---|---|---|
| Weight (g.) : | Before: | 10.4355 | After: | 4.5617 | Before: | 10.3387 | After: | 4.4378 | Before: | 10.3151 | After: | 4.3528 |
| Filter #: | H403 | | | | H405 | | | | H407 | | | |
| Filename ELPI: | ELPI_BentoniteMB300S_28062018 | | | | ELPI_BentoniteMB300S_28062018 | | | | ELPI_BentoniteMB300S_28062018 | | | |
| Filename CPC: | CPC_BentoniteMB300S_28062018 | | | | CPC_BentoniteMB300S_28062018 | | | | CPC_BentoniteMB300S_28062018 | | | |
| *All real-time monitors running and recording, start the pumps fore cyklone filter cassette and EM-sample/Hepa filtered air. Connect ELPI.* | | | | | | | | | | | | |
| *T0: Change the flow from bypass position to test position(air through drum)* | | | | | | | | | | | | |
| T0: Background | 10.34.00 | *Runs 5 min. All instr. ON* | | | 10.06.00 | | | | 11.36.00 | | | |
| T5: Start Drum | 10.39.00 | *Will rotate 1 min.* | | | 10.11.00 | | | | 11.41.00 | | | |
| T6: Drum stop rotation | 10.40.00 | *Let pumps run for 5 more min.* | | | 10.12.00 | | | | 11.42.00 | | | |
| T11: Air flow to Bypass | 10.45.00 | *Stop pumps and remove the filter.* | | | 10.17.00 | | | | 11.47.00 | | | |
| *Datacollection runs through all the tests!* | | | | | *Datacollection runs through all the tests!* | | | | *Stop data collection after the last test!* | | | |
| Amount of material (g): | 5.8738 | | | | 5.9009 | | | | 5.9623 | | | |
| Amount on filter (mg): | 0.1077 | | | | 0.1037 | | | | 0.0937 | | | |
| Dustiness Index (mg/Kg): | 48.02 | | | | 46.03 | | | | 41.16 | | | |

20. Click OK, read and report the values in the top of the document:

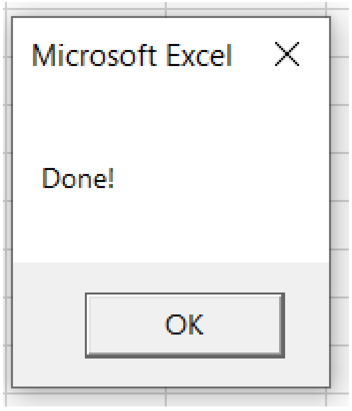


| | | | | | | | | | | |
|---|---|---|---|---|---|---|---|---|---|---|
| Sample | File | L:\PG-Nanotek data\befor | CPC_2021\CPC_TiO2JRCNM01005b_09122021.C07 | | | | | | | |
| Model | 3007 | | | Fitted particles generation rate [#/s] | Fitted particles generation rate per mg [#/mg/s] | Fitted tau [s] | Number based dustiness [#/mg] | Time for n50 [s] | Average total number concentration [#/cm3] | Emission rate time series [#/s] |
| | | | | 97440.78 | 16.24 | 18.29 | 974.41 | 48 | 387.3114754 | Negative number indicates faster removal than gener |
| Sample | # | 1 | | | | | | | | 6235.228849 |

# Annex C. Logbook file

| | | | | | | | |
|---|---|---|---|---|---|---|---|
| **Dustiness Test** | *Respirable dust is collected on 37mm. Filters, ELPI and CPC.* | | | | Date: | dd/mm/yy | |
| Material name: | | | | | | | |
| *Replica number:* | *#1* | | *#2* | | *#3* | | *#4 (if necessary)* |
| Filename ELPI (ELPI_institution name_name NM_number of test_ddmmyy): | | | | | | | |
| Filename CPC (CPC_institution name_name NM_number of test_ddmmyy): | | | | | | | |
| *Indicate testing times (see example below)* | | | | | | | |
| T0: Background | 10.19.00 | *Runs 5 min. All instr. ON* | 10.43.00 | | 11.07.00 | | 11.30.00 |
| T5: Start Drum | 10.24.00 | *Will rotate 1 min.* | 10.48.00 | | 11.12.00 | | 11.35.00 |
| T6: Drum stop rotation | 10.25.00 | *Let pumps run for 5 more min.* | 10.49.00 | | 11.13.00 | | 11.36.00 |
| T11: Air flow to Bypass | 10.30.00 | *Stop pumps and remove the filter.* | 10.54.00 | | 11.18.00 | | 11.41.00 |
| *Data collection runs through all the tests!* | | | *Data collection runs through all the tests!* | | *Stop data collection after the last test!* | | *Stop data collection after the last test!* |
| Amount of material introduced in the drum (g): | | | | | | | |

**Write here relevant observations (see an example below):**

ELPI did not record data on replicate #1

mass lost on filter replicate #2 while removal from the setup

Flow erros on CPC on replicate #3

# Annex D. Rotating drum dustiness report

Annex D consists of an Excel file containing a consolidated report of the ILC results from the Rotating Drum method.

# Annex E. Rotating drum statistical assessment

Annex E is composed by 5 pdf files named “Rotating Drum_DIinh”, “Rotating Drum_DIthor”, “Rotating Drum_DImass”, “Rotating Drum_DInumber”, and “Rotating Drum_DIpne”. These files contain the statistical assessment based on ISO 5725-2:2025 for inhalable, thoracic and respirable mass-based dustiness index, as well as particle number-based dustiness index and emission rate.

# Annex F. Small Rotating drum dustiness report

Annex F consists of two Excel files named “Small Rotating Drum_dustiness report_anonymised_granular NOAA” and “Small Rotating Drum_dustiness report_anonymised_fibrous NOAA”. These files contain a consolidated report of the ILC results from the Small Rotating Drum method for powders containing granular NOAA and powders containing fibrous NOAA.

# Annex G. Vortex shaker dustiness report

Annex G consists of an Excel file containing a consolidated report of the ILC results from the Vortex Shaker method.

# Annex H. Vortex shaker statistical assessment

Annex H is composed by 3 pdf files named “Vortex_DImass”, “Vortex_DInumber”, and “Vortex_DIpne” containing the statistical assessment based on ISO 5725-2:2025 for respirable mass and particle number-based dustiness index and emission rate.

# Annex I. Continuous drop dustiness report

Annex I consists of an Excel file containing a consolidated report of the ILC results from the Continuous Drop method.

# Annex J. Fluidizer dustiness report

Annex J consists of two Excel files names “Fluidizer_dustiness report_anonymised_granular NOAA” and “Fluidizer_dustiness report_anonymised_fibrous NOAA”. These contain a consolidated report of the ILC results from the Fluidizer method for powders containing granular NOAA and powders containing fibrous NOAA.

# Annex K. Venturi dustiness report

Annex K consists of an Excel file containing a consolidated report of the ILC results from the Venturi method.

# Annex L. Powders containing fibrous NOAA statistical assessment

Annex L consists of an Excel file containing a summary of the dustiness data generated for the Small Rotating Drum and the Fluidizer methods as well as the statistical assessment of the data, including Cochran C test, Dixon's Q test and calculation of the z-score.